Zinc Oxide Nanostructures for Optical and Optoelectronic Applications

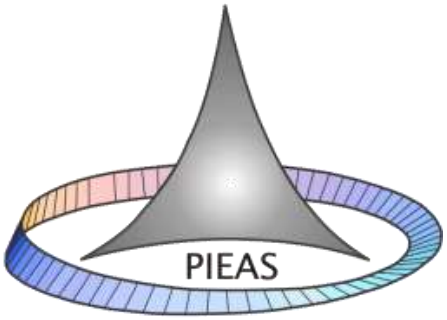

Hafiz Naeem-ur-Rehman

2015

Pakistan Institute of Engineering and Applied Sciences
Nilore, Islamabad, Pakistan

Thesis Submission Approval

This is to certify that the work contained in this thesis entitled **Zinc Oxide Nanostructures for Optical and Optoelectronic Applications**, was carried out by **Hafiz Naeem-ur-Rehman**, and in my opinion, it is fully adequate, in scope and quality, for the degree of **Ph.D.** Furthermore, it is hereby approved for submission for review and thesis defense.

Supervisor: _____
Name: **Dr. Mazhar Mehmood**
Date: 02 September, 2015
Place: PIEAS, Islamabad.

Head, DMME: _____
Name: **Dr. Mazhar Mehmood**
Date: 02 September, 2015
Place: PIEAS, Islamabad.

Zinc Oxide Nanostructures for Optical and Optoelectronic Applications

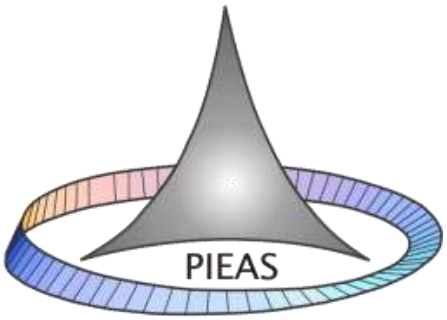

Hafiz Naeem-ur-Rehman

Submitted in partial fulfillment of the requirements
for the degree of Ph.D.
September, 2015

Department of Metallurgy and Materials Engineering
Pakistan Institute of Engineering and Applied Sciences
Nilore, Islamabad, Pakistan

Dedications

I dedicate my PhD Thesis

to my

BELOVED FATHER

Who passed away

just few days

before

the submission of

this thesis.

Declaration of Originality

I hereby declare that the work contained in this thesis and the intellectual content of this thesis are the product of my own work. This thesis has not been previously published in any form nor does it contain any verbatim of the published resources which could be treated as infringement of the international copyright law. I also declare that I do understand the terms ‘copyright’ and ‘plagiarism,’ and that in case of any copyright violation or plagiarism found in this work, I will be held fully responsible of the consequences of any such violation.

_____

(**Hafiz Naeem-ur-Rehman**)
02 September, 2015
PIEAS, Islamabad.

Copyrights Statement

Acknowledgements

First and foremost, I would like to thank my **creator** for His blessings. Because of Him I am able to finish this thesis without being ill or facing any obstacle. I thank Him for the gift of life, health and all opportunities in life. I offer my solemn gratitude to the Holy Prophet (Peace be upon Him) who is a foundation of supervision and acquaintance for humankind.

Afterwards, I would like foremost to give my heartfelt appreciation to my supervisor, **Dr. Mazhar Mehmood**, for his consistent guidance, productive criticism, continual encouragement and extended tolerance throughout my PhD tenure. He provided every possible help in flourishing and polishing my professional skills.

I would like to thank **Dr. Francis C. C. Ling** and his entire research group for their kind and bighearted support in research work during my stay at the Department of Physics, The University of Hong Kong.

Special thanks to Dr. Mirza Jameel Ahmad, Dr. Asim Rasheed, Dr. Farhat Ali, Dr. Mehmood Tahir and Dr. Irfan Ahmad and all other colleagues and friends for their sincere support.

All the credit goes to **my parents** who worked hard and suffered a lot in flourishing my career. Their prayers always remained with me in every difficult situation. It is because of them that I have reached this milestone in my career. Thank you ABU and AMMI. I am very blessed to have you in my life.

I am also grateful to **Higher Education Commission of Pakistan**, for providing me opportunity and financial support to carry out my research in Pakistan and Hong Kong under Indigenous and IRSIP fellowship scheme, respectively.

Table of Contents

List of Figures

List of Tables

Abstract

Wurtzite ZnO nano-structures with high crystalline quality have been grown by the electro-deposition of zinc on copper substrate followed by its hydrothermal oxidation in NaCl solution. Ni-doped ZnO nano-structures with up to 17 at% Ni have been formed for the first time without nickel-based impurity phase. The wire diameter decreases with Ni content, up to about 20-50 nm. Optical studies illustrate strong ultraviolet emission in the photoluminescence and cathode-luminescence spectra of ZnO nanostructures without, previously ever-existent, emission in the visible region, depending on the choice of NaCl solution (instead of pure water) and / or nickel doping. Annealing at 500 ºC in air causes emission in green and orange region, as accompanied by pronounced decrease in the intensity of UV emission. Annealing in argon results in intense green emission. As-synthesized doped and un-doped ZnO nanostructures obtained in this work are ideal choice for UV- based optical and optoelectronic devices. Gold nanoparticles have been attached to ZnO nano-structures by etching in potassium iodide followed by immersion in $HAuCl_4$ solution. The defect emission (in the visible region) intensified by etching almost completely vanishes after gold deposition. Photocatalytic activity of the ZnO nanostructures has also enhanced by attaching the gold nanoparticles.

Wurtzite ZnO thin films with high crystalline quality and almost perfect growth along c-axis have been formed by sputtering and PLD. These films, although composed of nano-crystalline columns present features of epitaxial growth on sapphire substrate. The ZnO film formed by PLD in air does not exhibit green and orange emission. Due to non-stoichiometric nature of ZnO film sputter-deposited in argon, green emission is observed. The charge carrier density is almost comparable in these films (about 2×10^{18} cm^{-3}), while the electron mobility in the former is significantly higher (about 35 $cmV^{-1}s^{-1}$) than the latter, owing to high crystalline quality as assessed by omega and phi scans in XRD analysis).

ZnO-Ge multilayer thin film structures have also been deposited by evaporation. Quantum confinement has been indicated by blue shift in the optical band gap of germanium.

List of Publications and Patents

Publications in Thesis

- **Naeem-ur Rehman**, Mazhar Mehmood, Farhat Ali, Muhammad Asim Rasheed, Muhammad Younas, Francis C. C. Ling, and Syed Mansoor Ali, *Heavily nickel-doped zinc oxide nanostructures prepared by hydrothermal oxidation of electro-deposited alloy films and their photoluminescence properties.* Chemical Physics Letters, 2014. **615**(2014): p. 35-43.

- **Naeem-ur Rehman**, Mazhar Mehmood, Rashid Rizwan, Muhammad Asim Rasheed, Francis Chi Chung Ling, and Muhammad Younas, *Control of optical properties of ZnO nanostructures grown by a novel two-step synthesis approach*. Chemical Physics Letters, 2014. **609**(2014): p. 26-32.

- **Naeem-ur-Rehman**, Mazhar Mehmood, Francis Chi Chung Ling. "*Annealing induced defects in ZnO nanostructures*". Submitted to journal.

- .**Naeem-ur-Rehman,** Mazhar Mehmood, Francis Chi Chung Ling, Abdul Faheem Khan, Syed Mansoor Ali. "*Comparitive study of the structural, optical and electrical properties of ZnO thin films prepared by PLD and sputtering techniques*". Submitted to journal.

- **Naeem-ur-Rehman**, Mazhar Mehmood, Francis Chi Chung Ling. "*Synthesis and Characterization of Gold nanoparticles modified ZnO nanostructures*". Submitted to journal.

- **Naeem-ur-Rehman,** Mazhar Mehmood, Francis Chi Chung Ling. "*ZnO-Ge multilayer thin film structures for photovoltaic applications"*. To be submitted.

Publications out of Thesis

- M Younas, LL Zou, M Nadeem, **Naeem-ur-Rehman**, SC Su, ZL Wang, W Anwand, A Wagner, JH Hao, CW Leung, R Lortz and Francis C. C. Ling, *Impedance analysis of secondary phases in a Co-implanted ZnO single crystal.* Physical Chemistry Chemical Physics, 2014. **16**(2014): p. 16030-16038.

- Farhat Ali, Mazhar Mehmood, Abdul Mateen Qasim, Jamil Ahmad, **Naeem-ur-Rehman,** Muhammad Iqbal, and Ammad H Qureshi, Comparative study of the structure and corrosion behavior of Zr-20% Cr and Zr-20% Ti alloy films deposited by multi-arc ion plating technique. Thin Solid Films, 2014(2014).

- W Aslam Farooq, Syed Mansoor Ali, Jan Muhammad, Syed Danish Ali, Muhammad Hammad Aziz, **Naeem-ur-Rehman**, and Muhammad Hussain, *Synthesis and characterization of Sn1Mg1− xO2 thin films fabricated by aero-sole assisted chemical vapor deposition*. Journal of Materials Science: Materials in Electronics, 2013. **24**(2013): p. 5140-5146.

- Syed Mansoor Ali, Jan Muhammad, Syed Tajammul Hussain, Shahzad Abu Bakar, and Muhammad Ashraf and **Naeem-ur-Rehman**, *Study of microstructural, optical and electrical properties of Mg dopped SnO thin films*. Journal of Materials Science: Materials in Electronics, 2013. **24**(2013): p. 2432-2437.

- Syed Mansoor Ali, Jan Muhammad, Syed Tajammul Hussain, Syed Danish Ali, **Naeem-ur-Rehman**, and Muhammad Hammad Aziz, *Annealing effect on structural, optical and electrical properties of pure and Mg doped tin oxide thin films*. Journal of Materials Science: Materials in Electronics, 2013. **24**(2013): p. 4925-4931.

- Syed Mansoor Ali, Syed Tajammul Hussain, Shahzad Abu Bakar, Jan Muhammad, and **Naeem-ur-Rehman**. Effect of doping on the Structural and Optical Properties of SnO2 Thin Films fabricated by Aerosol Assisted Chemical Vapor Deposition. in Journal of Physics: Conference Series. 2013: IOP Publishing.

1 Introduction

A brief overview of nano-materials has been presented in this chapter with particular focus on zinc oxide. Finally, objectives of the work have been outlined.

1.1 Nanotechnology and Nanomaterials

The significance of nanomaterials has been recognized in the area of advanced materials due to the exciting characteristics related with the nano-scale dimensions. Nanotechnology is the technology of the 21st century. It can be defined as the synthesis and engineering of materials at the nano level for possible device applications. The idea of nano-scale molecular device was first presented by, Richard Feynmann, in his famous lecture, “there is plenty of room at the bottom”. Materials less than 100 nm in at least one dimension have attracted a great deal of attention. Owing to their fine size and very high surface area, they possess dramatically different physical and chemical properties as compared to their bulk counterparts. This makes them ideal to study new physics at the nano-level in addition to the vast applications in versatile fields [1-2].

Nanoparticles behave quite different from their coarse-grained counterparts. The more loosely bound surface atoms constitute a significant fraction and they influence the behavior. For example, the melting point of gold is dramatically reduced when the particle diameter drops below 5 nm. Interestingly, nano sized gold is green in color which is a semiconductor while bulk is a noble yellow metal. Gold nanoparticles also change their color associated with surface Plasmon resonance.

Many interesting properties in nano-materials originate from the confinement of charge carriers in narrow dimensions [3-4]. Confinements could be mere electronic, excitonic or polaronic based on the size and excitation energy. Band gap energy often exhibits blue shift with very small sizes. Under some conditions, the energy bands of electrons and holes sometimes becomes close to discrete energy levels as of atoms/molecules. In addition to the large change in electronic/optical

properties, they also exhibit change in the effective redox potentials of photogenerated carriers [5-8].

1.2 Zinc Oxide

Zinc oxide (ZnO) is one of the versatile functional materials which have very appealing and broad-ranging history in diverse applications. ZnO has extensive use in various industrial applications such as a pigment in enamel coatings and paints, as an important ingredient in glass, cements, glue, tires, white ink, matches, cosmetics and dental cements [9-10]. The average annual production of ZnO to fulfill industrial demand is reported as ~ 100,000 tonnes [11]. The vast applications rely on various physical and chemical properties of ZnO such as the chemical activity, thermal and electrical conductivity, bioactivity and its UV absorption capability. It can also be categorized in the list of 'old' semiconductors. Reports on synthesis and characterization of ZnO have been available from as early as 1935 [4]. In 1960's improvements in the growth of single crystalline ZnO in epitaxial and bulk forms have transformed attentions in ZnO. Since then, synthesis of ZnO thin films has been an attractive field because of the strong potential for applications such as light emitters, transducers, sensors and catalyst. ZnO Nanostructures have attracted massive attention in recent period due to potential technological advantages and applications [12-16].

ZnO has some clear advantages as a wide band gap material.

- Exciton binding energy of ZnO is ~60 meV [17] that is considerably larger than that of GaN (~21-25 meV) [18]. Accordingly, the free exciton is stable at 300 K .
- Single crystal substrates in large sizes are available [19-21].
- Wet chemical processing is possible, and is compatible with Si technology [21].
- It possess greater resistance to radiation damage [22].
- It is one of the biocompatible Material [23].
- Optical pumping and lasing is possible at lower power threshold [24-25].
- It is easily available, cheap and is easily fabricated into nano-structures.

Large excitonic binding energy makes ZnO more striking for optoelectronic applications than GaN as the exciton stability increases by the higher exciton binding energy. It also enhances the luminescence efficiency by raising the possibility of radiative recombination.

ZnO also demonstrates good potential in a diverse range of applications in other areas, including sensor applications [23, 26-27], biomedical sciences [23] and spintronics devices [28-29]. It shows promise for space and nuclear applications, due to higher radiative resistance [30]. ZnO can also be used as a material for phosphors [31], varistors [32], piezoelectric transducers [33-34] and transparent conducting films [35-36].

Novel mechanical, electrical, chemical and optical properties introduce due to size reduction, and are believed to be due to improved crystal quality, surface and quantum confinement effects. Nano-scale structures of ZnO may enhance the compactness and efficiency of photonic and electronic devices including sensors, optical waveguides and LEDs. The structural, mechanical, chemical, electrical and optical properties of such kind of devices have already been enhanced by the small size of ZnO nanostructures. Although, ZnO has many applications in industry due to its bandgap in the near UV range and piezoelectric properties, but its utilization in optoelectronic devices still has not been successful because of the unavailability of reliable and proper p-type ZnO epitaxial layer. So in the absence of p-ZnO layer, hetero-epitaxy of ZnO with other p-type materials is being used to utilize its advantages. A p-n hetero-structure of n-type ZnO can be realized by employing a p-type material, while still using ZnO as an active layer. Much progress has been made in such kind of n-p devices. For example, n-ZnO/p-AlGaN heterojunction is successfully made to produce high-intensity UV emission in which ZnO served as the active layer [37]. Another potential application of ZnO is in homo-epitaxial devices.

Among the various ZnO nanostructures, nanorods or nanowires-like structures have higher potential for use in high performance devices and may be key material morphologies for future nanotechnology devices [38-40].

The formation of these nano-structures depends on the thermodynamic conditions and surface energy of different facets. The facet with higher surface energy usually extends to a smaller area, while that with lower energy extends to larger areas.

The highest growth rate is found along the c-axis, which means that $\{01\bar{1}0\}$ and $\{2\bar{1}\bar{1}0\}$ facets extend to form a high aspect ratio structures.

1.3 Defects and Luminescence in ZnO

The optical and electrical properties of semiconductor materials often depend on the quantity and nature of the defects present in it. Both extrinsic and intrinsic defects in ZnO affect for its luminescence properties. The donor and accepter energy levels present in ZnO below the conduction and above the valance bands are responsible for the ultraviolet near-band edge emissions. Deep energy levels are also found in the band gap of ZnO with different energies and result in the emissions in the whole visible region from 400-750 nm. Although, origins of these shallow and deep level emissions are still under debate for several years [31, 41-55].

The deep level emission (DLE) band in ZnO has been often attributed to different intrinsic defects in the crystal structure of ZnO such as oxygen vacancies (V_O) [56-60], oxygen interstitial (O_i) [48-50], zinc vacancies (V_{Zn}) [51-53], zinc interstitial (Z_{in}) [61] and oxygen anti-site (O_{Zn}) and zinc anti-site (Zn_O) [55]. The extrinsic defects such as substitution Cu and Li [58, 67] are also suggested to be involved in deep level emissions. The vacancy defects are formed when a host atom C is missing in the crystal and it is denoted by V_C. In ZnO, oxygen vacancy (V_O) and zinc vacancies (V_{Zn}) are the two most common defects. The single ionized oxygen vacancies in ZnO are said to be responsible for the green emission in ZnO. The oxygen vacancy has lower formation energy than the zinc interstitial and dominates in zinc rich growth conditions. The red luminescence from ZnO is attributed to doubly ionized oxygen vacancies [62].

The origin of the green emission in ZnO is the most controversial and many hypotheses have been proposed for this emission [43, 63-69]. Zinc vacancies were thoroughly investigated and suggested by many researchers to be the source of the green emission appeared at 2.4- 2.6 eV below the conduction band in ZnO [53, 70]. Many researchers also suggested oxygen vacancies as the source of green emission in ZnO [47, 71-72]. There are also reports that oxygen interstitials and extrinsic deep levels such as Cu are sources of the green emission in ZnO [11, 42, 73].

Recently it has been investigated that more than one deep levels are involved in the green emission in ZnO. i.e., V_O and V_{Zn} both contribute to the green emission [63, 74-75]. The blue emission in ZnO is said to belong to zinc vacancies. The blue emission is attributed to the recombination between zinc interstitial (Z_{in}) energy level to V_{Zn} energy level and it is approximately 2.84 eV (436 nm). It has been explained by the full potential linear muffin-tin orbital method, which explains that the position of the V_{Zn} level is approximately located at 3.06 eV below the conduction band and the position of the Z_{in} level is theoretically located at 0.22 eV below the conduction band [76].

The interstitial defects are formed when an excess atom D occupying an interstitial site between the normal sites in the crystal structure and it is denoted by D*i*. In ZnO, oxygen interstitial (O_i) and zinc interstitial (Z_{in}) are the two common interstitial defects. The zinc interstitial defects are normally said to located at 0.22 eV below the conduction band and play vital role in the visible emissions in ZnO by recombination between Z_{in} and different defects in the deep levels such as oxygen and zinc vacancies, oxygen interstitials and produce green, red and blue emissions in ZnO [76]. Oxygen interstitials defects are believed to be located at 2.28 eV below the conduction band and are responsible for the orange-red emissions in ZnO [68, 72]. The yellow emission in ZnO has often been attributed to oxygen interstitials [53, 72].

Anti-site defects are formed when atoms occupy wrong lattice position. In ZnO, the oxygen and zinc anti-site defects are formed when zinc occupies oxygen position or oxygen occupies zinc position in the lattice. These defects can be introduced in ZnO by irradiation or ion implantation treatments. The transitions at 1.52 eV and 1.77 eV above the valance band are attributed to O_{Zn} related deep levels [55].

Some cluster defects are also present in ZnO that are formed by combination of more than one point defect. The cluster defects can also be formed by a combination of point and extrinsic defects such as V_O Z_{in} cluster, which is formed by oxygen vacancy and zinc interstitial and it was reported that it is situated at 2.16 eV below the conduction band [55].

Extrinsic defects also play a vital role in the luminescence from ZnO. The ultraviolet (UV) emissions in ZnO at 3.35 eV are commonly related to the excitons

bound to the extrinsic defects such as Li, and Na accepters in ZnO [42]. The emission at 2.85 eV is due to copper impurities in ZnO [49, 77]. Recently the yellow emission observed in ZnO nanorods grown at low temperature by the aqueous chemical growth method was attributed to O_i and the Li impurities [49]. The yellow emission in the chemically grown ZnO nanorods was also attributed to the presence of $Zn(OH)_2$ that is attached to the surface of the nanorods. The yellow emission at 2.2 eV was observed in Li doped ZnO thin film and Li related defects and this is located at 2.4 eV below the conduction band [89, 90]. Mn, Cu, Li, Fe, and OH are common extrinsic defects in ZnO and these defects are involved in luminescence from ZnO. Defects with different energies produce the same color, for example ZnO:Cu and ZnO:Co have different energies but both emit green color [11].

Hydrogen has also been believed to play an interesting role in luminescence from ZnO. It is not a deep level defect and lie at 0.03-0.05 eV below the conduction band [78].

1.4 Diluted Magnetic Semiconductors and ZnO

The electronic devices employing the electronic flow and spin to function are studied in the field of spintronics. In this field diluted magnetic semiconductors (DMS) are considered as key materials as < 10% magnetically active atoms play their role to induce ferromagnetic properties along with semiconducting properties in the material. The potential use of DMS might be in the field of magneto-electronic, optoelectronic, or any device which use both electron charge and spin. DMS can be synthesized by substituting the cations in II-VI and III-V semiconductors with transition metals ions, e. g., Mn, Cr, Ni or Co. The transition ions at the cationic sites in the system cause exchange interaction between the *d* orbital electrons in magnetic ions and *sp* band electrons or holes leading to spin dependent anomalous Hall Effect.

DMS could be used to make a multifunction device on a single chip by replacing several components for logic, detection, storage and communications. Their optical properties also play a key role in converting the magnetic information in to an optical signal. But for a DMS to be considered as successful, its practical application should be similar to that of a well developed semiconductor. Thus major focus to

make DMS has been given to the conventional semiconductors, e.g. GaAs, TiO2, ZnO, GaN, GaSb, etc., by doping them with transition metals.

ZnO, as an important semiconductor material, have attracted much interest to develop dilute magnetic semiconductor material for spintronics applications. In order to build material for specific application, the doping of a proper material in ZnO is essential that tune the electronic, optical and magnetic properties [79-81]. Transition metals, i.e., Fe, Ni, Co, Mn, Cr, doped ZnO have shown potential to produces spintronics devices possessing spin polarized carriers. Among these, Ni is considered to be the efficient material to improve the optical and magnetic properties of ZnO nano-structures [82]. Along with spintronics applications, Ni doped ZnO nanostructures are also employed for the photo-catalysis of organic dyes and found to accelerate the process [83].

There are several methods that reported in the literature for synthesis of TM-doped ZnO nano-structures. These includes preparation of doped nanostructures by chemical route [84], hydrothermal method [83], sol gel method [85], thermal decomposition technique [86], chemical vapor deposition [87], thermal diffusion of TMs into ZnO [88], liquid phase evaporation deposition process [89]. Nevertheless, the doping of TM in ZnO is seen to form extra phases of TM oxides when the doping levels increased above a specific level. For instance, it has been found that employing the above mentioned synthesis methods, only up to 5% doping of TMs has been achieved without forming oxides of transition metals.

1.5 Methods for Growth of ZnO Nanostructures

1.5.1 Vapor Phase Transport (VPT)

In this method the vapors of the depositing material have been condensed on the substrate which has been kept at low temperature as compared to the target material. For example, the ZnO nano-combs were formed by evaporation of commercial ZnO powder in a tube furnace system at 1350−1450 °C under controlled condition [90].

Most commonly employed method for the growth of ZnO 1D nanostructures is vapor-liquid-solid (VLS) method, in which the vapor of the material to be deposited are exposed to a catalyst, e.g., Au particles, as a

result of which nanowires are formed. When the liquid becomes supersaturated in reactant materials, nanowire growth begins and continues as long as the reactant is available and the catalyst alloy remains in a liquid state [91]. Large-scale arrays of nanowires have been grown by this method [25, 92-93]

Similarly vapor-solid (VS) process has been employed by Meng et al., to grow arrays of highly aligned nanorods [94]. This chemical vapor deposition method (CVD) method has involved a thin ZnO base layer deposited by pulsed laser deposition (PLD) followed by VS process to synthesize the nanorods. Another study to grow nanocolumns was done in a catalyst free environment by using alumina substrates by the oxidation of zinc sulphide in tube furnace at 950 °C. In this method the substrate was kept far from the target at lower temperature [29].

The partial oxygen pressure and chamber pressure are important parameters influencing the growth mechanism that governs the final structure of the ZnO [18, 19]. By increasing the oxygen content under otherwise identical conditions, nanowires, dendritic side-branched/comb-like structures, and nanosheets can be synthesized.

Nanobelts of ZnO are usually grown [17] employing a catalyst free method by sublimation of ZnO powder. These nanobelts are actually kind of nanowires with well-defined geometrical shape and side surfaces.

Zinc oxide has a symmetric wurtzite crystal structure with two typical polar surfaces: $\pm(0001)$ and $(01\bar{1}1)$. During the synthesis process, when a nanobelt is formed due to the dominance of one of the polar surfaces, the dipole moment induces the spontaneous polarization resulting in the generation of electrostatic energy. The bending of nanobelt is then a way to decrease the electrostatic energy. But in fact, this bending of nanobelt will induce elastic energy. Hence, the competition between elastic energy and electrostatic energy lastly results in the formation of nanorings or nanosprings.

1.5.2 Chemical Vapor Deposition (CVD)

CVD process is often used in industry to produce semiconductor coatings. During the process one or more precursors are react or decompose to produce

desire coating on the substrate. Some by-products are also produced during the reaction which can be removed from the chamber by gas flow. [95]

Chemical Solution Method

Chemical solution method is often to deposit films and can produce thick films with micrometer dimensions in comparatively short times. The nano-structures can also be formed on the seeded substrate through the solution method. For example, the ZnO rod grown in an aqueous solution containing zinc nitrate and sodium hydroxide on a substrate which was initially coated with ZnO seed layer through sol–gel processing [96-98].

1.5.3 Hydrothermal Method

Hydrothermal method is often used to grow ZnO nano-structures and single crystalline ZnO ingots which have been cut into thin wafers to use as substrate. But this method has been widely employed to form nanostructures on bare substrates, patterned by lithography or have seed layer [99-100].

1.5.4 Thermal Oxidation

Sometimes high purity Zn foil or Zn powder has been heated under oxygen flow to form ZnO nano-structures with various morphologies [101]. The temperature range for oxidation process may be varies in the range from 400 to 1000 ^{o}C.

1.5.5 Precipitation Method

This method involves the formation of a solid from a solution or by the reaction of two or more solids during a chemical reaction or by diffusion in a solid. Un-doped and doped ZnO nanoparticles have been synthesized by this method [102].

1.5.6 Sol. Gel. Method

This method is used to deposit metal oxides in the form of nano-structures as well as thin films which are deposited by spreading the gel by a spin coater.

This method could also be employed to synthesized doped and un-doped ZnO nano-structures by making respective gels [85].

Physical Vapor Deposition

It is a kind of vacuum deposition method by which thin films or nano-structures have been deposited by condensing the vaporized material on substrates or on surface of some work-piece. ZnO nanorods, nanowires and thin films have been synthesized by PVD method [103-104].

1.5.7 Molecular Beam Epitaxy (MBE)

The epitaxial layers/films of semiconductor materials have been used to deposit by molecular beam epitaxy. Epitaxial growth of ZnO nano-structures [105-106] and thin films [107] is believed to have a defect free structure. The MBE deposited films are usually considered to be the single crystalline. Some researchers have also reported the deposition of p-type ZnO thin films by nitrogen doping using MBE [108].

1.5.8 Sputtering

This process is mainly deposit materials having high melting points. One can deposit metals, ceramics and even alloy materials. The deposited samples usually have elemental composition close to that of target material. So radio frequency magnetron sputtering has been a frequent method to grow ZnO films [109] and nanostructures [110].

1.5.9 Electrodeposition (ED)

This method is considered as a low cost and a simple method to deposit coating on metallic targets. Electrodes with large surface area can easily be coated using this method. This method is also used to grow ZnO nanostructures with different morphologies on metallic and semiconductor substrates like Si and GaN [111-113].

1.6 Control of Morphology of ZnO

The growth of nano-structures with reproducible features is also an issue of concern for many researchers. It is a widely acknowledged fact established after discussions at a variety of international meetings and conferences and reports by several authors, that morphology of ZnO nano-structures is extremely sensitive to the growth conditions (such as synthesis technique, pressure, temperature, and gas flow and substrate choice). This sensitivity of ZnO nano-structures makes it very tricky to achieve large area growth of structures with uniform and reproducible morphology by controlling the growth process. Generally, it has proven very difficult to reproduce such structures just by following a published growth method and using the same experimental conditions in another laboratory. Hence, to control growth adequately to synthesize a desired uniform and reproducible nano-structure morphology over a large area substrate will be one of the major challenges being faced by the ZnO research community.

In VLS, catalyst helps to form high aspect ratio nano-structures. But high temperatures are necessary in addition to use of PVD techniques for the deposition of catalyst.

1.6.1 Electrodeposition for Zn and Alloy Films

Electrodeposition presents a cost-effective method for deposition of large area thin films on substrate having arbitrary shapes with precise control of the film thickness. The temperature required for the process is very low. The high quality films can be grown by ED which usually presents strong adhesion with substrate surface. Another advantage of this technique is the deposition of alloys. For instance, anomalous co-deposition allows the preparation of zinc based films doped (alloyed) with transition metals like nickel even up to several 10's of percentage level.

1.6.2 Oxidation of Zinc Films

Qiang Xu et al. [114] have synthesized ZnO nanostructures by thermal oxidation of sputtered deposited Zn on Si substrates. The oxidation temperature used for Zn film was 700 ^{o}C. Similarly, Guo CF et al. [115] have grown ZnO nanostructures in a tube

furnace by the oxidation of Zn micro-structures at 300 ^{o}C. Rui-qun Chen et al. [116] had demonstrated the oxidation of sputtered Zn film in wet oxygen provided in quartz tube furnace at 420 ^{o}C. They have reported the formation of un-doped and doped ZnO nanobelts through this method.

1.6.3 Hydrothermal Oxidation of Electrodeposited Zn and Zn Alloy Thin Films

Zn and Zn alloy films can be grown on various conducting substrates. The growth rate can be controlled by current density and thickness can be controlled by charge passed during deposition. Similarly, solution chemistry can be controlled to provide with various levels of doping. The morphologies of the deposits also vary with deposition parameters.

It may be interesting to electro-deposit various Zn metal and alloy films and attempt to form doped and un-doped ZnO nano-structures. Various deposition and oxidation parameters may possibly help to form nano-structures with better control on size (diameter) and other morphological aspects.

Oxidation of these metal/alloy films in aqueous media with and without aggressive chloride ions may possibly form dense ZnO nano-structures well adhesive to the substrate. The fine grain size of nano-crystalline zinc and zinc-alloy films may also provide with high nucleation density and these facilitate the one-dimensional nano-structures with large population density. Finally it may be interesting to see if the alloy films can be oxidized to form highly doped ZnO nano-structures by hydrothermal method or not.

1.7 Thesis Outline

Chapter 1 presents general introduction to nanotechnology, nanomaterials and nanostructures to give a comprehensive overview about this field with special emphasis on zinc oxide, nano-structures of ZnO, its optical properties and factors effecting these properties supported by an ample literature review.

Chapter 2 summaries the experimental procedures that were employed for the synthesis of nano-scale structures and different techniques used in order to characterize these materials.

Chapter 3 discusses the synthesis of ZnO nanostructures by electrodeposition followed by hydrothermal oxidation at various temperatures and the effect of synthesis temperature on the nano-structures and optical properties.

Chapter 4 covers the effect of Ni doping in ZnO nano-structures on structure and optical properties.

Chapter 5 focuses the structure and optical behavior of ZnO nano-structures after annealing in air and argon environments.

Chapter 6 presents the attachment of gold nanoparticles on the ZnO nano-structures.

Chapter 7 the main emphasis of this chapter is to study the effect of oxygen partial pressure during RF sputtering deposition on the ZnO thin films.

Chapter 8 explains the various optical parameters of ZnO thin films deposited by pulsed laser deposition and radio frequency magnetron sputtering.

Chapter 9 gives a brief idea about the structural and optical properties of ZnO-Ge multilayer thin film structures.

Chapter 10 Summarizes the thesis by drawing main conclusions of the present work.

2 Experimental Techniques

The ZnO nano-structures and thin films prepared for the studies presented in thesis were synthesized by electrodeposition of metallic films on copper substrate followd by the hydrothermal oxidation and various PVD techniques, respectively.. For Un-doped, Ni-doped and Au attached ZnO nano-structures have been synthesized by wet methods. ZnO thin films and multilayer ZnO-Ge films have been deposited by PVD techniques. The structural, optical and electrical properties of these structures have been studied by employing various characterization tools.

2.1 Characterization Techniques

The characterization tools used in this study are listed below.

XRD
SEM
TEM
AFM
Photoluminescence
Cathodoluminescence
UV/Visible spectroscopy and Diffused Reflectance spectroscopy
Current-Voltage measurement (resistivity measurement)

2.2 X-ray Diffraction (XRD)

This non-destructive technique provides necessary information about different phases, crystal structures, crystal systems, lattice parameters and compressive and tensile stresses in a material [117]. XRD also helps distinguish between mono-crystalline and polycrystalline structures. The basic principle of XRD follows the Bragg's law. When monochromatic x-rays collide with atoms of a material, each atom becomes a scattering source. The diffraction occurs where Bragg's equation is satisfied:-

$$2dsin\theta = n\lambda$$

Where

θ = the angle of the diffracted x-ray

d = interplanar distance

λ = wavelength of x-ray beam

n = order of the diffracted beam

[117-121].[121-124].

The average crystallite size of the film is calculated using Scherer's formula [118],

$$d = \frac{0.9\lambda}{\beta Cos\theta}$$

Where

λ = wavelength of the x-ray beam

β = full width at half maximum (FWHM) of a certain peak expressed in radians.

2.3 Atomic Force Microscopy (AFM)

AFM provides extremely fine (detailed) information on the topographical properties of a material and roughness. [119, 125-126]. AFM is based on interacting force between sample and an extremely sharp probe (tip), on at atomic scale. Generally, the pyramid shape probe fixed on a thin cantilever is of a few microns of length with end radius of the order of nanometers [124-125]. In AFM, the limited area of sample is raster-scanned using the probe. Image can be achieved by measuring the lateral and vertical deflections of the cantilever with a laser. This deflection is the measure of atomic force between atoms at the tip and the sample. More commonly the deflection (force) is kept constant by upward and downward movement of the probe (or the sample) by a feedback control system. The control unit consists of a distinct feedback system having a piezoelectric xyz scanner that regulates the z-positioning along with horizontal 2-D scanning of the sample. [119, 126-127].

2.4 Scanning Electron Microscopy (SEM)

In *electron microscope* an electron beam (e-beam) is used to produce a magnified image of the sample. There are three principal types of electron microscopes: *scanning*, *transmission*, and *emission*. The electron beam is shined on the sample in the scanning and transmission electron microscope to produces an image, whereas in the field-emission microscope the sample itself is the source of electrons.

The scanning electron microscope is a characterization technique for examination of the structure and morphology of both bulk materials and films at higher magnification (>100000X) and higher resolution (few nanometers) [126, 128-130]. The magnification depends on the current delivered to scanning coils. The resolution is influenced by control of electron spot size which depends on wavelength of e's and on the e-optical system. A scanning electron microscope consists of an electron gun, magnetic lenses, set of scanning coils, an electron detector, and an oscilloscope. An electron beam (on either thermionic or field emission basis) is generated and is guided towards the specimen surface using electromagnetic lenses. The electron beam energy varies from few electron volts to 30-40 keV. The spot diameter of the beam lies in the range of 4Å to 5nm. The beam path creates a raster which matches to another raster comprising of pixels on screen. The electrons interaction with the specimen surface causes loss of their incident energy via elastic and inelastic scattering and consequently produces many signals. These signals are initially detected and then analyzed to provide information about the inner structure called image along with the composition of specimen. The most noticeable detection modes are characteristic x-rays, secondary electrons and backscattered electrons. The characteristic x-rays are generated as a result of removal of an electron from an inner shell of an atom of the specimen and its subsequent filling by an electron from some high-energy level. This causes the release of certain energy characteristic of each element. Characteristic x-rays are useful to determine the elemental composition of the material [126, 129-131]. Secondary electrons are generated through excitation of atoms due to incidence of electron beam. Backscattered electrons are in fact electrons of the primary beam. These electrons reflect back from the specimen because of elastic scattering. Secondary electrons give information regarding surface topography. Backscattered electrons, on other hand, help in identification of z-contrast or in other

words the elemental distribution within a specimen. Electrically conductive material surfaces (both metals and alloys) can easily be imaged with the help of SEM. The specimen is grounded to reduce chances of charge accumulation at the surface [132]. Non-conductive materials need nano-layer coating of some conducting material like platinum, gold or carbon [126] [127].

2.5 Energy Dispersive X-Ray (EDX) Analysis

This technique is both qualitative and quantitative to find out the localized composition of either a film or a bulk material [133-134]. In principle, all elements should be detected through EDX, but generally the technique is not accurate for lighter elements (lighter than Na, i.e. atomic number < 11). The accuracy of EDX measurements is close to $\pm$ 2%. Specimen shape and size (within applicable limits) have no restraint, and specimen holders are available for easy handling of samples. Nonconducting specimen are coated to provide a path for flow of incident electrons to the ground, thus avoiding specimen charging. A solid state detector e.g. Si (Li) or Si detector is used to acquire higher energy resolution. The detector is kept cool with liquid nitrogen to minimize electronic noise [130, 135-137] .

Energy dispersive x-ray analysis (EDX) is used to carry out the elemental analysis of the sample. The EDX analysis system always acts as an integrated aspect of a scanning electron microscope (SEM), and cannot operate individually exclusive of the latter [138-139].

In EDX Analysis, an electron beam is bombarded on the sample surface inside the scanning electron microscope. The bombarding electrons collide with electrons of specimen atoms and knocked some of these out during this collision. A higher energy electron from an outer shell ultimately occupies a vacant position created by an ejected inner shell electron. The outer electron imparts some of its energy by emitting an x-ray. The amount of energy released by electron transfer depends on corresponding shells involved in this transfer. The atom of every element emits x-rays with specific amounts of energy during the electron transferring. So, by measuring the energy of the emitted x-rays by a sample during bombardment, the identification as well as determination of the composition of each element is possible.

The EDX spectrum is a plot between the intensity of x-ray and energy of the emitted x-ray. It simply consists of peaks corresponding to those energy levels for which the majority of x-rays had been detected. Each peak corresponds to an atom, and therefore corresponds to a single element. Intensity of the peak is proportional the concentration of the elements in the specimen. An EDX spectrum not only identifies the element, but also the type of x-ray to which it's corresponding. For example, if a peak corresponding to the amount of energy possessed by x-rays emitted by an electron in the L-shell going down to the K-shell is identified as a K_α peak.

2.6 Rutherford Backscattering Spectroscopy (RBS)

Rutherford backscattering spectroscopy (RBS) is a non-destructive, quantitative analysis technique. It provides the information about the composition (the depth profile) of thin films as a function the scattering of incident beam of alpha particles. Alpha particles with energies ranges about 2-3 MeV are bombarded on the surface of the examining film/material under investigation. A part of the energy of incident ion is lost despite the elastic with surface atoms. A detector is used to count the energy of backscattered alpha particles. The energy loss by the incident ion is also a function of depth up to which it can penetrate before elastic collision and as a result scatter back. This kind of depth dependency of the energy is useful to determine the composition of a material [140-141]. The experimental technique is evenly suitable for depth profiling of multilayered coatings along with those of codeposited alloy coatings [142-144]. RBS is mainly helpful for identifying the heavy elements in a light matrix.

The sensitivity of RBS is low as compared to other elemental analysis techniques such as SRP and SIMS. The minimum detection limit is in the order of 10^{14} cm^{-2} atoms for a layer of thickness 10^{-5} cm corresponds to $10^{14}/10^{-5} = 10^{19}$ cm^{-3}. The sensitivity of RBS can be enhanced by using heavier ions than He, e.g. carbon. But heavy ions adversely affect the depth resolution. Another way to improve the depth resolution is tilting of the target. Maximum resolutions up to 2-5 nm have been achieved [145]. The additional advantages of RBS are determination of doping activation as well as degree of electrical activation.

2.7 Photoluminescence (PL)

Photoluminescence, also known as fluorometry, is a non-destructive technique for determining defects in semiconductors [146]. It is mostly suitable for the determination of shallow-level defects, but can also be applicable to certain deep-level defects, provided their radiative recombination [147].

2.8 UV/VIS/IR Spectroscopy

The response to electromagnetic radiation is related with optical properties of a material. When electromagnetic radiation interacts with a material, there are many processes that can arise as a result of the interaction between radiations and the material. Small amount of radiation may be lost and transformed into heat, which is absorption. However, some may pass without any loss, i.e. transmitted, and scattered back from the material, called reflectance.

2.8.1 Absorption

The Absorption depends on the frequency of radiation and the nature of materials interacting with radiation. For finding the band structure of a material, the most direct and easy technique is to measure the absorption spectrum. In the absorption process, a photon of known energy excites an electron from lower to higher energy state. Absorption coefficient 'α', is the relative rate of decreasing in light intensity in material, and is expressed as the absorption. The standard way for finding the electronic transitions, band structure and band energy of materials is by the absorption coefficient, particularly near the absorption edge. There are two types of optical transitions that can occur, direct and indirect transitions. Wave vector of electron remains same in case of direct transitions. However, in indirect transitions, the wave vector must change. Mott et al [148] reported following relation for the optical transitions, independent of temperature and free electron-hole interactions:

$$\alpha(\nu) = \frac{A\left(h\nu - E_{opt}\right)^{n}}{h\nu}$$

Where n = 1/2 or 3/2 for direct transitions depending on the transition whether it is allowed or forbidden, in amorphous materials absorption due to the interband

transition. Absorption in many non – crystalline materials is related with direct transitions, which obey the above equation [149].

2.8.2 Transmittance

The passage of radiation through materials without energy change is Transmission. This process depends on the frequency of radiation and the interacted concerned substance. The transmission coefficient is defined as "the amount to which a body passes through incident radiation, equal to the ratio of the flux" [150]. When a beam of radiation passes through a material, the amount of transmitted radiations depends upon the absorbed and the reflected radiation during interaction. It is also possible that diffused transmission may occur, that is transmission in which the laws of refraction are not obeyed on the microscopic scale and part of the radiation is scattered and lost from the beam without being absorbed.

2.8.3 Reflectance

Bounce back of incident radiation from the surface of material into same medium without changing of frequency rather than passing through the second medium is called reflection. Reflection depends upon the frequency of incident radiation and the material involved. A material has very small reflection that does not contain a high density of free charges such as glass. On the other hand, a metal possesses very dense free electrons and penetration by the radiations is very small, so has high reflectance. It is found that whatever the material is, the wavelength at which there is strong absorption, there will generally be a strong reflection [151].

2.9 Resistivity Measurements

Four Point Probe is a resistivity measuring technique. In this technique, a probe head with four tips or four different probes is used to contact the sample one wants to measure. Current is supplied by means of two specific current leads. These create, following Ohm's law, a voltage drop across the sample. Two additional voltage measuring leads are used to sense the voltage drop. The main advantage of four-terminal sensing is that the separation of current and voltage electrodes eliminates the impedance contribution of the wiring and contact resistances.

3 ZnO Nanostructures

Nanostructures exhibit unique and exceptional electrical, magnetic, optical, chemical and mechanical properties for the development of high performance devices [152-153]. Shape and size-dependent quantum confinements and large surface areas are attributed to enhance the chemical and physical properties of these nanostructures [154-156].

ZnO has a unique group of growth morphologies, such as nano-rods, nano-rings, nano-combs, nano-helixes/nano-springs, nano-wires, nano-belts, and nano-cages [153]. One-dimensional zinc oxide has been of great interest because of its potential applications in lasers, photodetectors, field emitters, nano-generators, photonic crystals, optical switches, field effect transistors, dye-sensitized solar cells, as well as in bio-devices because of its bio-compatibility [152, 157].

ZnO is a wide bandgap (3.37eV) semiconductor having large exciton binding energy (60 meV) [158]. Therefore, it exhibits reduced UV lasing threshold [25] and higher UV emitting efficiency [153]. ZnO has been considered to be one of the most promising UV emitting phosphors and is supposed to be potentially better than GaN [25].

To realize the use of ZnO in the UV emission devices, extensive studies have been done [24, 103, 157, 159-163]. The main problem hindering the achievement of UV emission devices based on ZnO is due to substantial green emission [164-165] which also tends to suppress the UV emission [99]. Preparation techniques, subsequent heat treatment and environment during preparation and heat treatment have been extensively focused upon to investigate the origins of luminescence and to optimize for maximum UV emission (or the visible one, depending on applications) [166-167].

Green emission in ZnO has often been related with crystalline imperfections like zinc and oxygen vacancies, which are commonly produced in the poor quality of crystalline structures [104, 168-171]. The emissions have also often been related with

surface related defects; for instance, green luminescence has been enhanced by the addition of some non-ionic surfactants [172]. Scanning electron microscopy equipped with photo-detectors have been successfully employed for cathode-luminescence to study the geometrical occurrence of visible as well as UV emission. For instance, UV emission has been predominantly seen at some top ends (i.e., c-plane) of nanowires, while the defect emission has been predominately seen along the prismatic surfaces where the UV emission is found to be extremely suppressed [173]. Such differences (i.e., position dependent emission) have also been related with the polarity of the (001) c-plane [174]. For the +ve polarity, the c-plane at the top or the bottom of the nanowires has been shown to exhibit enhanced UV emission in comparison with the side (prismatic planes), and the vice versa is true for the –ve polarity.

Researchers have used a range of techniques to prepare high-quality ZnO nanostructures required for UV optoelectronic devices such as electro-deposition [100, 103, 159], chemical vapor deposition (CVD) [161], physical vapor deposition [103-104], hydrothermal method [99, 175], sputtering [110] etc. However, ZnO nanostructures synthesized by these techniques exhibit a broad green emission.

This chapter presents the synthesis of high aspect ratio ZnO structures by a two-step process that is electro-deposition of zinc on copper substrate followed by hydrothermal oxidation in 3.5% NaCl solution at different temperatures and pressures. Photoluminescence (PL) and cathodoluminescence (CL) results of these samples show that green emission is absent. In addition, temperature (and pressure) of hydrothermal oxidation step plays an important role in determining the intensity of UV emission.

3.1 Experimental:

3.1.1 Electrodeposition:

Analytical grade $ZnCl_2$ and Boric Acid were used along with the doubly distilled water to prepare electrolytic solution for electro-deposition of zinc film on the copper substrate. The initial pH of the solution was 3.6 ± 0.1 (measured by pH meter Model PH 330/SET – 0, 82362 WTW, Germany) and during whole experiment it remained within the given error bars. Electro-deposition was performed using Potentiostat / Galvanostat AMEL Model-2051

at current density of 700 Am^{-2} for 20 minutes. The detailed procedure of electro-deposition process can be seen elsewhere [176].

3.1.2 Hydrothermal Treatment:

In the second step, electro-deposited zinc coatings were immersed in 100 ml of 3.5% NaCl solution in Teflon crucible. The crucible was then placed in the hydrothermal reactor (Model Limbo 350, Switzerland). Oxidation of zinc to form ZnO nanostructures was performed at various temperatures (and pressures) as given in Table 1. The temperature in the hydrothermal reactor was increased gradually to the reaction temperature, at which the sample was held for 24 hours and then allowed to cool to the room temperature. The samples were then removed from the reactor and thoroughly rinsed with distilled water.

X-ray diffraction (XRD) was performed by Bruker D8 Discover diffractometer with Cu Kα radiations. Transmission electron microscopy was performed by FEI Technai G2 20 Scanning TEM. Scanning electron microscopy as well as cathodoluminescence was performed by using JEOL JSM-7001F Field Emission Scanning Electron Microscope equipped with Gatan Monocol Cathodoluminescence recording system. The CL measurements were taken at 15 KV for all samples. Photoluminescence measurements were performed at 10 K with 325 nm He-Cd laser line (Melles Griot Series 56) at 15 mW.

Table 3-1 Temperatures and corresponding pressures employed for hydrothermal treatment of electrodeposited Zn films

Sr. No	Temperature (°C)	Corresponding Pressure (bar)
1	100	1.013
2	110	1.433
3	120	1.986
4	130	2.701

3.2 Results and Discussion:

Fig.1 shows SEM images of the ZnO nano-structures grown by hydrothermal oxidation of electrodeposited zinc in NaCl solution. At 100 ℃, the formation of nano-rods is evident as shown in Fig. 1(a). The diameter of these nanorods lies in the range of 100 to 750 nm. The nanorods tend to radiate outward from numerous originating / nucleation points in a flower-like pattern. Fig. 1(b) shows ZnO nanostructures formed at 110 ℃. Nanorods are numerously seen along with some microtubes (A) and extremely thin nano disks (B). The rods are more aligned mutually than that formed at 100 ℃. The rod diameter ranges from 0.35 to 1.3 μm a bit larger than that formed at 100 ℃. At 120 ℃, the rods become excessively aligned upward and their diameter is reduced in the range from 100 to 800 nm (Fig. 1 (c)). At 130 ℃, the small nanorods formed at lower temperatures are mostly replaced by much thicker microtubes. The hollow nature of these high-aspect ratio structures is clearly evident from fractured cross-sections. Their outer diameter varies up to about 3.2 μm, while the wall thickness remains about 0.9 μm. It seems that these microtubes are not formed by typical dissolution process, as the structures which are intact have a conical cap. A possibility is that initially nucleated large crystals cannot grow to thick micro-rods and they convert to microtubes. This seems partly related with growth stresses which are known to rise with thickness depending on growth conditions. This presumption is supported by a uniform wall thickness of about 0.9 μm, which must have been due to a compromise between various growth conditions and residual stresses. It is reported that depending on the growth conditions including the flux of zinc cations, a taper is produced and the tube is sealed at the top by a conical cap [177]. In addition to these microtubes, nanorods of 1 μm diameter and smaller are also seen.

When the reaction temperature is increased, the size of ZnO nanoparticles formed at initial stage of the oxidation of ZnO film is increased, providing the nuclei for the growth of nanorods with larger diameter. Accordingly, the size of the ZnO nanostructures tends to increase at higher synthesis temperature. The dispersity in the diameter of nanorods is believed to be caused by varying sizes of ZnO nanoparticles formed at the initial stage. It appears that stresses increase with diameter and above about 1 μm, stresses become so high that these nanorods are replaced by microtubes whose wall thickness remains of the order of 900 nm.

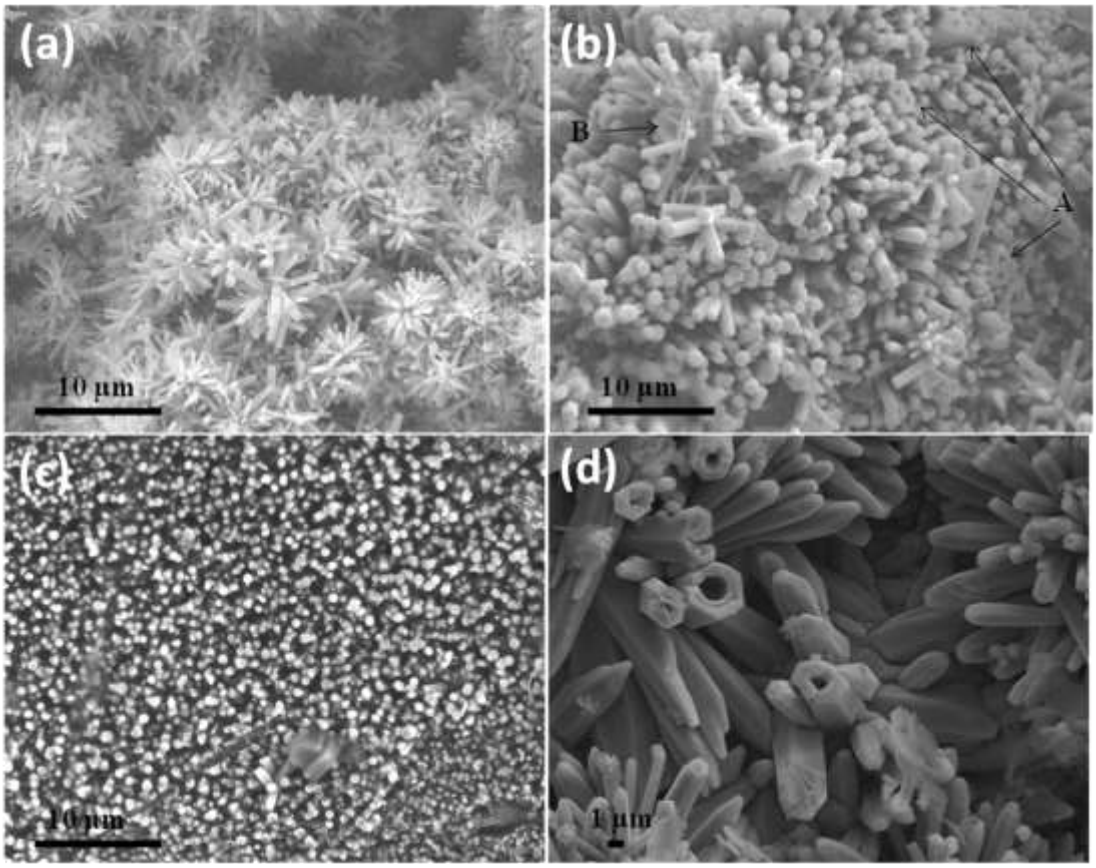

Figure 3-1 FESEM images of ZnO nanostructures grown at hydrothermal temperature of 100 ºC (a), 110 ºC (b), 120 ºC (c) and 130 ºC (d)

Fig. 2 shows typical XRD patterns of the samples prepared by hydrothermal oxidation of electrodeposited zinc film in NaCl solution. All the samples exhibit XRD peaks of hexagonal wurtzite ZnO (pdf card 01-070-8070). The formation of another minor phase, Zinc Hydroxide Chloride Hydrate (ZHCH) is also revealed by the XRD patterns (fitted with pdf card 01-072-1444) with the exception of 110 ºC. Its formation has been reported by our group in salt spray tests of zinc alloys [178]. Similarly Ueda et al [179] have also reported its formation by the chemical reaction of Zinc surface with a layer of sodium chloride in excessive humid atmosphere. Li et al [180] have observed that ZHCH tends to convert to ZnO with oxidation time. In the present work we have observed the simultaneous occurrence of ZHCH and un-oxidized Zn along with ZnO in the samples prepared at 100, 120 and 130 ºC. It appears that ZHCH is formed as an intermediate product as a result of oxidation of electrodeposited zinc and subsequently converts to ZnO. In order to confirm coexistence of the reactant Zn and the intermediate product ZHCH before complete conversion to ZnO, relatively thinner

samples (electrodeposited for 10 min) were hydrothermally oxidized at 120 and 130°C in the same solution. Figure 3 shows the corresponding XRD patterns that confirm that ZHCH is not retained after complete oxidation of electrodeposited zinc; ZHCH being the intermediate product formed in NaCl solution, particularly at 120 and 130°C.

It may be noticed that the kinetics of the reaction is partly dependent on temperature and crystallinity of ZHCH. For instance; at 100 °C, the samples exhibit diffraction peaks of unoxidised Zn when ZHCH peaks also appear. At the hydrothermal oxidation temperature of 110 °C, ZHCH phase vanishes in the XRD pattern and the electrodeposited Zn film is completely oxidized to ZnO. At further higher temperatures of 120 and 130 °C, both the un-oxidized zinc and ZHCH phase reappear. Furthermore, ZHCH exhibits higher crystallinity at these temperatures. It may be suggested that ZHCH with higher crystallinity covers the zinc surface better, providing a barrier layer to slow down its oxidation inspite of higher oxidation temperatures. Anyway the reaction kinetics seems to be faster at 110 °C in comparison with other temperatures employed in this work.

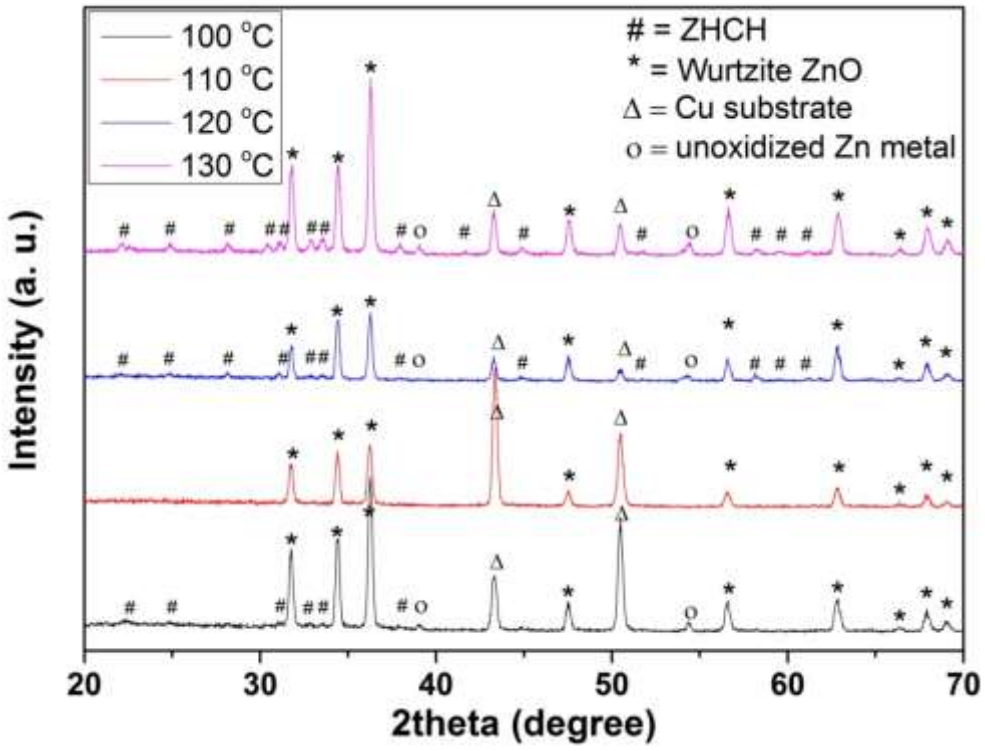

Figure 3-2 XRD patterns of ZnO nanostructures grown by hydrothermal oxidation of Zn film electrodeposited for 20 min.

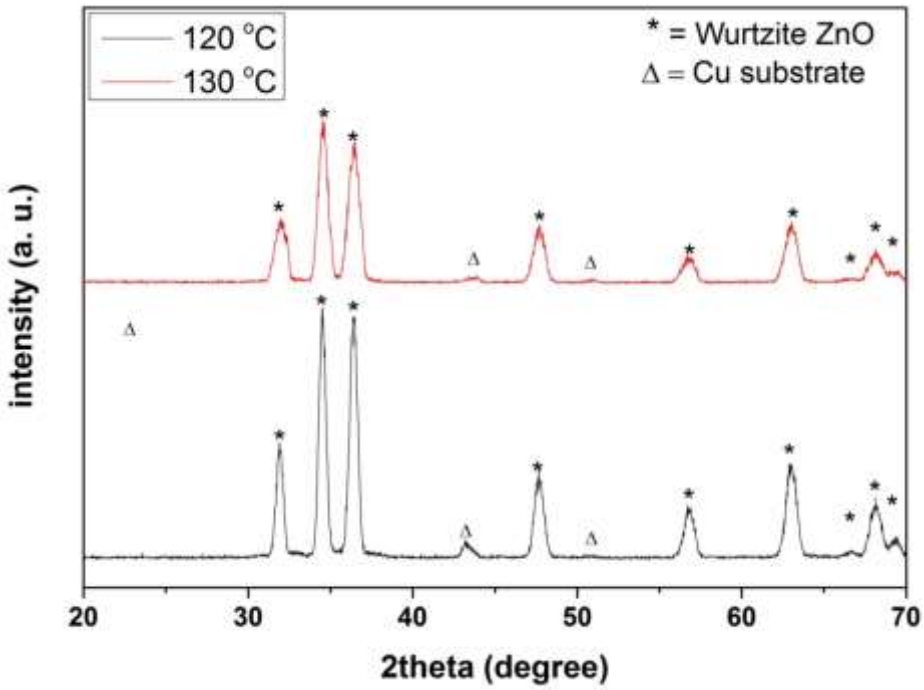

Figure 3-3 XRD patterns of ZnO nanostructures grown by hydrothermal oxidation of Zn films electrodeposited for 10 min

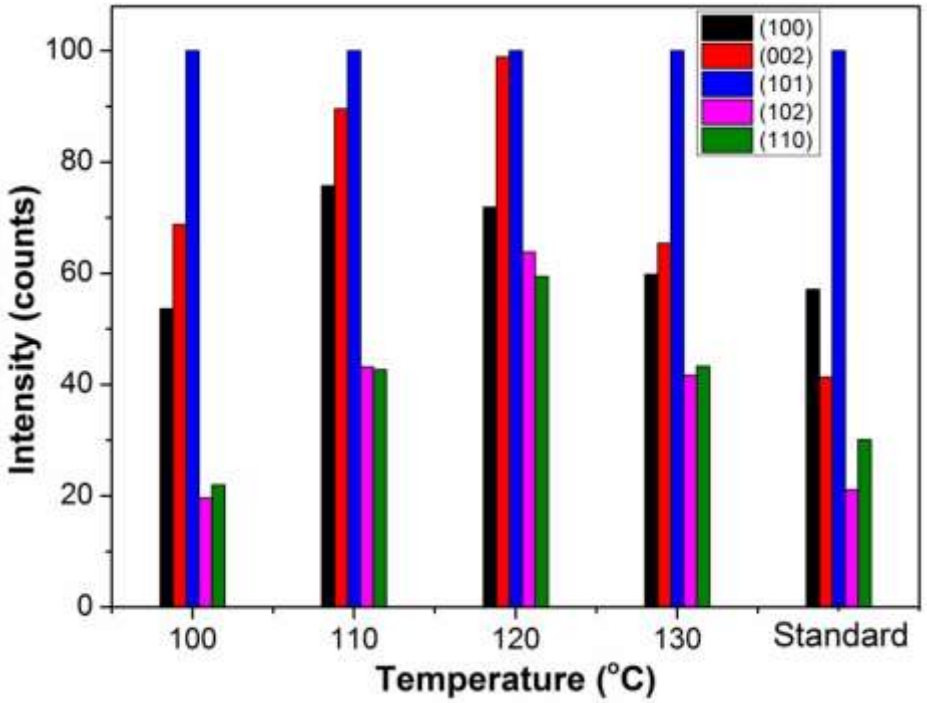

Figure 3-4 Intensity comparison of different XRD peaks of ZnO at different temperatures.

.

Fig. 4 compares the intensity of some of the XRD peaks of ZnO phase formed at different temperatures. For comparison, relative intensity of different XRD reflections in the standard powder data (pdf card 01-070-8070) has also been shown. In the standard data card, the (002) has lower intensity in comparison with (100) reflections; by contrast, our samples exhibit higher intensity of (002) as compared with (100) refection. This may be related with a general tendency of upward growth of ZnO nano-rods along c-axis. The highest relative intensity of (002) reflection is seen at the synthesis temperature of 120 ^{o}C. This is in agreement with the SEM observations showing the most pronounced upward alignment of nano-rods at this temperature. The changes in relative intensity of (002) reflection at other temperatures is also in agreement with the SEM observations.

Typical TEM images of ZnO nanostructures grown at different temperatures are shown in Fig. 5. The corresponding electron diffraction patterns are shown in the insets of the figure. From these diffraction patterns, the formation of wurtzite ZnO nanorods along c-axis is confirmed.

The low temperature (10 K) photoluminescence spectra of ZnO nanostructures grown hydrothermally at various temperatures are shown in Fig. 6. The PL measurement at low temperature isolates emission levels more clearly without suppressing (excluding) any emission just because of low measurement temperatures. The PL spectra of all the samples show strong band edge emissions in the ultra violet (UV) region except the sample prepared at 120 ^{o}C. On the other hand, green emissions (in the range 500 – 540 nm) which always appears in the case of samples prepared by wet chemistry is completely absent in our PL spectrum [25, 181-182]. This confirms excellent crystalline quality of wurtzite ZnO structures formed by hydrothermal oxidation of electrodeposited Zn films in NaCl solution. A zoom-in view at very low intensity scale (inset of Fig. 6) reveals the presence of very weak emissions in the violet and blue regions. These emissions are maximum for the sample prepared at 120 ^{o}C and minimum for the sample formed at 110 ^{o}C. The highest defect related emission intensity observed at 120 ^{o}C has a corresponding lowest UV emission intensity.

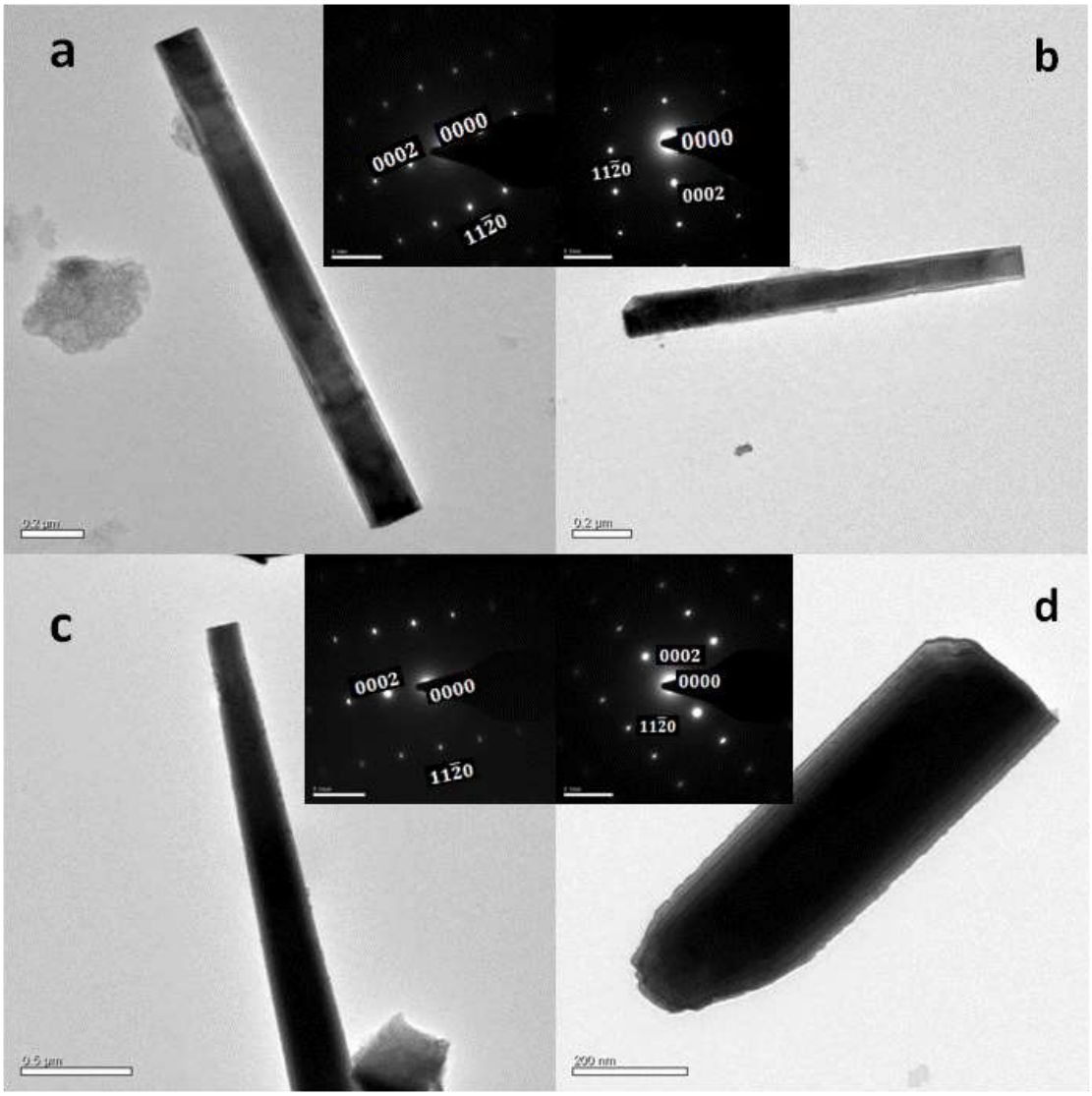

Figure 3-5 TEM images of ZnO nano-rods grown at 100 ºC (a), 110 ºC (b), 120 ºC (c) and 130 ºC (d). (Insets) In all SAED patterns the scale bar is equal to 5 nm-1.

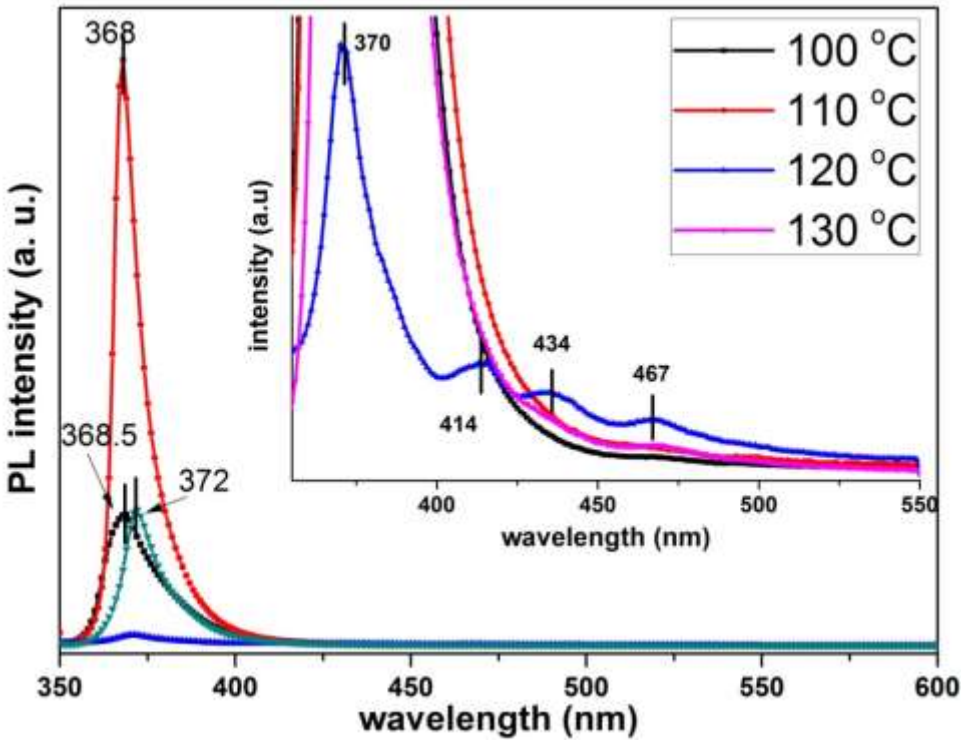

Figure 3-6 PL spectra of hydrothermally grown ZnO nanostructures taken at 10 K. Inset represents the magnified image of spectra.

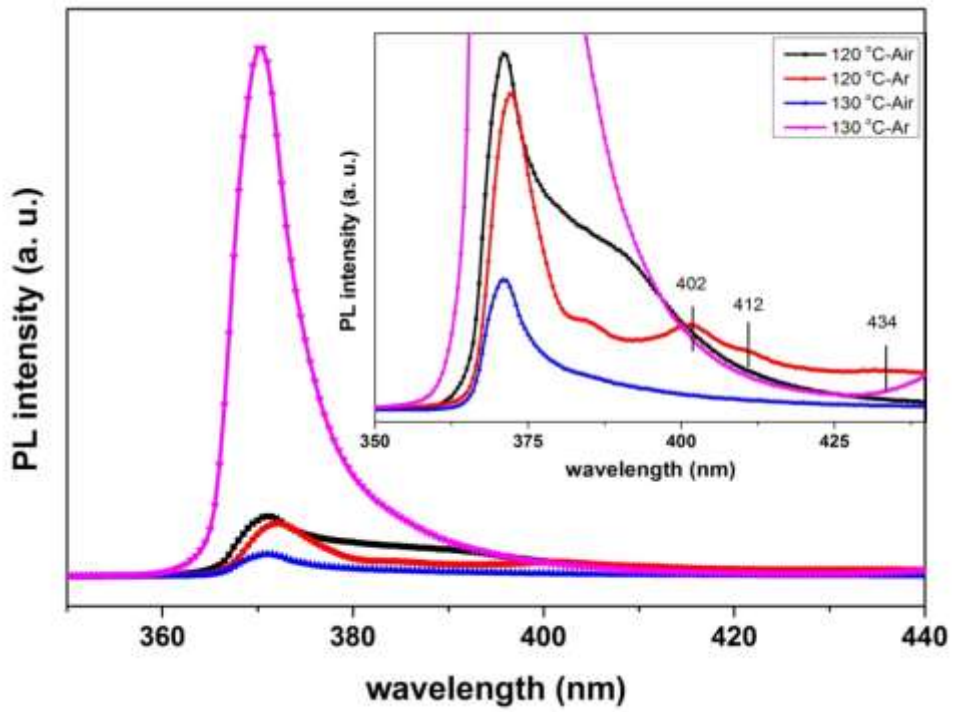

Figure 3-7 PL spectra (10 K) of ZnO nanostructures annealed at 500 °C. Inset represents the magnified image of the spectra.

The UV peak positions are 368.5, 368, 370 and 372 nm for the samples prepared at 100, 110, 120 and 130 ºC respectively. There is an obvious red shift in the UV peak position for the samples prepared at 120 and 130 ºC, as compared with the samples formed at 100 and 110 ºC. The shift of UV emission peak to lower energies could be attributed to the various factors including the size of ZnO nanostructures and electron hole exchange interactions at the surface of these nanostructures [183]. This red shift in the PL spectrum, according to the structural characteristics of ZnO, might be attributed to renormalization of bandgap by electron-hole plasma (EHP) process as a result of coulomb interactions among amplified free carriers at the band edge which leads to bandgap narrowing [184]. The EHP is produced due to the incident photon absorption by the electrons and holes in the conduction and valance band of the direct band gap semiconductors which are excited as a result of these photons having energy greater than the band gap energy of that semiconductor. The other possible reason of Red shift of UV peak in samples prepared at higher temperatures is due to donor (D) or acceptor (A) states which originates near the band minima and recombination between (A, e) or (D, h) causes the shifting of UV band to the higher wavelength. The exhibited red shift in energy for band-edge emission can also be emerged depending on the size and structure of the nanostructures.

There are three defect related emissions centres at 414, 434 and 467 nm with corresponding energies of 2.99, 2.85 and 2.65 eV, respectively. Lin et al [164] have reported the energy levels for intrinsic ZnO defects. Similarly, Kohan et al [185] have also calculate the energy of different emission levels in ZnO corresponding to various point defects that occur in the lattice. According to their calculations, zinc interstitial (Zn_i) being a shallow donor lies at level with energy 2.92 eV. Therefore, emission at 414 nm (~ 2.99 eV) (Fig. 5) is related to the defects that cause the violet emission and it can be ascribed to Zn_i. Two other emissions, violet at 434 nm (2.85 eV) and blue at 465 nm (2.66 eV) are also seen in the inset of Fig. 5. The origin of these two defect emissions is also possibly due to zinc interstitial. The difference in the energy seems to be due to the transition of electrons from the extended Zn_i states as discussed by the Zeng at al [156]. Varying atmospheric conditions or different oxidation states of these defects sites seem responsible for three emissions at different energies.

In order to confirm whether the defect emissions can be avoided by heat treatment, the samples prepared at 120 and 130 ºC were annealed in air and argon for

a period of about 2h at 500 °C, and PL was recorded, as shown in Fig. 7. It may be seen that violet emission seen in the as-prepared sample at 120 prevails after annealing in argon, although it almost vanishes after annealing in air. This supports the view that this defect emission is related with zinc interstitials. Sufficient supply of oxygen by air during annealing seems responsible for its recovery.

To further confirm the luminescent properties of ZnO structures, cathodoluminescence of selected areas was performed at ambient temperature. The accelerating voltage for incident electrons was 15kV, which is good enough for penetration into the ZnO upto a depth of about 300 nm, and thus photoluminescence excitation may not be limited to the surface regions of the nanowires. The collected CL images for all samples are shown in Fig. 8. It is evident from the CL images that UV emission is seen irrespective of the size and shape of ZnO nanostructures including nanorods and micro-tubes. The peak position of UV emission is slightly red-shifted and emission occurs at a broader range of wavelength for the cathodoluminescence in comparison with photoluminescence, which is primarily due to the difference in measurement temperature, as the cathodoluminescence was performed at ambient temperature. The emission from the inner sides of the micro-tubes (Fig. 8(d)) suggests that the inner surface of these micro-tubes exhibit similar (i.e. relatively defect free) structural characteristics as that of outer surfaces. The CL spectra corresponding to the ZnO structures shown above are plotted in Fig. 9. There is no sign of green emissions in the CL spectra as well. Red shift in UV emission for the sample prepared at 130 ºC is also evident which is in agreement with PL study.

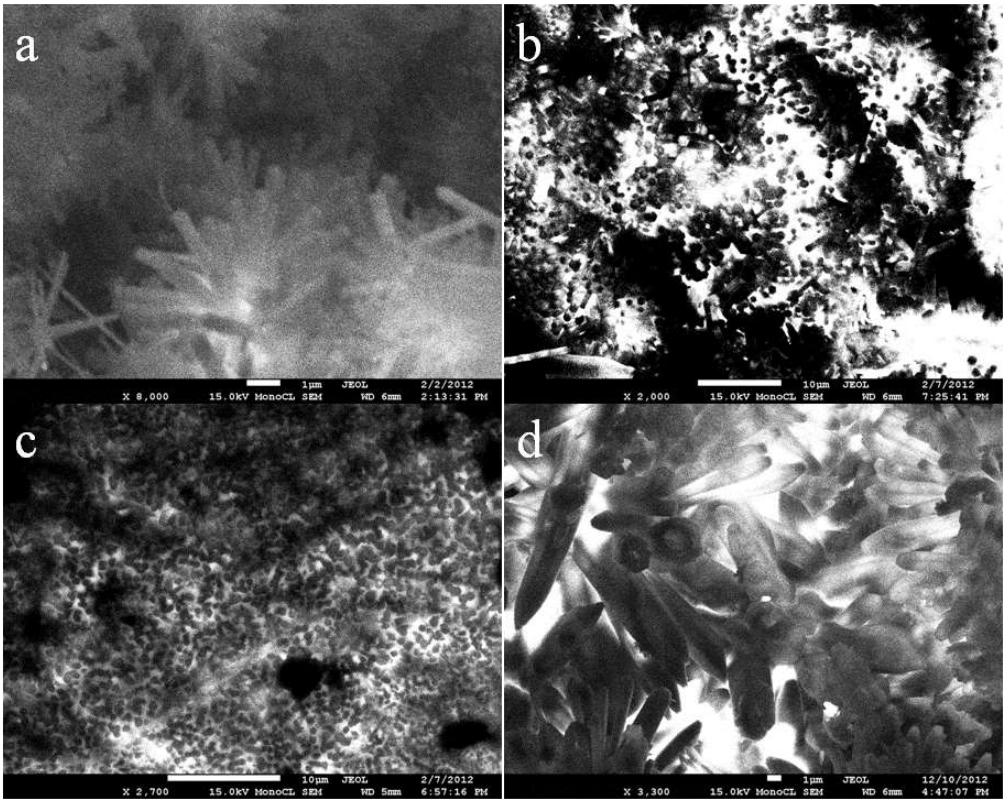

Figure 3-8 Selected area CL images of ZnO nanostructures grown at temperatures 100 ºC (a), 110 ºC (b), 120 ºC (c) and 130 ºC (d).

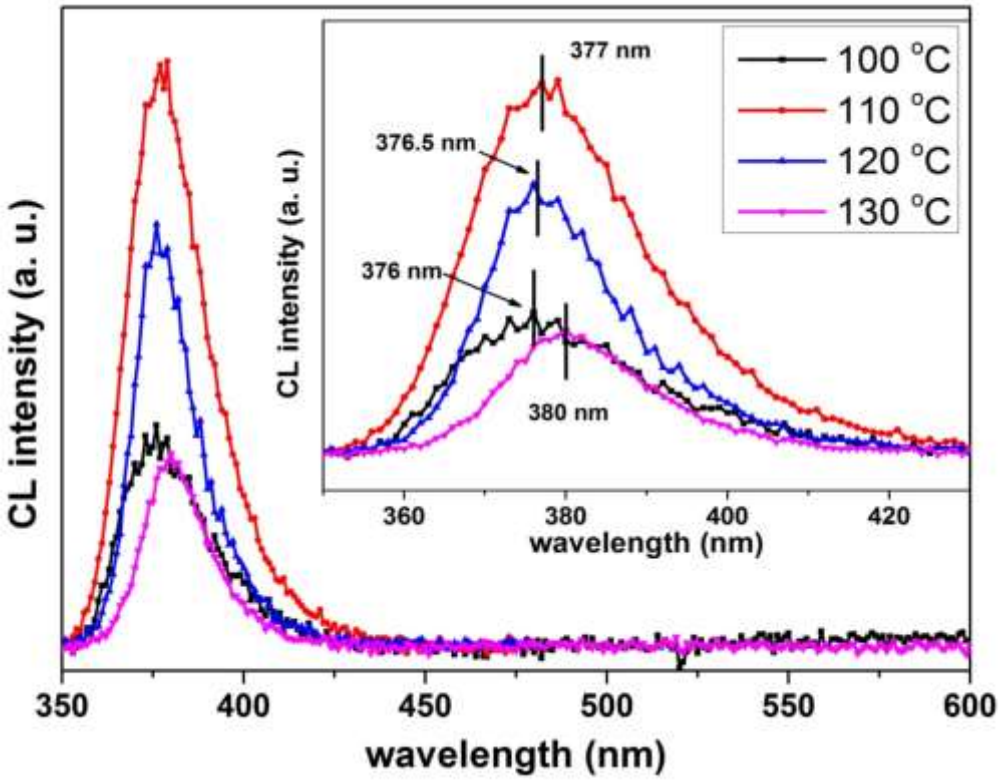

Figure 3-9 Cathodoluminescence spectra of different ZnO nanostructures shown in Fig. 8.

3.3 Conclusions:

The highly crystalline ZnO nano and micro-structures are formed as a result of two-step synthesis approach. This method consists of electrodeposition of zinc followed by hydrothermal oxidation in NaCl solution at temperatures ranging from 100 to 130 ºC. The morphology and nanostructures is found to be temperature dependent. With the increase in temperature, the diameter of nanorods increases from 0.1-0.75 μm at 100 ºC, to 3.2 μm at 130 ºC. The rod-like morphology is mostly converted to micro tubes at 130 ºC. The top of the nanorods are flat at lower temperatures and become conical at higher temperatures. The wall thicknesses of micro tubes are 0.9 μm and are found to be independent of the tube diameter. Zinc hydroxyl chloride hydride is also formed during hydrothermal oxidation of Zn film which gets more crystalline at higher temperatures and restricts the complete oxidation of electrodeposited Zn film. The ZHCH along with unoxidised Zn in the samples affect the luminescent properties of ZnO nanostructures. The luminescence properties also provide the evidence of lower crystal defects and showed very strong UV emission peaks but the green luminescences were absent completely. The violet and blue emissions were found to be dependent on the amount of unoxidised Zn. It provides the excess Zn to be present at the interstitial positions and exhibit minimum intensity where Zn film is completely oxidized to ZnO. The removal of green luminescence and reduction of other defect related emission makes these nanostructures suitable for UV photonic applications.

4 Ni-doped ZnO Nanostructures

Functional nanomaterials exhibiting interesting optical, electrical and magnetic properties have recently gained huge interest of the researchers because of novel properties related with nano-scale dimensions and large surface area. ZnO nanostructures are interesting for their exceptional physical properties, e.g., high electrical conductivity, transparent nature, photoluminescence in ultra-violet and visible region, etc., in addition to ability to form various morphologies [22, 33, 38, 186].

ZnO nanostructures are synthesized by a diverse range of techniques including chemical vapour deposition [187-189], vapour transport [190-191], thermal oxidation [101], vapour-liquid-solid growth [192-193], precipitation [102], sol gel [194] and hydrothermal processes [195], etc. Variation in synthesis parameters affects the crystallinity and optical properties of ZnO nanostructures [43, 168, 186]. Nevertheless, defect-free ZnO nanostructures are very difficult to form as photoluminescence spectra almost always exhibit defect-related emissions in the PL spectra [49, 168, 186, 196-197]. Some degree of control is however exercised by post heat treatments in highly controlled atmospheres [198].

Doping of transition metals in ZnO nanostructures is of considerable interest. Nickel is considered to be the most efficient transition metal dopant due to its exceptional chemical stability and ability to tune electrical, optical and magnetic behaviour of ZnO nanostructures [84]. Nickel has been successfully doped up to about 5% in wurtzite ZnO nanostructures by co-precipitation [84, 86, 102, 194]. At 10% and higher nickel content in the sample, segregation of some nickel to form NiO has been seen inevitable.

As reported in chapter 3, ZnO nano-structures have been by hydrothermal oxidation of electrodeposited zinc in NaCl solution. The structures exhibited interesting optical properties. For instance, green emission was almost absent, although prominent blue emission was seen in some cases, with strong UV emission.

In the present chapter, un-doped and heavily Ni-doped ZnO nanostructures have been formed by hydrothermal oxidation of electrodeposited Zn and Zn-Ni alloys. Comparative study of hydrothermal oxidation in water and in NaCl solution has been performed. Particular emphasis has been laid on the structural and morphological changes and photoluminescence properties of ZnO nanostructures as a function of oxidation environment and nickel doping.

4.1 Experimental:

Analytical grade $ZnCl_2$, $NiCl_2.6H_2O$ and Boric Acid were used for electrodeposition bath. The pH of the bath was 3.6±0.1 (measured by pH meter Model PH 330/SET – 0, 82362 WTW, Germany). Electro-deposition of metal and alloy films was performed (on copper substrate) at a constant current density of 350 $A.m^{-2}$ for a period of 10 min using Potentiostat/Galvanostat AMEL Model-2051. Other details can be seen elsewhere [199].

Electrodeposited Zn and Zn-Ni films were immersed in 70 ml of pure water or 3.5% NaCl solution in a Teflon-lined Stainless Steel (SS) autoclave. The autoclave was then placed in an electric oven (Heraeus vacutherm VT 6130P). The temperature of the oven was slowly increased to 100 ^oC, which was maintained for a period of 24 h followed by slow cooling to room temperature. The sample was then removed from the autoclave and thoroughly washed with distilled water.

X-ray diffraction (XRD) was performed by Bruker D8 Discover diffractometer with Cu Kα radiations. Scanning electron microscopy (SEM) and compositional analysis were performed by using Field Emission Scanning Electron Microscope (FEI Nova NanoSEM 430) equipped with EDX system (EDAX). High resolution transmission electron microscopy (HRTEM) was performed by FEI Technai G2 20 Scanning TEM. Photoluminescence (PL) spectra were obtained at Room temperature (RT) and 10 K using 325 nm He-Cd laser line (Melles Griot Series 56) at 15 mW.

4.2 Results and Discussion:

Figure 4-1 and 4-2 show SEM images of zinc and zinc-nickel alloy films electrodeposited on copper substrate in various chloride baths at a current density of 350 $A.m^{-2}$. Composition of these alloy films, as determined by EDX analysis, is shown in Table 1. Percentage refers to atomic percent in this manuscript. It has been reported by our group that the concentration of zinc and nickel chlorides in the bath has pronounced effect on the composition and morphology of alloy deposits, although the deposits remain rich in zinc due to anomalous co-deposition [199].

Table 4-1 Composition of precursor solution for electrodeposition and resulting Ni contents in deposited alloy films.

Sr.No	$ZnCl_2$ in sol. (g/L)	$NiCl_2.6H_2O$ in sol. (g/L)	Ni contents in alloy (at %)
1	200	0	0
2	200	50	7
3	200	200	12
4	50	200	17

Figure 4-3 shows XRD patterns of ZnO nanostructures formed by hydrothermal oxidation of zinc and zinc-nickel alloy films in pure water and NaCl solution. After hydrothermal oxidation, wurtzite ZnO is formed. The electrodeposited alloy film is almost completely oxidized in NaCl solution (Fig. 4-3(a & b) and 4-4(a)), except for the alloy containing 17 % Ni (Fig. 4-4(b)). In pure water, metal film is completely oxidized to ZnO (Fig. 4-3(a)); XRD patterns for alloy films indicate some un-consumed alloy phase (Ni_2Zn_{11}) (Fig.4-3(a) and 4-4(a & b)). The oxide layer formed on the alloy deposits seems to passivate the underlying metal / alloy and resist further oxidation in water. In NaCl solution, chloride ions accelerate the oxidation due to which the alloy films are mostly consumed to form ZnO nanostructures.

It may be seen in the XRD patterns (Figs. 4-3 & 4) that FWHM of (002) peak of wurtzite ZnO formed in NaCl solution is smaller than that in pure water, which suggests an improved crystallinity or lower growth (residual) stresses for ZnO nanostructures formed in the former than in the latter oxidizing medium.

It may be interesting to mention that multiple peaks of ZnO are seen in XRD patterns. As will be shown later, the samples are composed of ZnO single crystal nanorods that grow along c-axis, but radiating from the surface in different directions with respect to sample's surface (i.e., not normal to the surface alone). As the foot print of X-ray beam on the sample is about 1 mm wide and about 10 mm high, XRD response corresponds to large number of rods; a small fraction of which should contribute to one XRD peaks, while some others should contribute to another peak, depending on their orientation in the diffraction geometry.

As shown in Fig. 4-5(a), the oxidation of electrodeposited zinc film in water results in the formation of nanorods with diameters in the range of 45 to 150 nm. Figure 4-5(b) represents the nanorods formed by the oxidation of 200-50 zinc-nickel alloy sample containing 7% nickel. The diameter of most of the nanorods lies in the range of 40 to 100 nm, although some rods with a diameter of up to 180 nm are also seen. In comparison with Fig. 4-5(a), the top ends of these nanorods give relatively rough appearance. With further rise in the Ni content of the precursor alloy film to 12% and 17%, the rod diameter decreases significantly, as shown in Fig. 4-6(a) and (b), respectively. Particularly for the sample prepared by oxidation of 17% Ni alloy film; very thin nanorods are formed with a diameter lying mostly below 50 nm, except for some longer and thicker nanorods with a diameter of above 100 nm. The primary reason for the decrease in the rod diameter with increase in nickel content of the precursor alloy may be the higher level of nickel doping in the ZnO nanorods. The surface appearance of the nanorods also depends on nickel content. For instance, Fig. 4-5(a) and (b) reveal relatively rougher surfaces of the nanorods; while more well-defined hexagonal shape with sharper edges and smoother faces are seen in case of the samples containing higher nickel content, as shown in Fig. 4-6(a) and (b).

Figures 4-7 and 4-8 show SEM images of the electrodeposited zinc metal and zinc-nickel alloy films oxidized in 3.5% NaCl solution at 100 ºC. It may be noticed that the number density of rods, in general, increases as compared with oxidation in

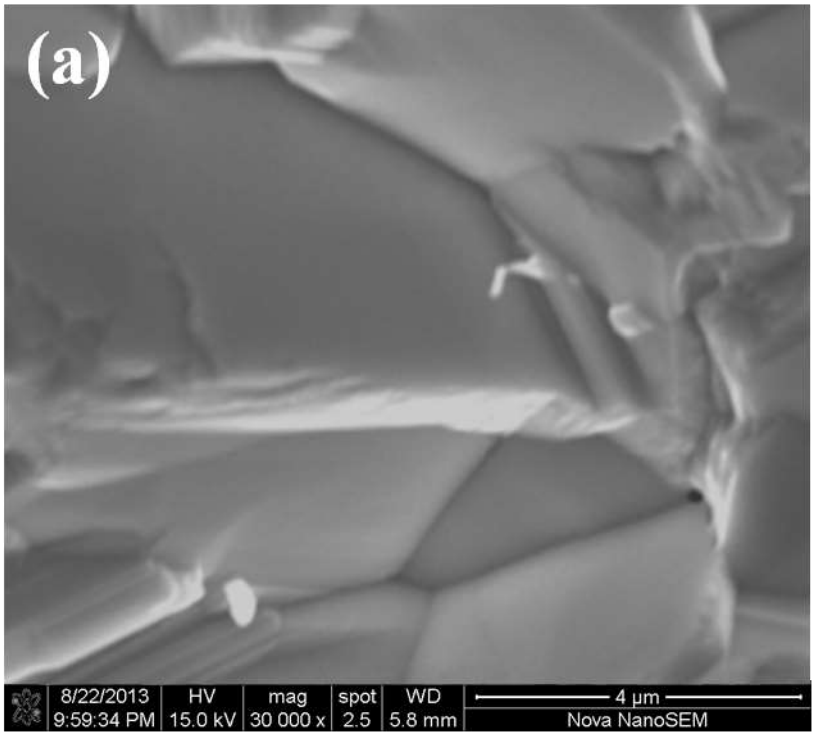

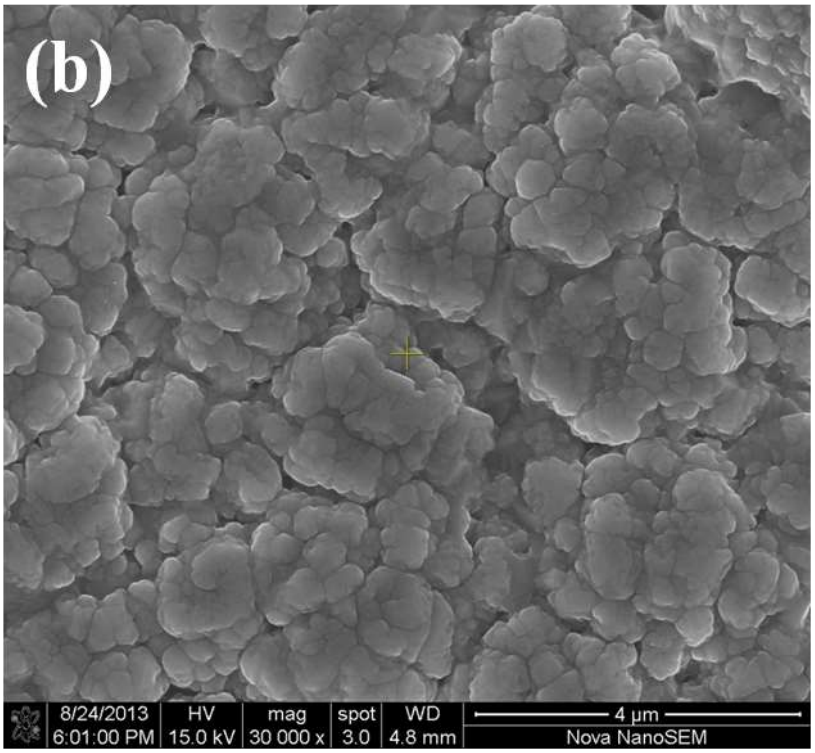

Figure 4-1 SEM images of the electrodeposited films; (a) Zn, (b) Zn-7%Ni. (Percentage of nickel is in atomic percent.)

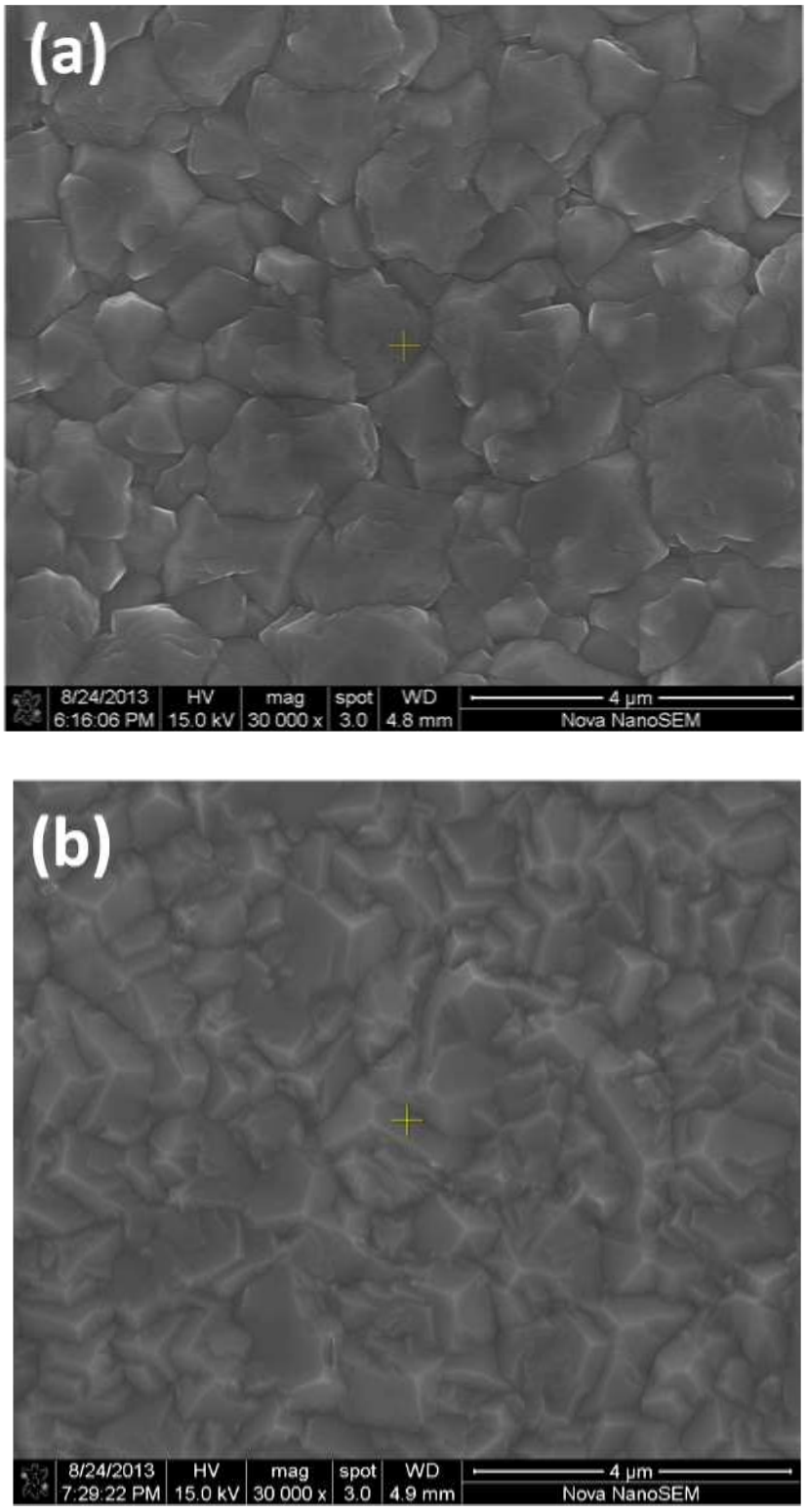

Figure 4-2 SEM images of the electrodeposited films; (a) Zn-12%Ni, (b) Zn-17%Ni. (Percentage of nickel is in atomic percent.)

pure water. When compared with Fig. 4-6(a, b) for oxidation of the alloy containing 12-17% Ni in water, Fig. 6-8(a, b) reveal the formation of considerably thinner nanorods in NaCl solution. It may be noted in Fig. 6-8(b) that the diameter of most of the nanorods lies in the range of 20-50 nm.

Comparing the corresponding images in Figs. 4-5, 6, 7 & 8, for both the metal and alloy films, better well-defined / undamaged hexagonal structures are observed when oxidized in NaCl solution than in pure water. Chloride ions in the solution may partly influence growth kinetics by increasing the oxidation rate of zinc and its alloys and providing enhanced flux of the cations to the growth interface. Chloride ions are also known to form zinc hydroxyl-chloride [180, 200]. It has been seen in [201] by the present authors that zinc hydroxyl-chloride is formed as an intermediate product in chloride solution. Naturally the nature of intermediate product must somehow affect the quality and appearance of the final product, i.e., the wurtzite ZnO nanostructures. Another possibility is that the chloride ions adsorbed at the growing end, i.e., c-plane, affect its polarity / surface reconstruction. This might influence the growth kinetics of ZnO nanostructures with improved diffusivity of the cations and anions at the growth surface and thus forming relatively defect-free and compact nanostructures with smoother morphological appearances. The presence of chloride ions has also facilitated the formation of relatively thinner nanorods. This may be either due to larger nucleation density, for chloride ion attack on the metal / alloy surface generating high flux of zinc cations, or due to adsorption of chloride ions at the surface restricting the growth along prismatic (side) planes.

Figure 4-9 shows the typical EDX patterns of Ni-Zn alloy coating with 17 at% Ni and the corresponding ZnO nanostructures formed by the oxidation of these alloys in water and NaCl solution. These patterns exhibit the incorporation of Ni dopant in ZnO nanostructures. A comparison of dopant's content in the oxide nanostructures with the precursor alloy film has been shown in Figure 4-10. It may be seen that mostly the nickel content of the oxidized sample remains close to that of the precursor alloy film (Percentage of doped nickel refers to $\frac{\text{Ni}}{\text{Ni+Zn}}$ x 100, as determined by EDX analysis). Ni composition in the ZnO nanostructures has been determined by EDS measurements.

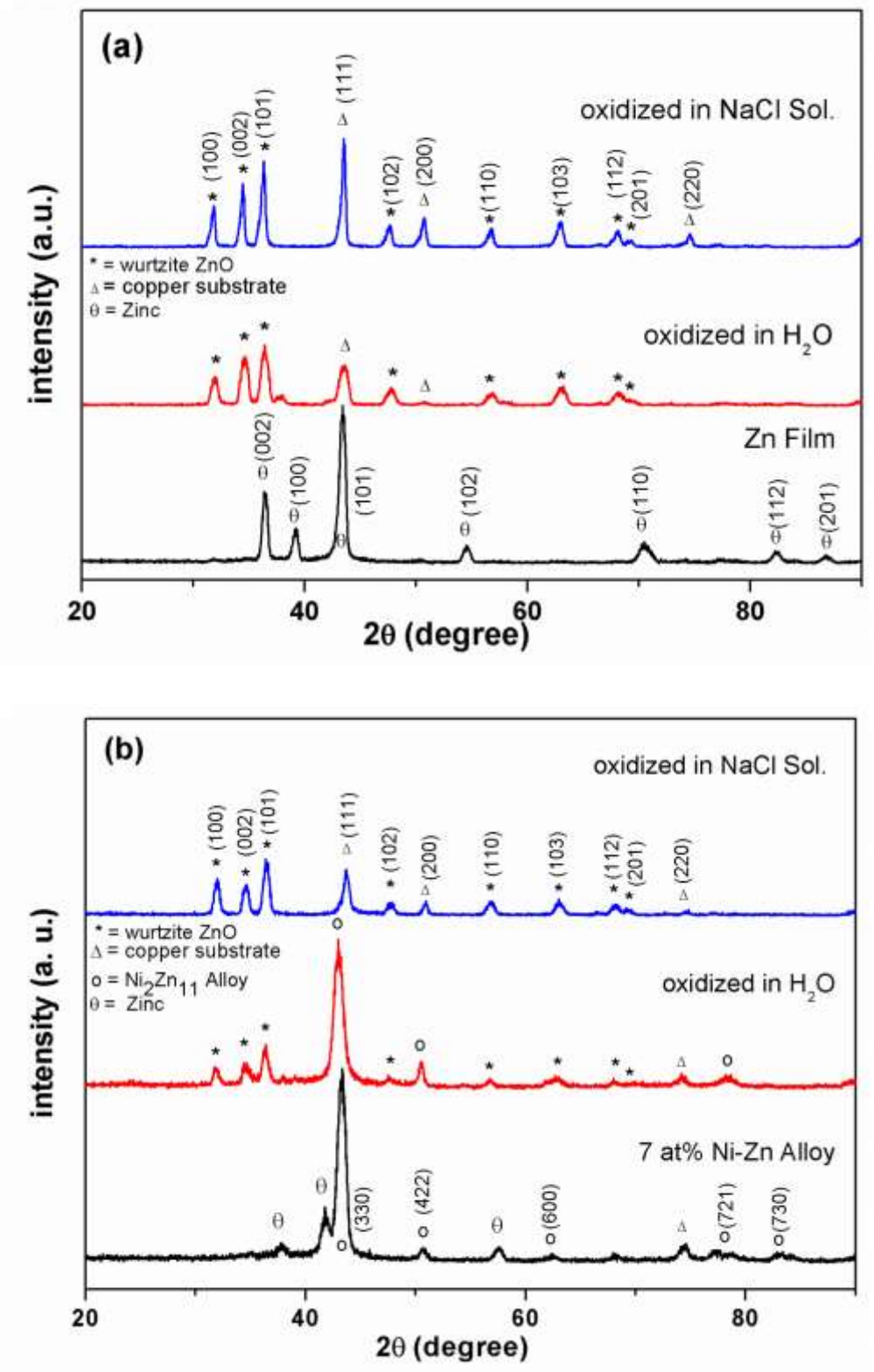

Figure 4-3 XRD patterns of electrodeposited metal and alloy films before and after oxidation in water and 3.5% NaCl at 100 ºC; (a) Zn, (b) Zn-7% Ni

.

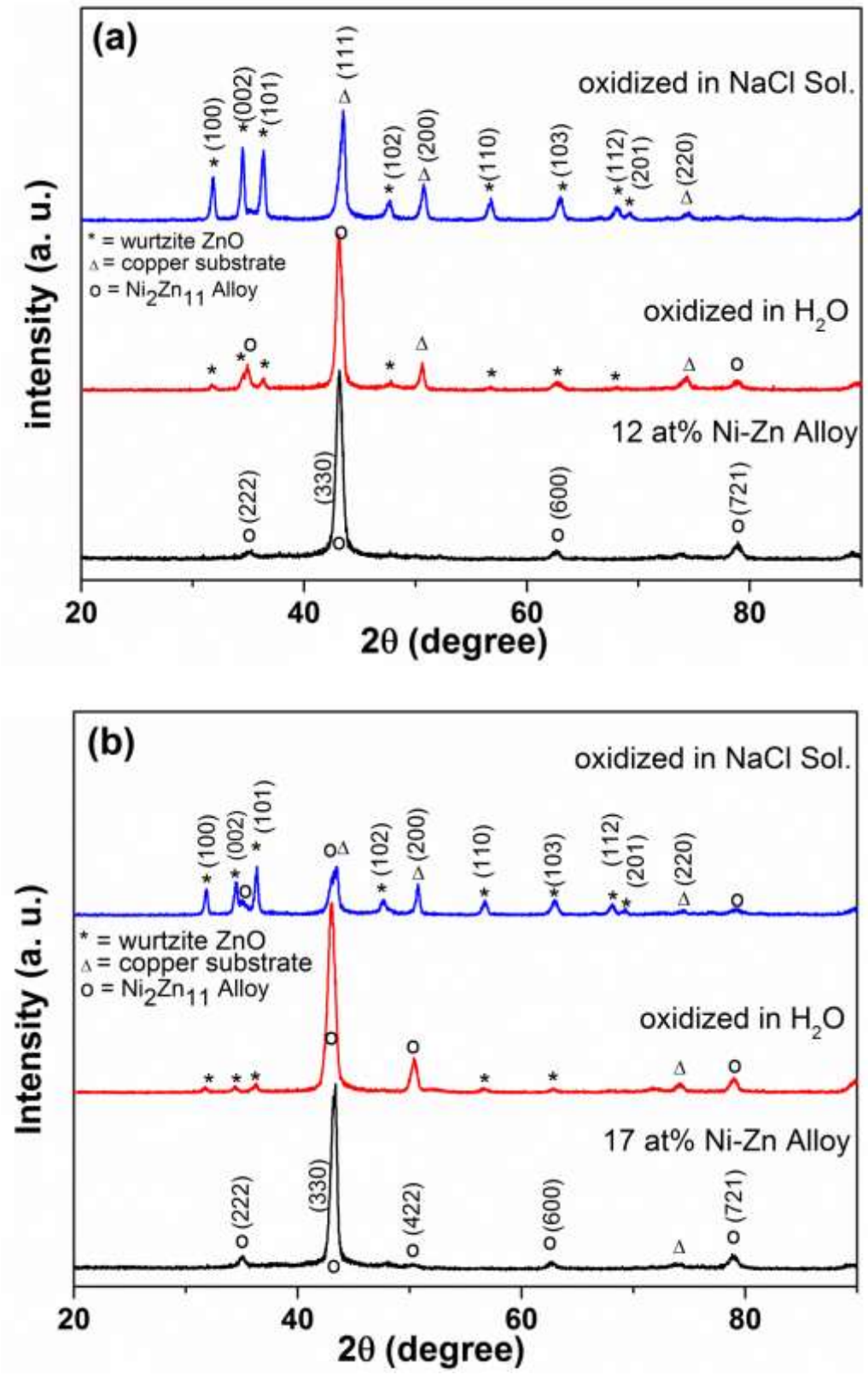

Figure 4-4 XRD patterns of electrodeposited metal and alloy films before and after oxidation in water and 3.5% NaCl at 100 ºC; (c) Zn-12% Ni, (d) Zn-17% Ni

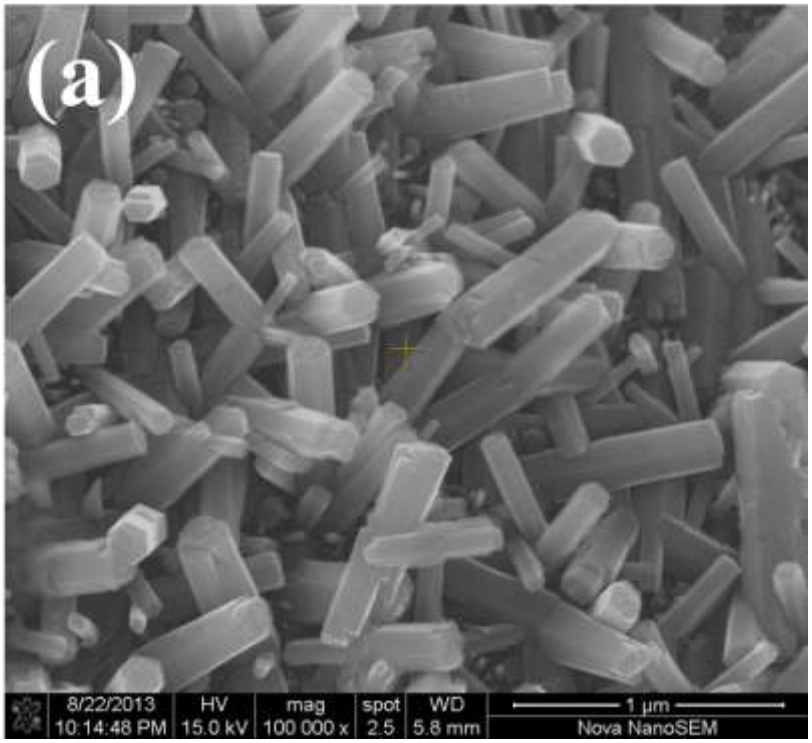

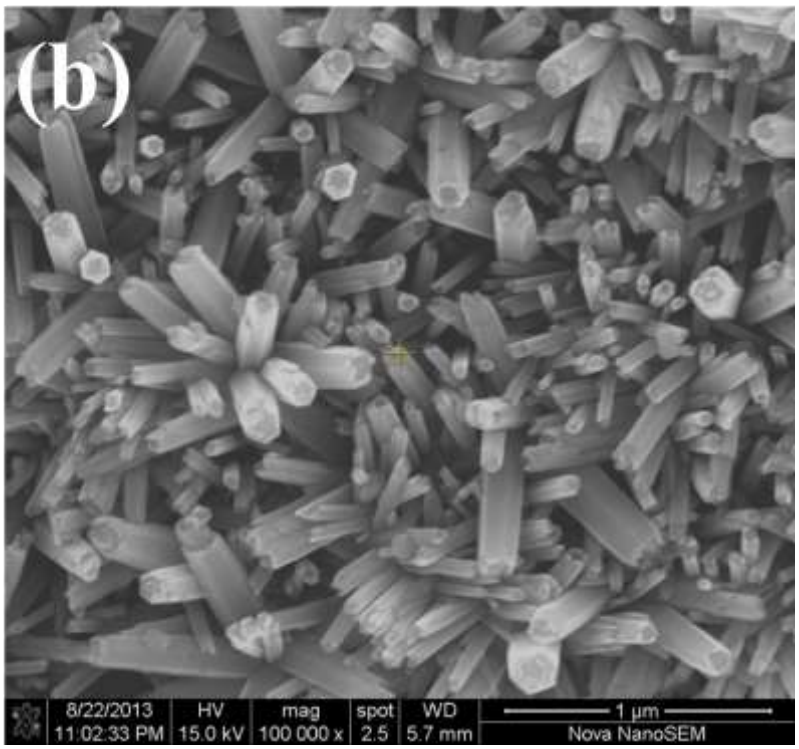

Figure 4-5 SEM images of the ZnO nanorods formed by the hydrothermal oxidation of electrodeposited films in pure water t 100 ºC; (a) Zn, (b) Zn-7%Ni.

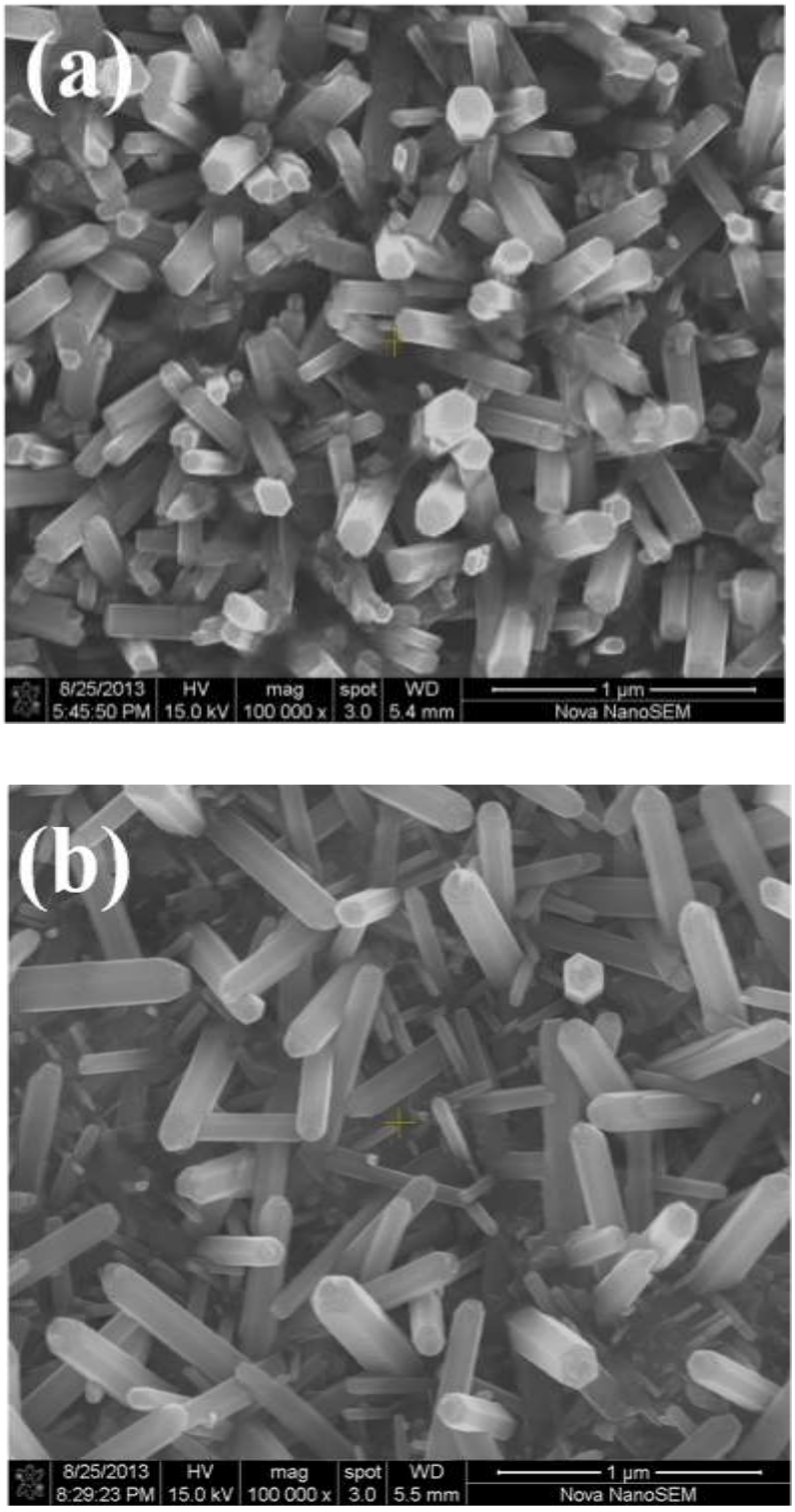

Figure 4-6 SEM images of the ZnO nanorods formed by the hydrothermal oxidation of electrodeposited films in pure water at 100 ºC; (a) Zn-12%Ni, (b) Zn-17%Ni.

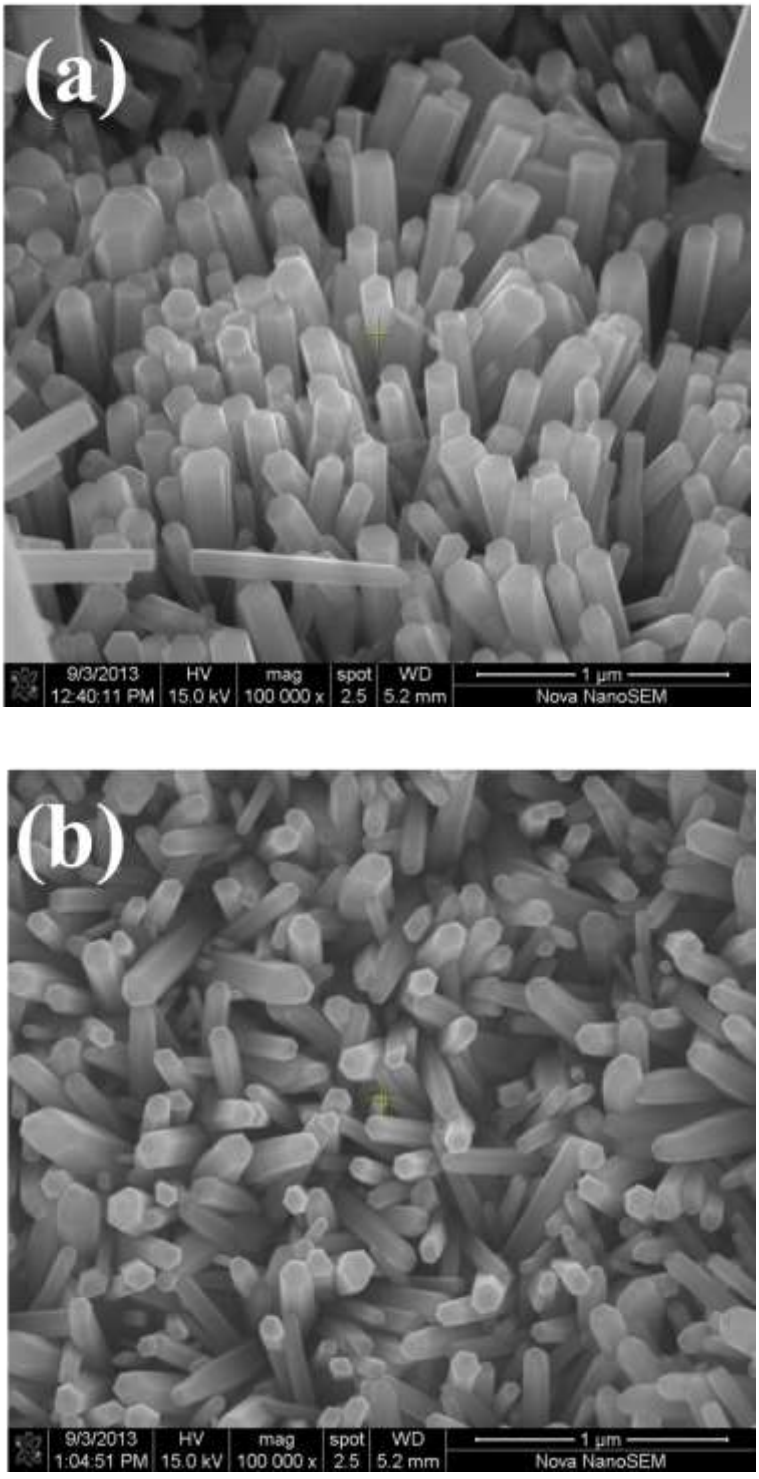

Figure 4-7 SEM images of the ZnO nanorods formed by the hydrothermal oxidation of electrodeposited films in NaCl solution at 100 ºC; (a) Zn, (b) Zn-7%Ni.

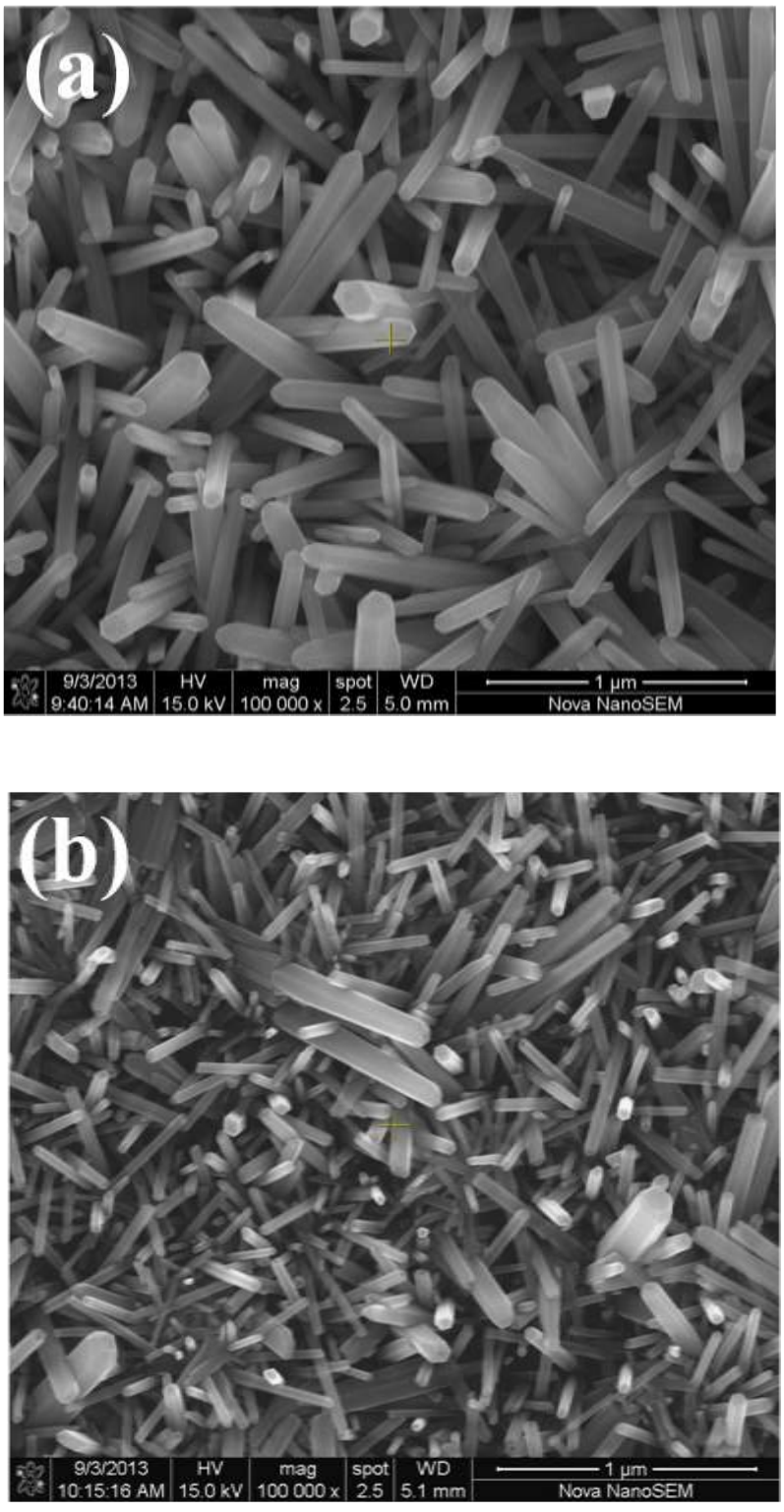

Figure 4-8 SEM images of the ZnO nanorods formed by the hydrothermal oxidation of electrodeposited films in NaCl solution at 100 ºC; (a) Zn-12%Ni, (b) Zn-17%Ni.

This is one of the best techniques for measurement in the solid state. If measured by more accurate elemental analysis (wet techniques) techniques, analysis of isolated ZnO is not possible; due to which one was never sure if the analyzed sample is really ZnO or not.

The point whether EDS is good enough for elemental analysis or not, it is true that it cannot provides the quantitative analysis of lighter elements (Z<11), but for higher elements credibility of results mostly depends on the homogeneity of the samples under test. If the samples are not homogenous, discrepancy between results should be expected in the first place.

For the detection of Nickel (Z=28) in ZnO nanostructures multiple step analysis have been done e.g., in electrodeposited alloy coating before oxidation and then in Ni-doped ZnO nanostructures after hydrothermal oxidation. The concentration of Ni doping has reported after confirming the results for several experiments.

Figure 4-11(a) and (c) represents typical TEM images of ZnO nanorods prepared by oxidation of alloy film containing 17%Ni in water and NaCl solution, respectively, along with selected Area electron diffraction patterns. Single crystalline nature of ZnO nanorods is obviated by electron diffraction patterns. Typical HRTEM images of are also shown in Fig. 4-11(b) and (d) The measured inter-planer distance (0.52 nm) matches well with (0001) plane in wurtzite ZnO indicating the growth of nanorods along the [0001] direction [202-204]. The electron diffraction patterns clearly reveal that growth of ZnO nanorods takes place along c-axis. The formation of any other phases and shapes has not been revealed by TEM including electron diffraction. Clusters of any other phases in the nanorods have also not been seen by HRTEM.

It has often been reported in literature that attempts to form highly doped ZnO nanostructures mostly fail due to segregation of the dopant to form additional oxides. Mostly these attempts have relied on the use of mixed precursor solutions for co-precipitation. Under these conditions, nucleation of the, otherwise, dopant's oxide cannot be avoided due to its large supersaturation. In our technique, up to 17% nickel has been doped in ZnO nanostructures without the formation of any other oxide phase.

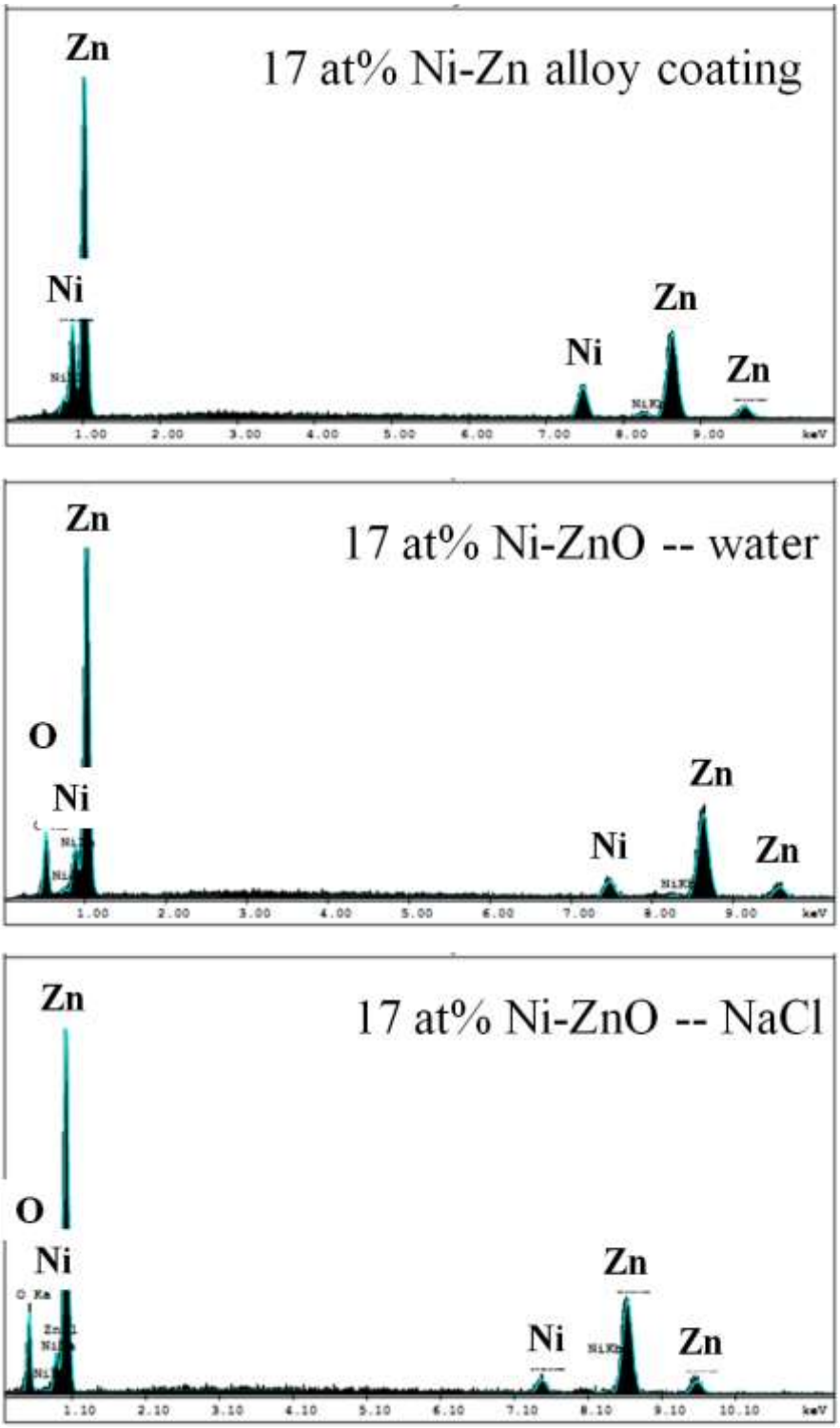

Figure 4-9 EDX of 17% Ni-doped ZnO samples.

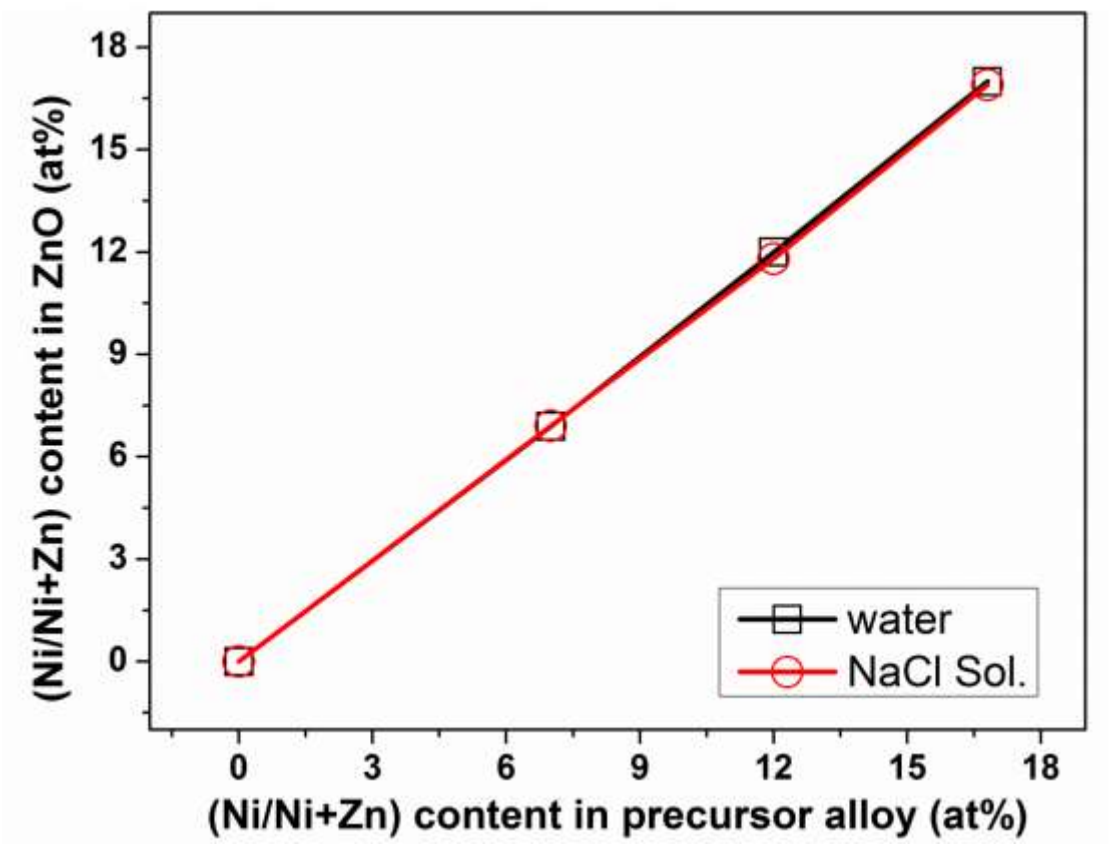

Figure 4-10 Comparison of Nickel contents in the oxide nanostructures and precursor alloy films.

In fact, the precursor alloy oxidizes gradually / slowly due to some degree of protectiveness provided by the overlying oxide layer that passivates the alloy surface, due to which the cations are formed at the metal-oxide interface or the defects in the passive oxide layer. Accordingly, the slowly formed cations of the dopant (nickel) join the ZnO nanostructures without forming its own oxide.

Typical photoluminescence (PL) spectra of the doped and un-doped ZnO nanostructures formed by the hydrothermal oxidation of the electrodeposited films are shown in Fig. 4-12 & 13. Substantial excitonic band edge emission in the ultra violet (UV) region is seen irrespective of the oxidizing conditions and nickel content in the nanostructures. The UV emission is observed at a narrower range of wavelength at 10 K than at room temperature, due to sharpening of the band edges at low temperatures.

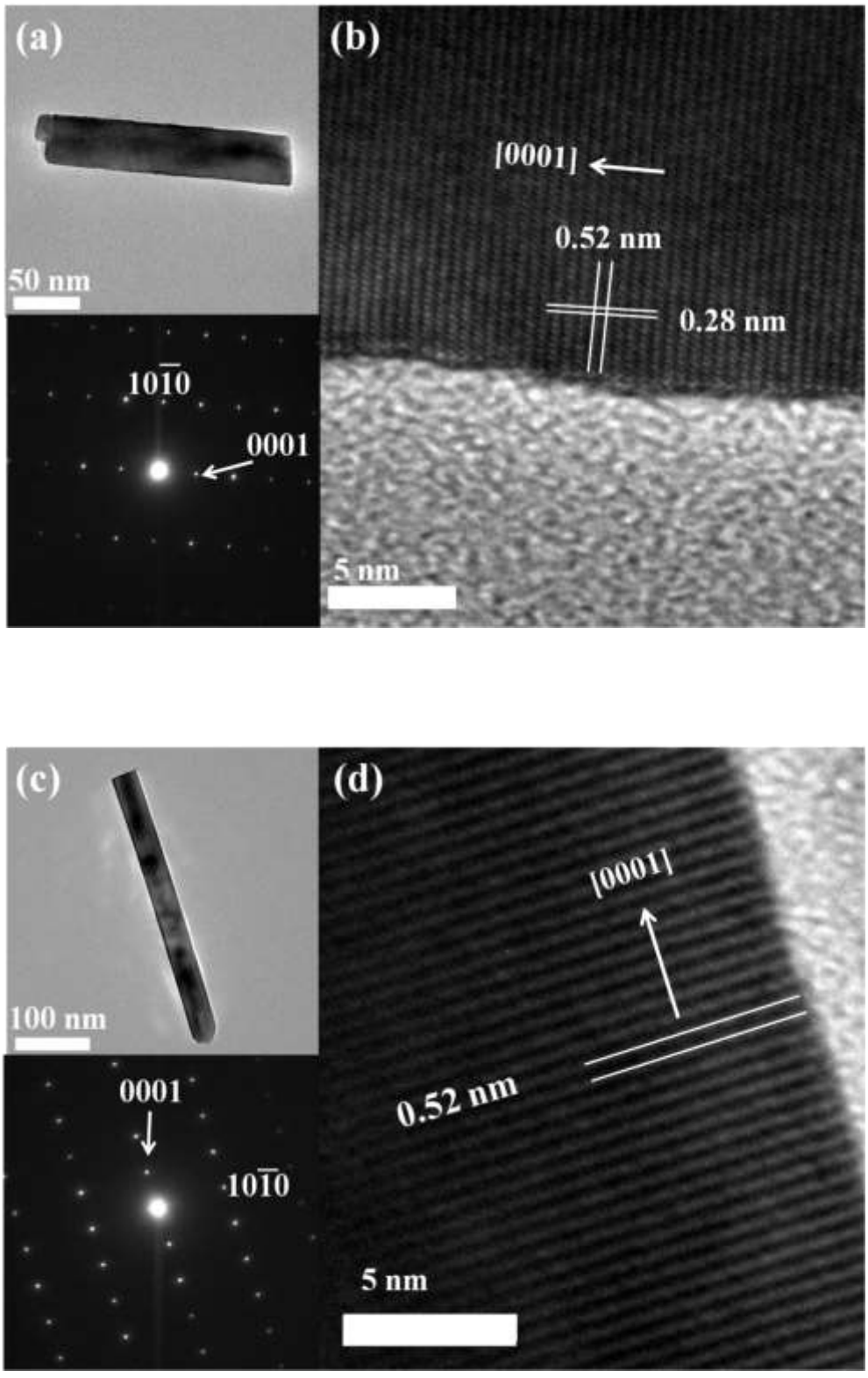

Figure 4-11 TEM images of 17% Ni doped ZnO nanorods grown by the oxidation in water (a) and NaCl solution (c). The corresponding HRTEM images and SAED pattern are also shown in (b) and (d), respectively.

At 10 K, the nanostructures formed in NaCl solution exhibit relatively sharper UV emission in comparison with nanostructures formed in pure water. This may be attributable to higher crystalline quality of the oxide nanostructures formed in NaCl solution.

Optical band gap has been determined from the peak position of the UV emission, as shown in Fig. 4-14. The optical band gap exhibits a blue shift with nickel doping, which is in agreement with literature [194, 205-206]. Such a blue shift in heavily-doped n-type structures (including Ni-doped ZnO) has been explained by Moss-Burstein band filling effect [194, 207-208]. The optical band gap measured at 10 K is slightly lower for the samples prepared in NaCl solution than in pure water. This may partly be due to adsorbed chloride ions. At room temperature the optical band gap does not appreciably depend on nickel content as well as on the oxidizing conditions, due to pronounced thermal affects that predominate the overall response. The band gap values of the Ni-doped ZnO nanostructures have generally shown a blue shift with increase in the Ni doping, both in case of water and NaCl oxidation synthesis. There is no justification for higher bandgap value for this one sample (12% Ni doped ZnO/oxidized in water). However, the difference is minor and can be due to experimental limitations / errors.

The reason for the changes in UV peak intensity with composition is not clear. In general, it may depend on absorption efficiency for the incident radiation, thickness (volume) of the absorbing medium, as well as the alternative transitions at lower energy levels, apart from orientation / alignment of the sample with the incident beam. Anyway, it is clear that defect emission in the visible region is affected by nickel addition and by oxidizing medium. It may be noted that emission in the visible region, clearly seen in the un-doped ZnO nanostructures, becomes almost negligible for the doped ZnO samples prepared in water. More interestingly, the visible emission vanishes both for the doped and un-doped ZnO samples prepared in NaCl solution. This may partly be due to high crystalline quality of ZnO nanostructures formed in NaCl solution, owing to the formation of an intermediate Zinc hydroxyl-chloride at the ZnO-Zn interface (chapter 3).

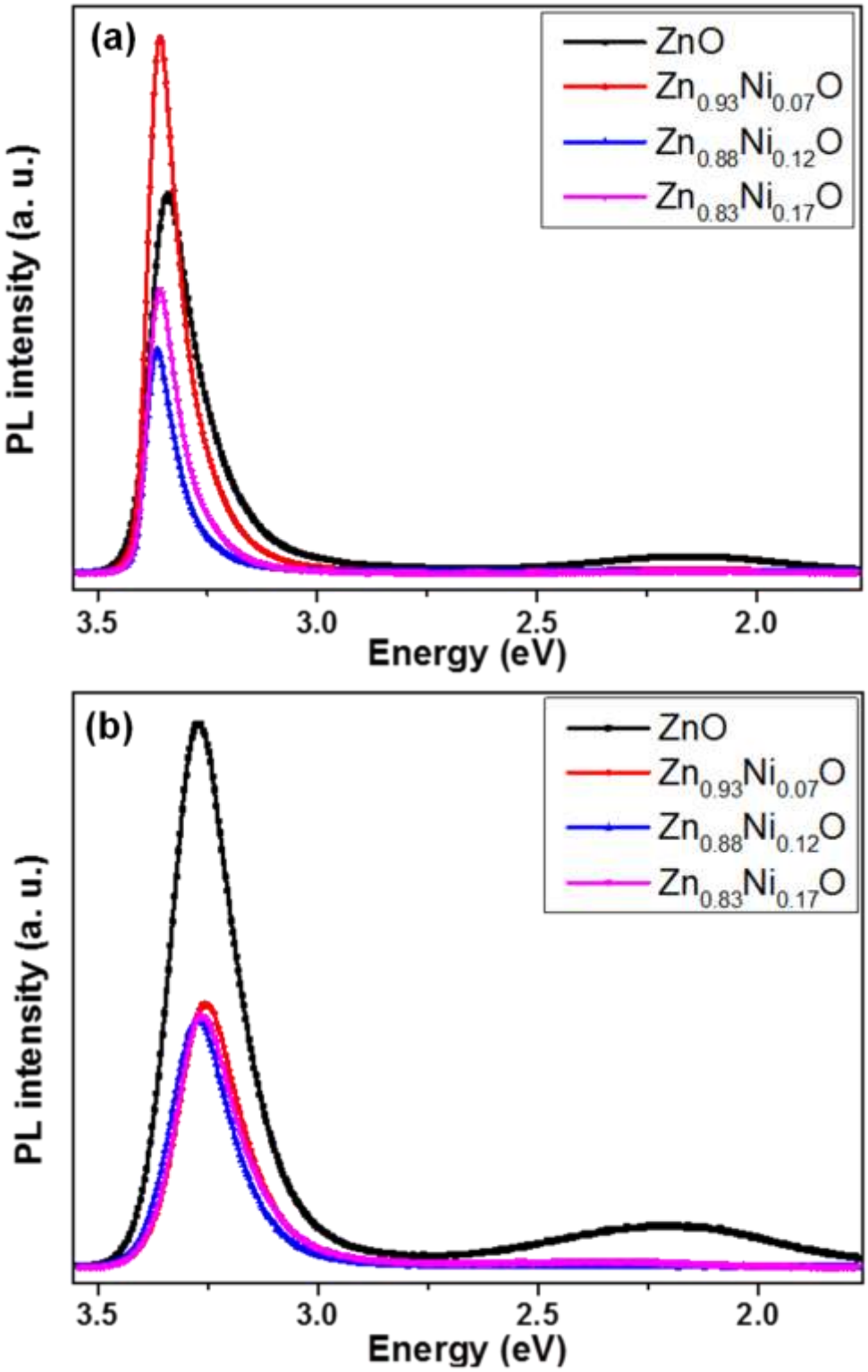

Figure 4-12 PL spectra of Zn(Ni)O nanostructures formed by hydrothermal oxidation in water (a) at 10 K and (b) at room temperature.

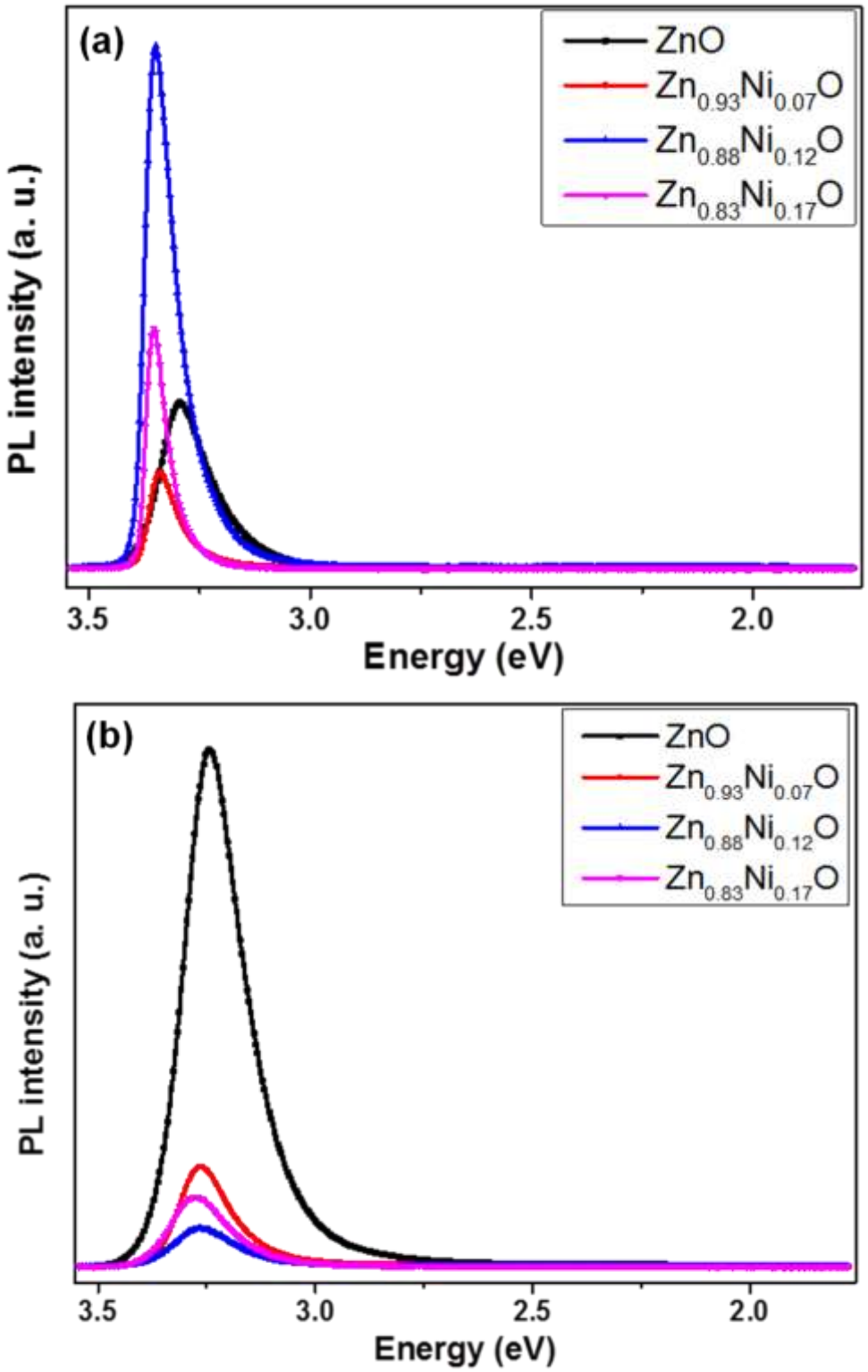

Figure 4-13 PL spectra of Zn(Ni)O nanostructures formed by hydrothermal oxidation in and NaCl solution (c) at 10 K and (d) at room temperature.

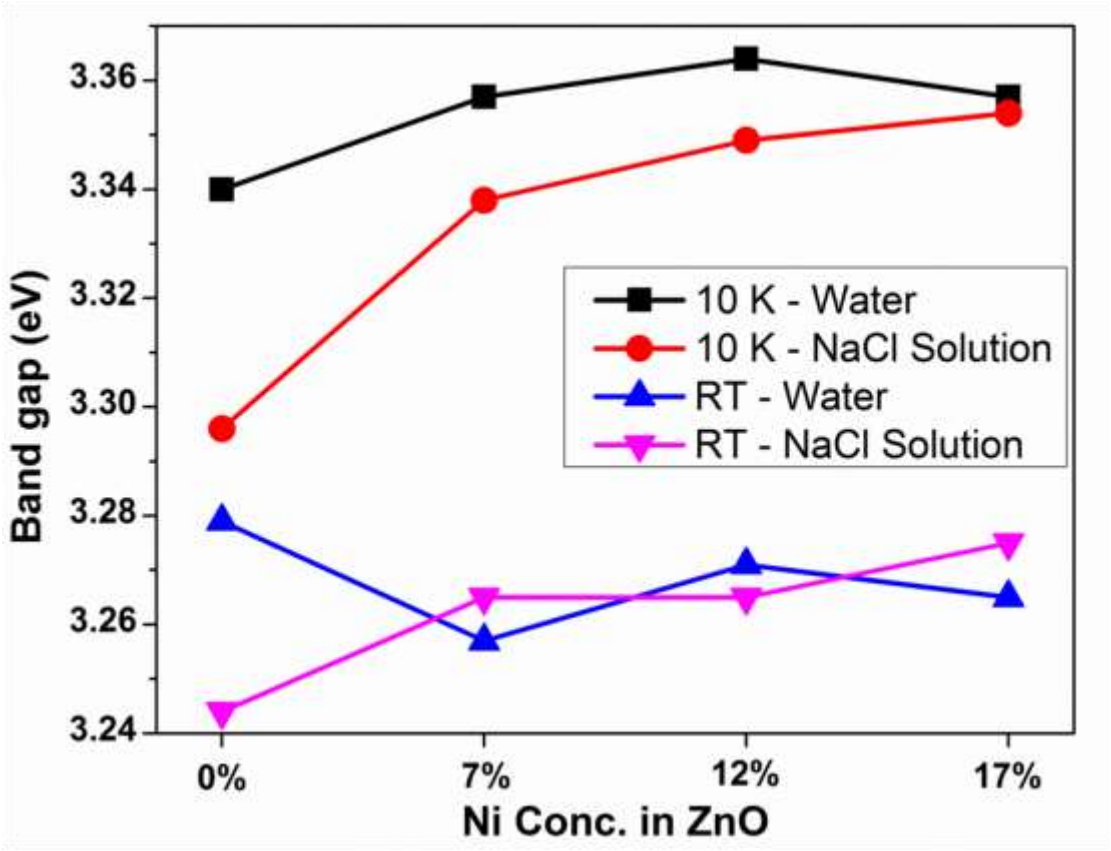

Figure 4-14 Optical band gap estimated from UV emission is shown in (e).

It may be noticed that the minor visible emission in Ni-doped ZnO nanostructures prepared in water is featured with fine structures (Fig. 4-15(a)). This behaviour is similar to [194]. The origin of these fine structures is not clear. One argument can be that the otherwise broad emission is possibly a result of multiple origins. Several researchers have attempted to estimate energies associated with various defect levels [156, 164, 196, 209-211]. For instance, the violet emission observed at 2.86 eV (Fig. 4-15(a)) can be assigned to zinc interstitials [156], as has been schematically shown in Fig. 4-15(b). Zinc vacancies might be responsible for the emissions featured at 2.64 eV and 2.46 eV, associated with electronic transition from conduction band and zinc interstitials, respectively, to zinc vacancy [210-211]. The emission at 2.23 eV may be attributed to transition from conduction band to oxygen vacancy [196, 212]. Further emissions in the yellow to red region could be assigned to oxygen interstitials [196]. Anyway, the visible emission in these samples is very minor, and might be originated from isolated defects of various types including, for instance, different surface features and other two-dimensional and one-dimensional

defects associated with growth stresses, apart from the point defects. These extremely weak emissions may also possibly be related with additional energy levels introduced by nickel itself. Anyway, further investigation is necessary for clarification.

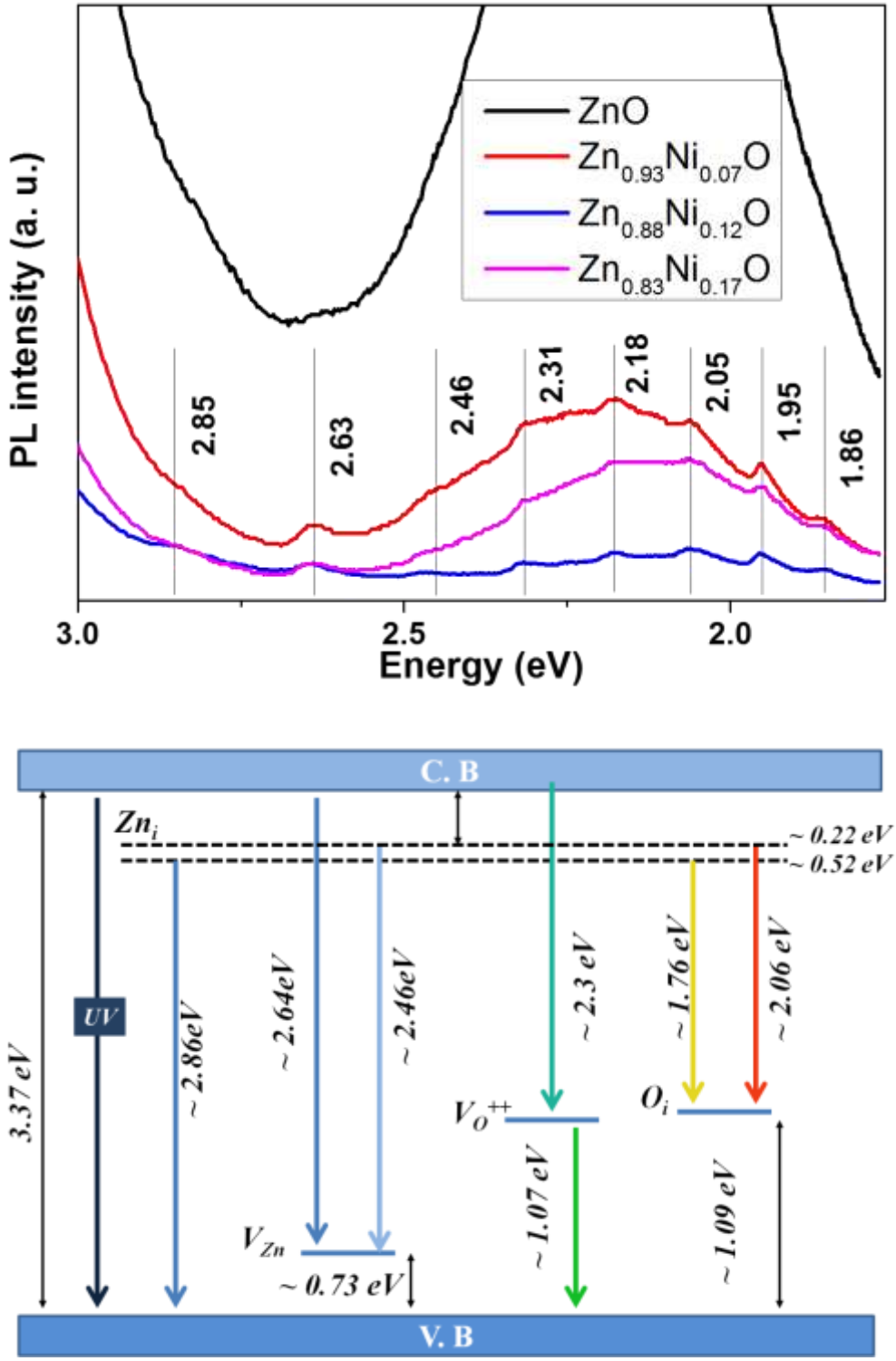

Figure 4-15 PL spectra exhibiting the multiple sub-peaks in the visible region of Ni-doped ZnO naostrutures prepared in water. (b) Proposed energy level diagram for various intrinsic defect levels in ZnO. [Ref. 156, 164, 196, 209-211]

4.3 Conclusions:

ZnO nanorods with up to 17 at% doped nickel have been successfully formed by hydrothermal oxidation of electrodeposited Zn-Ni alloy films in pure water and in 3.5% NaCl solution at 100 ℃. Wurtzite ZnO is seen without any indication of NiO. Chloride ions in the solution enhance oxidation rate. The crystalline quality is also better in case of chloride solution, in addition to lesser physical defects / etching marks. Nickel doping strongly affects the diameter of the ZnO nanostructures. Significant decrease in diameter is seen for highly doped ZnO in comparison with un-doped ZnO. The diameter of most of the nanowires becomes as low as 20-50 nm for 17 at% Ni-doped ZnO formed in NaCl solution. UV emission at 10 K exhibits blue shift, along with peak sharpening with nickel doping. Substantial visible emission (about 10% of the UV emission) exhibited by ZnO nanostructures formed in water almost vanishes with nickel doping. Synthesis in chloride solution eliminates the visible emission completely.

5 Annealed ZnO Nanostructures

ZnO nanomaterials including nanowires, nanorods, nanoneedles, **n**anotubes, etc., have attracted substantial attention due to the exceptional morphology and broad range of applications in diverse areas including electronics, photovoltaics, nanogenerators, sensors, actuators, and so on [213-224]. This is also a well established fact that the properties of ZnO nano-structures are strongly dependant on their sizes, morphologies and various kind of defects, e.g., vacancies, interstitials etc.

Particularly, the variation in optical properties of ZnO nanostructures with morphology, synthesis temperature and post growth annealing are supposed to be mostly related with different defects. Contradictory reports are often seen in this regard. Annealing of nanostructures in reducing environment (H_2 + N_2 gas) has been shown to enhance broad green PL emission due to oxygen vacancies [225]. On the other hand, Leung et al. [226] have reported that green emission most likely originates from complex defect formations, which may also contain zinc vacancies.

The nanostructure have been shown to sustain high temperature (800 ^oC) annealing in argon environment but changed to some other morphology when exposed to air at the same temperature along with the suppression of green luminescence [227].

Eswar et al. [228] observed change in the average ZnO particles sizes upon the post-growth annealing. This also resulted in change in luminescence properties of these nano-structures. Mhlongo et al. [229] observed the morphological variation from "flower-like" structure of ZnO nanorods to randomly oriented "worm-like" ZnO nano-structures with annealing. They further observed extinction of V_{Zn} and/or Z_{in}. Hadia et al. [230] have observed the formation of ZnO nanoparticles of around 33 nm size by heating the hydrothermally prepared hydrozincite plate like-particles at 350 ^oC. The high temperature annealing increased the particle size up to 350 nm with corresponding optical band gap shift from 3.26 to 3.30 eV. Annealing in oxygen environment caused incorporation of oxygen in the nano-structures up to 550 ^oC and

reducing the oxygen vacancy related emission in the PL spectra and then increase in vacancy related PL emission above 700 ^{o}C.

As presented in Chapter 3 and 4, nanowires of ZnO have been formed by hydrothermal oxidation of electrodeposited Zn and Zn-Ni alloy films. Ni addition and/or use of NaCl solution for hydrothermal oxidation have been extremely effective to fabricate nanorods with high crystalline quality, with UV emission without defect related emissions. It has been extremely interesting to note that visible emission seen in the sample prepared by hydrothermal oxidation in water was almost negligible for the samples prepared by hydrothermal oxidation in chloride solution. This may extremely useful for potential applications in UV devices, which is a real dream to replace GaN based devices.

In general, heat treatment is known for improvement in crystalline quality of materials. Also, it can also introduce or conversely lower various point defects, i.e., vacancies, interstitials, etc., depending on the annealing conditions. In this chapter, ZnO nano-structures have been formed by hydrothermal oxidation of Zn films in NaCl solution at 120 and 130 ^{o}C and effects of annealing have been investigated at 500 ^{o}C, in argon and air environments. It may be interesting to see if morphology and optical properties are affected by these treatments or not.

5.1 Experimental:

The formation of ZnO nanostructure has been achieved by the hydrothermal oxidation of electrodeposited Zn films. Initially Zn films were electrodeposited on Cu substrate for which analytical grade ZnCl2 and boric acid have been used to prepare solution for electrodeposition. The pH of the solution (measured by pH meter Model PH 330/SET – 0, 82362 WTW, Germany) has been maintained at 3.6 ± 1 before and during the electrodeposition process. Electrodeposition was performed at two current densities of 350 and 700 Am-2 for 10 minutes using Potentiostat / Galvanostat AMEL Model-2051. The details of substrate preparation and electro-deposition process can be seen elsewhere.

The electrodeposited Zn coatings were immersed in 70 ml of 3.5% NaCl solution in Teflon lined Stainless Steel (SS) autoclave. The SS autoclave was then

placed in oven for hydrothermal oxidation of these Zn coatings at 120 and 130 °C. The temperature in the oven was increased gradually to the reaction temperature, at which the samples were held for 24 hours and then allowed to cool to the room temperature. The samples were removed from the autoclave and thoroughly rinsed with distilled water. These samples then exposed to air and argon environments for annealing at 500 °C for two hours.

The structural, morphology and luminescent properties of as deposited and annealed samples have been studied by scanning electron microscopy (SEM), X-ray diffraction (XRD) and photoluminescence (PL). SEM was performed by using FEI Nova Nano SEM 430 Field Emission Scanning Electron Microscope. X-ray diffraction (XRD) was performed by Bruker D8 Discover diffractometer with Cu Kα radiations. Photoluminescence measurements were performed at 10 K and room temperature (RT) by exciting the sample with 325 nm He-Cd laser line (Melles Griot Series 56) at 15 mW.

5.2 Results and Discussion:

Fig. 5-1 shows typical SEM images of ZnO nanostructures formed by the hydrothermal oxidation of electrodeposited Zn film (at current density ~ 350 Am^{-2}) in NaCl solution. The ZnO nanorods formed at 120 °C have diameters in the range of 100 to 600 nm (Fig 1). The growth direction of these nanorods is mostly normal to the substrate surface. Generally the nanorods have a conical cap at the top.

When these samples are annealed at 500 °C in air, as shown in Fig. 5-2, the surface gets even smoother. By contrast, the sample exhibits tendency of inter-diffusion (ostwald ripening) among nanorods and relatively rougher appearance, particularly of the conical tops after annealing in argon atmosphere, as shown in Fig 5-2(b).

There is another important observation regarding these samples, which is the delamination of the films containing ZnO nanorods (from the substrate) after annealing in Ar environment, as shown in Fig. 5-3. This peeling-off phenomenon is not substantial when the samples are annealed in air, as shown in Figure 5-4. Apparently, inter-diffusion and Ostwald ripening has caused substantial adjustment of

nanorods among themselves causing pronounced stresses at their interface with the substrate, which has resulted in pronounced delamination in case of annealing in argon.

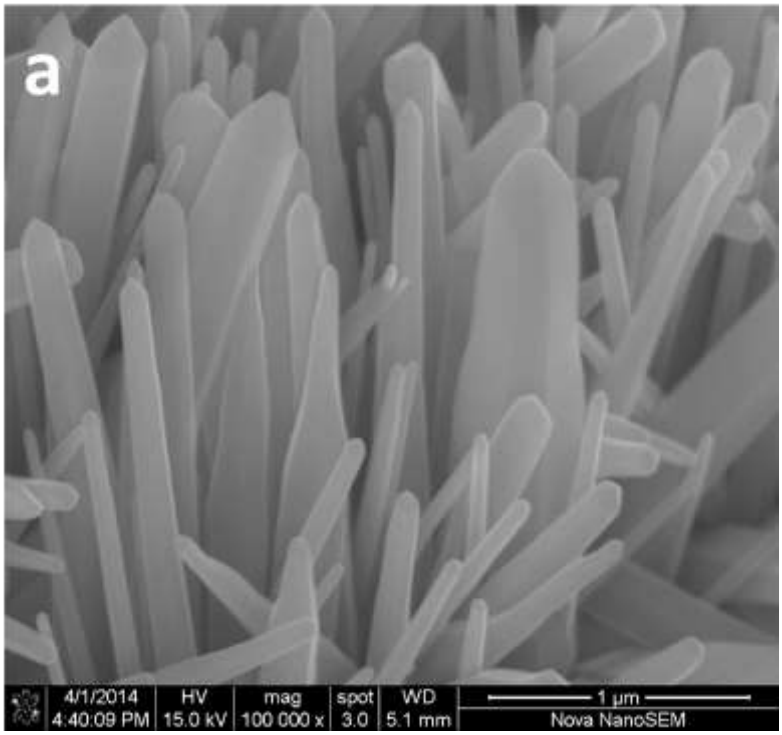

Figure 5-1 ZnO nanostructures formed by hydrothermal oxidation of Electrodeposited Zn film (current density 350 Am^{-2}) at 120 ºC

Fig. 5.5 shows SEM images along with EDS results for backside of a typical ZnO nanostructured layer delaminated from the substrate. Fig. 5.6 shows the same for the substrate surface exposed by delamination. The EDX analysis for Fig. 5.5, confirms Zn and oxygen and rules out diffusion of copper into the ZnO nanorods. The substrate with some residual ZnO exhibits copper, zinc and oxygen in the EDS results (Figure 5-6). The diffusion of Cu from substrate and Zn form upper coating has formed a layer producing stresses at the interface of ZnO and Cu-Zn regions. That leads to the removal of ZnO coating.

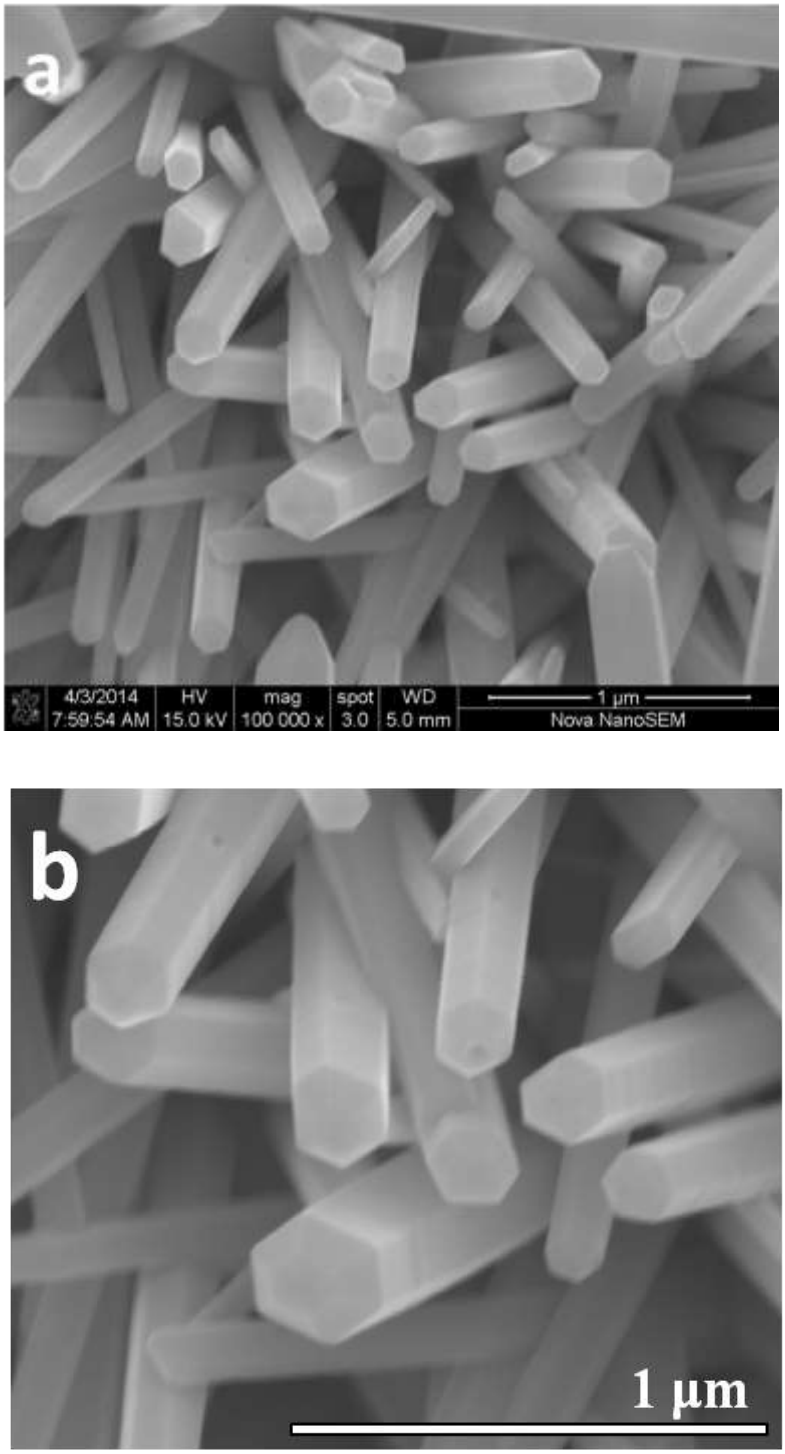

Figure 5-2 ZnO nanostructures (prepared at 120 ºC) Annealed in Air at 500 ºC for 2 hours, (a), enlarged view of nanorods (b).

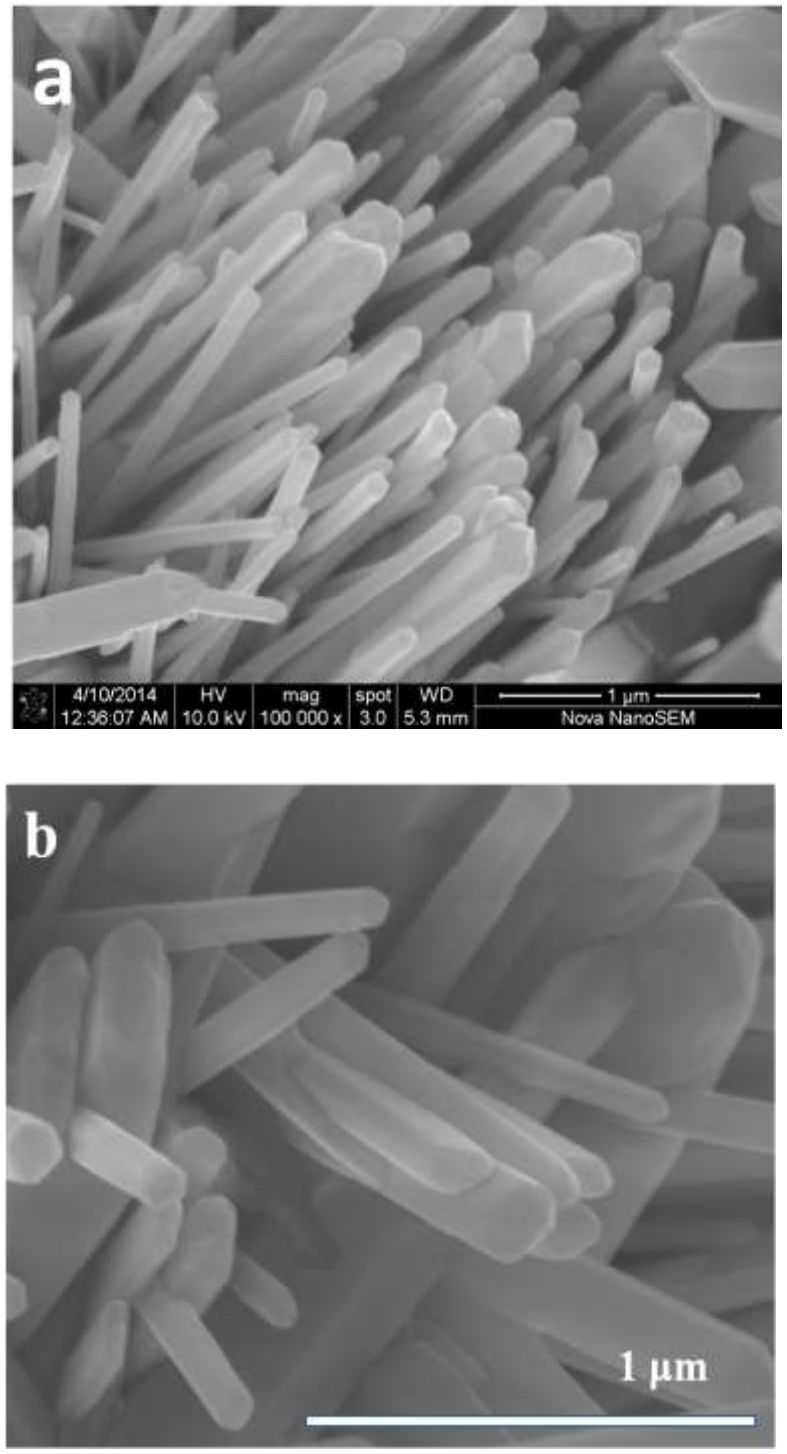

Figure 5-3 ZnO nanostructures Annealed in Ar at 500 ºC for 2 hours (a); enlarged view of nanorods (b).

Figure 5-3 The coating containing ZnO nanostructures after Annealing in Ar environment.

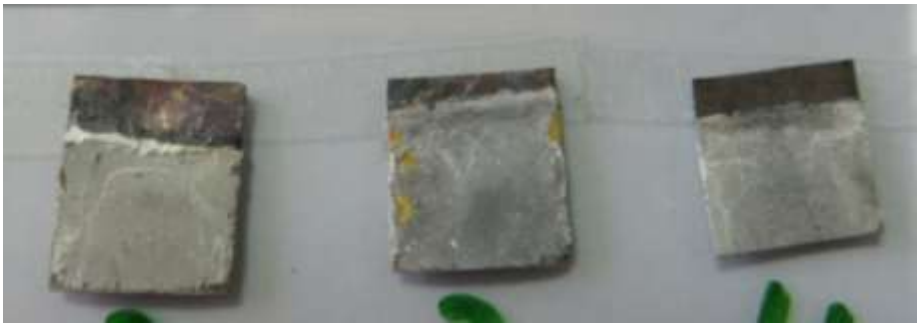

Figure 5-4 The coating containing ZnO nanostructures after Annealing in Air.

Elemnet	Wt%	At%
O	19.61	49.92
Zn	80.39	50.08

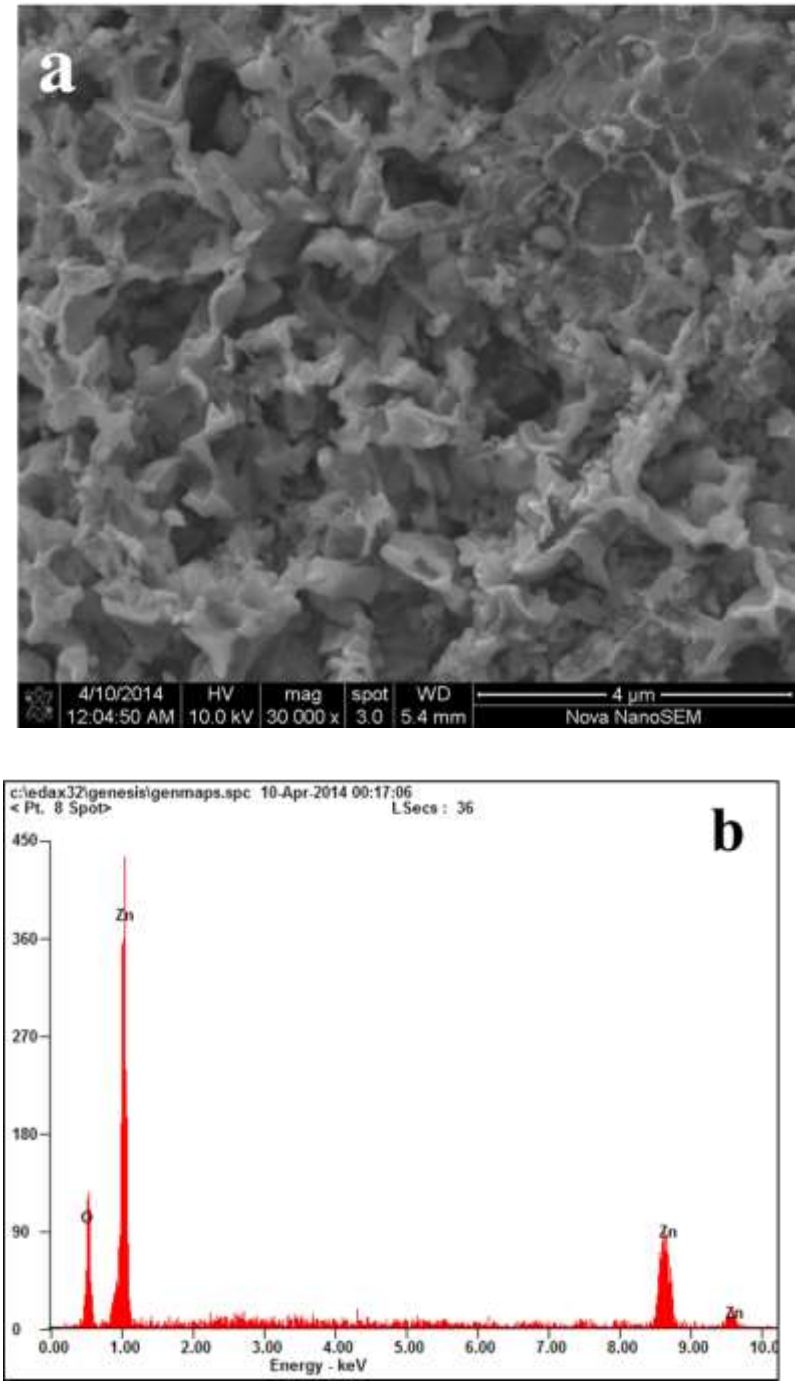

Figure 5-5 Back side of the ZnO coating along with its EDX spectrum (synthesized at 120 oC)

Element	Wt%	At%
OK	5.14	17.90
CuK	54.95	48.13
ZnK	39.90	33.97

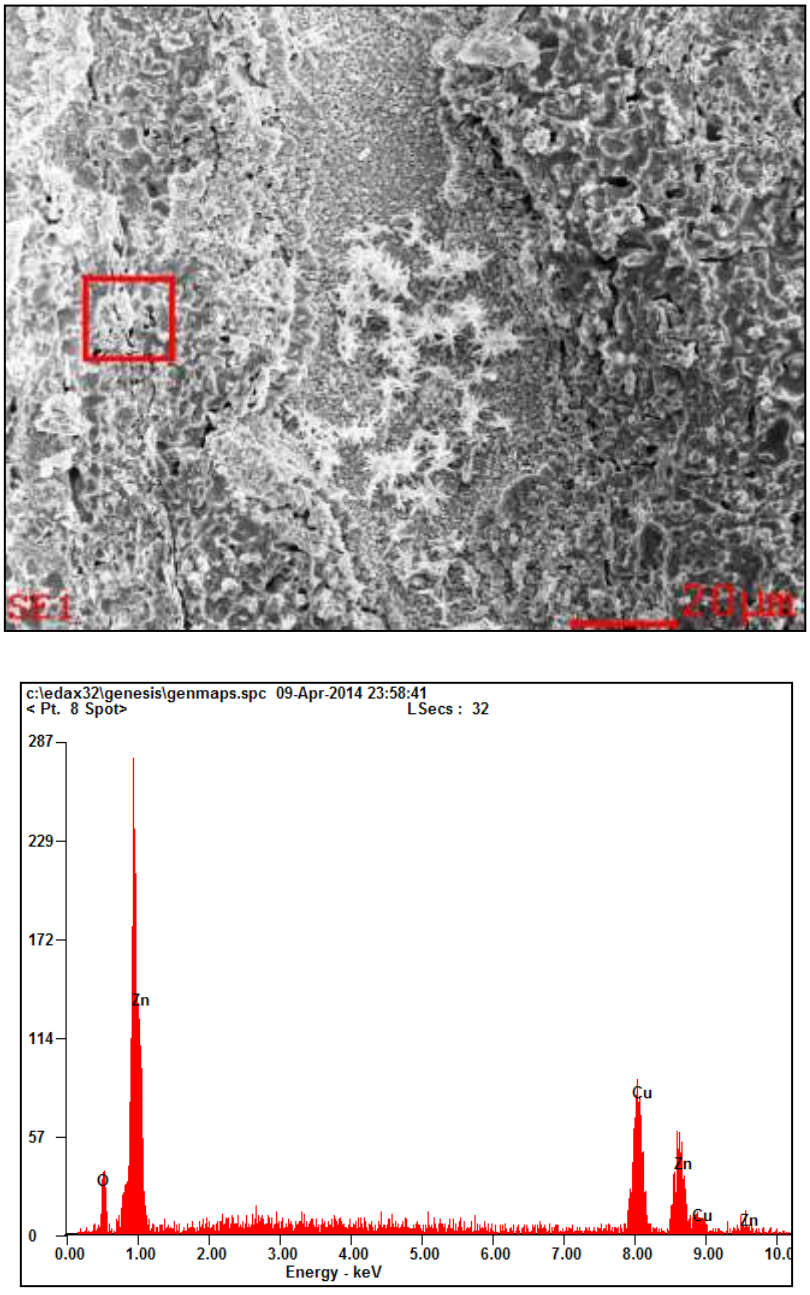

Figure 5-6 Substrate surface after removal of coating containing ZnO nano-structures as a result of argon annealing and its EDX spectrum.

Figure 5-7 & 5-8 shows XRD patterns of ZnO nanostructures before and after annealing in air and argon environments. After hydrothermal oxidation of electrodeposited Zn films, wurtzite ZnO is formed. The electrodeposited metallic film is almost completely consumed during oxidation in NaCl solution for all samples. In NaCl solution, generally, chloride ions accelerate the oxidation process due to which the metallic film mostly consumes to form ZnO nanostructures.

The XRD patterns of annealed samples confirm that ZnO retains the hexagonal wurtzite structure, although another minor phase appears in the XRD patterns after annealing . This crystallographic phase is identified as an inter-metallic phase of cubic CuZn by comparison with the XRD patterns database JCPDS card No.008-0349. The presence of this inter-metallic phase possibly points towards the inter-diffusion of Cu and ZnO as a result of the annealing at 500 ^{o}C. Allabergenov et al. [231] have deposited a Cu-ZnO bi-layer using electron beam evaporation followed by the heating these layers at temperatures 500 ^{o}C and above. That resulted in oxidation and diffusion of copper into ZnO forming Cu- doped ZnO. In our samples, diffusion of Cu mostly occurs at the interface of Cu substrate and ZnO region, even in argon atmosphere. This interlayer diffusion might possibly be mediated by partial deoxygenation of ZnO at the interface allowing to form an intermetallic phase, containing varying amount of dissolved oxygen depending on annealing atmosphere. Anyway, this diffusion does not extend through ZnO nanorods lying over this intermediate layer, as has been confirmed by EDX analysis of the bottom as well as the top of the ZnO nanrod structure.

The PL response of annealed ZnO nanostructures is quite different from that of un-annealed structures as have been discussed in the 3rd chapter. For reference the PL spectra of un-annealed ZnO nanostructures is also shown in Fig. 5-9. The spectrum of sample prepared at 120 ^{o}C, exhibits multiple emissions in the UV region which corresponds to various type of exciton recombination, e.g., free exciton and bound exciton. While the nanostructures formed at 130 ^{o}C only shows an intense ultraviolet emission. After annealing, ZnO nanostructures have exhibited different kind of defect related emissions, depending on annealing environment. The PL spectra of the air annealed exhibit a specific trend by emitting two types of luminescences in the visible region, e.g., green and orange/red (Fig. 5-10 to 13).

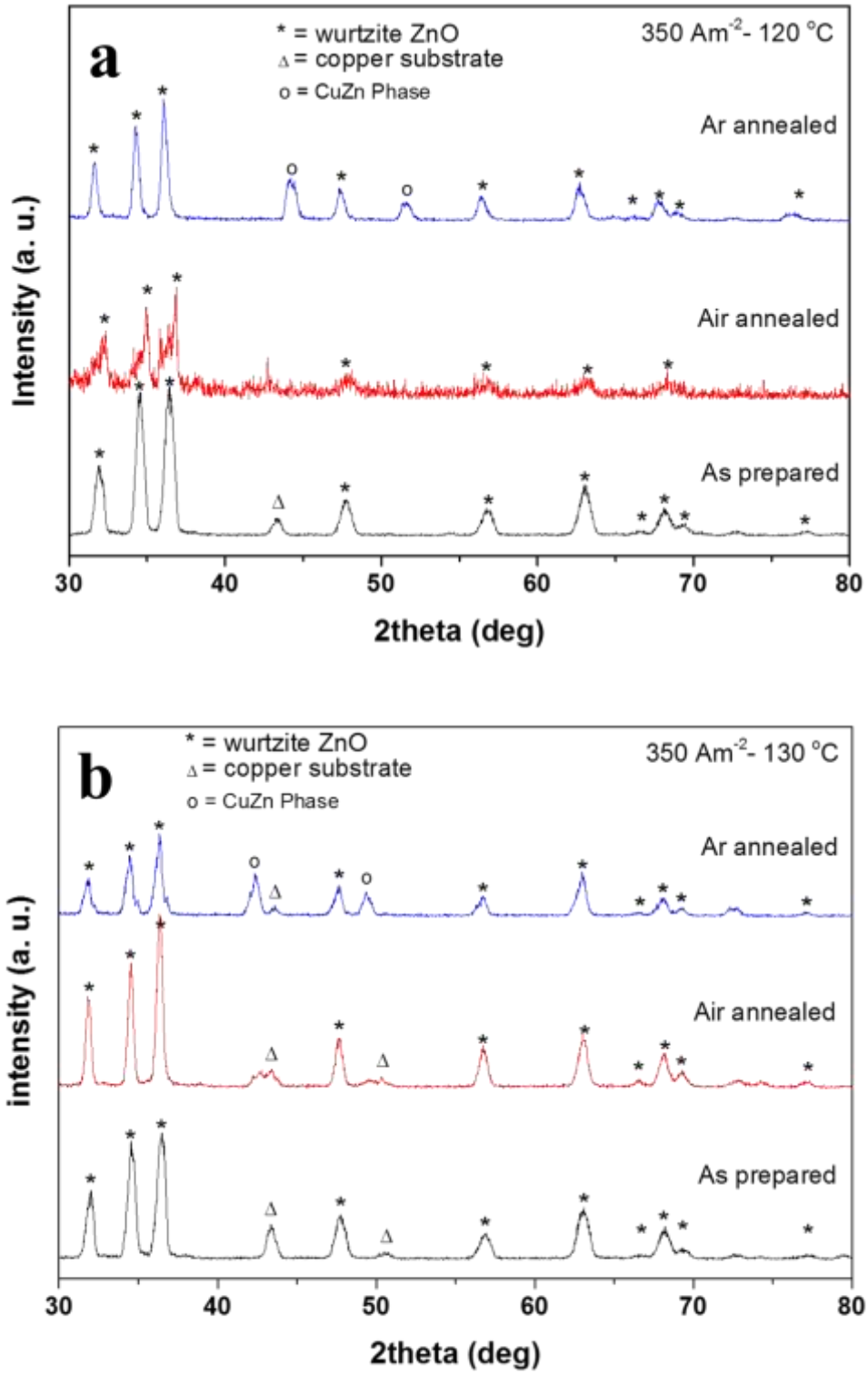

Figure 5-7 XRD patterns of ZnO nanostructure formed by oxidation (a) at 120 ºC (b) at 130 ºC, of electrodeposited Zn film at 350 Am^{-2}.

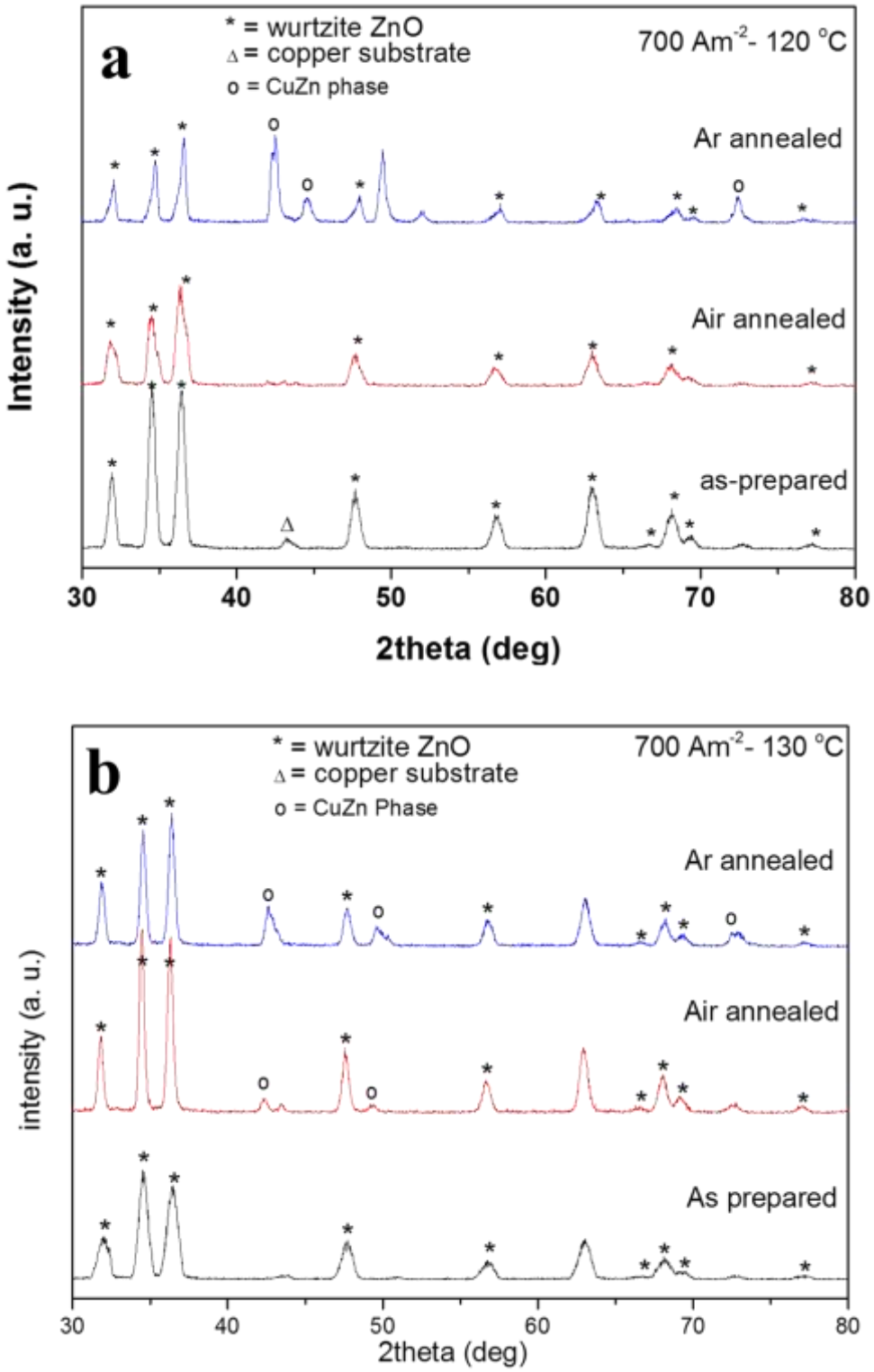

Figure 5-8 XRD patterns of ZnO nanostructure formed by oxidation (a) at 120 ºC (b) at 130 ºC, of electrodeposited Zn film at 700 Am^{-2}.

This behavior of PL spectra is quite different from that of the as-synthesized ZnO nanostructures, as shown in Fig 5-10. The major outcome of annealing nanostructure in air is the evolution of orange emission in the PL spectra. This deep level emission is strong in samples 700 Am^{-2}/120 and 130 ^oC (Fig 5–12 & 13), while the intensity has been decreased for sample 350 Am^{-2}/120 ^oC (Fig. 10) and becomes negligible in case of 350 Am^{-2}/130 ^oC (Fig. 11). For un-doped ZnO nanostructures, it is well established that the deep level emission results from the intrinsic ZnO defects including oxygen vacancy (V_O), zinc vacancies (V_{Zn}), interstitial oxygen (O_i), interstitial zinc (Z_{in}) and anti-site oxygen (O_{Zn}). There is no doubt that many changes/defects are introduced to the ZnO nanorods by the annealing process. The one of the possible origin of orange emission (~630 nm) is the excess oxygen content which might be incorporated at the interstitial positions during oxygen annealing. The appearance of the orange emission with annealing observed here could be an indication of transformation of non-radiative defects through annealing to radiative defects associated with excess oxygen incorporation [232]. Several reports have indicated that electronic transitions from conduction band to O_i or Z_{in} to O_i could have been the reason to generate orange emission [169, 211].

The PL spectra of 350 Am^{-2}/120 ^oC and 700 Am^{-2}/130 ^oC also show the deep level green emission at 502 nm. This deep level emission points towards the presence of some other point defect in ZnO nanorods. The annealing in the oxygen rich environment might have reduced the possibility of oxygen vacancies, which is generally supposed to be responsible for green emissions. Surface modification of nanostructures is the other possible reason for green luminescences [233]. Djusiric et al. [196] reported that the air annealing supported the enhancement of the orange/Red emission while quenching of the yellow and orange/Red emissions were observed by annealing the nanostructures in argon environment which pointed their relation to excess oxygen. These observations are in agreement with the present results.

As it can be seen in the Fig 5.10 to 5.13, the Pl spectra of nanostructures after argon annealing reveal strong green emissions around 500 nm for all the samples irrespective of their synthesis parameters. For the oxide semiconductors, oxygen vacancy is the most common defect and it usually acts as the radiative center to produce luminescence, and it is also accepted by several researchers that in ZnO, the almost ever-present visible luminescence originates from the oxygen vacancies [234-

237]. Oxygen vacancies, usually, create different energy levels with its different charge states located in the ZnO band-gap [238-239], and these oxygen vacancies with charge states in ZnO are responsible for the various luminescences at different wavelengths in the visible region [240-241]. Liao et al.[242] have reported the emission energy of these states as the origins of blue (2.78 eV), green (2.48 eV) and yellow (2.00 eV) luminescences from ZnO are attributed to the electronic transition from the neutral oxygen vacancy (V_O) centers to the valence band edge, the electronic transition from the V_O^+ centers to the valence band edge and recombination of delocalized electrons close to the conduction band to the V_O^{++} center, respectively. Therefore, the deep level emission produced after the argon annealing could be attributed to the oxygen vacancies that have been produced in the nanostructures due to the heating in oxygen deficient/reducing environment. The corresponding energy is in agreement with the reported value for this defect emission.

There is a blue shift in the position of UV peak when the measurements are taken at room temperature, which corresponds to the excitation of the carriers due to the thermal energy provided to these carriers at this temperature.

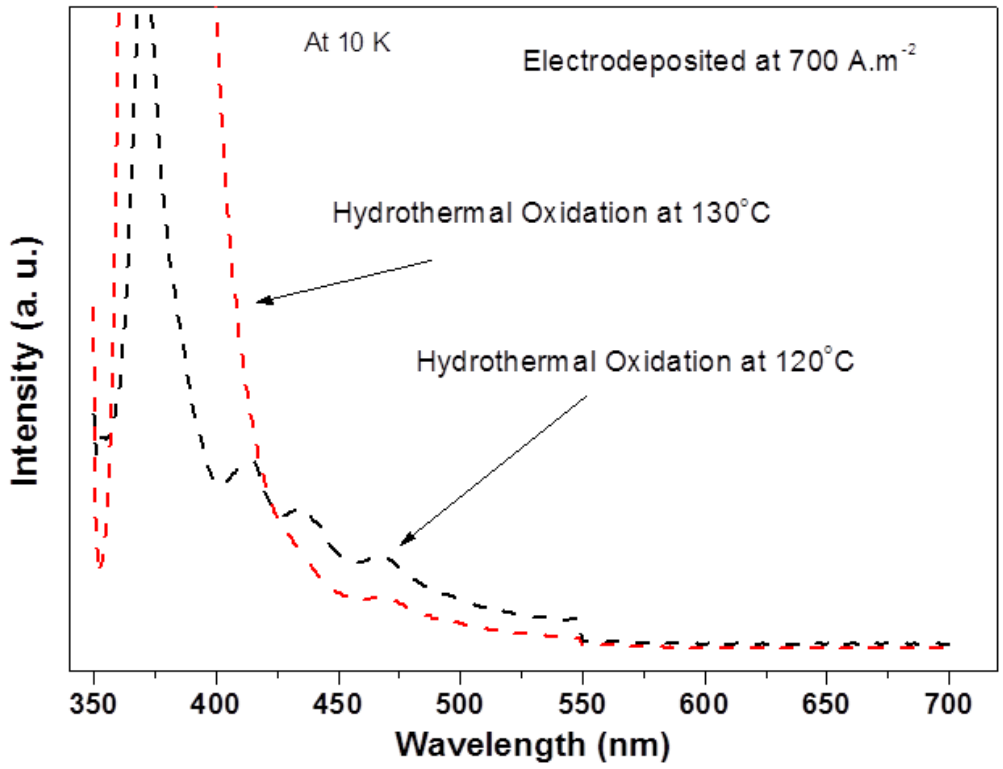

Figure 5-9 PL spectra of ZnO nanostructure formed by oxidation (a) at 120 ºC (b) at 130 ºC, of electrodeposited Zn film at 700 Am^{-2}.

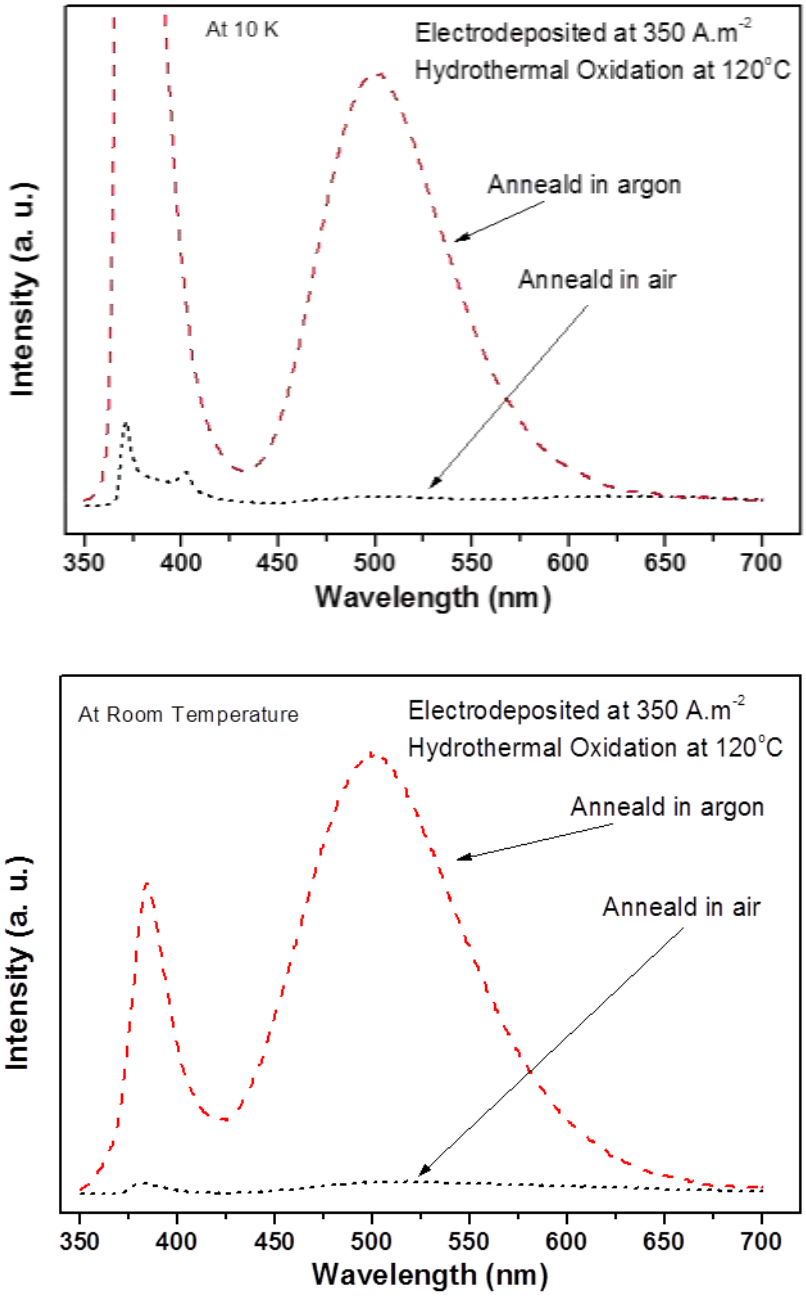

Figure 5-10 PL spectra of ZnO nanostructure formed by oxidation at 120 ºC, of electrodeposited Zn film at 350 Am^{-2}.

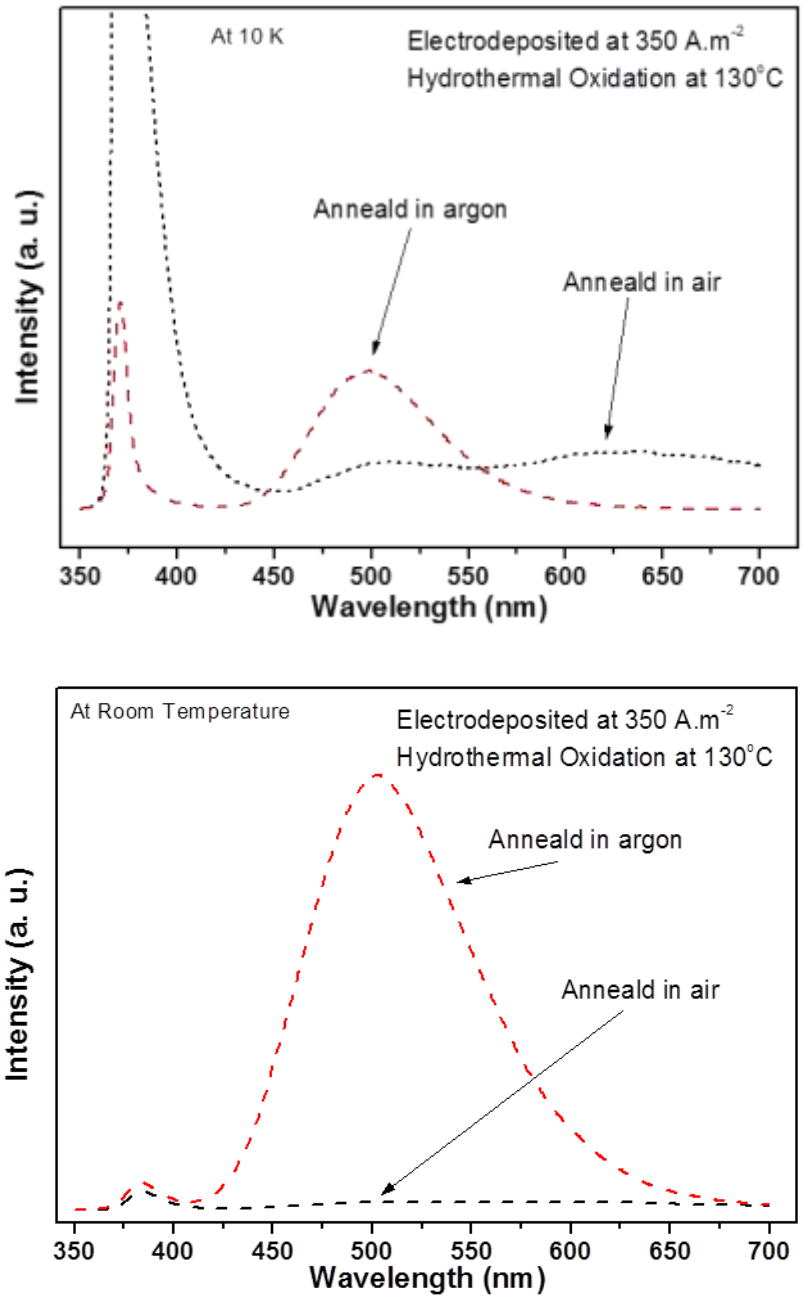

Figure 5-11 PL spectra of ZnO nanostructure formed by oxidation at 130 ºC, of electrodeposited Zn film at 350 Am^{-2}.

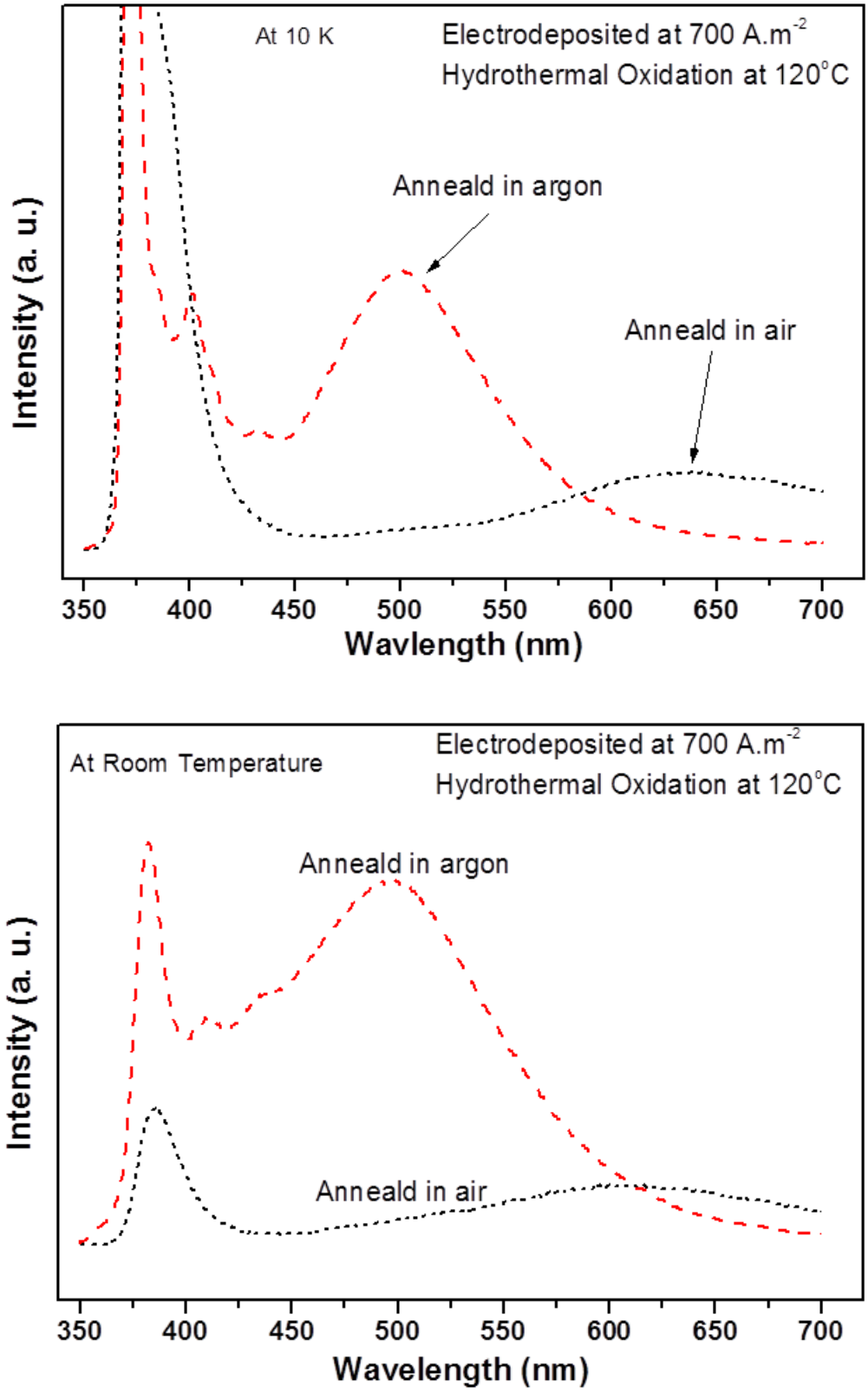

Figure 5-12 PL spectra of ZnO nanostructure formed by oxidation at 120 ºC, of electrodeposited Zn film at 700 Am^{-2}.

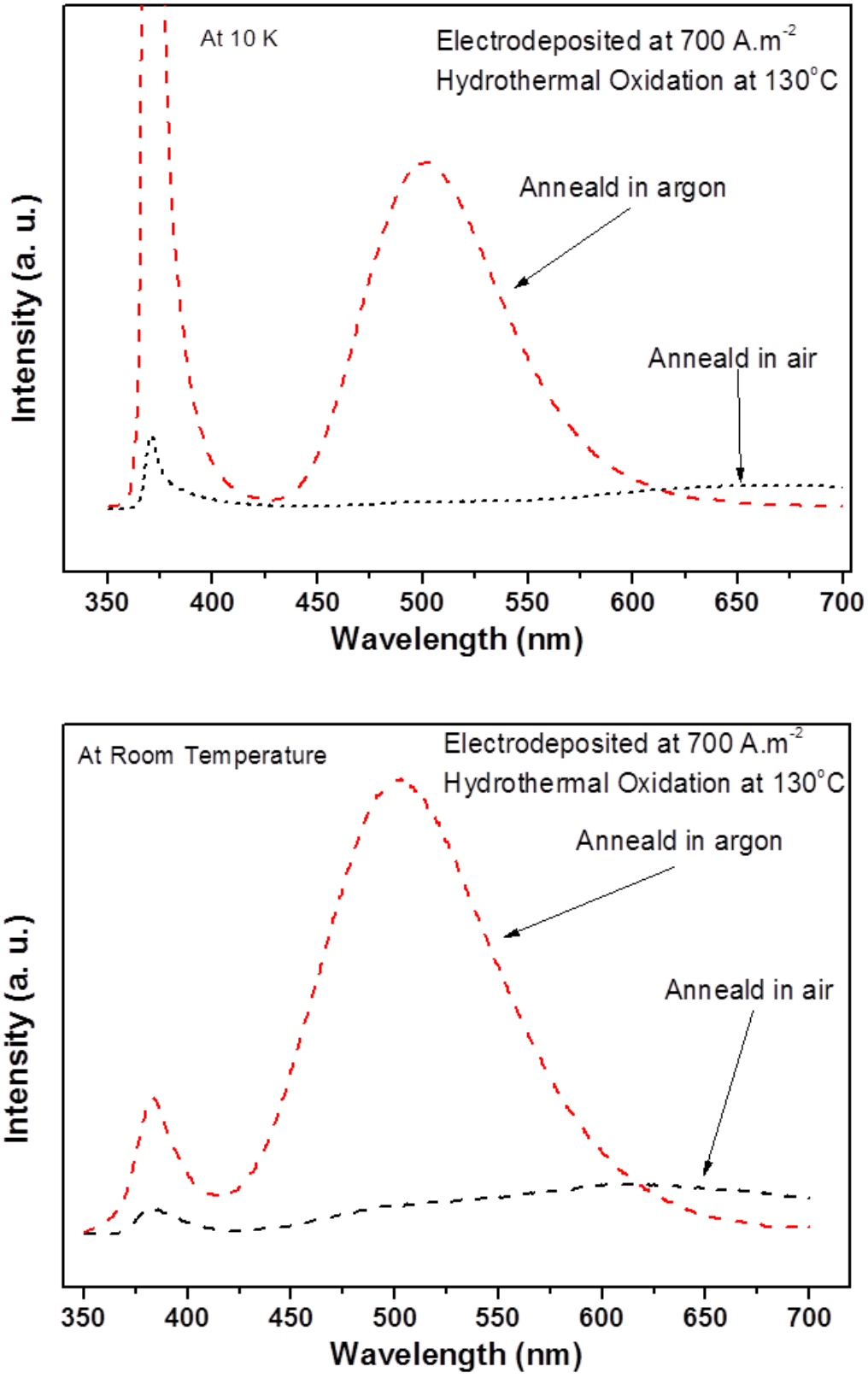

Figure 5-13 PL spectra of ZnO nanostructure formed by oxidation at 130 ºC, of electrodeposited Zn film at 700 Am^{-2}.

Figure 5-14 Emission of light from the sample when exposed to a laser.

Figure 5-14 shows a photograph obtained from a typical sample annealed in air while being shined by UV radiations. The intense blue / green emission observed for this sample indicates that these samples can be well employed for optoelectronic devices involving visible radiations.

It may be worth-mentioning here that annealing is often employed for lowering / defect emissions. By contrast, defect emissions originate by annealing in case of our samples prepared by hydrothermal oxidation of electrodeposited zinc in NcCl solution. This further supports our view that the novel approach presented in this thesis (Chapters 3-4) involving hydrothermal oxidation of electrodeposited zinc is the most suitable approach to form ZnO nanostructure with high crystalline quality, intense UV emission without defect emissions. The usual approach reported in literature to partly overcome visible emission by annealing (the samples that are almost always exhibiting defect emissions in the as-synthesized form) is not suitable. This is because heat treatment both in air as well as in argon can introduce defects and it has always been extremely difficult to optimize annealing conditions to achieve

pure UV emission. Also, annealing can cause other problems, for instances, morphological changes in the nanostructures and deteriorating adhesion with the substrate.

5.3 Conclusions:

Annealing of the ZnO nanorods formed by hydrothermal oxidation of the electrodeposited zinc in NaCl solution has been performed. It has been firmly concluded that our approach reported in chapter 3-4 is the best choice for ZnO nanostructures for UV devices. The air annealing has provided an environment to improve the shape of nanorods and the underlying un-oxidized Zn metal to oxidize using oxygen at high temperature. The argon annealing have enhanced the pitting of the nanorod's top and created cups and troughs. Apart from minor modifications to the nanorod's morphology, the annealing of the samples in air and argon created an inter-metallic CuZn layer at the Cu/ZnO interface. The higher diffusion rate of the Cu/Zn in the argon annealed samples pushed ZnO film to peel off from the substrate as a result of the lattice mismatch between the oxide and inter-metallic layer and the stresses produced as a result of morphological changes in nanostructures due to argon annealing.

6 Gold-decorated ZnO Nanostructures

Composite nanostructures exhibit unique optical and electronic properties. For example, ZnO/ZnS and ZnO/V2O5 core/shell nanostructures [243], CdSe/ZnS Quantum dots [244], ZnO/TiO2 nano-composites arrays [245], WO3/ZnO nanorods arrays [246], ZnTe/ZnO nano-heterostructures [247], graphene oxide/ZnO nanorods hybrids [248] and Cu2O/ZnO composite structures [249] have been synthesized to tailor optical, electrical and photo-catalytic properties.

In metal-semiconductor composite systems, metals attached with semiconductors have electron storage capability, which facilitates charge separation [250]. Fermi level of this composite system can be tuned by varying the size of the attached metal nanoparticles [251]. Gold and silver metals have been popular metals to construct the metal-semiconductor nano-composite structures.

ZnO nanostructures decorated with gold nanoparticles have been successfully utilized in many applications such as glucose biosensors [252], photo-electrodes in dye-sensitized solar cells [253] and photo-catalytic activity for the degradation of organic pollutants, exhibiting strong [254].

One major application of metal-semiconductor composite systems is the photocatalytic degradation of organic pollutants in organic industries. The main restraint in achieving good efficiency of photocatalytic degradation using semiconductor nanoparticles is the rapid recombination of charge carriers which prevents the availability of the carriers required to enhance the photocatalytic activity. To provide the carriers in the solution, attaching metal nanoparticles to the semiconductor nanostructures is found to be the most successful method [255-257].

In this chapter, attachment of gold nanoparticles on ZnO nanorods formed by hydrothermal oxidation of electrodeposited zinc has been reported. Surface activation to facilitate this attachment has been provided by potassium iodide. Changes in optical properties of ZnO nanostructures by iodide treatment and then gold attachment

have also been focuses upon. In addition, photocatalytic activity of the nanostructures has also studied.

6.1 Experimental:

Analytical grade $ZnCl_2$, $NiCl_2.6H_2O$ and Boric Acid were used for electrodeposition bath. The pH of the bath was 3.6±0.1 (measured by pH meter Model PH 330/SET – 0, 82362 WTW, Germany). Electro-deposition of zinc metallic films was performed (on copper substrate) at a constant current density of 350 $A.m^{-2}$ for a period of 10 min using Potentiostat / Galvanostat AMEL Model-2051.

ZnO nanostructures were formed by the hydrothermal oxidation of zinc films. Electrodeposited Zn films were immersed in 70 ml of pure water in a Teflon-lined Stainless Steel (SS) autoclave. The autoclave was then placed in an electric oven (Heraeus vacutherm VT 6130P). The temperature of the oven was slowly increased to 100 ^oC, which was maintained for a period of 24 h followed by slow cooling to room temperature. The sample was then removed from the autoclave and thoroughly washed with distilled water.

The prepared ZnO samples were then immersed in 0.1M potassium Iodide solution for 24 hours followed by soaked them into two separate solutions each containing 10 mL of 0.05M and 0.025M $HAuCl_4$ solution for further 24 hours. Then these samples were taken out and rinsed thoroughly with de-ionized water. The complete synthesis method can be seen in the schematic diagram shown in Figure 1.

Scanning electron microscopy (SEM) and compositional analysis were performed by using Field Emission Scanning Electron Microscope (FEI Nova NanoSEM 430) equipped with EDX system (EDAX). Photoluminescence (PL) spectra were obtained at Room temperature (RT) and 10 K using 325 nm He-Cd laser line (Melles Griot Series 56) at 15 mW. The catalytic activity of these samples for degradation of Methylene Blue (MB) dye was checked by using commercially available 10W ultraviolet lamp. The photocatalytic activity of the ZnO and Au-ZnO nano-composite has been analyzed by the photocatalytic degradation of Rhodamine B (RhB) solution. The concentration of RhB aqueous solution was determined by a UV-visible spectrophotometer Labomed Spectro UV/VIS double beam UVD 3500

spectrometer. The absorbance of RhB solution was measured after every 20 minutes in the wavelength range of 250 – 800 nm by taking out the sample from the solution.

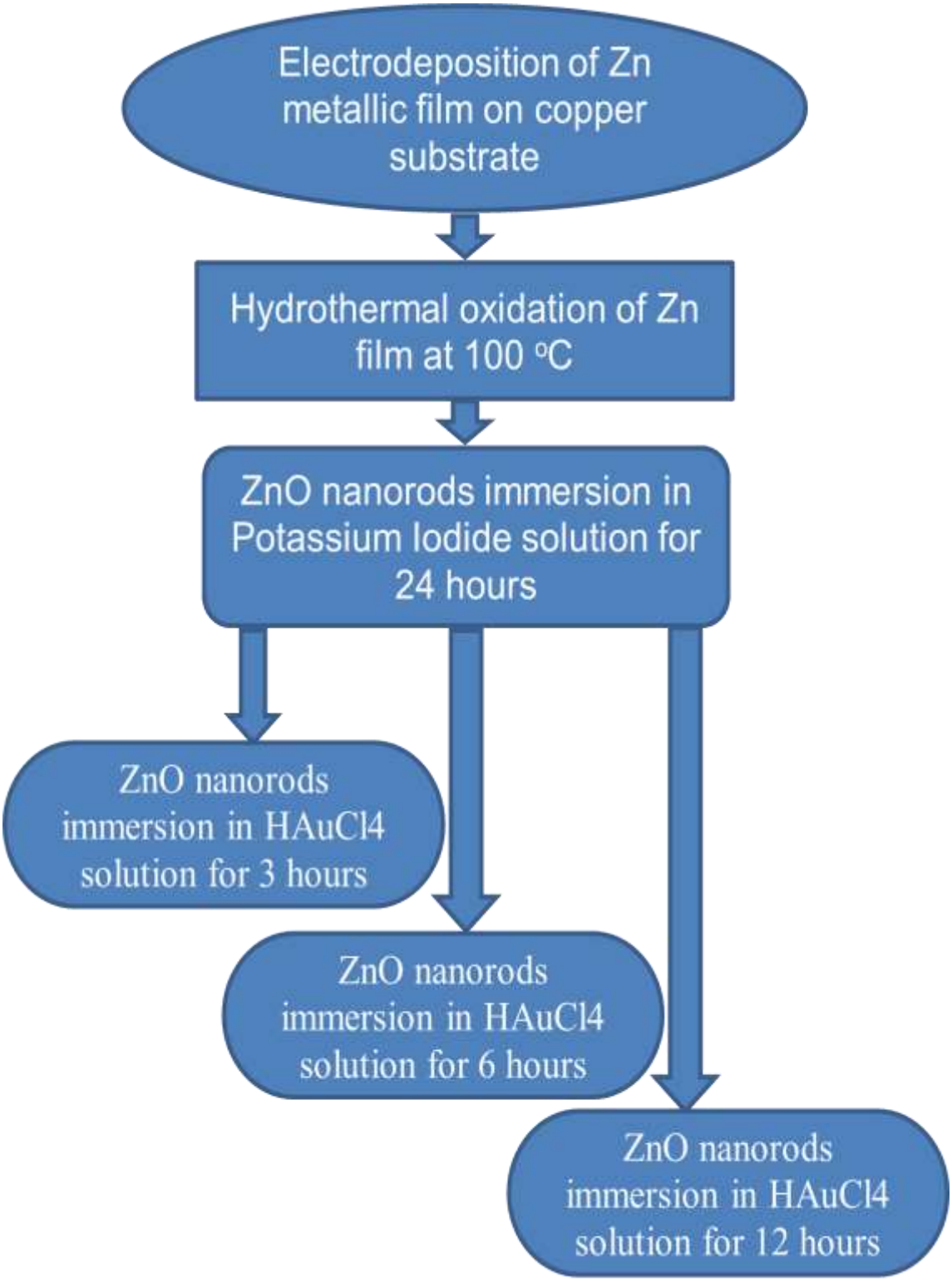

Figure 6-1 The flow chart showing the procedure for preparing Au/ZnO nano-composite structures.

6.2 Results and Discussion:

SEM image of the as-synthesized ZnO nanostructures are shown in Figure 6-2. The rods formed possess clean hexagonal geometry having a sharp tip at the ending point. Figure 6-3 shows the morphology of the ZnO nanorods after immersion in potassium Iodide (KI) solution for 24 hours. The surface of these nanorods has been affected by the KI solution treatment. More pronounced damage has been seen at the conical tops of nanorods. The faces making the tips of nanorods are relatively high energy surfaces. The non-polar {100} surfaces are apparently less affected in the solution (Figure 6-3). Any contamination or incorporation of KI has not been detected by EDX analysis as shown in Fig. 6-4.

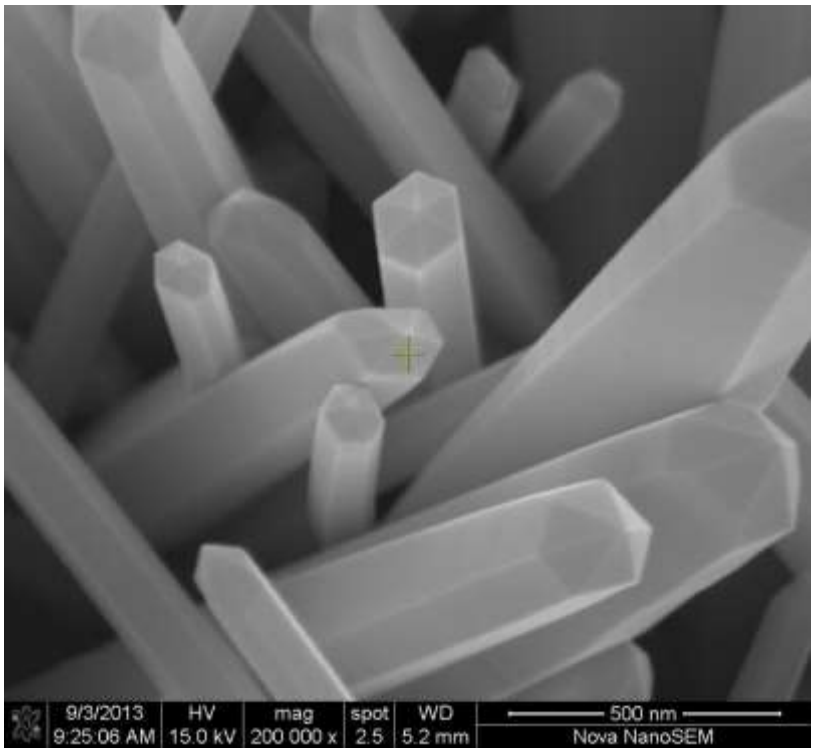

Figure 6-2 SEM image of ZnO nanorods formed after hydrothermal oxidation of electrodeposited Zn film.

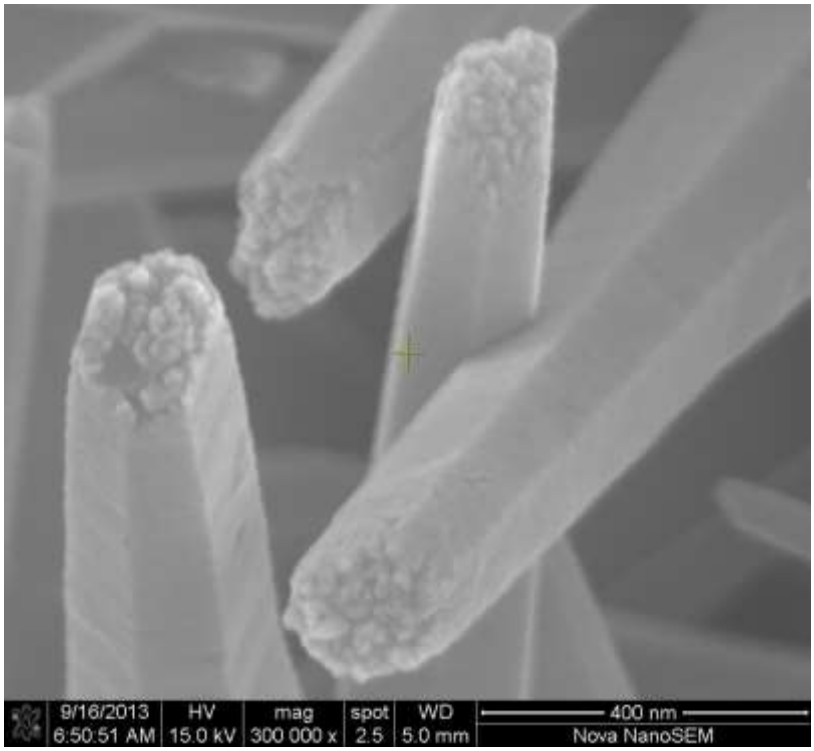

Figure 6-3 Magnified view of ZnO nanorods after immersion in the potassium iodide solution.

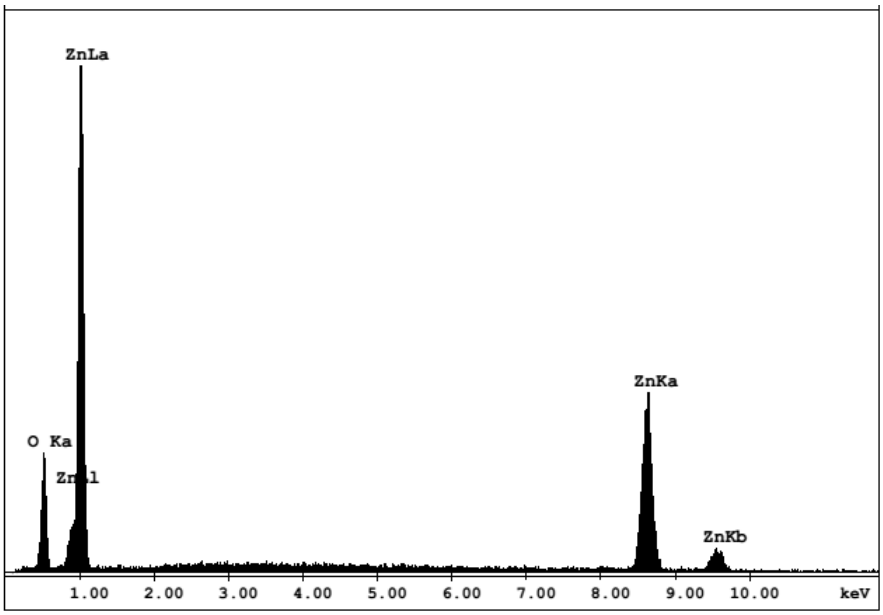

Figure 6-4 EDS spectrum of ZnO nanorods taken after immersion in the potassium iodide solution.

The nano-scale Au/ZnO composites have been formed as a result of reaction between KI modified ZnO nanorods and $HAuCl_4$ solution for 3, 6, and 12 hours as represented in Figure 6-5, 7 and 9, respectively. It can be seen that upon increasing the immersion time of ZnO nanorods in $HAuCl_4$ solution, the number of Au nanoparticles decorated on the surface of the ZnO nanorods increases, and their size also increases slightly Another important aspect regarding the coverage of nanorods with gold is the formation of a thin Au film on the whole nanorod surface irrespective of the formation of visible gold nanoparticles. For instance, ZnO nanorods at a relatively low lying region do not show visible gold nanoparticles, yet region still shows some gold in the EDX analysis (Fig. 6-13).

The low-temperature (10 K) PL spectra of the ZnO nanorods and Au-ZnO nano-composites with different Au contents have shown in Figure 14(a). The two emission bands located at ~371 and 575 nm are clearly revealed in the spectra. The sharper and more intense emission peak at ~371 nm has been frequently assigned to the near-band-edge emission in ZnO, while the depressed and broad band in the visible spectral range (with peak at ~575 nm) has been attributed to the electronic transitions to the intrinsic defects such as oxygen interstitials or some complexes of point defects in ZnO.

The suppression of visible emission with the improved Au coverage is an important aspect of this study. It can be seen that intensity of the band related to visible emission has increased for the first Au-ZnO nano-composite sample as compared to as-synthesized ZnO nanorods. But it tends to decrease as the coverage surface of the ZnO nanorods has increased by the Au NPs. The ratio of visible emission intensity to ultraviolet emission intensity has been plotted against the immersion time of ZnO in the Au solution, as shown in figure 14(b). Initially, the surface of the ZnO nanorods has been modified by the KI solution which might have created defects states at the surface as can be seen in the SEM images. So when the nanorods have been immersed for 3 hours in the Au solution, the surface of the ZnO nanorods is not completely covered exposing those defect states to the radiation which results in the intense visible emission.

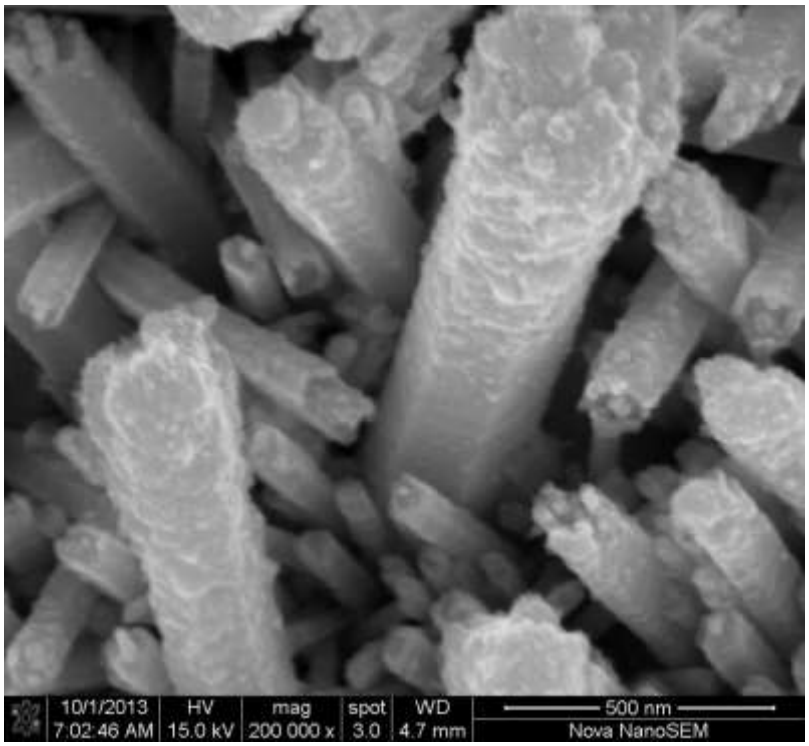

Figure 6-5 SEM images of Au/ZnO nano-composites formed after 3 hours.

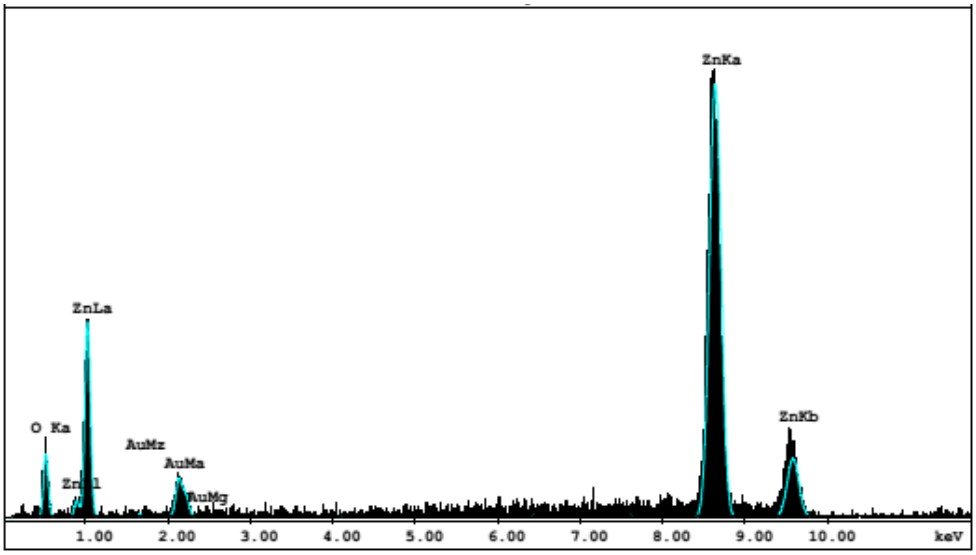

Figure 6-6 EDX epectrum of ZnO nanorods after 3 hours immersion in Gold solution.

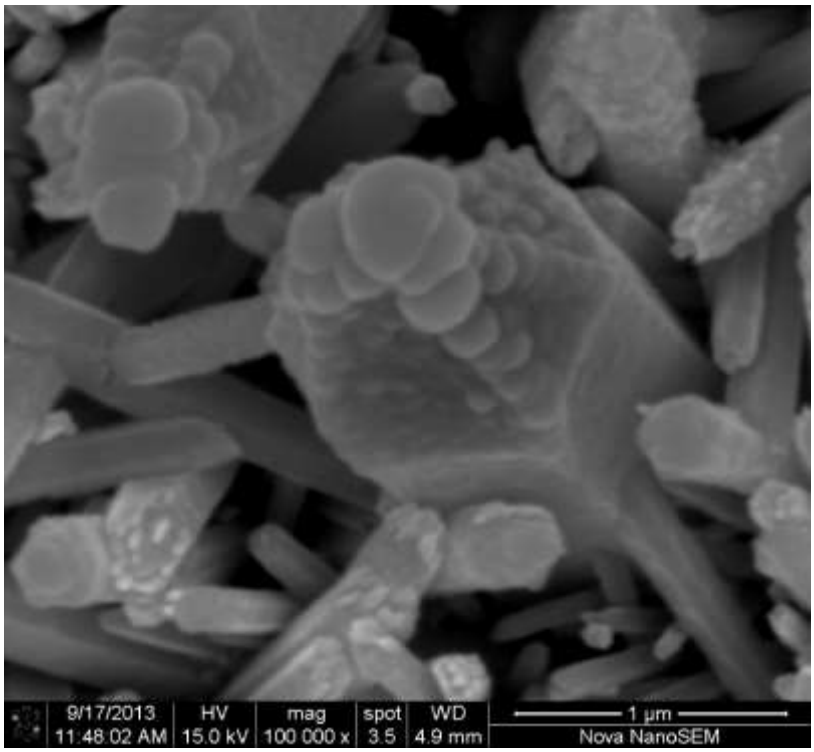

Figure 6-7 SEM images of Au/ZnO nano-composites formed after 6 hours.

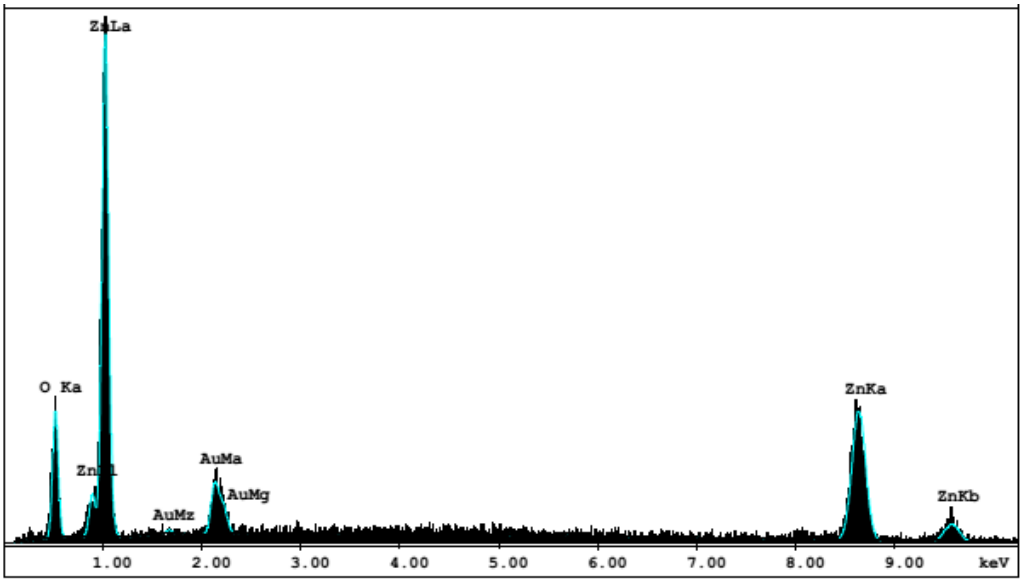

Figure 6-8 EDX epectrum of ZnO nanorods after 6 hours immersion in Gold solution.

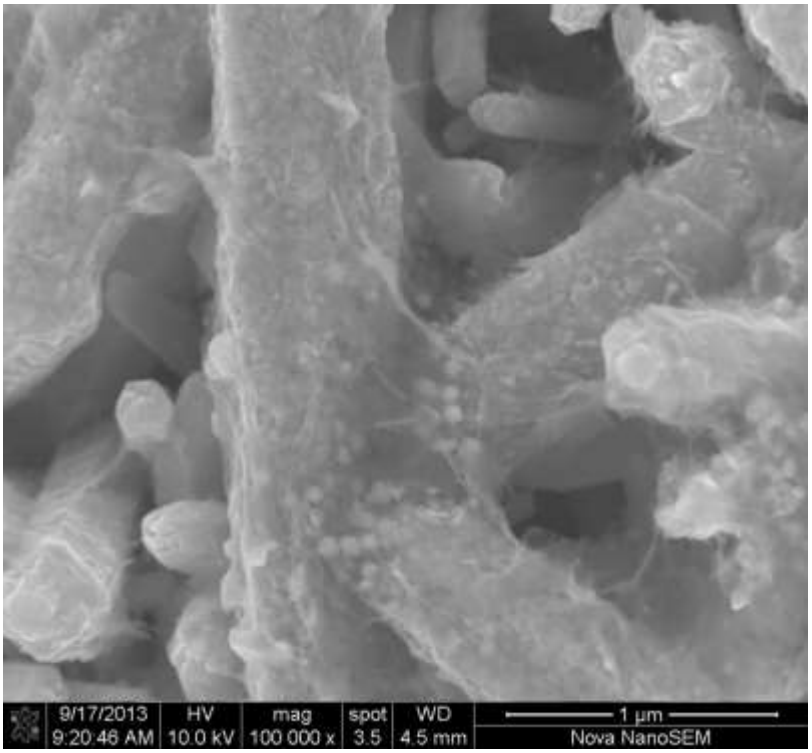

Figure 6-9 SEM images of Au/ZnO nano-composites formed after 12 hours.

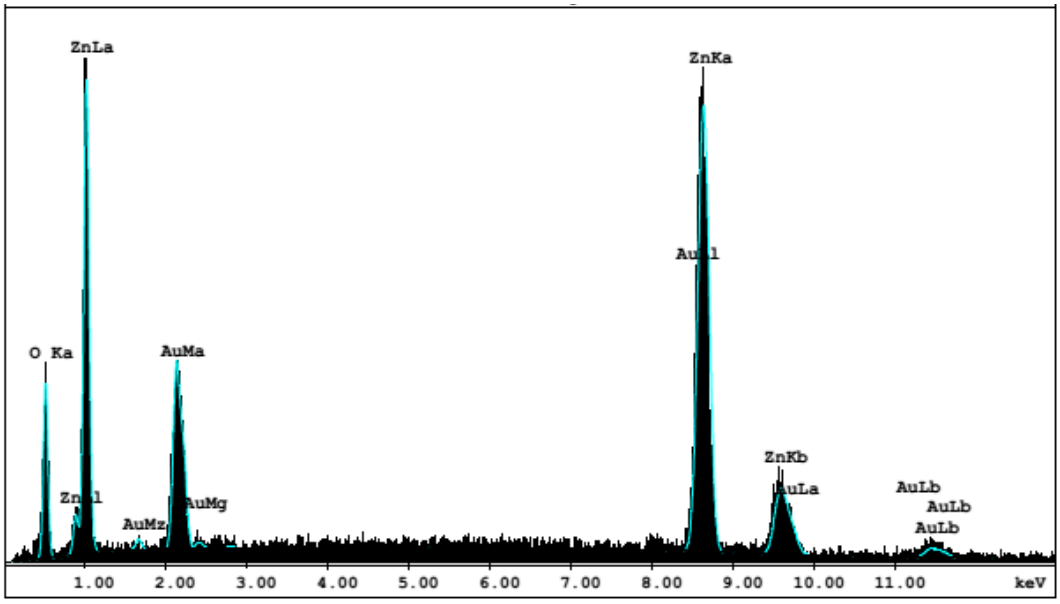

Figure 6-10 EDX epectrum of ZnO nanorods after 12 hours immersion in Gold solution.

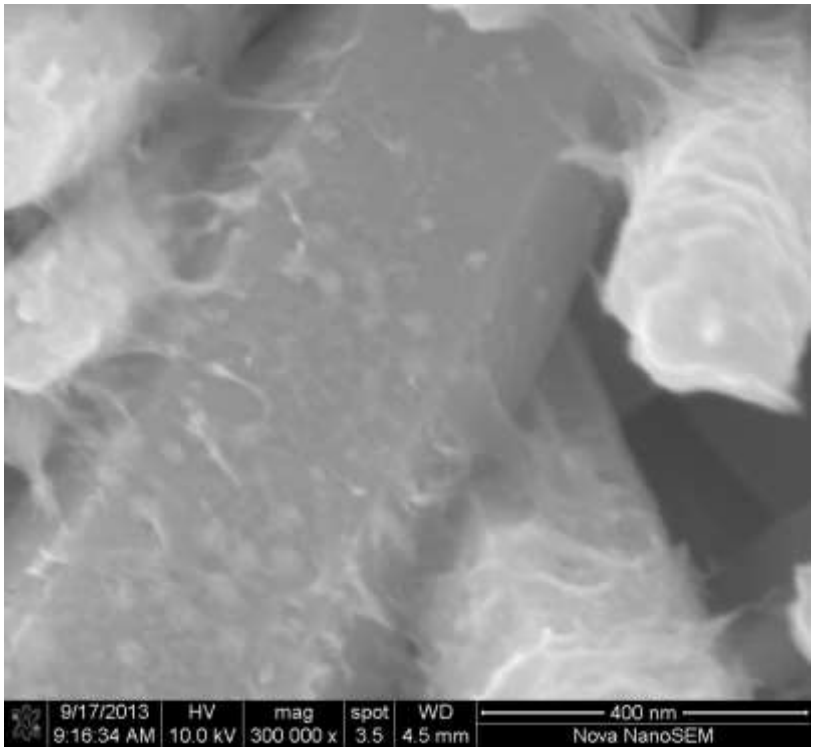

Figure 6-11 Au nano-particles formed on the side surface of ZnO nanorods.

But this visible emission tends to decrease when the coverage of nanorods surface and/or the size of In such composites, the diminution of surface state defects causes an enhancement in the near band-edge emission by improving the number of energetic electrons available in the conduction band to recombine with holes in the valence band. The similar effect has been reported in case of CdSe quantum dots functionalized with Au nanoparticles and ZnO/Ag_2O nano-composites [258-259].

The photocatalytic activity of the ZnO nanostructures has been demonstrated by the degradation of RhB. Figure 6-15 shows UV/Vis absorption spectra which has obtained from the degradation of 10 ppm solution of RhB by bare ZnO nanorods. It can be seen that with increasing UV irradiation time, the absorption peak intensity corresponding to RhB diminishes gradually because of the photodecomposition of the organic dye solution. The concentration of the RhB solution was approximated by the maximum absorption peak intensity at approximately 556 nm in the UV–Vis spectra which can be seen in Figure 6-16. It is clearly seen that the photocatalytic activity of ZnO nanorods was significantly enhanced by the deposition of gold NPs on ZnO nanorods.

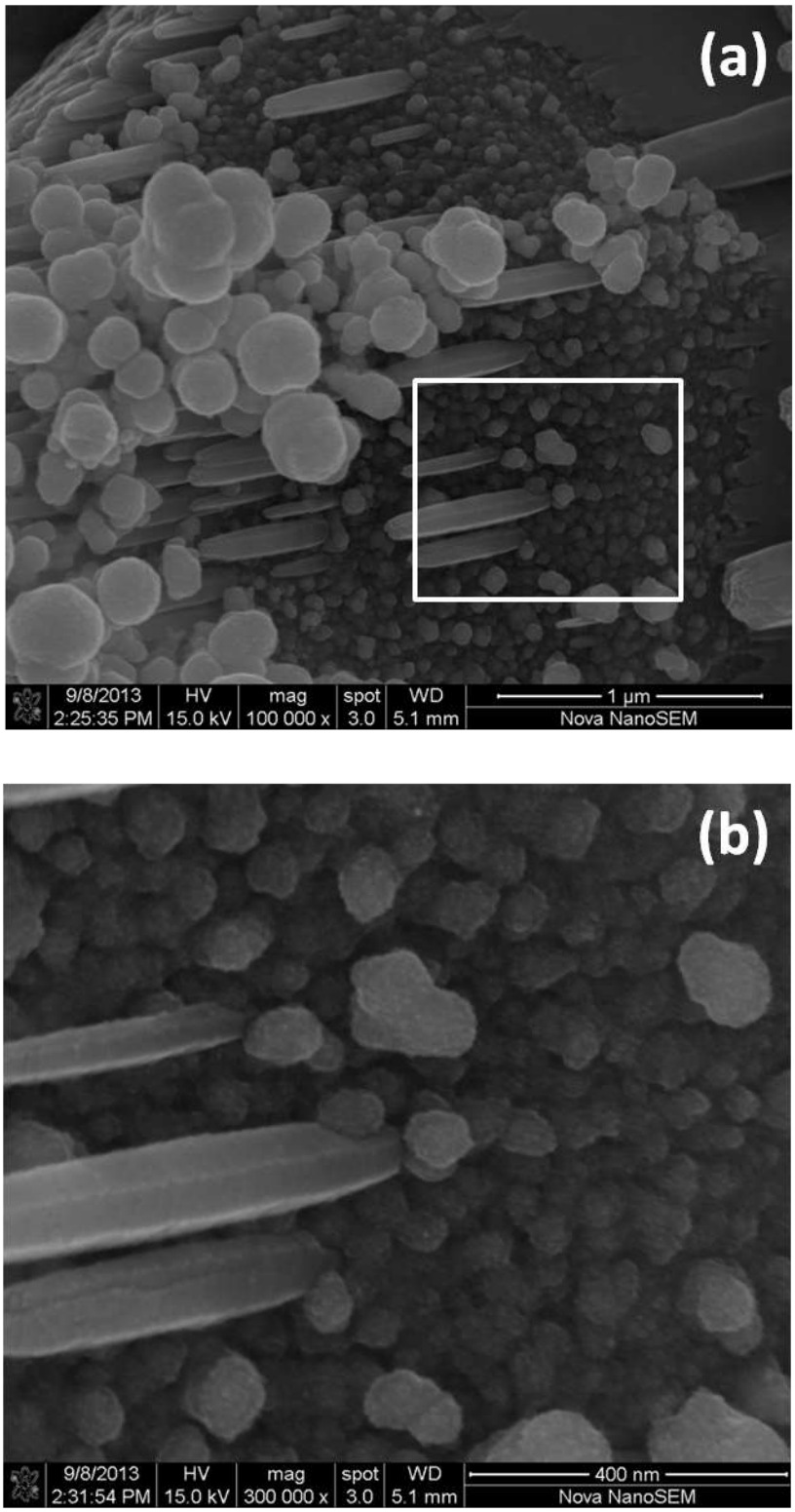

Figure 6-12 Magnified views of morphological appearance of conical tops of ZnO nanorods after Au deposition (a) enlarge view of the squared area (b).

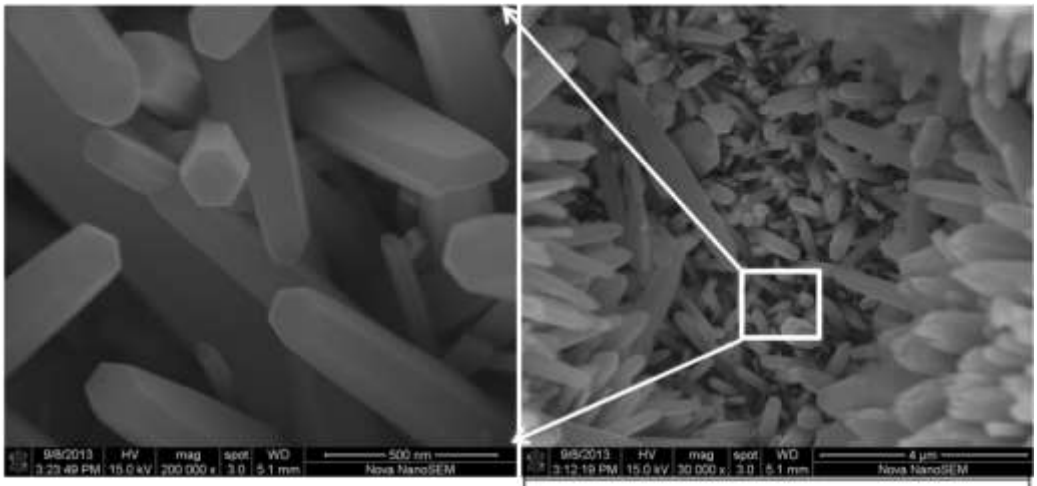

Element	Wt%	At%
O	21.61	54.35
Au	6.37	1.30
Zn	72.03	44.35

Figure 6-13 Morphology and compositional analysis of low lying ZnO nanorods in valley region.

In order to understand the effectiveness of Au nano-particles decorated ZnO nanorods in photocatalytic reaction can be explained by drawing the band diagram of metal-semiconductor contact, as shown in Figure 6-17. Generally, the Fermi level energy of ZnO is estimated to be larger than the Au work function. This contact of Au and ZnO forces the Fermi level to reposition it at equilibrium value close to the conduction band of ZnO. The new Fermi level of Au/ZnO nano-composite forms below the energy level of the bottom of the conduction band of ZnO, the electrons would transfer from ZnO to Au due to the energy difference under UV irradiation.

Mostly, photocatalysts being used in industry consist of powder-like nanoparticles. These nanoparticles are usually used by making a suspension in aqueous solution, which makes it difficult to reuse these catalysts. The recycling of the theses catalysts would only be possible unless some accessorial means such as high-speed centrifuge is provided to separate it from the treated solution. This complexity in recycling would make them discouraging in practical applications

irrespective of having high catalytic activity for the degradation of organic pollutants. However, the synthesis of ZnO nanostructures on substrate makes them suitable to reuse for several time without any kind of recycling of nanostructures from the solution. This in turn will reduce the cost of operation for the degradation process

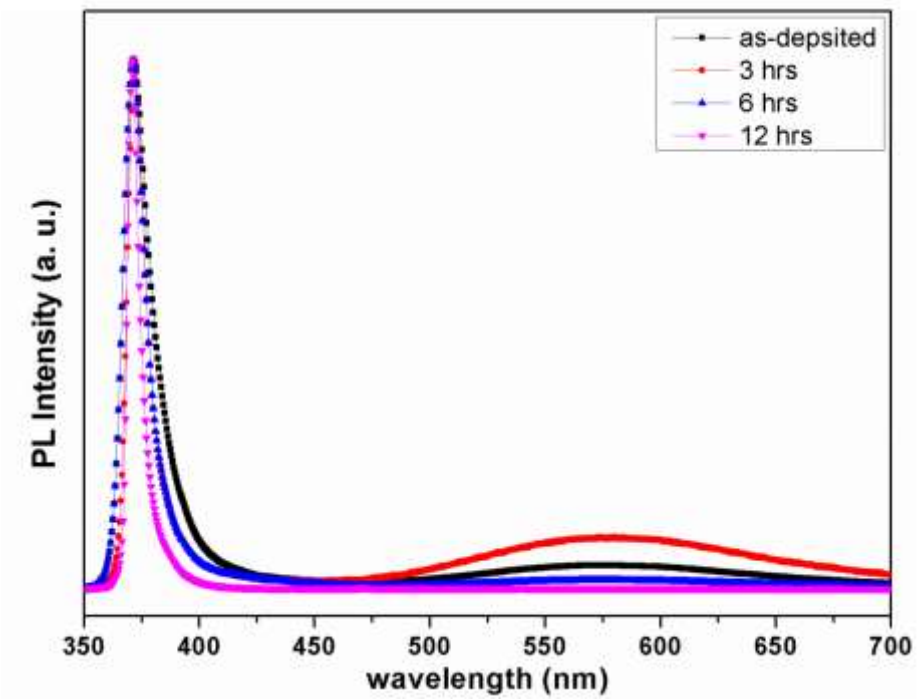

Figure 6-14 PL spectra of pure ZnO and Au /ZnO nano-composites

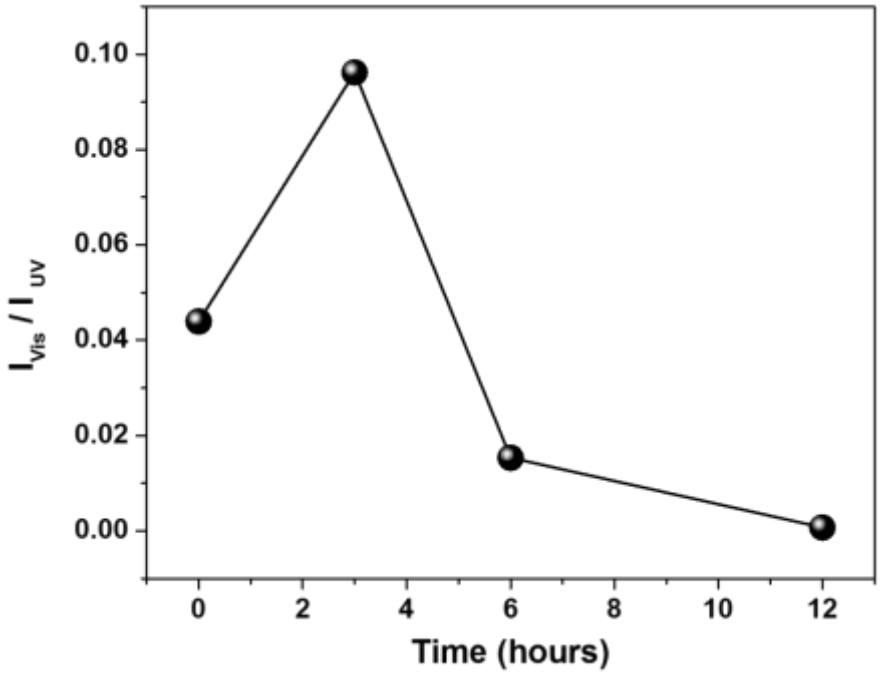

Figure 6-15 Plot for the ratio between the defect emission intensity to UV emission intensity.

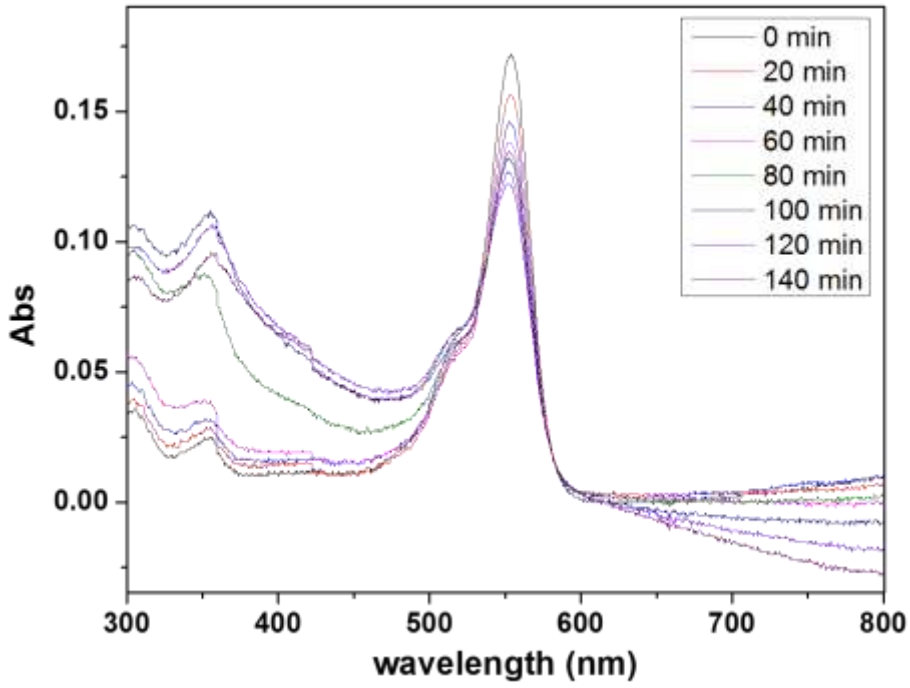

Figure 6-16 UV–vis absorption changes of Rh.B (10 M) in the presence of pure ZnO NRs in different UV irradiation time.

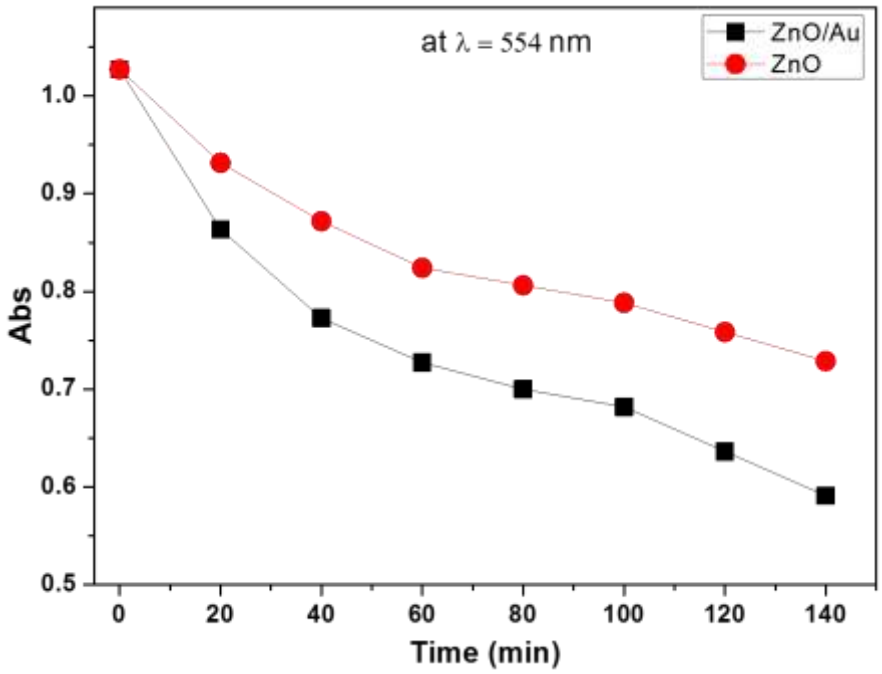

Figure 6-17 Photocatalytic degradation kinetics of the MO aqueous solution of the synthesized samples.

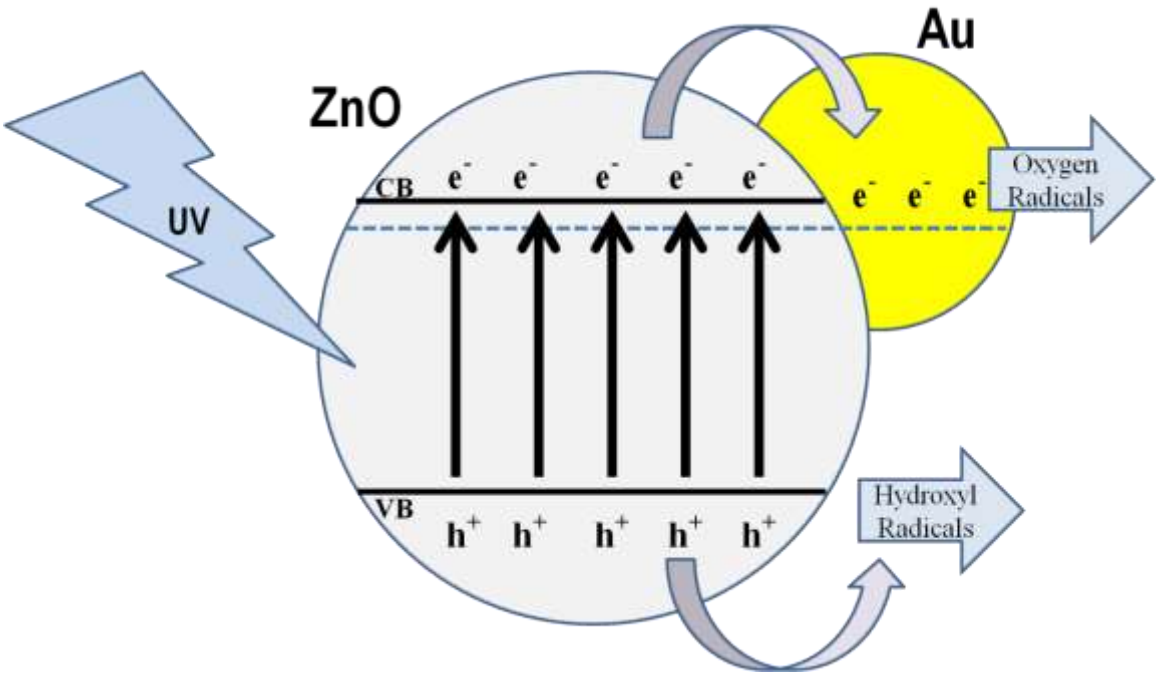

Figure 6-18 Schematic illustrations for the photo-induced charge separation of the Au/ZnO nano-composite structures.

6.3 Conclusions:

In Summary, a unique and simple method has been adopted to synthesize the Au decorated ZnO nanorods. Potassium iodide solution has been come out with an exceptional ability to etch ZnO nanorods surface to provide states for the formation of Au nano-particles. The size of the Au nanoparticles increased as a function of time for which nanorods immersed in the HAuCl4 solution. The defect emissions in the luminescence spectra have also minimized by the increased coverage of the ZnO nanorods by Au particles. The surface defects produced by KI might have been covered by the Au particles which make possible to suppress these defect emissions. In the same way, the photocatalytic activities have also been enhanced by the gold deposition. These properties make these nanostructures a wonderful candidate for optical devices and for chemical industry for photocatalysis.

7 RF Sputtered ZnO Thin Films

Zinc Oxide is a prospective semiconductor material for thin film optoelectronic [260-262] and piezoelectric [263-265] devices, due to its wide band gap (3.37 eV) and built-in piezoelectricity for the wurtzite crystal structure. Large exciton binding energy (about 60 meV) permits excitonic recombination at elevated temperatures and makes ZnO a prospective candidate for light emitting devices (LED) in ultraviolet and visible regions [261]. It can also endure higher powers because of the higher breakdown voltage. Such variety in properties make ZnO to be used in various device applications, such as solar cell, UV lasers, transparent conductive contacts, varistors, thin film transistors, laser diode, etc.

There are numerous means of deposition of ZnO thin films including molecular beam epitaxy (MBE) [266], pulsed laser deposition (PLD) [267], chemical vapor deposition (CVD) [268], metal organic chemical vapor deposition (MOCVD) [269], ion beam deposition [270], radio frequency (RF) magnetron sputtering [271] and atomic layer deposition (ALD) [272].

RF magnetron sputtering provides high deposition rate, deposition at low substrate temperature, good adhesion of the film to the substrate and the simple and less expensive apparatus [273].

The morphology, composition and properties of ZnO thin films are affected by many factors involved in the growth process such as choice of substrate, growth temperature, rate of sputtering and gas flow rates, etc. Oxygen in the environment affects the characteristics plasma, rate of sputtering, as well as, stoichiometry of oxide film. It is well established that amount of oxygen vacancies in the ZnO films effects the luminescence and the optoelectronic response of ZnO. This chapter presents work performed on ZnO thin films, prepared by RF magnetron sputtering. Particular emphasis has been laid on the role of oxygen partial pressure on the crystalline quality of the films.

7.1 Experimental Procedure:

The ZnO target for the sputter deposition was prepared using ZnO powder with 99.99% purity. The ZnO powder was pulverized thoroughly for two hours, and then a pellet of 50 mm diameter and 3 mm thickness was prepared with subsequent sintering at 1200 ℃ for 12 h. ZnO films were deposited on the c-plane sapphire substrates. The substrates were cleaned subsequently with acetone, ethanol and deionized water each for 10 minutes before deposition. RF magnetron sputtering technique was employed to deposit ZnO thin films. The deposition chamber was evacuated to a base pressure of 5.5×10^{-4} Pa before deposition. Substrates were placed at the substrate holder 8 cm away from the ZnO target and the deposition temperature for the ZnO was kept at 600 °C. The Argon gas (99.999% pure) was introduced into the chamber as sputtering medium. The Argon to Oxygen ratio was varied as given in Table 1. Pre-sputtering was performed for about 10 min to clean the surface of the target. The total working pressure during the deposition was kept at 1 Pa and the deposition time was 4 hours.

The crystal structure of both samples was analyzed using Bruker D8 Discover x-ray diffractometer equipped with Cu Kα line (0.1541 nm). The thickness and composition thin films were measured by Rutherford backscattering spectroscopy (RBS). The measurements was performed using 5UDH-2 Pelletron (5 MV Pelletron Tandem Accelerator) with He^{2+} beam with average energy 2 MeV. The analysis was performed by keeping the scattering angle at 170°. All RBS measurements were made using Cornell geometry. Cross-sectional and Surface morphology of the films were investigated by field emission scanning electron microscope (FEI Nova NanoSEM 430). Optical transmittance spectra of the ZnO films were obtained at room temperature using Mapada UV-3200PC Spectrophotometer in the wavelength range of 200 nm to 800 nm.

7.2 Results and Discussion:

The morphology and growth pattern of the ZnO thin films has been studied by taking the cross-sectional images by scanning electron microscopy (Fig 7-7). The cross-sectional views of these thin films have shown clearly columnar growth. The films for which oxygen supplied during the deposition process, the deposition rate has been

decreased as a function of oxygen partial pressure in the deposition chamber. The columns seem to form due to growth of ZnO along c-axis.

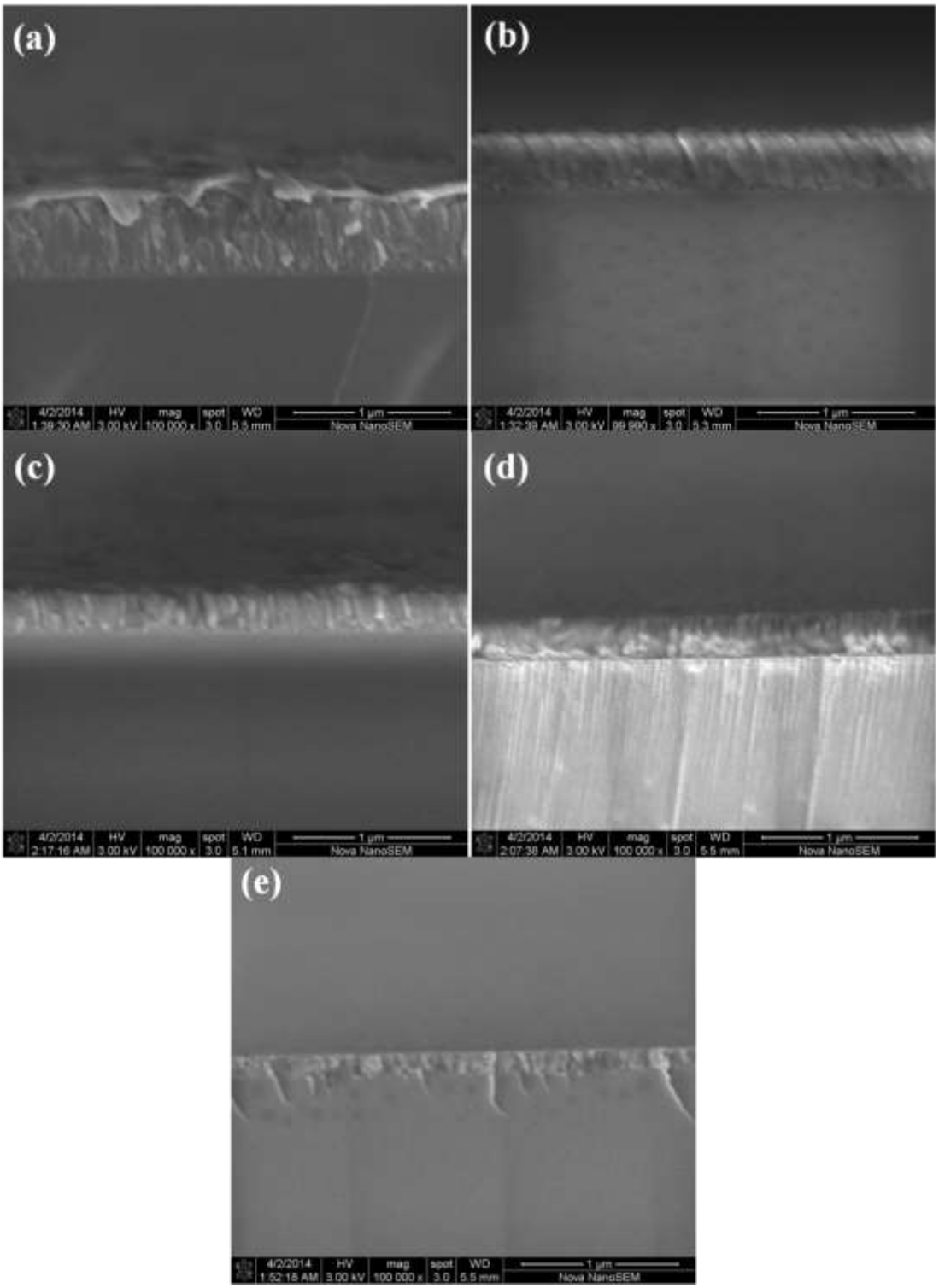

Figure 7-1 Cross-sectional SEM images of ZnO thin films deposited with, (a) 0% oxygen, (b) 0.5% oxygen, (c) 5% oxygen, (d) 10% oxygen and (e) 20% oxygen.

The RBS results along with their simulated fitting are shown in Fig. 7-2 to 7-6. The Zn edge, corresponding to the energy of the scattered particle form Zn nuclei at the surface has been indicated by an arrow around channel # 1400. The width of the Zn band varies for different films. The band width is related with energy loss for the incident particles travelling through the film along with the energy loss for the scattered particle moving outward. Accordingly, the band width relates with film thickness. The other aspect is the edge for the counts for the particles scattered from the substrate. This edge is shifted to lower energies (i.e., smaller channel #) for the thicker films.

The relative intensity of Zn, oxygen and substrate, width of the bands and position of substrate counts on energy scale also provide with the basis to determine the stoichiometry of ZnO films. The details of thickness and composition of zinc and oxygen in the deposited thin films estimated from simulated fitting of RBS spectra are given in table 7-1. It may be seen that the zinc to oxygen ratio in the deposited films varied as a function of oxygen to argon ratio in the sputtering chamber. ZnO films deposited by sputtering in pure argon atmosphere contain about 45% oxygen, and the oxygen to zinc atomic ratio in deposited thin films becomes unity when oxygen in the sputtering chamber reaches a threshold level of 10%. The other parameter which has been influenced by oxygen in the chamber is the thickness of the deposited films. Decrease in thickness with increase in oxygen partial pressure in the sputtering environment seems partly related to the reduced sputtering yield due to lower mass of oxygen than argon [274]. This alone does not explain complete behavior. For instance, environment still contain much larger quantity of argon than oxygen, while the film thickness is several times lower than in pure argon. One possibility is the lower oxygen at the target surface due to preferential sputtering. Due to excessive broken bonds, in the oxygen-deficient surfaces in case of argon atmosphere, sputtering yield might be higher as compared with relatively oxygen-rich environment.

The X-ray diffraction analysis of these ZnO thin films has been performed to judge the crystalline quality of thin films. Fig. 7-7 shows the results of detector (2θ) scans. It can be seen in the detector scan (Fig. 7-7) that 002 peak of wurtzite ZnO for most of the films lies around 34.4 degrees. Corresponding to the peak positions of 002 peak, rocking curve have been obtained as shown in Fig. 7-8. The rocking curves are

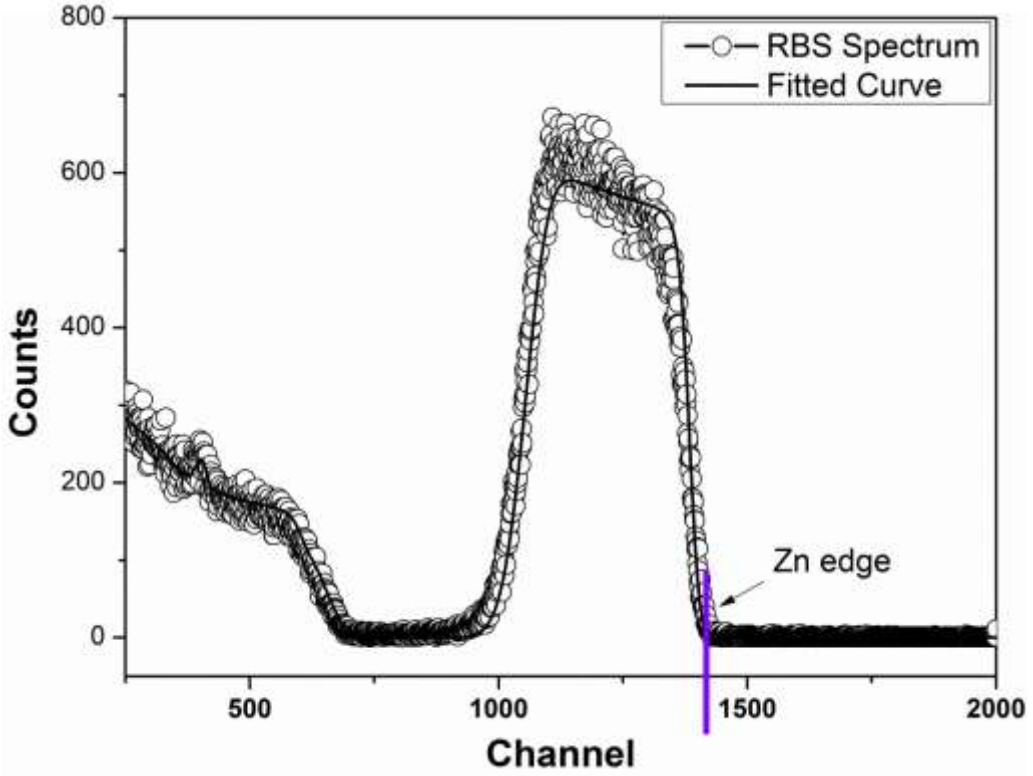

Figure 7-2 RBS spectrum of ZnO film sputtered by pure argon in sputtering chamber.

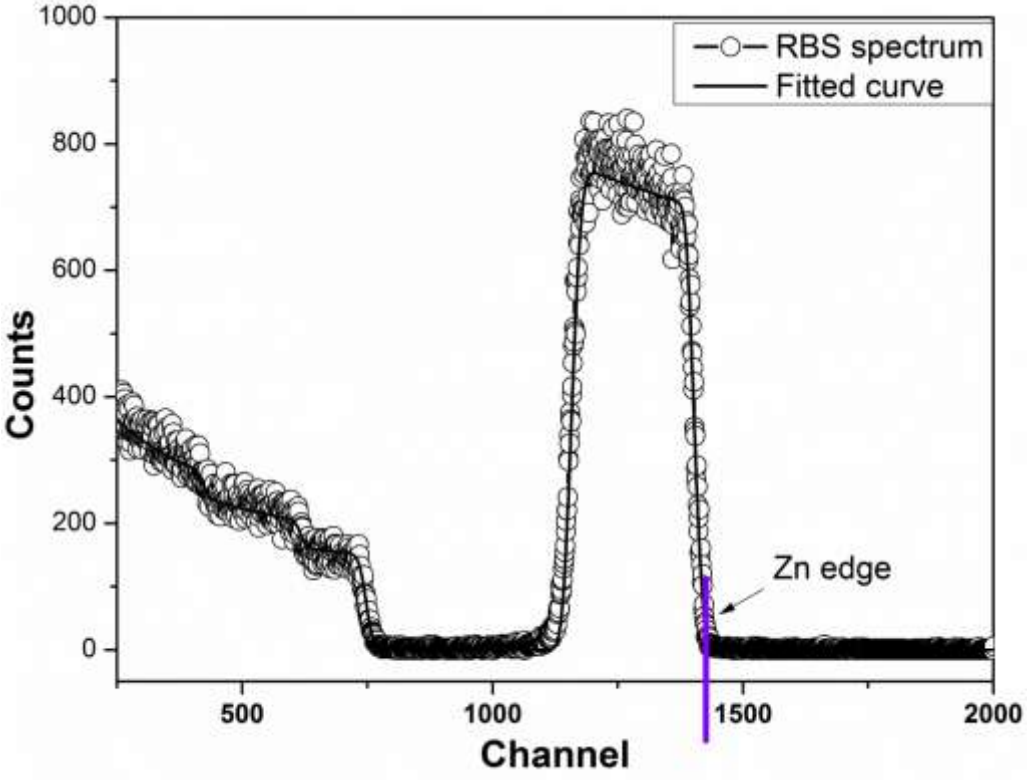

Figure 7-3 RBS spectrum of ZnO film sputtered by 0.5% oxygen in sputtering chamber.

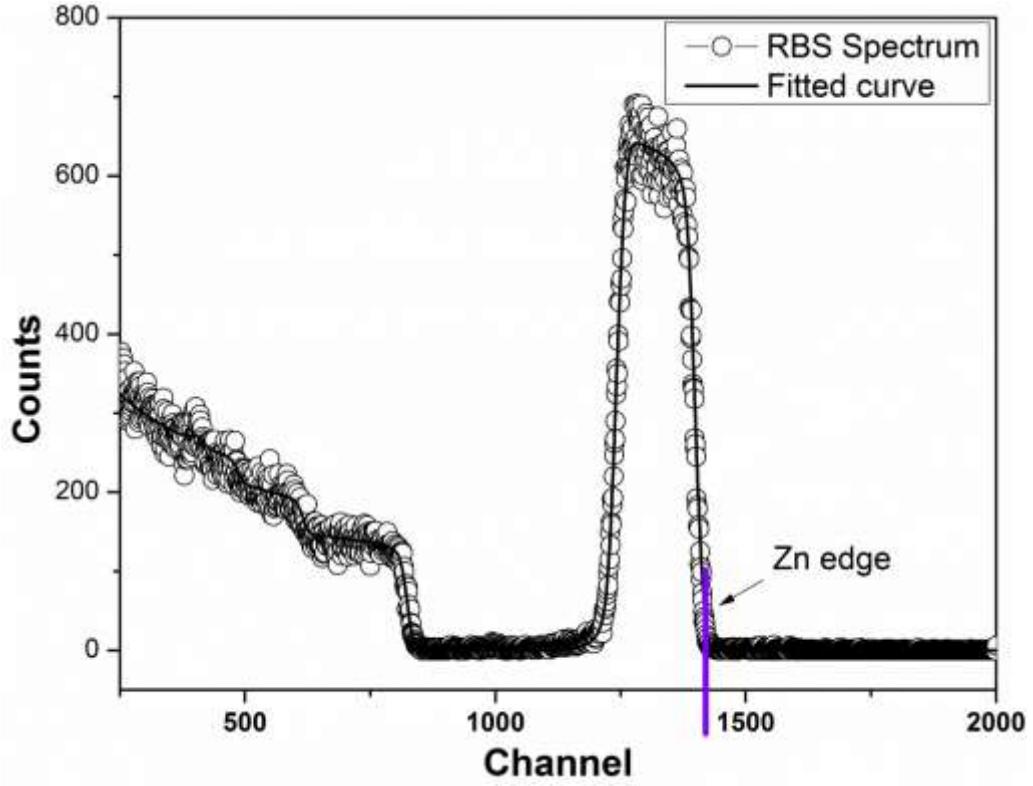

Figure 7-4 RBS spectrum of ZnO film sputtered by 5% oxygen in sputtering chamber.

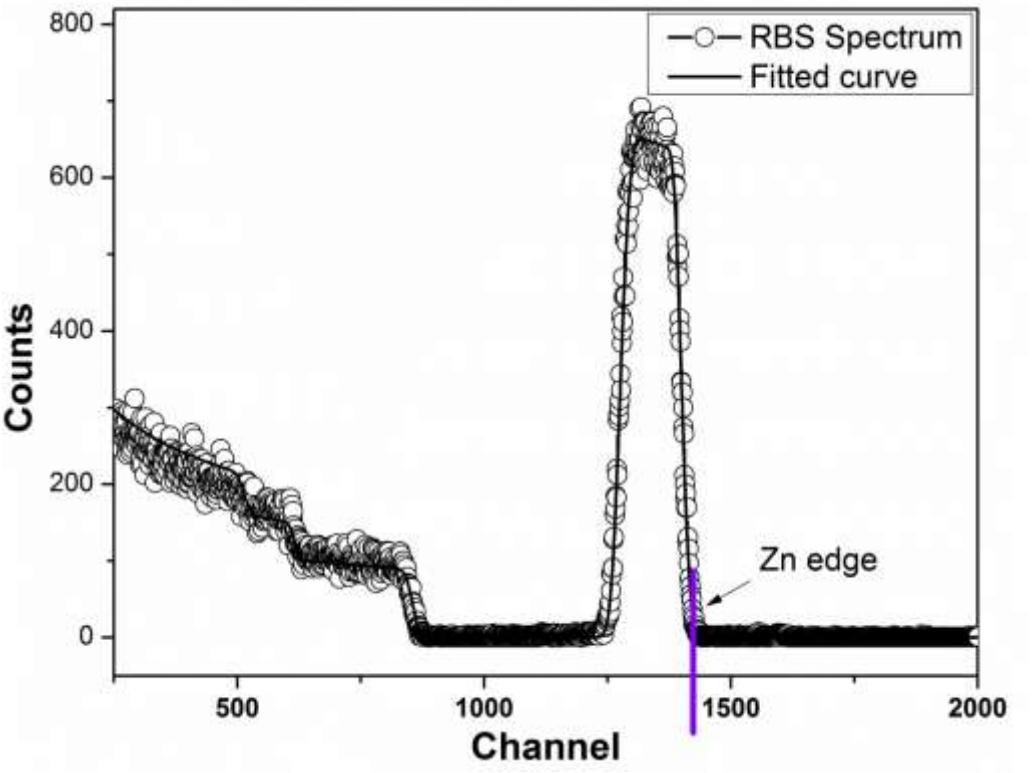

Figure 7-5 RBS spectrum of ZnO film sputtered by 10% oxygen in sputtering chamber.

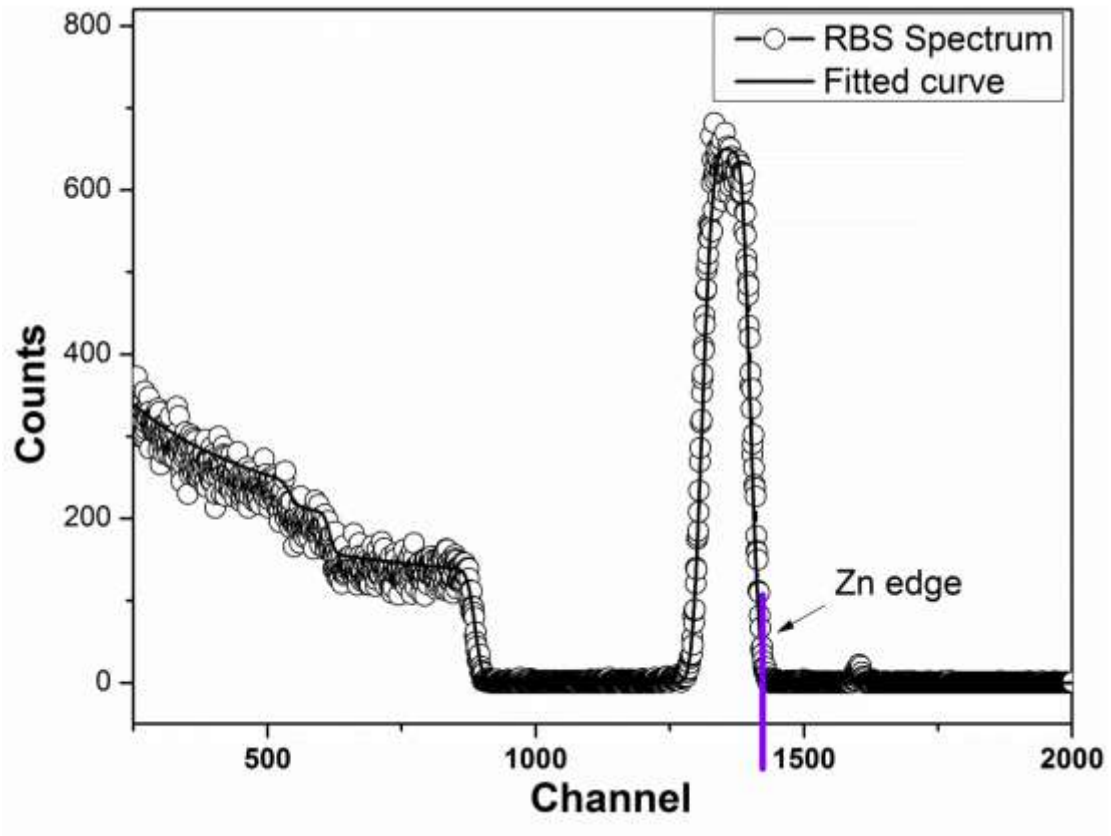

Figure 7-6 RBS spectrum of ZnO film sputtered by 20% oxygen in sputtering chamber.

Table 7-1 Ratio of Sputtering gases, estimated film thickness by RBS and structural parameters.

Sr. No	Ar/O_2 (%)	Thickness (nm)	Composition estimated by RBS (at%)		FWHM (rocking curve)	Lattice parameter c (Å)
			Zinc	Oxygen		
	100/0	477	55	45	3.5	5.2077
	99.5/0.5	365	56	44	5.2	5.2078
	95/5	226	52	48	2.9	5.1933
	90/10	175	50	50	2.54	5.2079
	80/20	127	50	50	2.21	5.2102

obtained by keeping 2θ constant and scanning on the omega scale. In this scan, only those crystals can contribute to diffraction for which incident and diffraction beams make an angle of θ with the diffraction plane, i.e., 002 in this case (2θ = 34.4°). For a polycrystalline sample with random orientation, a peak should not be observed in omega scan; rather a uniform intensity should appear as a function of omega. As can be seen in Fig 7-8, counts start appearing at 12°, rise till an angle of 17° followed by a decrease in intensity up to 22°. The FWHM of peak in omega scan has been shown in table 7-1. The FWHM lies in the range of 2 to 5°. As maximum number of crystals contributes to omega($17.2 \sim \frac{2\theta}{2}$), hence most crystals have placed parallel to sample's surface. For the FWHM of 2°, about 60 percent crystals should have grown within a maximum misorientation of 1° with respect to sample's normal, for the sample grown at 20% oxygen in the sputtering environment. For pure argon this should be of the order of 1.7°. The FWHM tends to decrease with oxygen in the atmosphere which apparently reflects improved epitaxy/texture.

Phi scan of ZnO (104 peak) thin films has been carried out in order to investigate the in-plane orientation of grown films in comparison with sapphire substrate. The typical phi pattern (Figure 7-9) of ZnO film deposited by pure argon gas exhibits six distinct peaks separated by 60° associated to six fold symmetry of wurtzite ZnO. But there were some difficulties to isolate 104 diffraction peak in case of other ZnO films because of lean intensity.

Figure 7-10 is a typical XRD phi scan for the (101) peak of ZnO films. The phi scans have been collected by keeping the omega ~ 18.13°, 2θ ~ 36.26° and Chi at 61.5°. Mutual misorientation of ZnO crystals in the phi-axis is not pronounced, as confirmed by the 6-fold rotation symmetry of the101 reflection (pointed as **a** in figure 7-10). The intensity of (101) peaks has been reduced as the oxygen partial pressure for the deposition increases. This reduction in intensity might be correlated with the reduction in the film thickness of the respective samples. In addition with 6 peaks from ZnO crystal, there are some other peaks which also appear in the phi patterns. The sharp peak (**b** in figure 7-10) present between every two **a**-type peaks, repeats itself after every 60° and this has arisen from the sapphire substrate. The same are also seen in the bare sapphire substrate (figure 7-11). The low intensity reflection with six-fold symmetry might be due to surface region. In addition to this 6-fold symmetry

from sapphire substrate, 3 pairs of some unknown peaks also appeared in the phi scan. One pair marked by c_1 and c_2 exhibits 3-fold symmetry about sample's normal (c-axis). As oxygen in the chamber increases, relative intensity of these pairs increases on the phi scan. It appears that some trigonality develops with increase in oxygen partial pressure. Thinner films formed at higher oxygen partial seem to have been influenced by the trigonal substrate and associated epitaxy stresses. This tend to introduce some trigonality in the crystals that are misoriented with hexagonal crystals at 10's of degrees, which mean that they have a drastically different orientation relationship with the substrate.

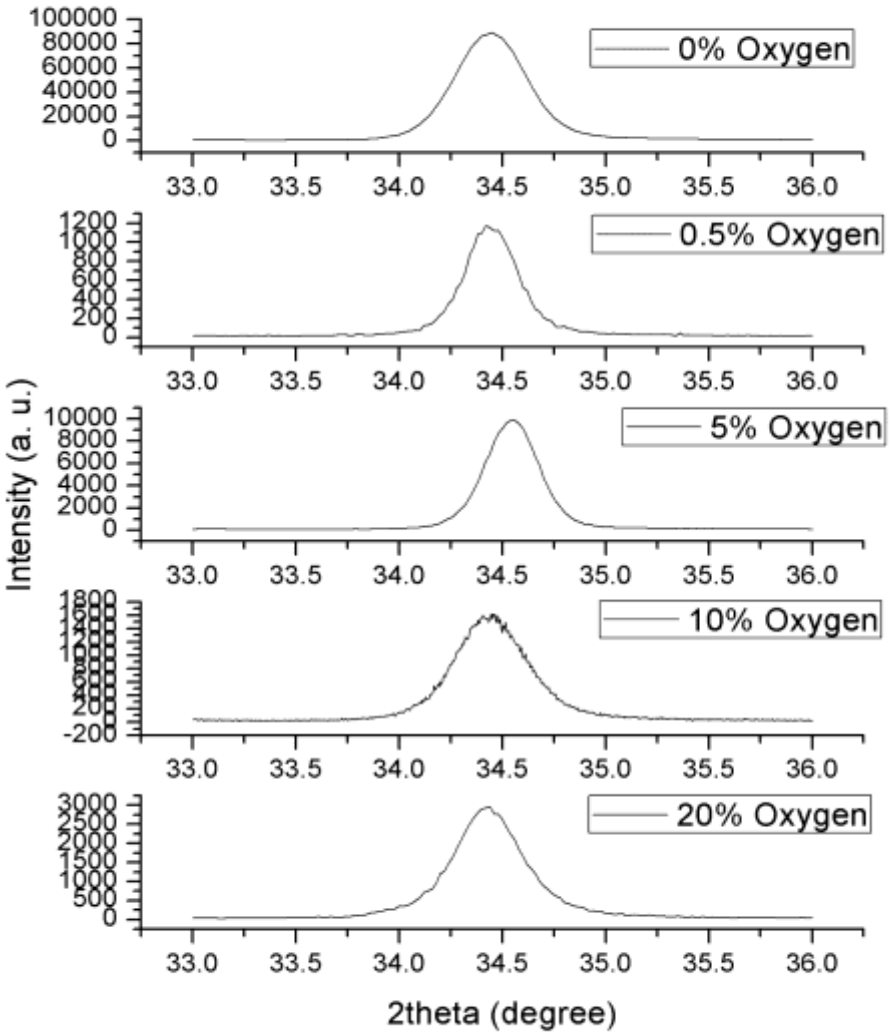

Figure 7-7 XRD detector scan showing the 002 peak of different ZnO thin films deposited in various oxygen partial pressures.

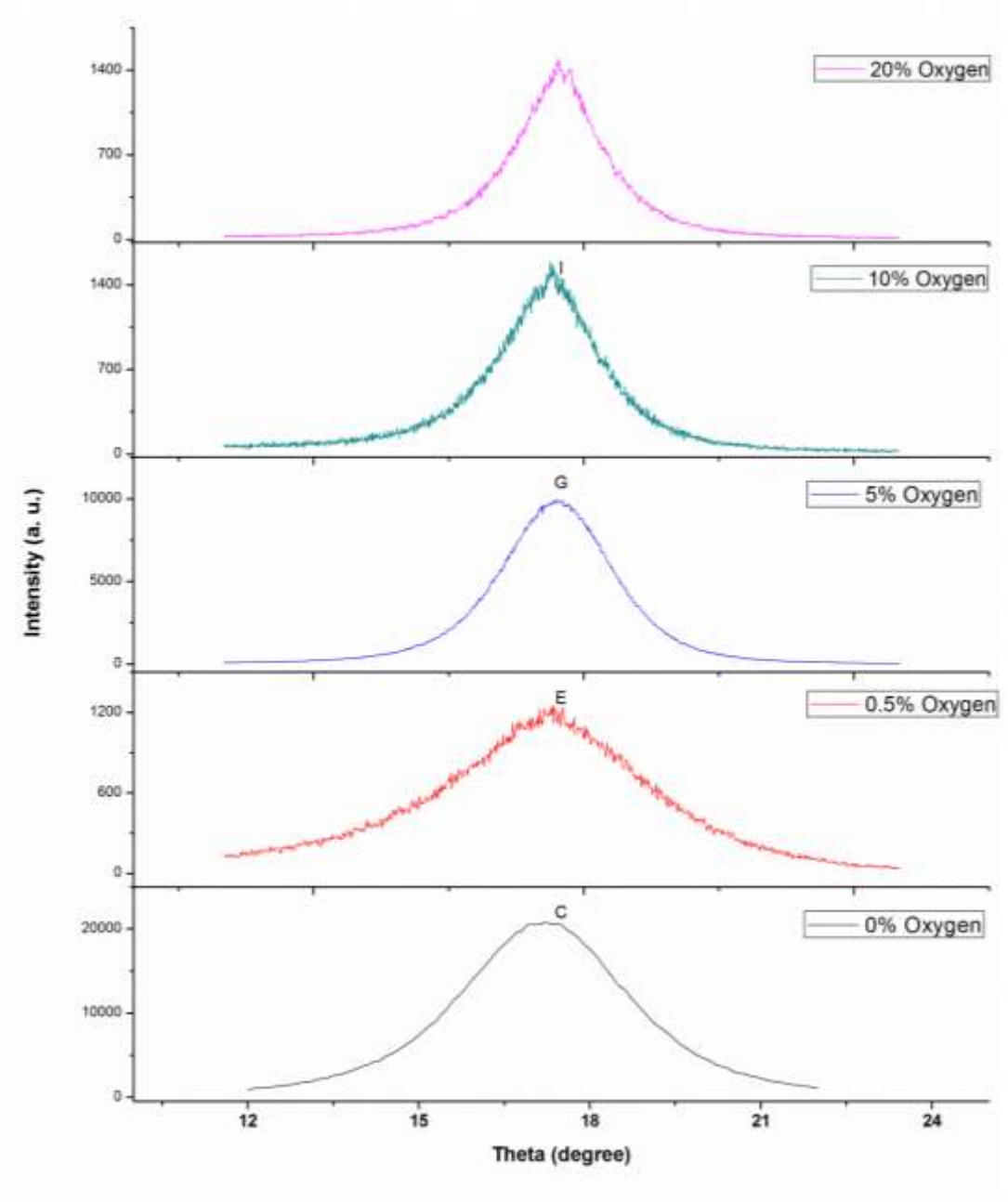

Figure 7-8 XRD rocking curve of 002 peak of different ZnO thin films deposited in various oxygen partial pressures.

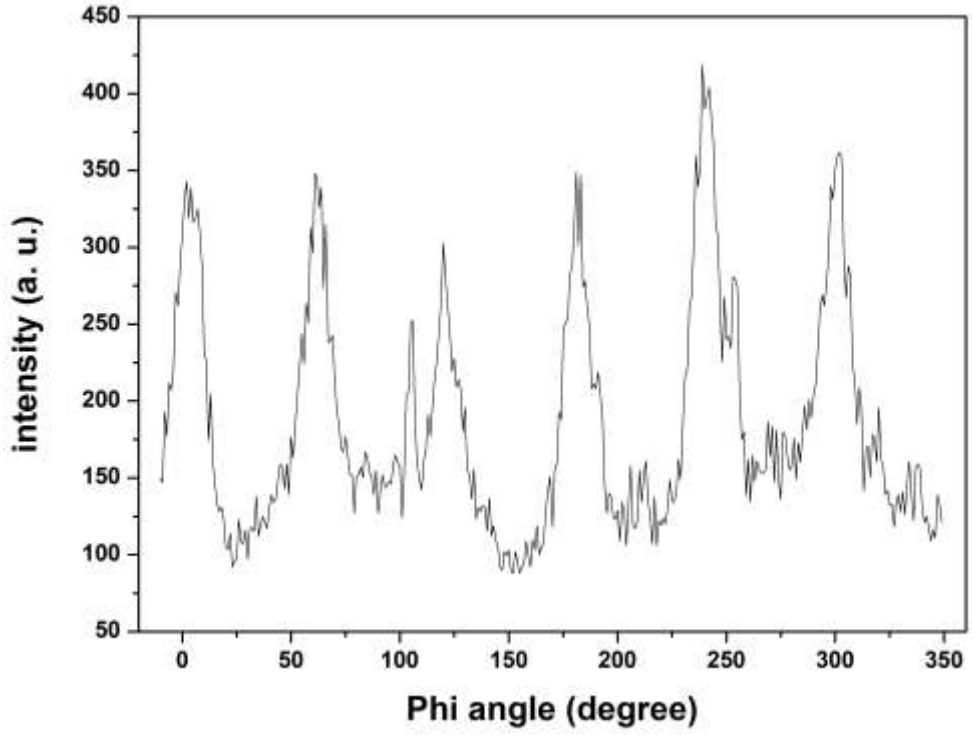

Figure 7-9 Phi scan of ZnO (104) diffraction peak.

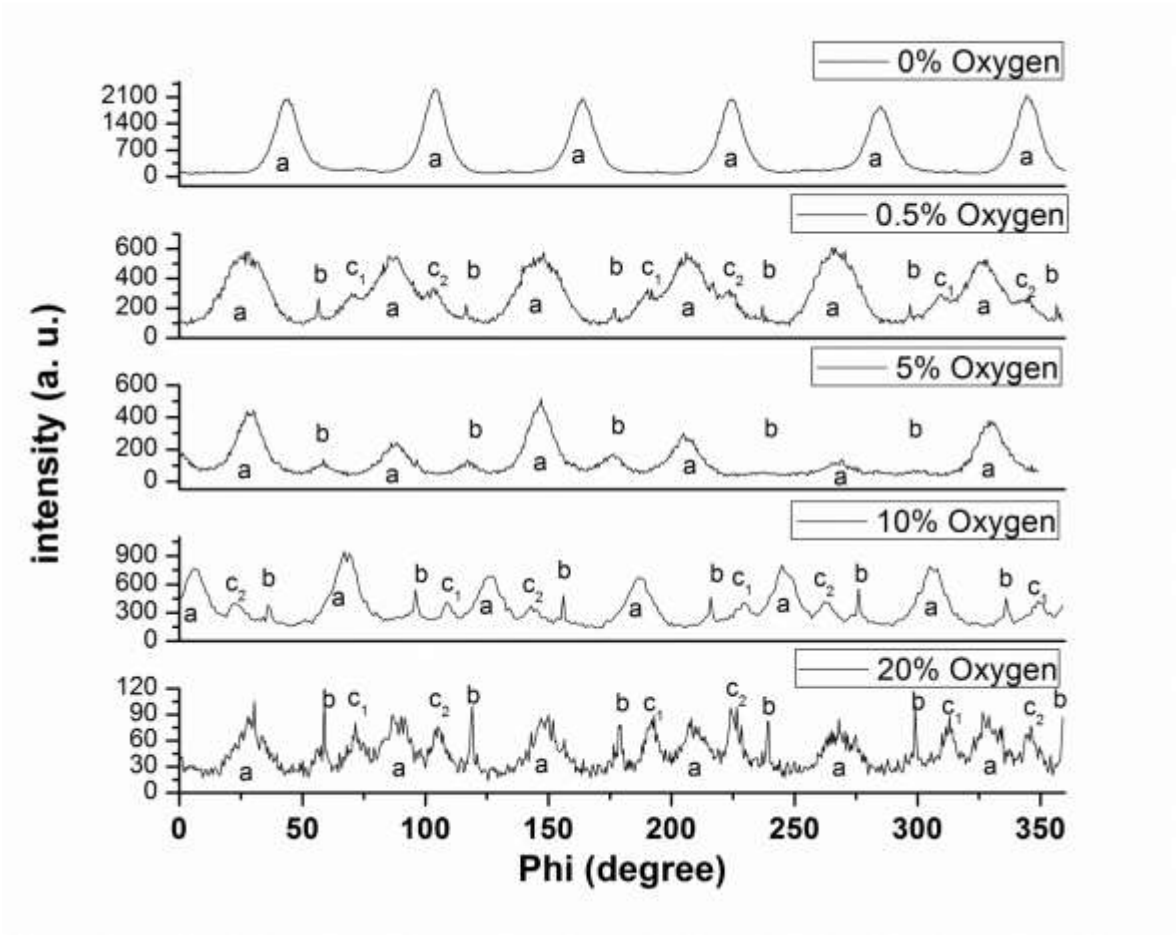

Figure 7-10 Phi scan of 101 peak of different ZnO films.

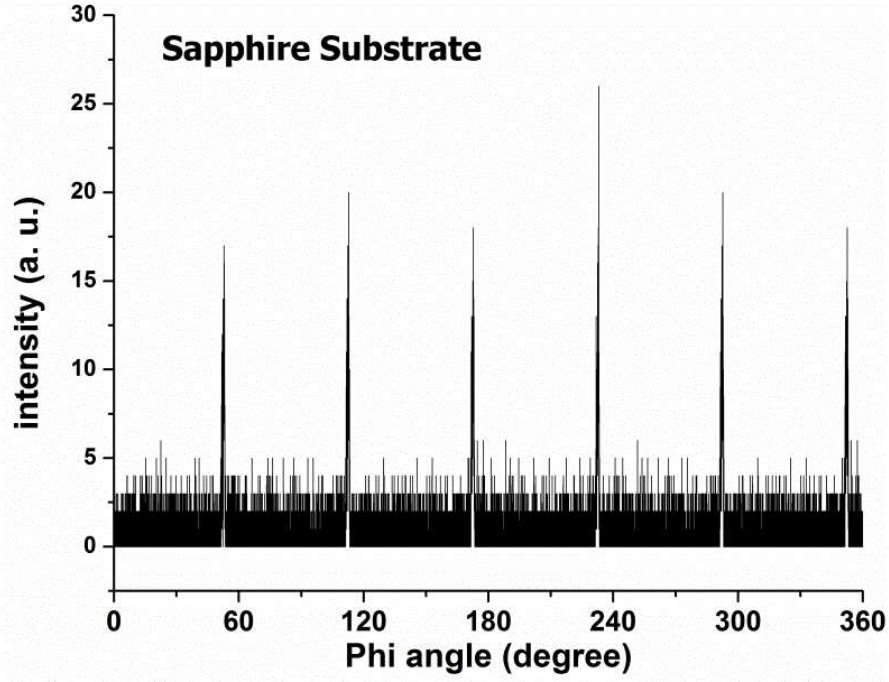

Figure 7-11 Phi scan of Sapphire substrate taken at Chi angle 61.5 and theta 18.13 degrees.

Figure 7-12 shows the diffused reflectance spectra of ZnO thin films sputterd at various oxygen partial pressures. The fringe patterns of optical reflectance in the visible wavelength range have shown a random trend. The overall reflectance has initially decreased below a 20% value for 0.5% and 5% samples in comparison with that sample deposited with pure argon gas. But for the two samples deposited at higher oxygen partial pressure the overall reflectance has raise about 25% value. Similar trend has been seen for the case of absorption edge in the reflectance spectra. The initial small insertion of oxygen made the absorption edge to follow red shift as compared to the 0% sample while the 10% and 20% samples clearly exhibit a blue shift. The blue shift in the absorption edge is considered to be the signature of good crystalline nature of ZnO thin films.

The product of carrier concentration N and the mobility μ of carriers in the films in the visible region is found to be a function of film thickness x and reflectance R and can be calculated by the given relation.

$$\mu N = \frac{4.\varepsilon_{\circ} c}{e.x}\left(\frac{1}{1-R}\right)$$

The product values of the ZnO films have shown a systematic rise as a function of the thickness of the films (Fig. 7-13). This trend points towards the less resistivity due to the better crystallinity and less hindrance to the carrier mobility in their movement through the thickness of the samples. The increase in the crystallinity of the ZnO films is reason for increase in the mobility of the carriers as the oxygen increases in during the deposition process.

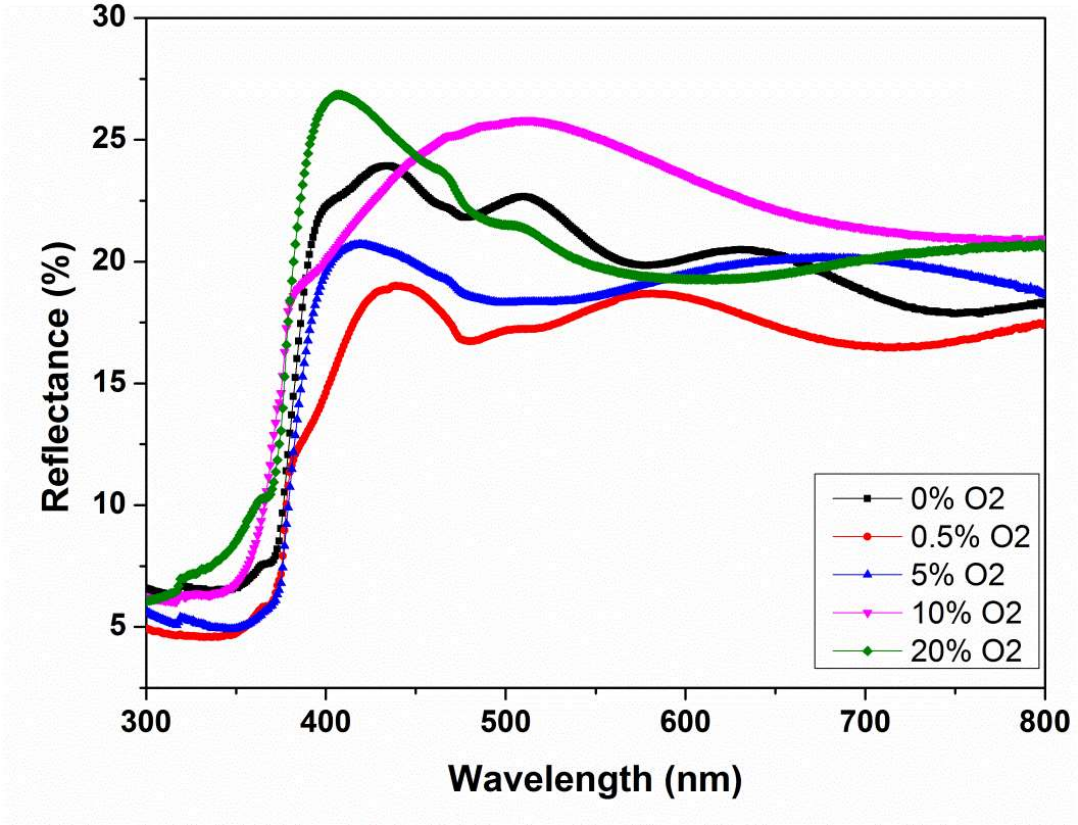

Figure 7-12 Diffused reflectance spctra of ZnO thin films.

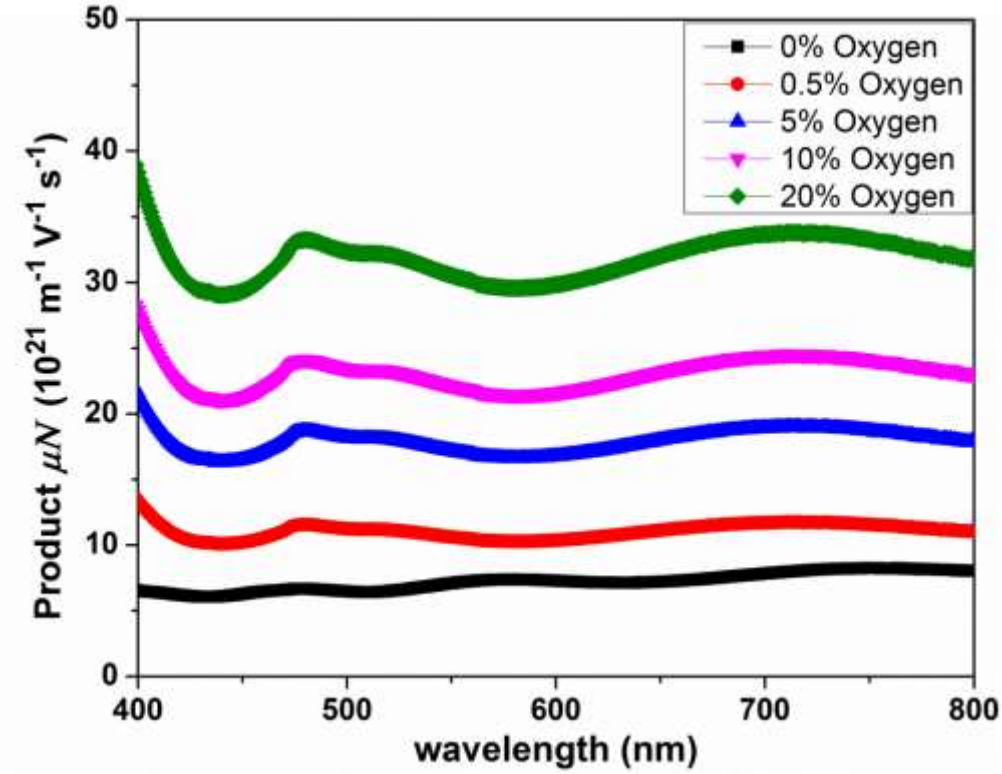

Figure 7-13 Plot for the product of carrier concentration and mobility vs wavelength

7.3 Conclusions:

From the above results it can be concluded that oxygen partial pressure during the sputter deposition have played a significant role on the structural and optical properties of ZnO thin films. The deposited ZnO films consist of the vertically aligned columns. By increasing the Ar/O_2 ratios in the sputtering chamber during the deposition process, deposition rate has been reduced that in turn responsible for thinner film deposition. The less percentage of heavy ions is the main cause of such reduction of deposition rate. The Zn to oxygen ratio in deposited thin films reached to unity after a threshold of 10% oxygen in the sputtering environment. The XRD rocking curves of the films have pointed towards improved crystalline quality of the thin films as a function of oxygen partial pressure. The ZnO films exhibited the tendency to grow in wurtzite structure with six fold symmetry during phi scan of ZnO 101 XRD peak. In contrast, a signature of trigonal symmetry has also appeared in the phi scans that suggest the formation of some misoriented crystals near the film-substrate interface. The mobility of the carriers in the ZnO films has also found to increase with a rise in oxygen pressure.

8 High Crystalline Quality PLD and Sputtered ZnO Films

Zinc Oxide (ZnO) is one of the widely used semiconductor materials due to its large and direct band gap (3.37 eV) making it suitable for a variety of electrical and optical device applications [275-276]. Due to its large exciton binding energy (60 meV) at room temperature in comparison with GaN (26 meV), it can be employed for many potential applications in optoelectronic devices such as solar cells, gas sensors, lasers, wave devices, luminescent materials, etc [277]. Presently most of the industrial applications employ the wide band gap semiconductors especially GaN (a III-V group semiconductor) and its alloys. However, GaN based light emitting diodes (LEDs), as well as, laser diodes (LDs) generally have higher threshold and are unable to work at higher temperature because of its small excitonic binding energy of about 26 meV. On the other, owing to better properties of ZnO at elevated temperatures and higher excitonic binding energy, it is a good choice to replace GaN for working in harsh environment and at high temperatures [22, 278].

The larger exciton binding energy of ZnO makes it a promising material for exciton emission at room temperature under low binding energy. That's why; it has potential use for short wavelength optoelectronic devices. The increased usage of short-wavelength optoelectronics devices in industry has forced the researchers to explore the structural, optical, electrical and optoelectronic properties of ZnO at room temperature as well as at elevated temperatures. Henceforth, there are continuous efforts to report synthesis and characterization of ZnO in the form of bulk material as well as thin film. Zu *et al.* [279] investigated the optical emission properties of ZnO thin films prepared by molecular beam epitaxy at room temperature for optoelectronic applications. They concluded that optical response of ZnO thin films covers two regions: one is the excitonic near the band edge and the other is deep level emission due to defects in the visible range. Deep level emission arises due to intrinsic defects such as oxygen vacancies, interstitial, zinc vacancies, extrinsic impurities, etc [233]. Generally, UV emission is thought to be due to exciton transition [280]. Anyway, the

precise origin of visible emission is still under debate. It is generally well accepted that the optical, electrical and optoelectronic properties of ZnO films are sensitive to crystalline quality and smoothness of the films. Consequently, most of the work has been performed on controlling the defects of ZnO thin films. It has been often seen that the improvement in the crystal quality effects a sharp and strong UV emission and a suppressed and week emission in the visible region [201, 281-282].

The p-type doping of ZnO faces difficulties while this material exhibits intrinsically *n*-type conductivity and very high electron densities of up to 10^{21} cm^{-3}. It is difficult to obtain low-resistivity reproducible *p*-type ZnO because of the effects arising from the presence of native defects and hydrogen impurities [78]. Several groups have postulated the use of *p*-type ZnO doped with nitrogen, arsenic, or phosphorus [283-285]. However, the choice of dopant and growth technique remains controversial and the reliability of *p*-type ZnO is still under debate [286]. As an intrinsic n-type material, ZnO needs a p-type semiconductor material to make a p-n junction for LED. Stable and reproducible p-type conductivity for ZnO is still a very difficult task. Some groups have reported the deposition of p-ZnO and used it for making homojunction with n-ZnO to get an LED [287-290]. Based on above-mentioned limitations, many researchers have used GaN [291-294], Si [295-297] and NiO [298-300] as a p-type material for combination with ZnO to have a successful p-n junction diode. Unlike other p-type materials, GaN has the wurtzite crystal structure resembling that of ZnO with comparatively very low lattice mismatch ~1.8% [301] and a comparable band gap. Moreover, GaN is technically more stable for longer duration than all its counterparts.

ZnO films have been deposited by various techniques such as evaporation [302], molecular beam epitaxy [108], pulsed laser deposition [17], sputtering, metal organic chemical vapor deposition [9, 18], electrodeposition [303], etc. Nevertheless, Pulsed laser deposition (PLD) has advantages such as oriented growth of films (at low substrate temperature), high deposition rates, deposition at high oxygen pressure and good quality of films. Whereas, sputtering offer good adhesion, high deposition rate, high degree of crystallinity with (002) peak (and rocking curve having less full width at half maxima), high optical transmittance and sputtering of almost any compound. RF Magnetron Sputtering [293, 304] and PLD [301] have been employed by different groups to make heterojuction of n-ZnO on p-GaN substrate.

These ZnO films have also been deposited on the p-type GaN substrate to compare their morphology and investigate and correlate the structural, optical and electrical characteristics of ZnO films. Growth patterns of ZnO heterostructures on GaN were probed for respective deposited films in order to understand the basic phenomenon behind various optical and electrical properties. ZnO/GaN heterojunction grown by PLD has been found to be better in efficiency (in terms of higher current and lower threshold voltage) in comparison with RF magnetron sputtering owing to its inherent controlled growth conditions.

In chapter 7, it has been seen that RF sputtering can be employed to produce high quality ZnO thin films on sapphire substrate at oxygen to argon ration of 10 and 20%. It was however, difficult to grow thin films at a reasonable deposition rate. In the present chapter, another technique has been employed, i.e., PLD to grow thin films of ZnO. Its characteristics have been compared with ZnO thin films grown by RF sputtering in argon.

8.1 Experimental:

The ZnO target for the sputter deposition was prepared using ZnO powder with 99.99% purity. The ZnO powder was pulverized thoroughly for two hours, and then a pellet of 50 mm diameter and 3 mm thickness was prepared with subsequent sintering at 1200 ℃ for 12 h. Two types of substrates were used in this study. For structural properties ZnO films were deposited on the c-plane sapphire substrate while the current-voltage study of the p-GaN/n-ZnO heterojunction were studied by depositing ZnO films on the commercially available p-Mg:GaN (carrier concentration ~ 5×10^{18} cm^{-3}) deposited on c-plane sapphire. The substrates were cleaned subsequently with acetone, ethanol and deionized water each for 10 minutes before deposition. PLD and RF magnetron sputtering techniques were employed in this experiment. The first sample was prepared by using PLD system (with Coherent COMPexPro 102 KrF laser, wavelength – 248 nm, max pulse energy = 400 mJ). The chamber was evacuated to a base pressure of 6×10^{-4} Pa before deposition with substrate temperature at 600 ℃ and target to substrate distance was maintained at 8 cm. A laser beam of 300 mJ with a frequency of 2 Hz was used to ablate ZnO target. The oxygen partial pressure during the deposition was kept at 2 Pa and depositing time was 60 min. Film

thickness (~180 nm) was measured by field emission scanning electron microscopy (FESEM). The second sample was deposited by the RF magnetron sputtering system using the same ZnO target. The deposition chamber was evacuated to a base pressure of 5.5×10^{-4} Pa before deposition. Substrates were placed at the substrate holder 8 cm away from the ZnO target and the deposition temperature for the ZnO was kept at 600 °C. The Argon gas (99.999% pure) was introduced into the chamber as sputtering medium. The pre-sputtering was performed for about 10 min to clean the surface of the target. The working pressure during the deposition was kept at 1 Pa and the deposition time for ZnO film was 6 hours. The thickness of the film was estimated to be ~860 nm during deposition.

The crystal structure of both samples was analyzed using Bruker D8 Advance x-ray diffractometer equipped with Cu Kα line (0.1541 nm). Surface morphology of the films was investigated by atomic force microscopy (Quesant Universal SPM, Ambios Technology, USA) in non-contact mode. Room temperature photoluminescence (PL) measurements were performed with 325 nm He-Cd laser line (Melles Griot Series 56) at 15 mW. Room temperature electrical properties were determined using Hall Effect measurement with van der Pauw configuration by the Accent HL-5500PC system. Optical transmittance spectra of the ZnO films were obtained at room temperature using Mapada UV-3200PC Spectrophotometer in the wavelength range of 200 nm to 800 nm. The current-voltage measurements for the ZnO/GaN heterostructures were obtained by using hp 4155A Semiconductor Parameter Analyzer in the voltage range of 10 to -10 V.

8.2 Results and Discussion:

Fig. 1 represents XRD patterns for the ZnO thin films deposited by PLD and RF sputtering techniques on c-plane sapphire substrates. Both samples exhibit a preferred (002) oriented growth along c axis. Similar results have been obtained by Lee *et al.* and Kumar *et al.* [305-306] for ZnO films prepared by PLD. To further investigate the film quality and crystallographic orientation, rocking curves for the (002) peak were obtained as shown in Fig. 8-2. These curves reveal the variation in the degree of texture in both samples. The full width at half maximum (FWHM) of peaks was calculated to be 1.87º and 4.75º for the PLD and sputter grown ZnO films,

respectively. The FWHM for the PLD sample is much narrower and which may be related with higher crystalline quality or improved orientation relationship with the substrate in comparison with the sputtered film.

Zhao-yang et al [307] have reported that the quality of the films improves with the increase in substrate temperature due to higher thermal energy/ diffusivity of the adatoms. In our case substrate temperature is same for both the films. Nevertheless, PLD technique is characterized by extremely high energy of the vaporized atoms in the plume. The energetic flux of incident atoms seems to provide additional energy to the atoms at the surface for higher crystalline quality of the film with excellent growth along c-axis. The tendency of high energy incident particles to relieve the internal stresses of the film, thereby improving the crystallinity is also in agreement with Aravind et al [308].

Fig. 8-3 illustrates phi scan of the ZnO (104) peak, which was employed to have some insight of in-plane orientation of both ZnO thin films in comparison with sapphire substrate. This peak was approached by suitably aligning the substrate with respect to diffraction geometry. As can be seen, both the samples exhibit six distinct peaks separated by 60º related with six-fold symmetry that clearly manifests the tendency of wurtzite ZnO to undergo epitaxial growth on single crystal c-plane sapphire. The sharp peaks with a FWHM of 6-8º for the PLD deposited sample depicts a picture of good epitaxial growth as compared to the RF sputtered sample in which the peaks are much broader and of low peak to background ratio. Kim *et al*. [309] reported the relatively high temperature deposited PLD ZnO films yields an improvement for in-plane and out-of-plane crystallinity.

Fig. 8-4 depicts the typical top view AFM images of the PLD and RF sputtered samples. The bar assists to present z-height variation in the sample's surface. It may be noted that z-height variation in case of PLD film is of the order of 15 nm, much smaller than about 50 nm in sputtered film. On x-y scale also the PLD film exhibits finer structure. The RMS roughness of PLD film is about 4.3 nm, which is much smaller than that for sputtered film, i.e., 12.9 nm. The surface roughness increases for sputtered films as compared to PLD prepared films showing non-uniform distribution of grain sizes clear from Fig. 8-4.

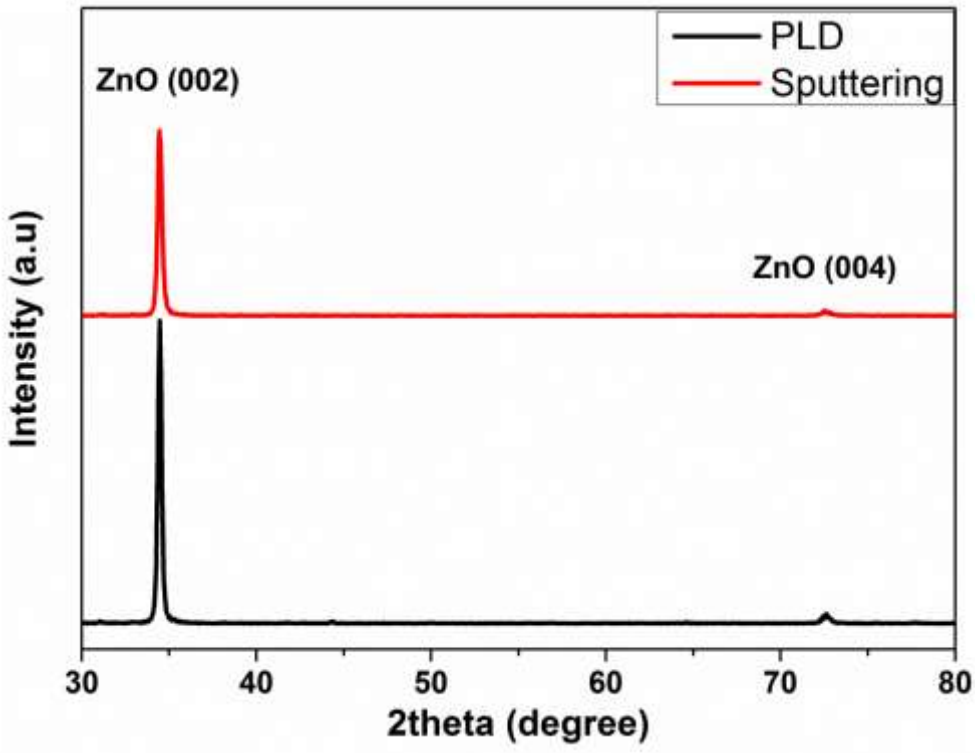

Figure 8-1 XRD patterns of ZnO films.

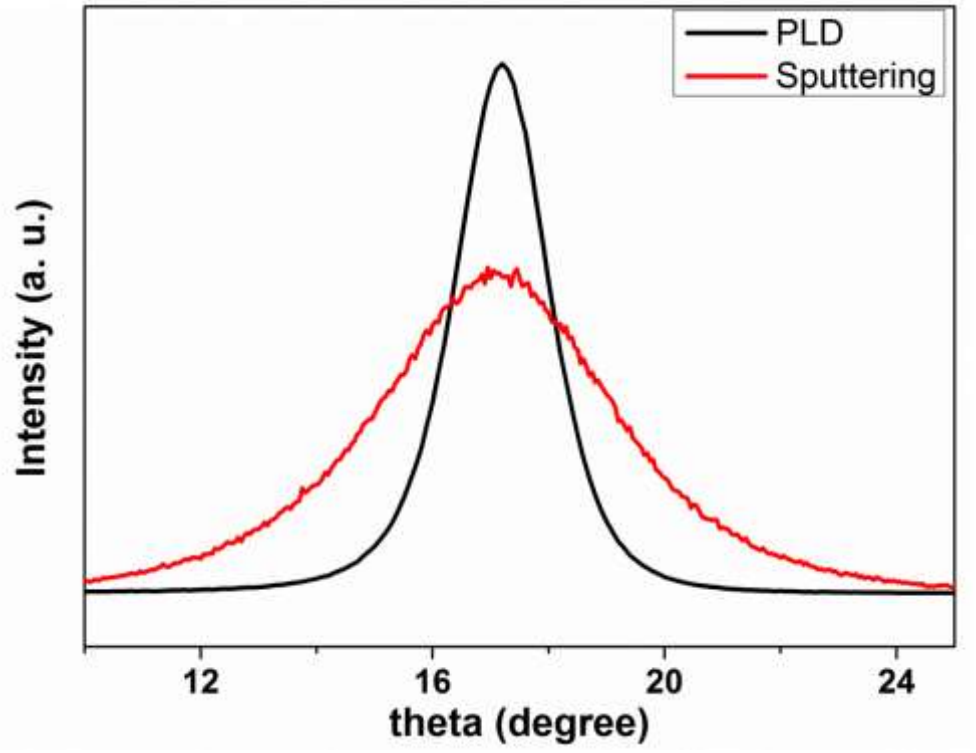

Figure 8-2 XRD Rcking curves of ZnO films

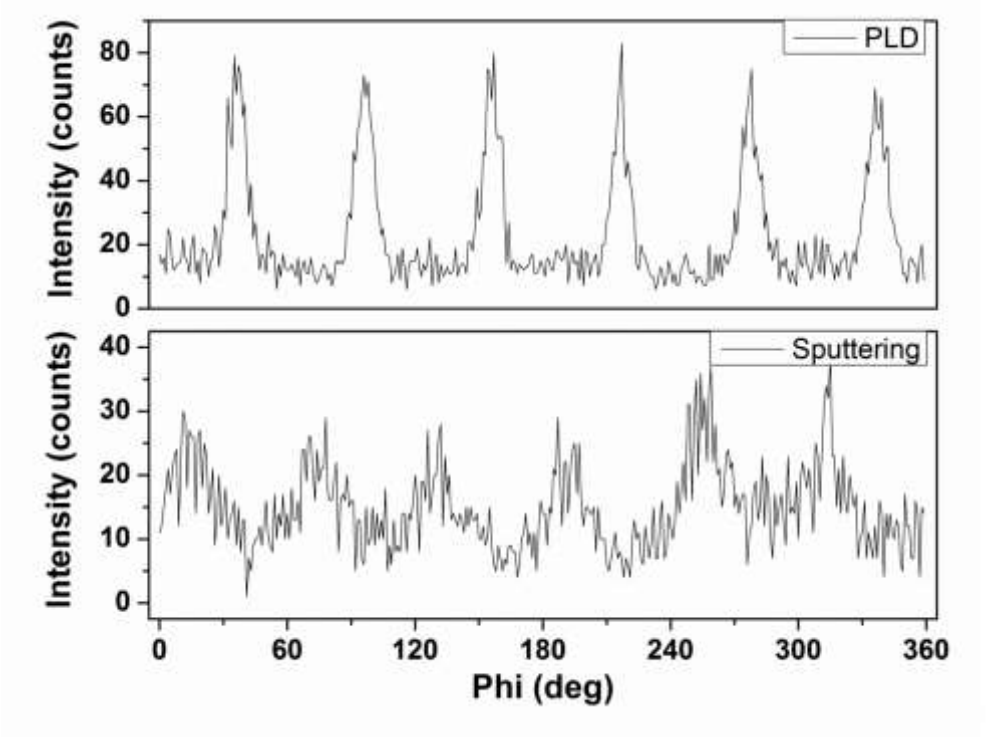

Figure 8-3 Phi scan for the 101 peak of ZnO thin films.

It may be suggested that films nucleate on the substrate in typically epitaxial manner. However, due to large lattice mismatch, perfect 2-D growth does not take place. The growth stresses are relaxed by forming islands, which finally grow upward in the form of columns. These columns have certain degree of orientation relationship with the substrate that gives rise to six fold in plane symmetry in Phi-axis. This orientation relationship is much stronger in case of PLD films, as the FWHM of the peaks along phi-axis is much finer in comparison with sputtered film. High energy of incident particles seem responsible for annealing out the defects and forming compact deposits with solid and dense inter-column boundaries in case of PLD films. Accordingly, the crystals/columns during growth do not find sufficient space to relax, as a result of which crystals continue their growth almost in the same axis without much rotational adjustment. As a result, PLD film exhibits very small FWHM of peak in omega scan for the surface planes of (002) as well as in Phi scan for an oblique angle plane of (104).

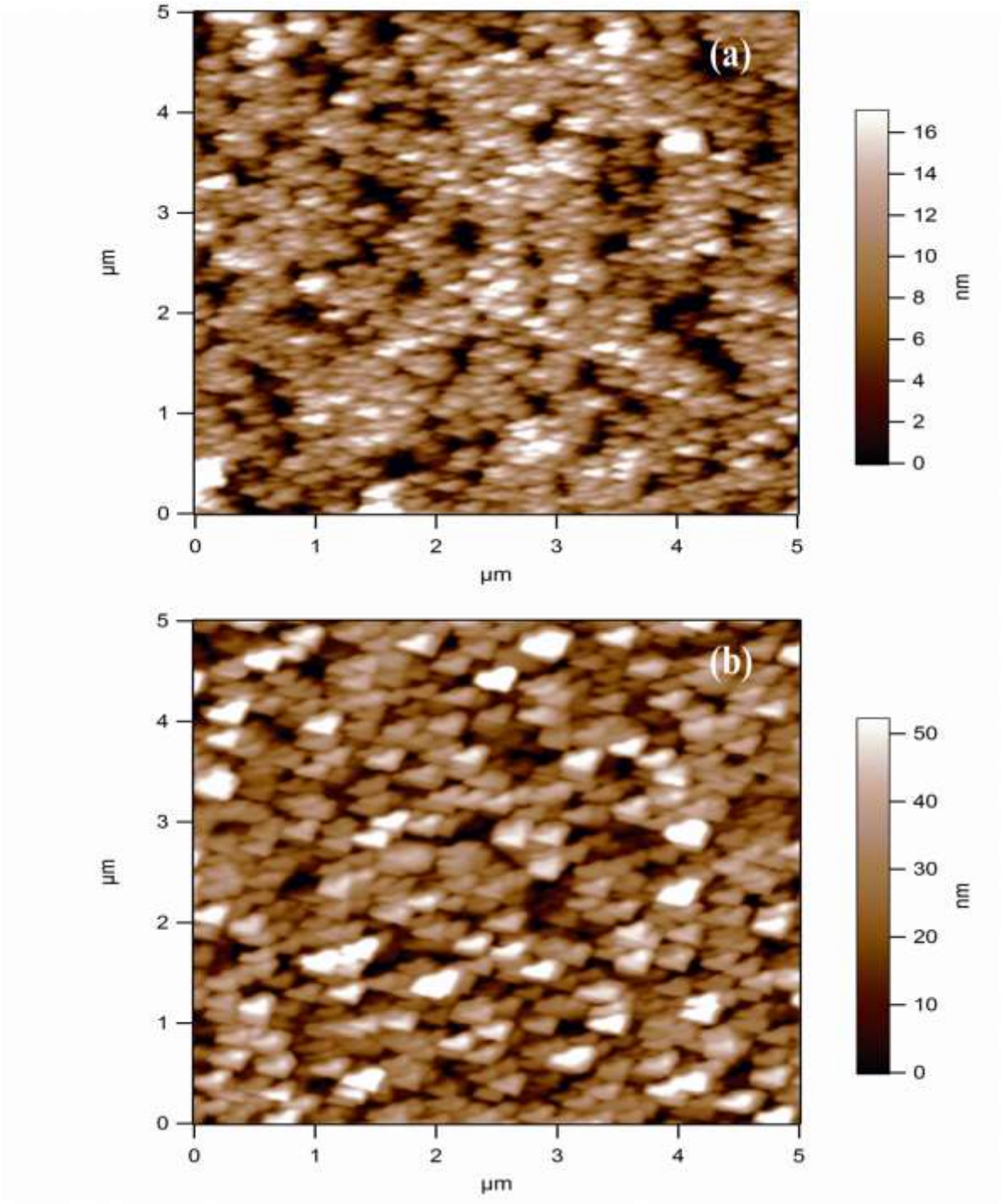

Figure 8-4 AFM images of the ZnO thin films.

Fig. 8-5(a) and (b) compare the top view SEM images of the films, while Fig. 8-5(c) and (d) present the cross-sectional views. The coarser structure of sputtered film in comparison with PLD films is in close agreement with AFM images (Fig. 8-5(a,b). In both the cases, columnar growth is evident from Fig. 8-5(c) and (d). These columns may possibly be crystals and / or sub-crystals separated by large and small-angle grain boundaries. Furthermore, a relatively more compact nature of the film formed by PLD is clearly evident (Fig. 8-5(c & d)). Higher energy incident particles in PLD may be responsible for compact deposits.

Fig. 8-6 illustrates photoluminescence spectra of ZnO films formed by PLD and sputtering. UV emission peak centered at 3.30 eV corresponds to near-band edge emission related with the direct recombination of free excitons [310]. Both the films exhibit a blue emission peak centered at 2.61 eV, while the sputtered film shows an additional green emission peak at 2.29 eV. Photoluminescence of ZnO in the visible region is generally related with intrinsic defects such as oxygen vacancies, zinc vacancies and zinc interstitials, etc. [311]. However, green luminescence is mostly observed in case of nanowires and nanorods, while blue luminescence is frequently observed in thin films. Son *et al* [312] have observed shift from green luminescence for the films formed at lower temperatures to blue luminescence for the films formed at relatively higher temperatures with appearance of coarser columnar grains. Blue emission in spite of very high crystalline quality of the film formed by PLD suggests that this is not related with simply intrinsic intra-crystalline point defects; but it is related with defects in the inter-crystalline boundaries. For instance, the blue emission at 2.61 eV is attributable to the transition of charge carriers from zinc interstitial to ionized zinc vacancy level [212, 313].

This pair of defects may be situated at inter-columnar boundaries where crystals of high quality meet generating a boundary with variety of defects. Intensity of blue emission is increased in sputtered films inspite of a possible decrease in the overall column boundary regions due to larger size of columns. This seems related with the fact that mutual misorientation of these columnar crystals along x-y plane, where prismatic planes meet, is much less for the PLD films than for the sputtered film (Fig. 8-5(c & d)) as a result of which the former films have relatively lower number density of defects along the grain boundary.

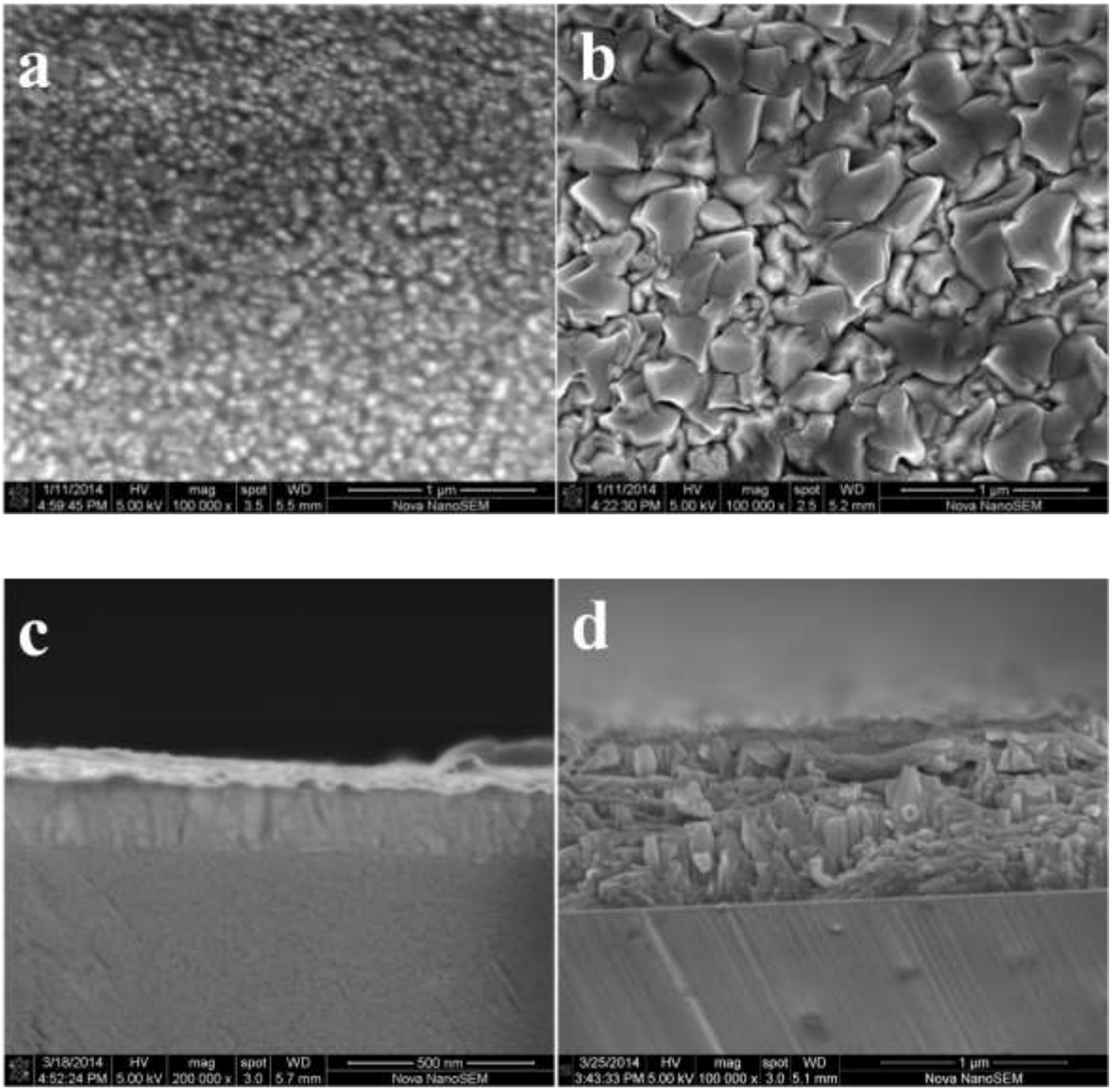

Figure 8-5 Surface morphology and the cross-sectional view of ZnO thin films by PLD (a & c) and RF sputtering (b & d).

The green peak emission by sputtered ZnO sample might be related with common intrinsic point defects related with oxygen vacancies. One reason may be significant deficiency of oxygen/deviation from stoichiometry, as these films were formed in argon atmosphere; although lower crystalline perfection in sputtered film may be regarded as another reason for bluish-green emission by the sputtered films.

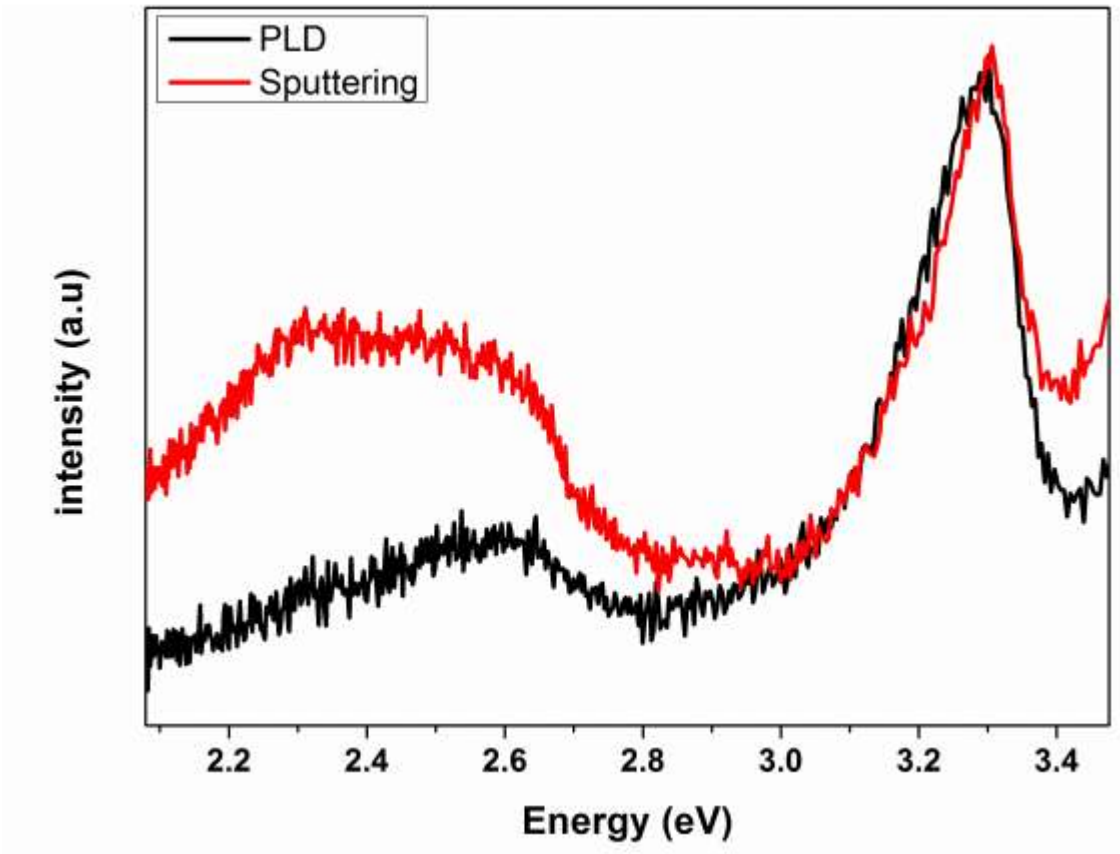

Figure 8-6 Photoluminescence spectra of ZnO thin films.

Fig.8-7 shows the room temperature optical transmittance spectra of the PLD and sputter deposited ZnO thin films. From the spectra of films, it is evident that the average transmittance value of around 90% lies in the visible wavelength range, and absorption of at around 378 nm indicating high crystalline and optical quality, which indicates that the obtained films have low impurities and few lattice defects [314-315]. The absorption edge corresponds to transition from valence band to conduction band whereas; the absorption in the visible range is associated with intrinsic defects in the films [316].The apparent steep drop off at 378 nm in the transmission line for PLD deposited ZnO films is shifted towards lower wavelength as compared to that of Sputtered film also indicating that the optical gap in the film deposited by PLD is larger than in film deposited by sputtering method. The band gap of both films can be estimated by calculating the absorption coefficient expressed by the relation[317]:

$$(\alpha hv) = A(hv - E_g)^{1/2}$$

Where A is a constant, α is the absorption coefficient, h is Plank's constant and v is the frequency of incident radiation. E_g is determined by extrapolating the straight line portion of the spectrum to $\alpha hv = 0$. The observed direct band gap energy of the ZnO films deposited by sputtering and PLD as listed in the table are 3.28 and 3.29 eV respectively. Interestingly, the band gap energy of the pure ZnO thin films increases with substrate temperatures [318]. In comparison to the band gap energy of single crystal ZnO (3.37 eV), these obtained values are somewhat smaller. This small variation of the band gap energy has been attributed due to defects in ZnO thin films. These optical band gap values are in well matches with the reports on spray pyrolysis [319], rf sputtered [320], dc reactive magnetron sputtered [321] and ion beam sputtered [322] films. The higher band gap of PLD deposited ZnO films suggests that the PLD films have better crystalline quality than sputter deposited ZnO films.

The reflectance of ZnO thin films deposited by PLD and RF magnetron sputtering is shown in Fig. 8-8. The reflectance behavior of both films is appeared to be different as PLD film show a continuous while sputtering sample has shown an oscillatory fringe pattern in the measured range of wavelength reflects the optical homogeneity of the deposited films [323].

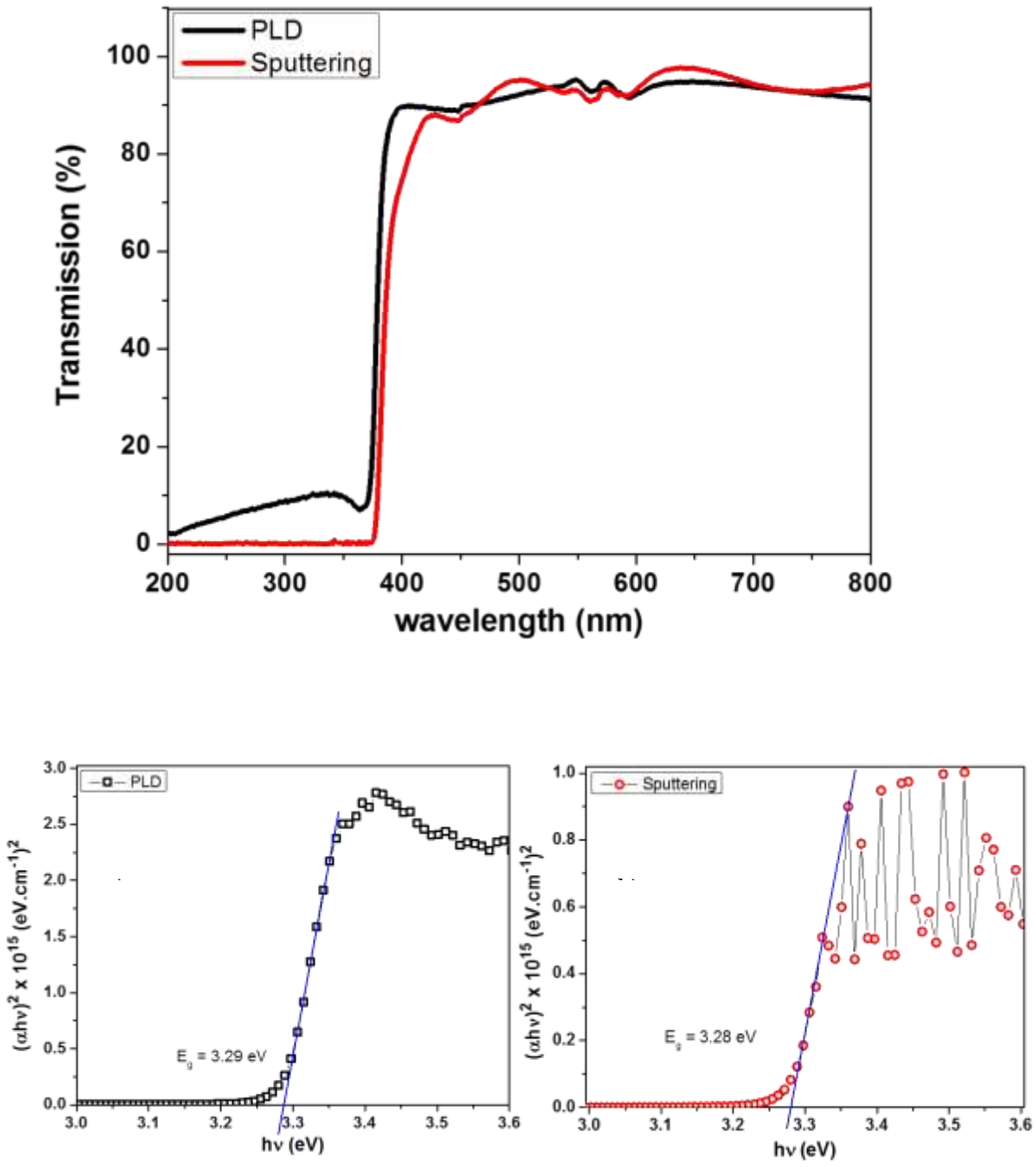

Figure 8-7 Transmission spectra and the optical band gap of ZnO thin films.

As seen, sputtered film exhibits a slightly low reflection as compared with PLD films in the wavelength range 300-500 nm. The reduction of the reflection can be explained as for the transmittance in terms of free surface morphology. The intensity of diffusely transmitted light is controlled by the differences in the refractive index of ZnO and sapphire substrate, the ratio of light wavelength (λ) and the vertical r.m.s value (R) according to the scattering theory [324]. In the case of $R \ll \lambda$, the intensity of diffusely transmitted light is higher and less amount of reflection losses. This theory shows a good agreement with our experimental results.

The refractive index of these films can be calculated from the reflectance data by the following relation [325]:

$$n = \sqrt{\frac{1+\sqrt{R}}{1-\sqrt{R}}}$$

And the calculated refractive index has been plotted against wavelength in the visible region shown in Fig. 8-9. The reflective index behavior of both films is exhibited to be different as PLD film show a continuous while sputtering sample has shown an oscillatory fringe pattern. It is observed that the refraction behavior of films tends to decrease and exhibits an oscillatory behavior with wavelength in the visible regions. This may be due to the polarization process as it is related to the extent of polarization [326]. The similar pattern reported previously by Hamad and Nahhas *et al*. [327-328]. It can be seen that refractive index of PLD deposited ZnO film exhibit almost same value around 1.25 for the entire wavelength region. In contrast the sputtered ZnO thin film has shown an oscillatory (from n_{min} = 1.09 to n_{max} = 1.29) behavior which tends to decrease with decreasing wavelength. These values of the refractive index are approximately close to the value reported for bulk material [329-330].

The complex refractive index of thin films is defined as

$$n^* = n - ik$$

Where n^* is the complex refractive index and k is known as the imaginary part of n^* and is known as extinction coefficient.

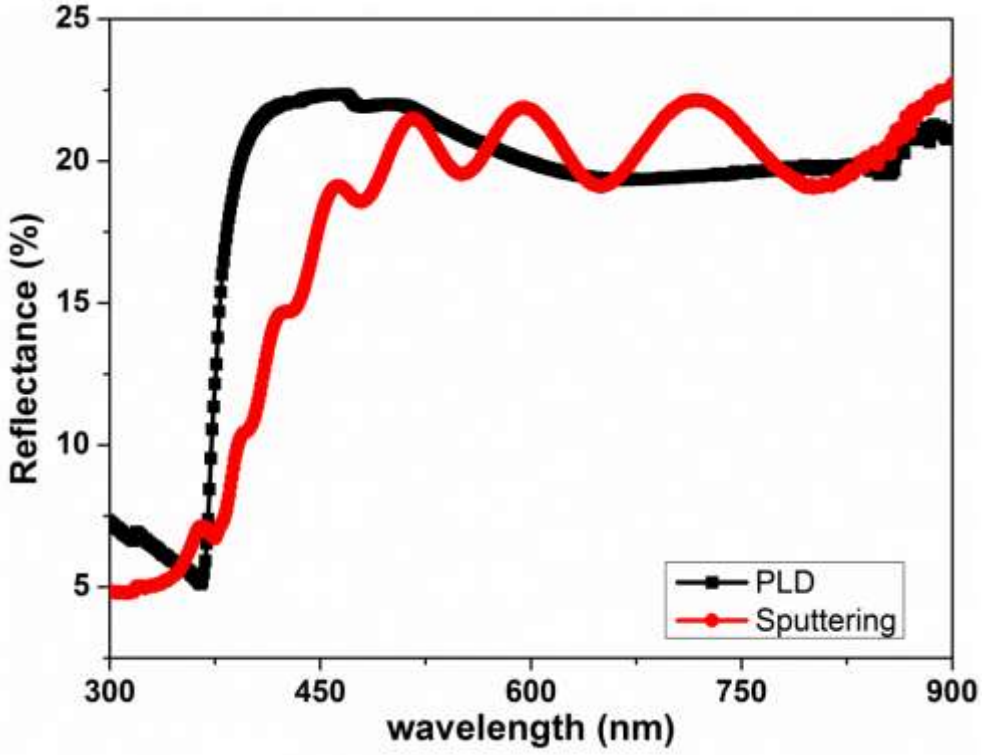

Figure 8-8 Optical reflectance of ZnO films.

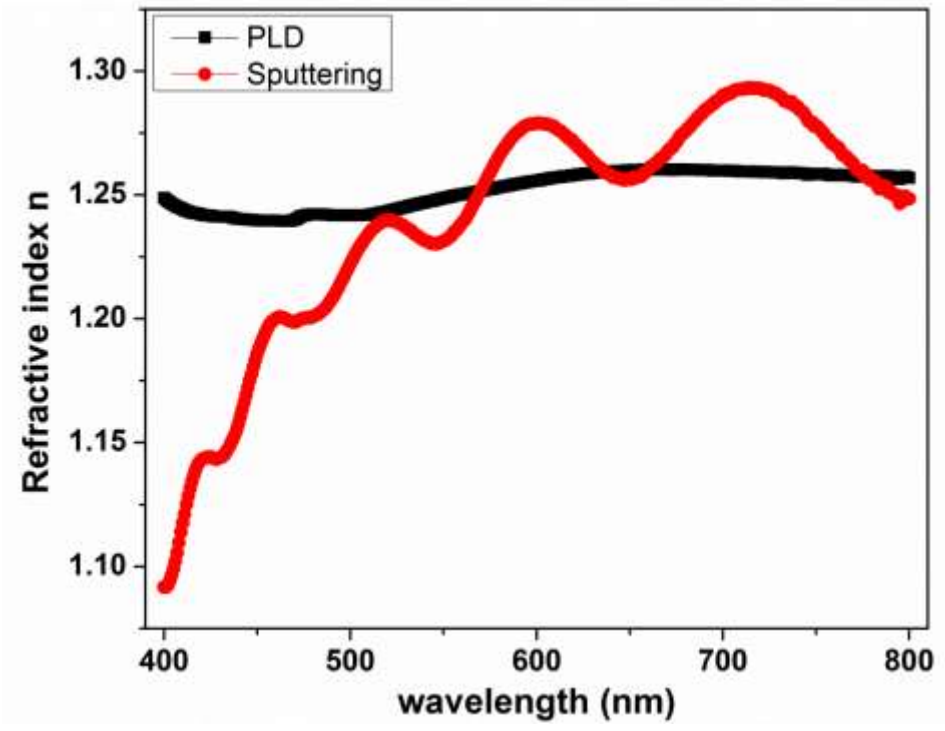

Figure 8-9 Plot of refractive index vs wavelength of ZnO thin films.

It can be calculated from the relation [331]

$$k = \frac{\alpha\lambda}{4\pi}$$

And in this equation α is the known as absorption coefficient and it can be calculated from the transmittance data using equation [332]

$$T = e^{-\alpha x}$$

Where T is transmittance and x denotes the thickness of the deposited film. By using these two equations, the extinction coefficient has been calculated as a function of wavelength and plotted in Fig. 8-10. The value of k is finding to be consistent in the visible wavelength region with negligible variations for both samples. The steep rise (for sputtered ZnO films) in the value of the extinction coefficient near the band edge (<420 nm) is due to the inter-band absorption [333].

The relative permittivity ε of the PLD and the sputtering grown thin films has determined using the relation $\varepsilon = n^2$ and is plotted as a function of wavelength as shown in Fig.8-11. The low frequency shows a larger dielectric constant, which is due to the presence of space charge polarization [334]. The decrease of dielectric constant with increasing frequency can be explained by the fact that the frequency of electric charge carriers cannot follow the alternation of the ac electric field applied beyond a certain critical frequency [335]. The higher frequencies show very small dielectric constant, which is key for the fabrication of materials for photonic and electro-optic devices [336]. The relative permittivity which is also known as optical dielectric constant, exhibit nearly a constant value for PLD grown ZnO film while for sputtered film its value show sinusoidal variations in the range 1.2 to 1.65 with the wavelength.

The optical conductivity of thin films as a result of the incident photons can be calculated by employing the absorption coefficient and the refractive index using following equation [337]

$$\sigma = \alpha . n . c/4\pi$$

The range of optical conductivity for sputtering grown ZnO thin film is quite narrow as compared to the PLD grown ZnO thin film (Fig. 8-12).

The product of carrier concentration *N* and the carrier mobility μ in the visible wavelength region is shown in the figure 8-13 which is found to be dependent on the reflectance R and film thickness *x* as related by this equation

$$\mu N = 4.\frac{\varepsilon_o\, c}{[e.x(1-R)]}$$

It can be seen in Fig. 8-13 that the overall range of product values for PLD sample lies in the higher quadrant as compared to sputtered sample. However, some variations are observed in the product of carrier mobility and carrier concentration for PLD thin film as a function of incident photons wavelength and the product values increase above 550 nm. But for the sputter deposited sample the product values found to be quite consistent with the wavelength with no major variation.

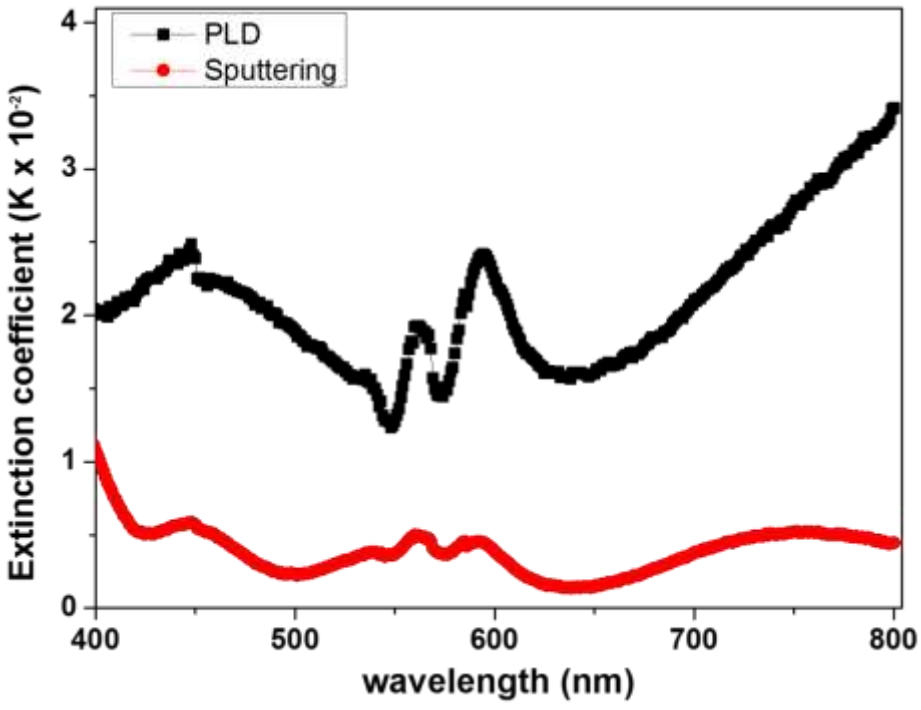

Figure 8-10 Plot of extinction coefficient *k* vs wavelength of ZnO thin films.

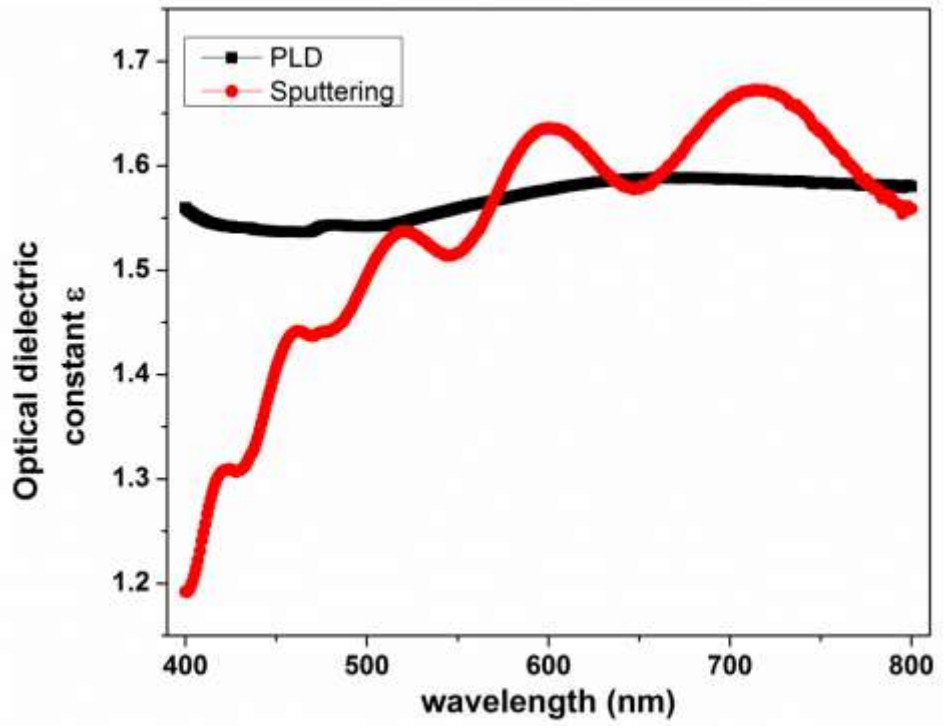

Figure 8-11 Plot of optical dielectric constant ε vs wavelength of ZnO thin films.

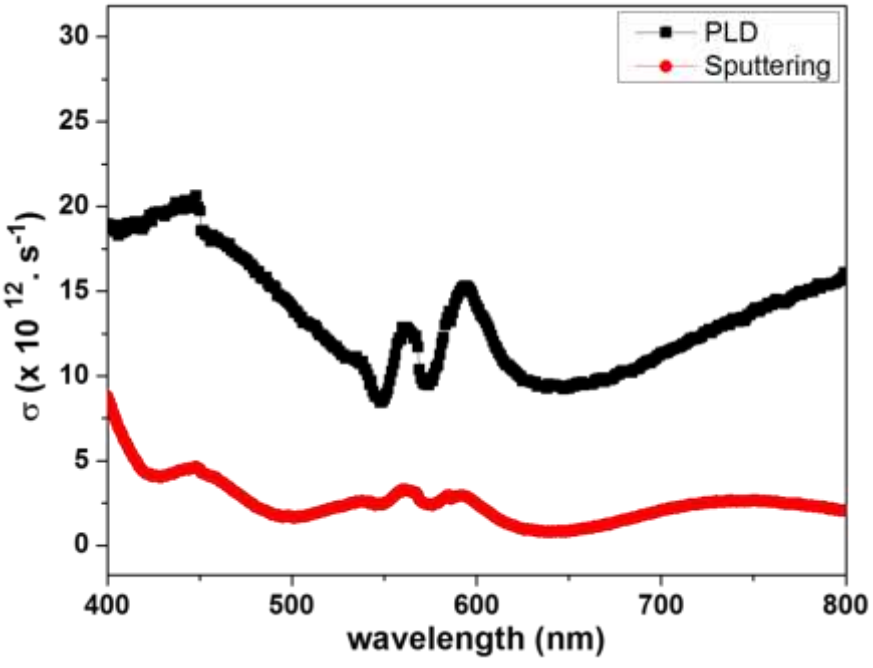

Figure 8-12 Plot of optical conductivity σ vs wavelength of ZnO thin films.

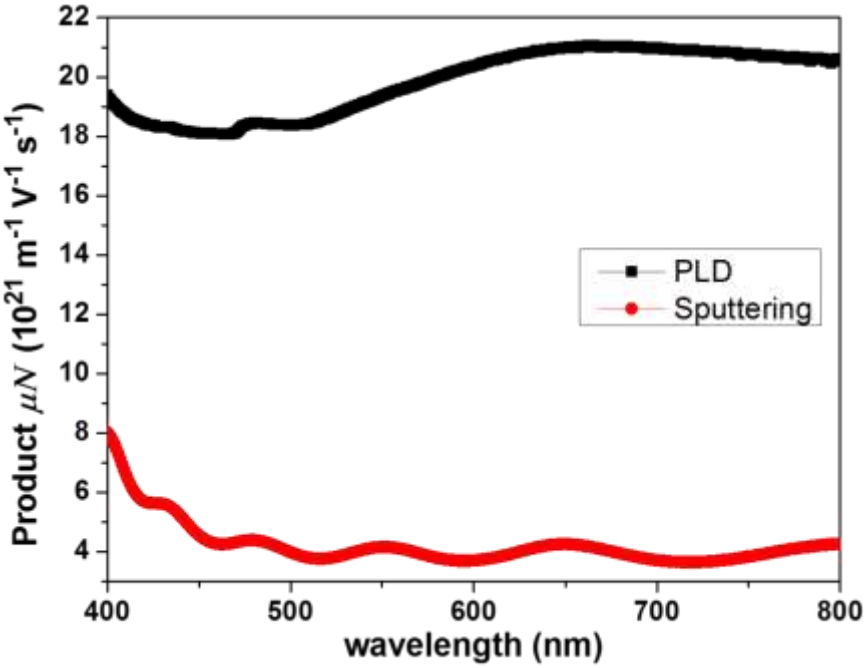

Figure 8-13 Plot of the product of carrier mobility μ and carrier concentration N vs wavelength of ZnO thin films.

Table 8-1 Electrical parameters measured by Hall measurement and optical band gap.

	Resistivity (Ω-cm)	Mobility (cm^2/V-sec)	Carrier Concentration (cm^{-3})
PLD	0.0792	34.6	2.28×10^{18}
Sputtering	0.4832	7.5	1.73×10^{18}

Table 1 describes room temperature electrical properties of the PLD and sputtered films. The carrier concentrations of these films are supplied from donor sites, which are associated with oxygen vacancies and excess metal ions. It is generally believed that the conduction characteristics of ZnO films dominated by oxygen vacancies and Zn interstitial atoms. The resistivity is inversely proportional to the product of carrier concentration and mobility. Therefore, the change in resistivity with increase in substrate temperature is due to the change in carrier concentration or mobility.

It can be seen that the carrier concentration of ZnO films grown by PLD and sputtering is almost same. Difference in resistivity is mainly due to the variation in the carrier mobility in each type of film. The columnar growth of ZnO provide high ratio of the grain boundary area as compared to the grains which in turn provide defective states that are responsible for restriction of the carrier mobility. In PLD sample the higher crystallinity of the film make us to believe in the formation low angle grain boundaries among the grains which in turn decrease the defect density in these regions. On the other hand, the crystallinity of sputtered ZnO film suggests the existence of higher number of defect centers in the grain boundary area among the columnar grains. The grains in sputtered film are combined through high angle boundaries which increase the grain boundary area to grain ratio and hence higher defect density in that area to effect the mobility of charge carriers. Moreover, the stoichiometry of pulsed laser deposited ZnO films is better than sputter deposited, which also facilitates the higher conductivity of PLD films. Recent investigations suggest that none of demonstrate characteristics consistent with a high concentration shallow donor. Van de Walle [338-339] gives comprehensive explanation of the native defects and their complexes. He suggested that conductivity is attributed to presence of hydrogen and its complexes with some native defects, which is universal and present during film growth process. Hydrogen impurities react with oxygen vacancies and the resulting complex $(V_OH)^\bullet$ behave as a shallow donor. In this case, as the PLD deposited films demonstrate better stoichiometriy within the grains. But there is a chance for the defects (e.g. oxygen vacancies) present at the grain boundaries to make complexes with $(VoH)^\bullet$. These complexes act as the shallow donors and provide charge carriers for conductivity. Meanwhile, in sputtered sample, the carries provided by these complexes may be scattered or captured by some compensating defects present in the grain boundary area.

The I-V characteristics of ZnO/GaN junctions are measured by changing the bias voltage from +10 to -10 V The contact behaviour of In on ZnO and Ni/Au on GaN posses ohmic behaviour and it has been reported in several published articles previously. However, for the sake of confirmation, the above mentioned contacts have been checked by I-V characteristics and results shown ohmic behavior (Figure 8-14). . Fig. 8-15 clearly demonstrates the rectifying behavior of the p-n junction diodes.. The forward bias series resistance shown by sputtered deposited sample is larger in

comparison to PLD grown, while reverse bias leakage current for both heterostructures is negligible. The turn on voltage value of PLD deposited ZnO/GaN junction is 3.8 V while that of sputtered made junction is 5.2 V. The main reasons for the high turn on voltage in case of sputtered sample include the existence of the interfacial defects and the crystal quality of the ZnO film deposited by the RF Magnetron sputtering. As it is evident from the AFM analysis that the surface roughness of sputtered sample is higher than that of PLD sample, so this higher roughness of the film results in accumulation of interfacial defects at the ZnO/GaN interface. These interfacial defects are responsible for the electron capture when the device is working in the forward bias [340]. The other possible reason is the crystal quality of the ZnO film. As we have seen from the XRD results that ZnO film made by sputtering has a slightly poor crystalline structure as compared to PLD.

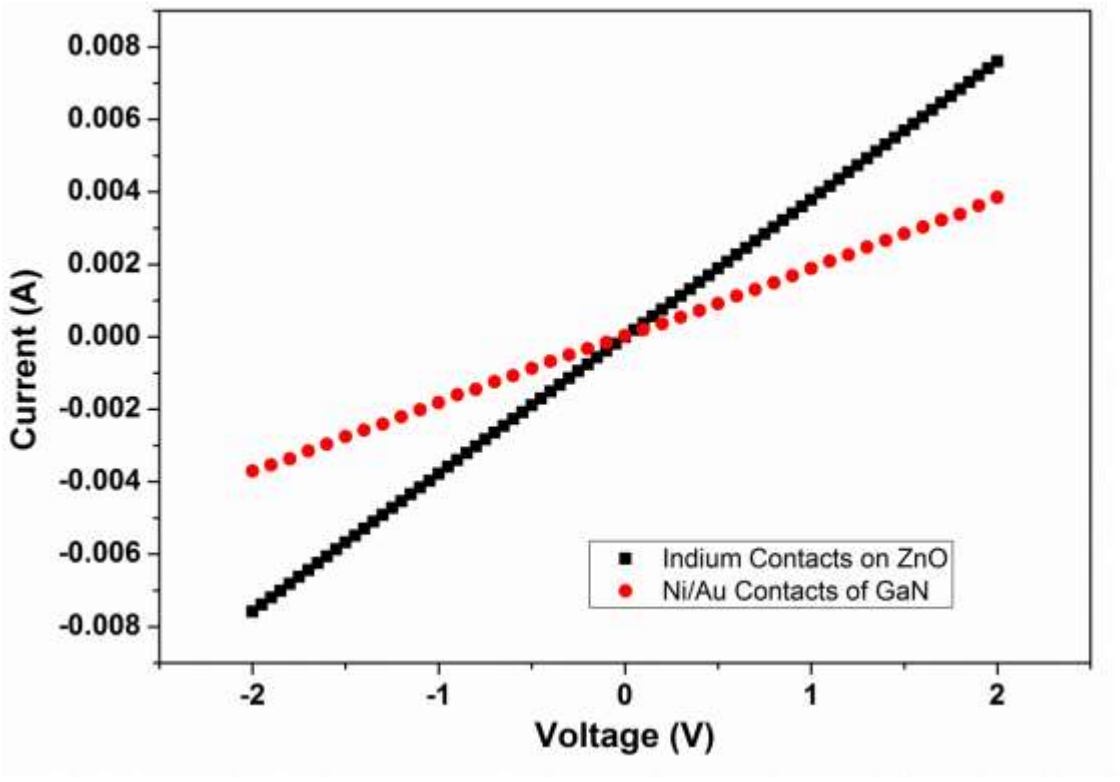

Figure 8-14Contact behaviors of p-n junction devices

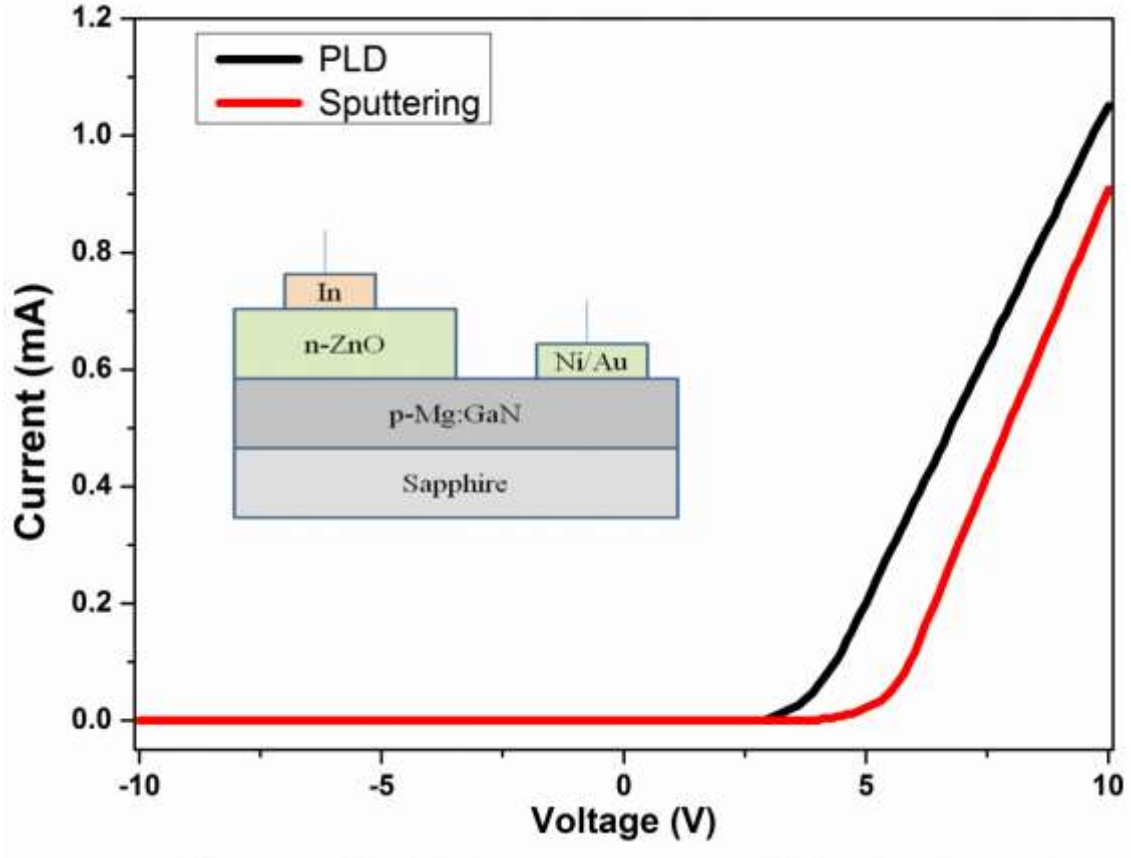

Figure 8-15 Current-Voltage characteristics of n-ZnO/p-GaN heterojunction. Inset shows the device structure.

8.3 Conclusions:

ZnO films have been grown on the c-plane sapphire substrate by pulsed laser deposition and the RF magnetron sputtering. The sample deposited by PLD is showing more crystallinity and smooth surface as compared to the RF sputtered sample. The higher crystalline quality of PLD grown film is attributable to energetic flux of incident atoms that provide additional energy to the atoms at the surface. These high energy incident particles have tendency to relieve the internal stresses of the film, which in turn improve the crystallinity of thin film. Phi scan of an oblique angle ZnO (104) plane exhibits the tendency of growth of wurtzite ZnO with six-fold symmetry and higher degree of epitaxial growth in case of PLD deposited sample.

More compact columnar growth has been observed in the PLD sample as compared to sputtered one. The columns are separated by large angle boundaries in sputtered sample and give rise to more defects in this region as compared to PLD sample in which columns are bound by low angle boundaries and posses less number of defects. These defects may be responsible for the reduced electronic mobility in sputtered ZnO film. The blue emissions are observed in the PL spectra of both samples which is attributable to the transition of charge carriers from zinc interstitial to ionized zinc vacancy level. In sputtered sample the oxygen deficiency has produced strong green emission along with UV and blue luminescence. Both types of defects have expected to be mostly lying in the large angle boundary region of the sputtered sample. The small roughness of PLD deposited ZnO on p-GaN caused the small number of interfacial defects which results in higher current flow and lower turn on voltage for the p-n junction diode. This comparison showed that good crystal quality and low surface roughness are the key factors to be cause for the good electrical behavior of a heterojunction device and by controlling these factors we can get a best p-n junction diode for LED applications.

9 ZnO-Ge multilayer thin film structures

Zinc oxide is a promising wide band gap semiconductor material (Eg ~ 3.37 eV) with a wide range of application in the electrical, optical and optoelectronic industry as varistor, surface acoustic wave devices, UV light-emitting diodes and lasers, and window material for display and solar cells etc[341-343]. During last decade, ZnO has diverted the attention of researchers towards the deposition of transparent conducting oxide (TCO) films using zinc oxide which possesses very high optical transmission, high electrical conductivity, high chemical and mechanical stability together with its abundance in nature makes it a lower cost material when compared with the most currently used TCO materials (ITO, SnO2). In the ZnO lattice; the two native defects (excess Zn and Oxygen vacancy) effect result in an n-type conductivity but the conductivity due to these "intrinsic" defects is not high enough to enable ZnO thin layers to act as an electrical contact for thin-film solar cells [344]. In order to satisfy the diverse requirements in devices, various approaches have been taken to amend optical properties of ZnO. There are so many approaches which have been adopted by researchers to manipulate the optical properties of ZnO. Intensive studies on the subject depositing multilayer structures or by doping exotic dopants to achieve above purpose have been done using Ce, Ga Er, Al, In, Ge, Na, Li, etc., as foreign materials [345-351].

Ge is an indirect band gap semiconductor having smaller energy difference between direct and indirect band gap (ΔE = 0.12 eV), high refractive index, possessing small effective mass and high mobility. The small ionic radii difference between Ge and Zn make it the suitable candidate which can be used to change the electronic properties easily. The employment of the Ge nanoparticles in the TCOs can produce the quantum confinement effects and it is successfully used to tune the band gap of the films [352]. Previously many researchers have worked on the multilayer structure of Ge with other materials to sort out its potential application in the field of photovoltaic [352-357]. In this work we have studied the optical response of ZnO/Ge multilayer by the varying number of multilayers.

ZnO/Ge multilayers have been deposited to harvest their photovoltaic applications due to the production of potential wells among ZnO-Ge layers giving rise to the Quantum confinement of carriers. In this report, structural and various optical properties of ZnO/Ge multilayer thin films deposited by physical vapor deposition methods have been reported. ZnO and Ge layers were deposited in alternate sequence forming 2, 4 and 6 layers thin film structure.

9.1 Experimental Procedure

ZnO-Ge multi-layer thin films were deposited on BK7 glass substrates using electron beam evaporation of ZnO powder (99.999%) and resistive heating of Ge powder (99.999%) as a starting material. These films were deposited in the form of 'sets of two, four and six layers' periodically starting with Ge (15 nm adjacent to substrate) and ZnO (30 nm) on the top and so on as shown in Fig. 1. The chamber was pumped out to a vacuum level below 1 x 10^{-5} mbar. Oxygen pressure in the chamber was 4.0×10^{-4} mbar during growth of each ZnO layer. During deposition substrate temperature was kept at 100 ^{o}C and rotated at 30 RPM.

Rutherford backscattering (RBS) was performed to confirm the layer structure across the thickness of the multi-layer films. Incident particles were the He ions accelerated to energy of 2 MeV. The XRD spectra of multi-layer films were recorded by using Bruker D8 Discover diffractometer equipped with Cu K_{α} radiation. Surface morphology of the films was analyzed by Atomic Force Microscopy (Quesant Universal SPM, Ambios Technology) in non-contact mode. Optical transmittance and reflection spectra of these films were measured by Perkin Elmer UV/VIS/NIR Lambda 19 spectrophotometer in the wavelength range 300–2500 nm. The current-voltage (I-V) characteristics of the multi-layer structures were measured using Keithley 6487 pico-ammeter meter with DC voltage in the range of 0 to 2V.

9.2 Results and Discussion:

The films deposited on glass substrate show good adhesion to substrate. Peel off, cracking or blisters are not found in the as-deposited films. Fig. 1 shows initial proposed layer structure of the ZnO-Ge films. The thickness of the layers was planned about 15 nm and 30 nm for Ge and ZnO, respectively. The films have been deposited

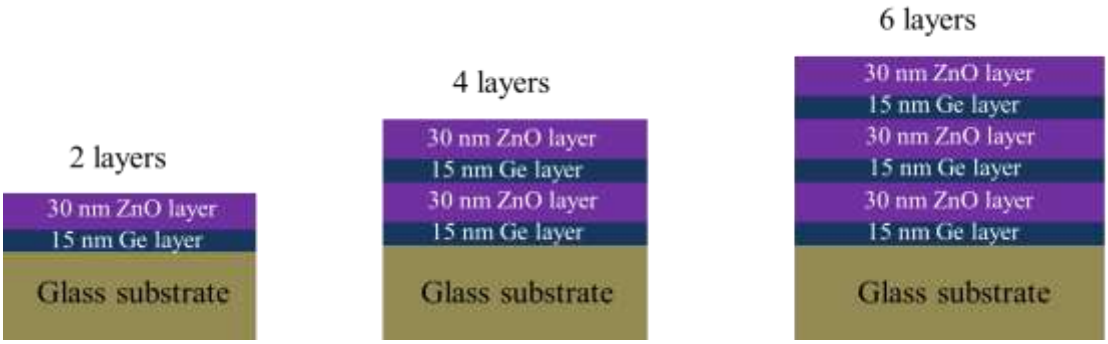

Figure 9-1 Initial proposed layer structure of Multi-layer ZnO-Ge thin films.

accordingly by monitoring the layer thickness using quartz crystal monitor during the deposition. After deposition, RBS has been used to analyze the composition and thickness of the multilayer film. The RBS spectra of two, four and six multilayer film structure along with the simulated spectrum as shown in Fig 9-2,3&4 respectively. The layer formation has been confirmed by the simulated fitting of these RBS spectra. The thickness and composition of elements in these layers have been tabulated in tables 9-1,2&3. This analysis has revealed that the thickness of the layers has not been the same as has been detected from the quartz crystal monitor. The thickness for the ZnO layers has been estimated to be thinner while the deposited Ge layers have been found thicker in comparison with the values shown by qurtz crystal monitor. The thinner ZnO layers might be the result of re-evaporation of ZnO from the glass substrate. On the other hand, compositional analysis has shown the diffusion of oxygen in the Ge layers. There may be two possible reasons for this diffusion, first is the diffusion of oxygen between the layers after deposition. The other might be during deposition. As initially, we have deposited Ge layer on glass substrate, then oxygen gas had been inserted in to the chamber for the growth of ZnO layer. So during this time some of the Ge might have been oxidized by the oxygen before the deposition of ZnO layer.

The Fig. 9-5 shows the 3D AFM images of the ZnO-Ge multi-layers which clearly revealed that the surface layer is deposited in the form of big clusters in all three type of multi-layer structure. But the surface roughness of the films is seemed to be increased with the increase in the number of the deposited layers.

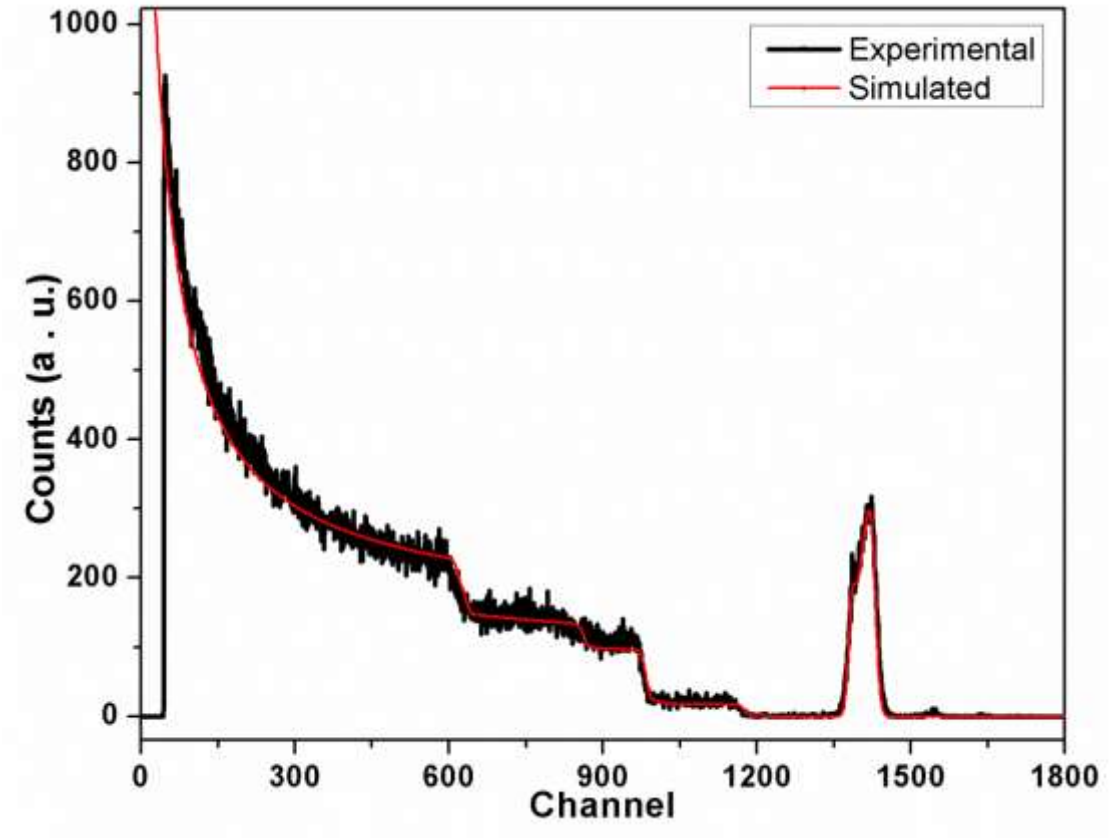

Figure 9-2 RBS spectrum of 2-layer ZnO-Ge film along with simulated fitting.

Table 9-1 composition and layer's thickness estimated by the fitting of RBS spectrum of 2-layers ZnO-Ge film.

Layers (bottom to Top)	Composition		ZnO/Ge 2-layers Calculated Thickness (nm)
Ge	Ge = 0.75	O = 0.25	26.1
ZnO	Zn = 0.5	O = 0.5	12.1

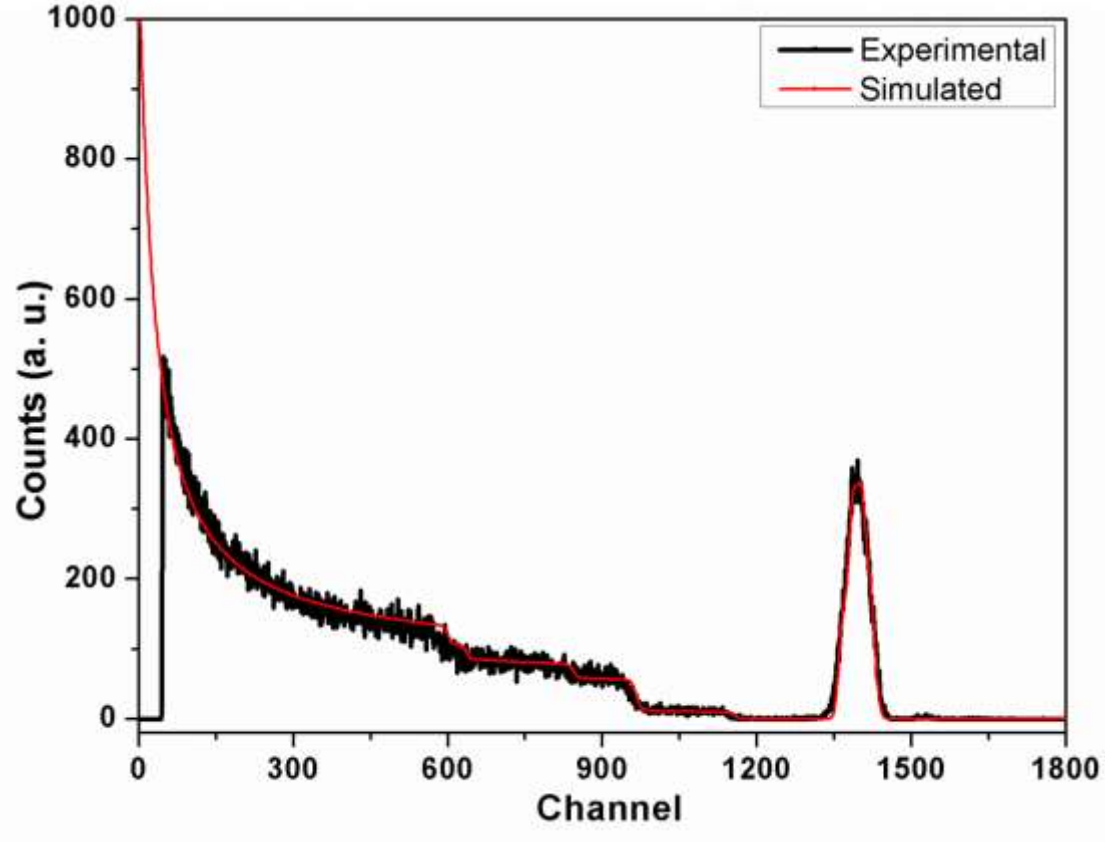

Figure 9-3 RBS spectrum of 4-layers ZnO-Ge film along with simulated fitting.

Table 9-2 Composition and layer's thickness estimated by the fitting of RBS spectrum of 4-layers ZnO-Ge film.

Layers (bottom to Top)	Composition		ZnO/Ge 4-layers Calculated Thickness (nm)
Ge	Ge =0.95	O = 0.05	26.4
ZnO	Zn = 0.5	O = 0.5	16.9
Ge	Ge 0.95	O = 0.05	26.4
ZnO	Zn = 0.5	O = 0.5	16.3

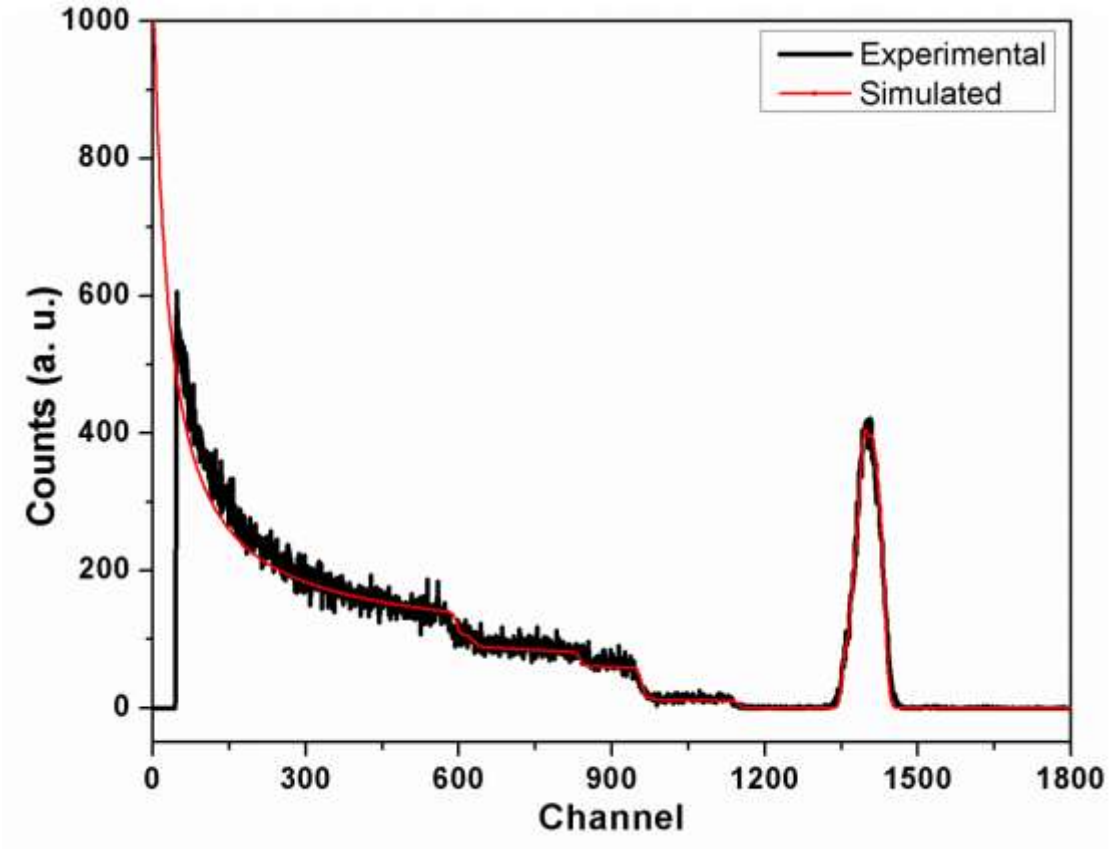

Figure 9-4 RBS spectrum of 6-layers ZnO-Ge film along with simulated fitting.

Table 9-3 Composition and layer's thickness estimated by the fitting of RBS spectrum of 6-layers ZnO-Ge film.

Layers (bottom to Top)	Composition		ZnO/Ge 6-layers Calculated Thickness (nm)
Ge	Ge = 0.85	O = 0.15	31.3
ZnO	Zn = 0.5	O = 0.5	8.4
Ge	Ge = 0.85	O = 0.15	31.3
ZnO	Zn = 0.5	O = 0.5	8.4
Ge	Ge = 0.95	O = 0.05	35
ZnO	Zn = 0.5	O = 0.5	3.6

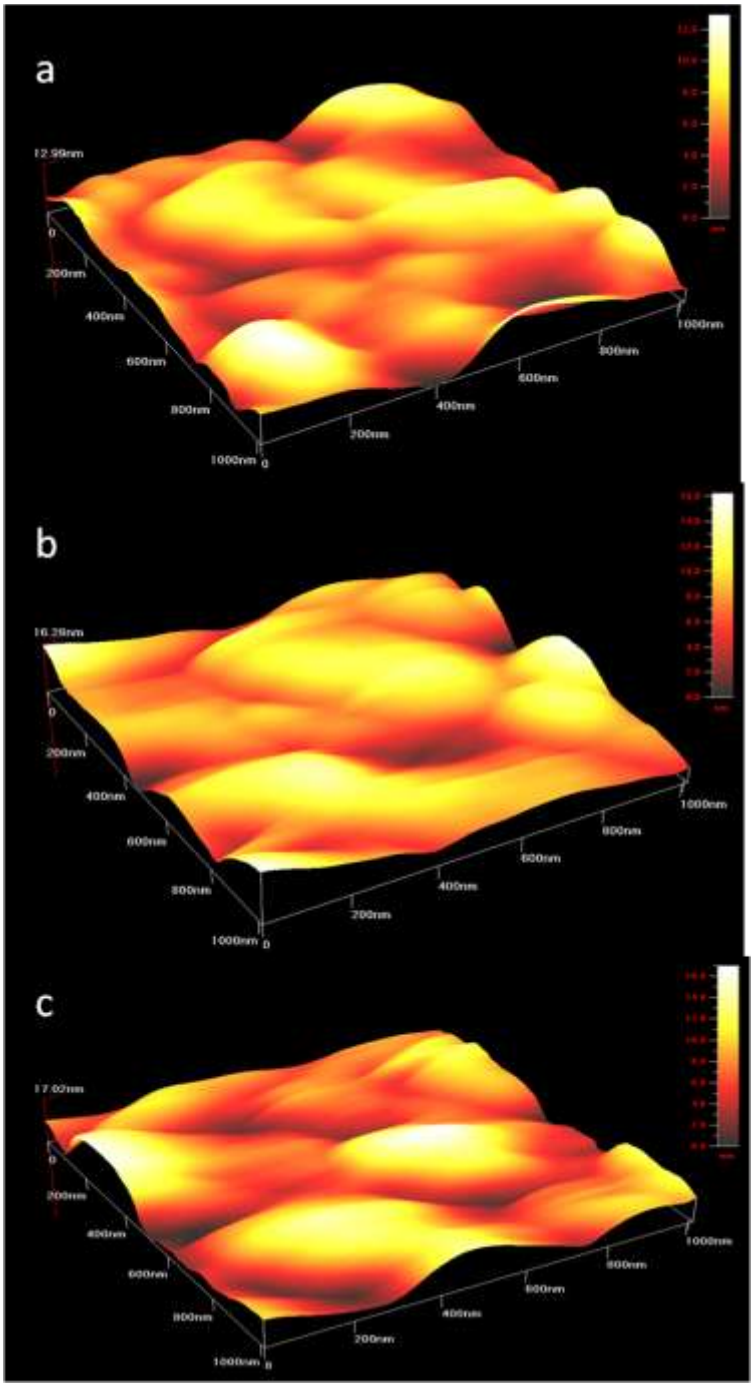

Figure 9-5 AFM images of 2 (a), 4 (b) and 6 (c) layers ZnO-Ge films.

X-ray diffraction (XRD) patterns of as-deposited multi-layer ZnO-Ge thin films performed in the range of 20°–90° at room temperature is shown in Fig. 9-6. All the films are amorphous. The XRD patterns of these multi-layer films shows a diffused scattering (centered at about 25^{o}) coming from glass substrate [1]. The amorphous nature of these multi-layers may be due to germanium layers. In as-deposited form pure ZnO thin films, deposited by electron beam evaporation in similar conditions, show crystalline nature while pure Ge films show amorphous nature. The Ge layers [2] provide hindrance to ZnO atoms to deposit in crystalline form. Moreover, the large lattice mismatch between ZnO and Ge crystals is another cause of amorphous nature of these films.

The transmittance spectra of ZnO-Ge multilayer thin films deposited on glass substrate is shown in Fig. 9-8. tthe decrease in the transmittance with the increase in the number of depositing layers is clearly observed in the Fig. all the as deposited multilayer thin films have a relatively large band tail which due to the amorphous nature of the deposited films as described by the XRD results. The lattice mismatch at the interface of two layers would produce a region with high density of defects. The amounts of these traps in different number of interfacial regions alter the band gap of the multilayer thin films.

Fig. 9-9 shows absorption coefficient (α) of the multilayer films plotted as a function of photon energy ($h\nu$). In Fig 9-9 a and b we can see that there are two linear regions while in c, there is only one region at the smaller energy value. These two regions may arise from the direct band gap at 0.66 eV, 1.06 eVand 1.08 eV for Ge and at 3.66 eV and 3.02 eV for ZnO. While in the 6 layer film the band gap for the ZnO may be suppressed due to the large amount of deposited Ge.

It appears that the Ge layers in the multilayer films manifest themselves predominantly as direct band gap materials, the absorption activity at indirect band gap (0.66-1.08 eV) being insignificant, in contrast to bulk Ge that is predominantly an indirect band gap material. This is an interesting aspect arising from quantum confinement effects in nanostructure Ge layers.

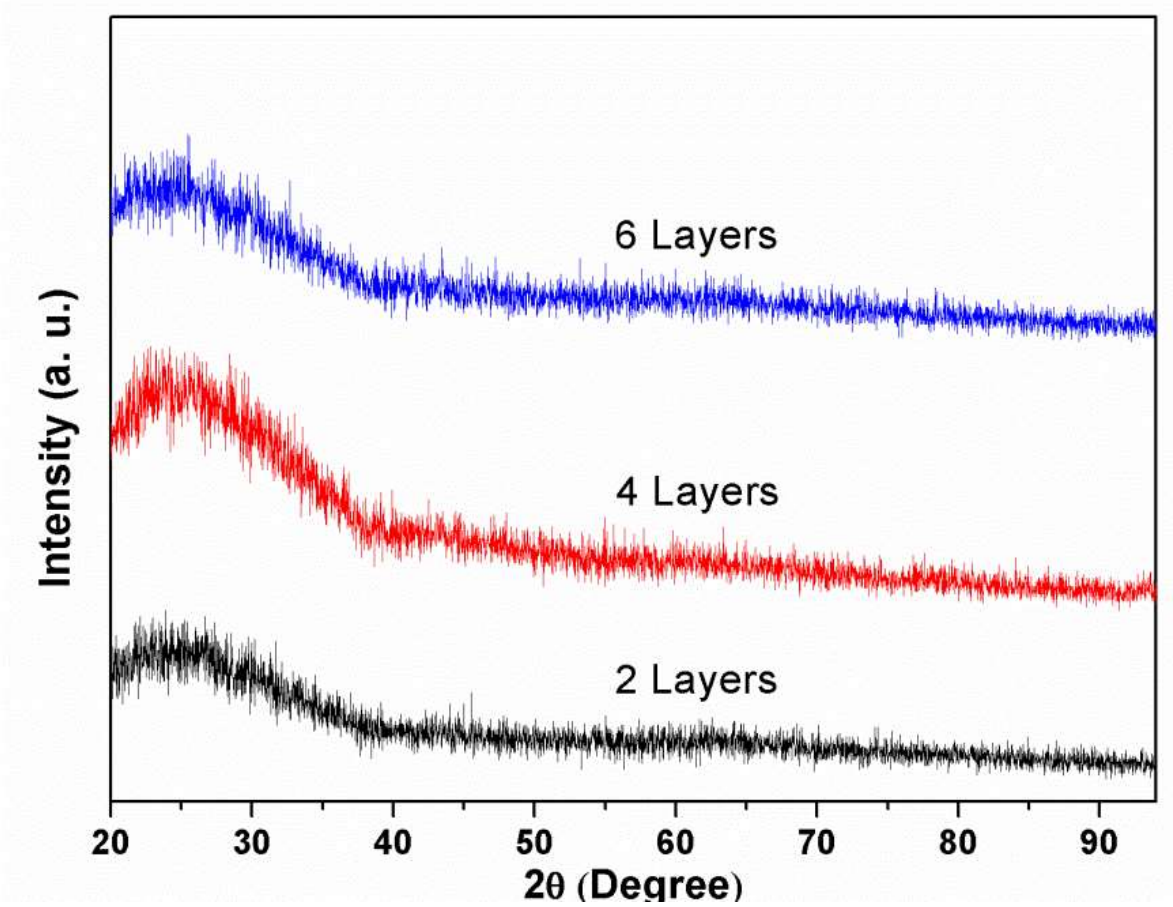

Figure 9-6 XRD patterns of ZnO-Ge multilayer films.

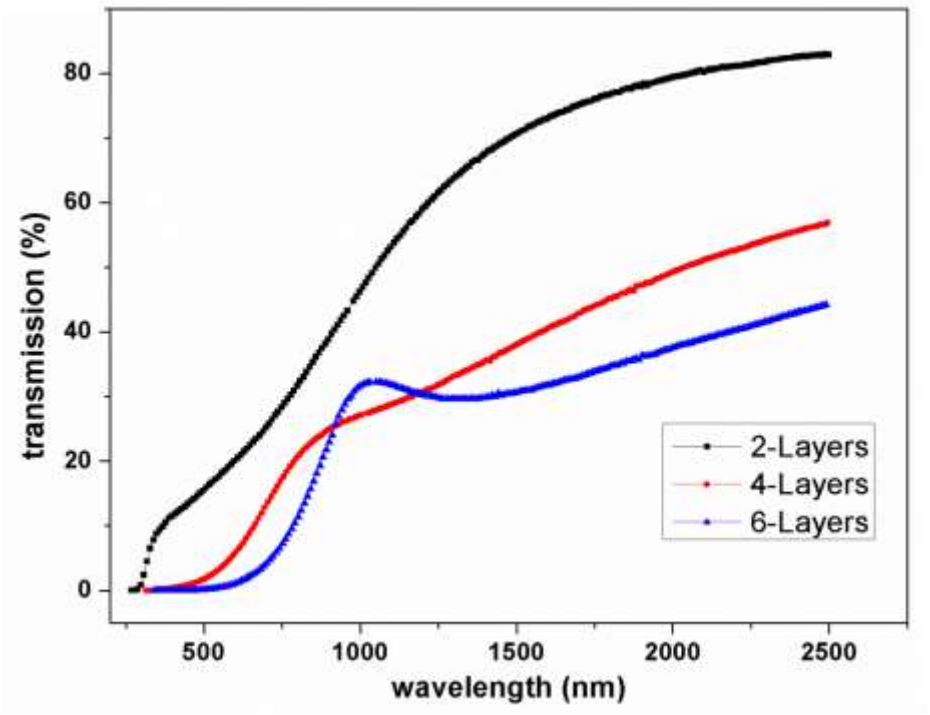

Figure 9-7 Transmission spectra of multilayer thin films

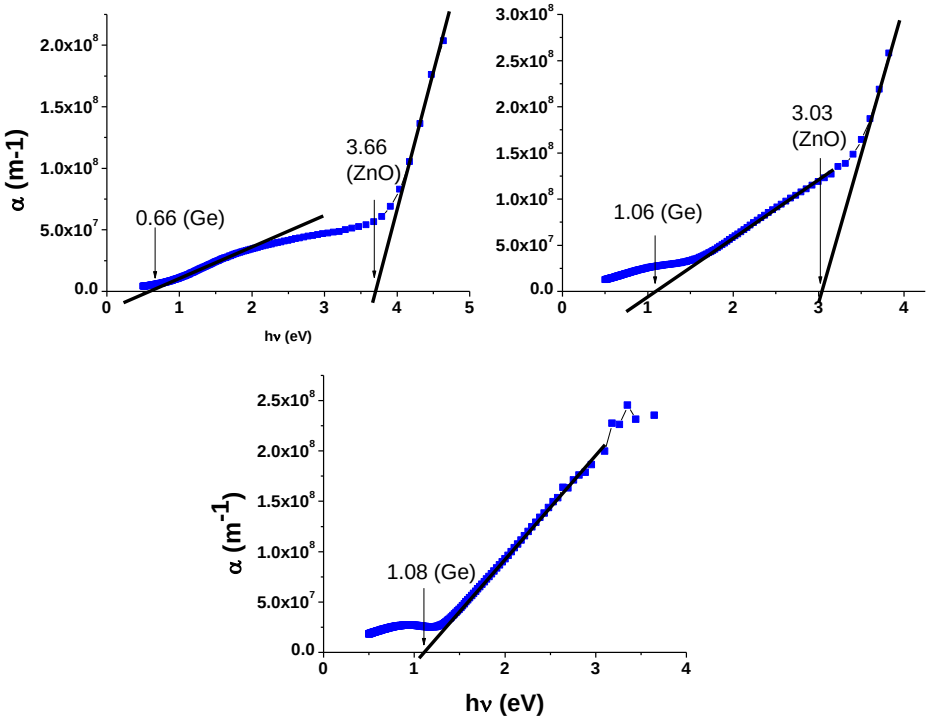

Figure 9-8 Tauc plot used for calculating optical band gap of multilayer films.

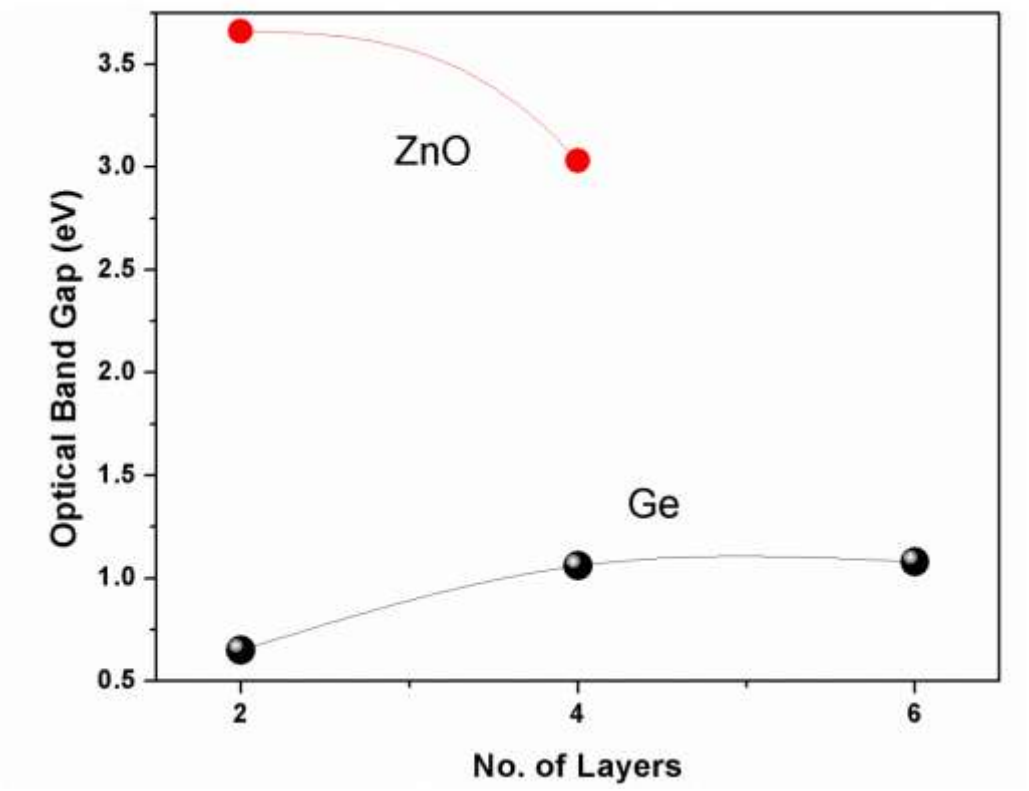

Figure 9-9 Plot of band gap variation as a function of number of layers.

Fig. 9-11 represents the reflectance of the multilayer thin films as a function of wavelength. The multilayer films have shown a specific trend which has certain maximum value of reflectance around specific wavelength region. The 2 layer film represents two maxima at 1346 and 600 nm. These maxima shifted towards lower wavelength region and also decreased in magnitude as the no. of multilayer increased.

The reflectance was used to measure the refractive index of the films using this relation [358].

$$n = \sqrt{\frac{1+\sqrt{R}}{1-\sqrt{R}}}$$

The refractive index of the films has shown for two regions from 200-1000 nm and 1000-2500 nm separately (Fig. 9-12). There has been a rapid decrease in refractive index from a higher value to about 1.20 in the UV region and then maintained a nearly steady magnitude between 1.13 – 1.20 in the visible and near IR region.

But in the infra red region, as the no. of multilayer increased, the refractive index showed a linear trend with decreasing slope. Six layer film have slightly less variation with value between 1.13 – 1.14, while this value increased to 1.13- 1.18 for four layers and 1.15 -1.29 for two layers.

This graph in Fig. 9-13 represents the value of refractive index at 589.3 nm, as a function of the no. of multilayer. At this wave length the value of refractive index in the case of four layers is higher than that of two and six layers.

The complex refractive index n* is defined as

$$n^* = n - ik$$

where k is the imaginary part of n* known as 'extinction coefficient' and is given by the relation [150, 359]

$$k = \frac{\alpha\lambda}{4\pi}$$

Fig. 9-14 represents the extinction coefficient of the film calculate using above equation as a function of wavelength. The extinction coefficient is found to be nearly constant in the wavelength range of 1250 - 2500 nm. But in the lower wavelength range it decreased with increasing wavelength and formed a lower edge which shifted towards right as the number of multilayer increased.

The relative permittivity of the multi-layer films was determined from the relation $\varepsilon = n^2$ as shown in Fig. 9-15. The permittivity of the multilayer films decreased rapidly in the visible region followed by a gradual increase in the IR region. The increasing trend of permittivity in the IR region is more prominent in case of 2 layer film as compared to the 6 layer film.

The equation given below has been used to study the optical conductivity of the normally incident photons on the ZnO-Ge multilayer films [359-360].

$$\sigma = \frac{\alpha \,.\, n \,.\, c}{4\,\pi}$$

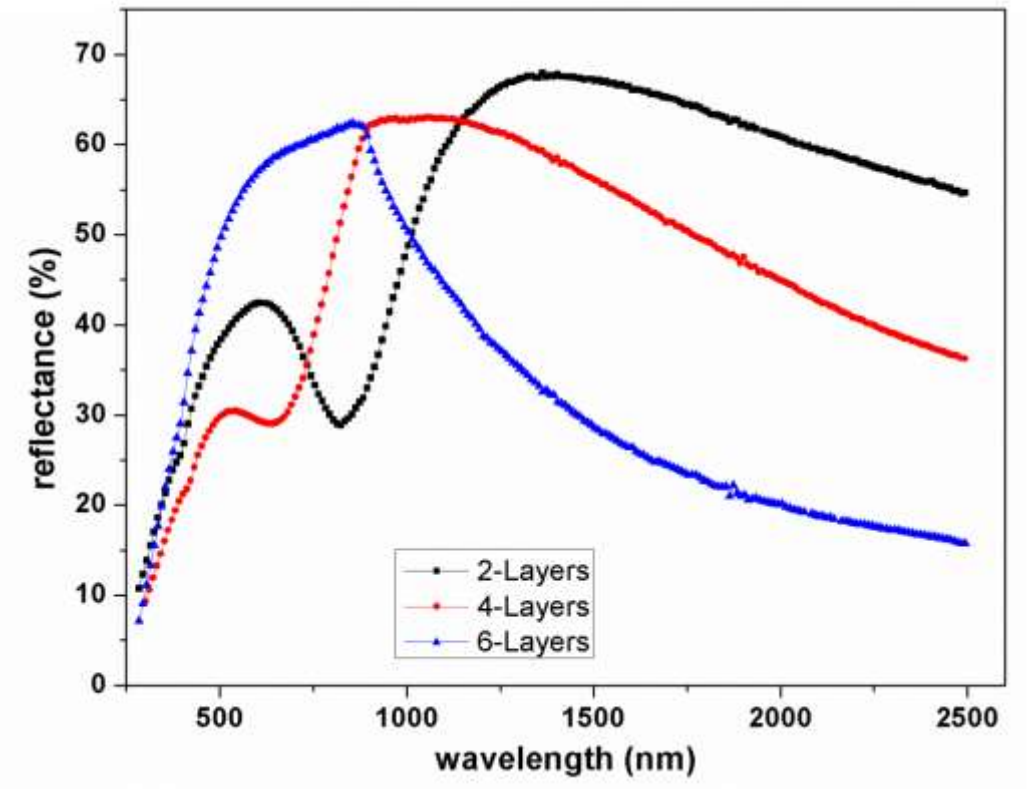

Figure 9-10 Reflection spectra of ZnO-Ge multilayer films.

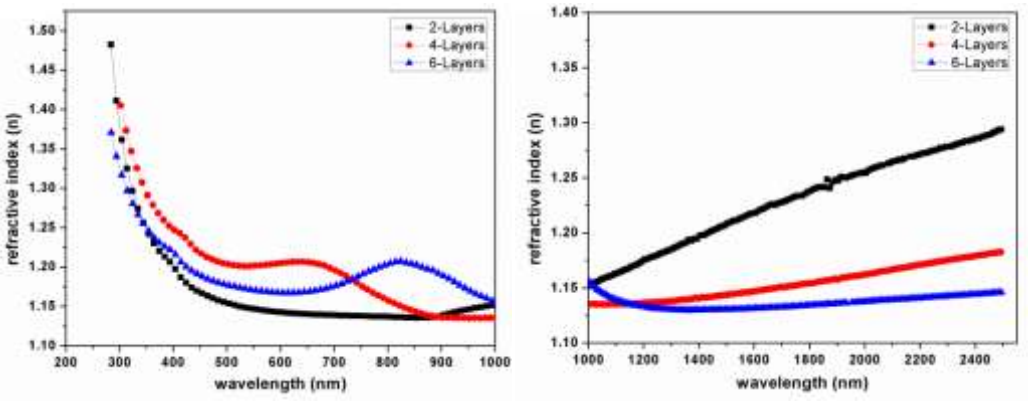

Figure 9-11 Refractive index of multilayer films estimated from the reflection data.

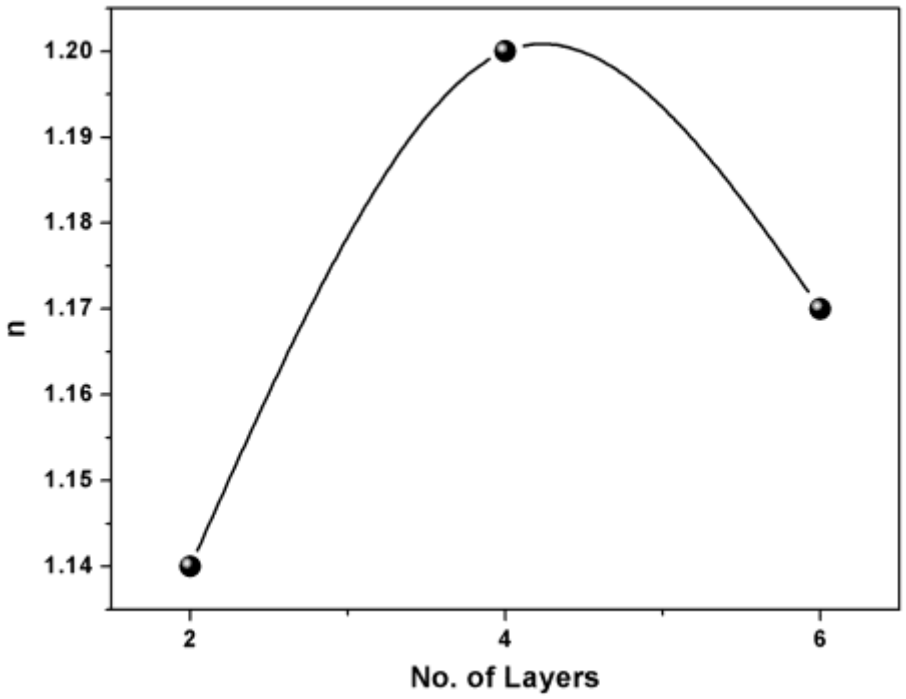

Figure 9-12 Plot of variation of refractive index as a function of number of layers.

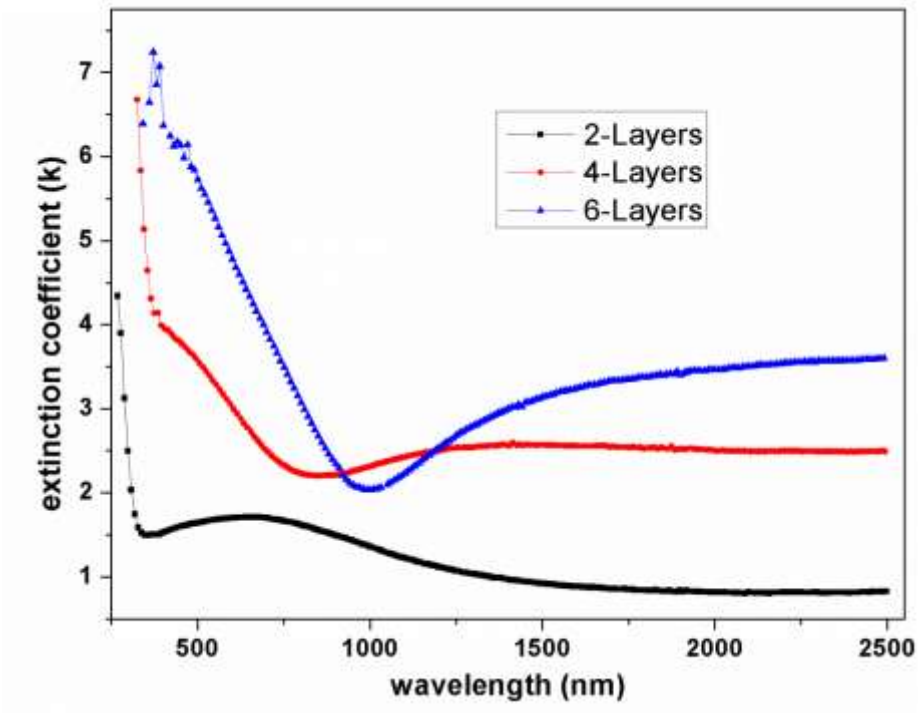

Figure 9-13 Plot for extinction coefficients of multilayer films.

The fig 9-16 shows a rapid decrease of optical conductivity in the visible region. But after that it gained a nearly constant value of σ in the IR region. The σ showed an increasing trend with the increase in the number of multi-layers of the films

Product of carrier concentration N and mobility μ was found to be a function of reflectance R and thickness x of films in the IR region as expressed below [361-362]:

$$\mu N = \frac{4\,\pi\varepsilon^0 c}{e\,.\,x}\left[\frac{1}{1-R}\right]$$

The product μN in the IR region has been calculated as a function of wavelength and number of layers of the films. It is observed that μN decreases with wavelength (Fig 9-17). Furthermore μN shows variations (increase) with respect to the number of layers in the films.

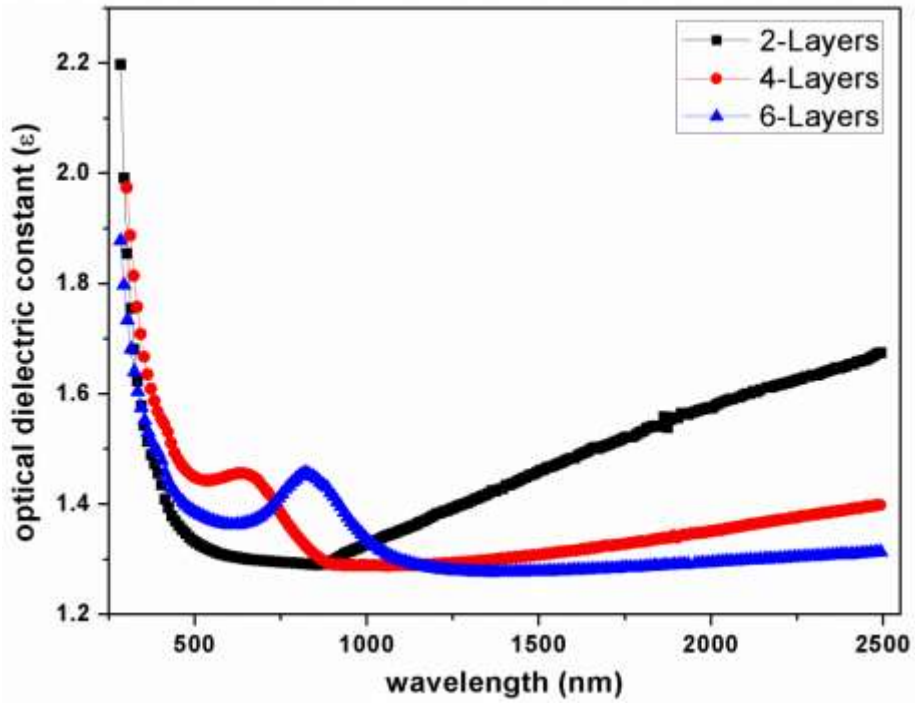

Figure 9-14 Optical dielectric constant of multilayer films.

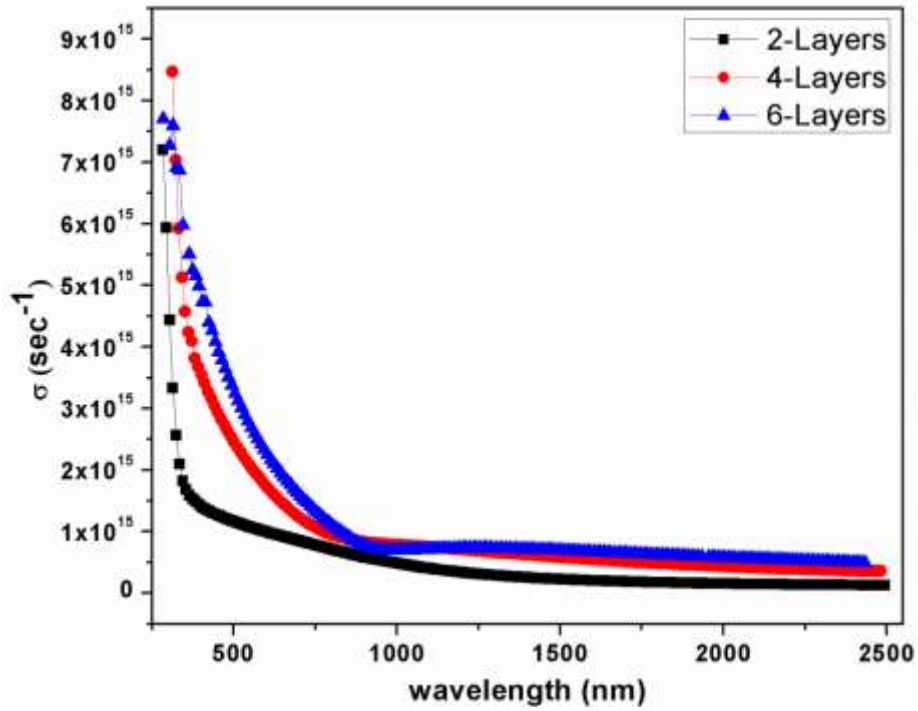

Figure 9-15 Optical conductiveity of mulitlayer films with change in wavelength.

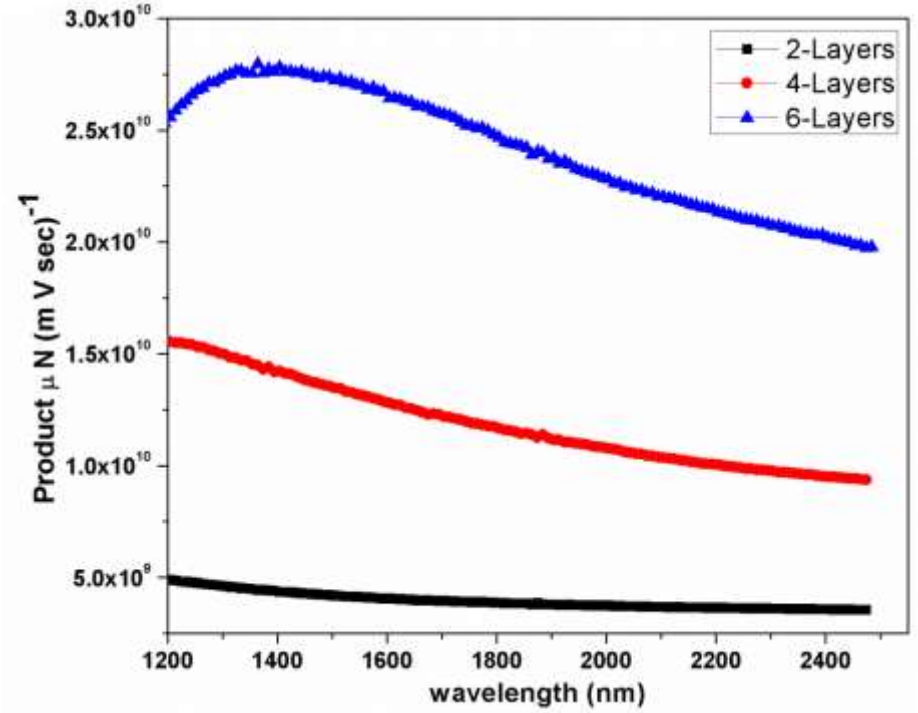

Figure 9-16 Effect of wavelength change on the product of carrier concentration and mobility of carriers in the multilayer films.

The current-viltage caharacteristics of multilayer films has been measured by using four probe method. The curves are taken in the range from 0 to 2 V. it can be seen (Fig. 9.18) that the conductivity of the multilayer films has been increased as the no. of deposited layers are increased. The electrical conductivity of the multilayer films has been calculated by estimating the slope of I-V curve and then putting in the following equation.

$$\sigma = \frac{slope\ of\ I-V\ curve}{thickness\ of\ film}$$

The plot of conductivity vs number of layers in the film is plotted in Figure 9-19. It clearly reaveled the increasing trend of conducvity as the number of multilayers in the films increased.

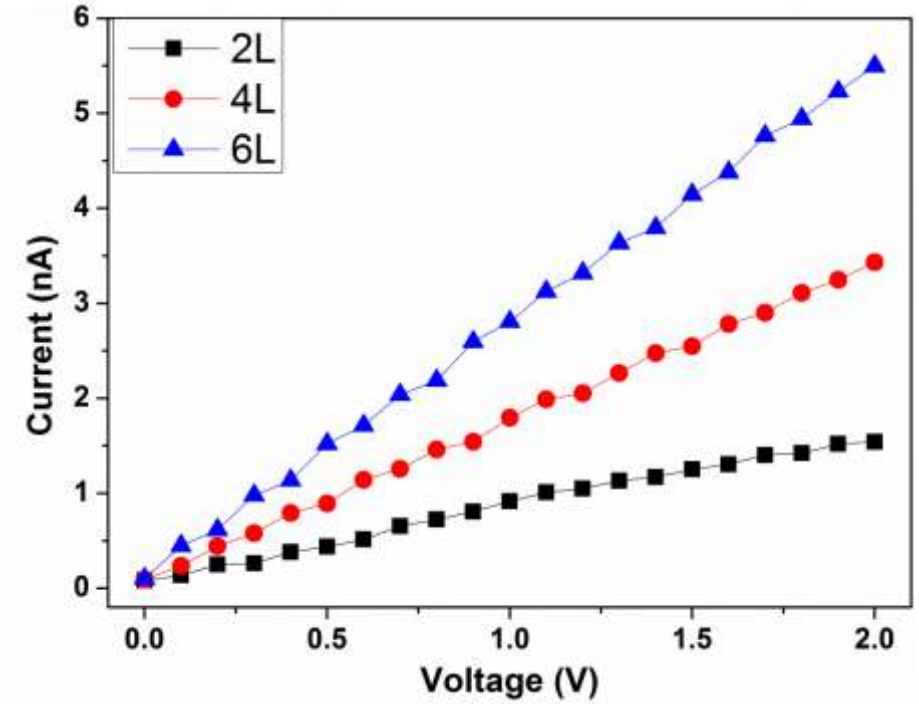

Figure 9-17 Current-Voltage characteristics of ZnO-Ge multilayer films.

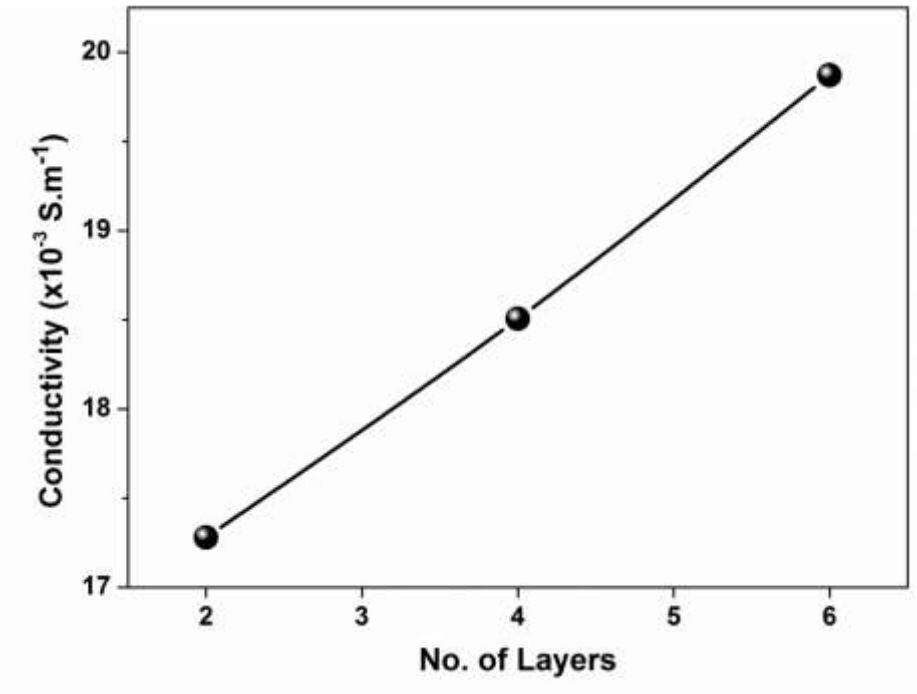

Figure 9-18 Plot of conductivity vs no. of layers in the films.

9.3 Conclusions:

ZnO-Ge multilayer films have been successfully deposited by employing electron beam evaporation and resistive heating for ZnO and Ge alternate layers, respectively. The overall crystal structure of multilayers has been found as amorphous. The low deposition temperature might be the reason for this behavior. The un-wanted oxygen diffusion in the Ge layers might have been done during the deposition. The thickness of the layers have found difficult to control and results in the higher surface roughness as the number of layers increased. The optical band gap has shown a shift of indirect ti direct band gap for germanium. The separate band gaps calculated from the tauc plot represents the quantum confinement of the carries. The optical and electrical conductivities are also increased to certain extent by increasing layers.

10 Summary

ZnO nanorods and nanowires have been formed by employing a new approach, which has also been proved useful for heavily Ni-doped ZnO nanostructures. In this approach, initially, zinc metal or (zinc-nickel) alloy films are formed by electrolytic deposition in chloride bath at a current density of 350-700 A m^{-2}; then, these films are oxidized hydrothermally to form ZnO nanostructures. In this way, ZnO nanorods are formed on conducting substrate of interest.

The effect of oxidation temperature on the structure and optical properties of un-doped ZnO nano-structures has been studied. Highly crystalline wurtzite ZnO nano-structures have been grown by the electro-deposition of zinc on copper substrate followed by its hydrothermal oxidation in NaCl solution at 100-130ºC. Scanning electron microscopy has revealed the formation of nanowires and nanorods (with a diameter of about 100 nm to more than 1 μm). By HRTEM and electron diffraction, these rods are confirmed to single crystalline grown along c-axis. With the increase in temperature, the diameter of nanorods increases from 0.1-0.75 μm at 100 ºC, to 3.2 μm at 130 ºC. The rod-like morphology is mostly converted to micro tubes at 130 ºC. The top of the nanorods are flat at lower temperatures and become conical at higher temperatures. For microtubes of various diameters, the wall thickness remains about 0.9 μm. Optical studies illustrate strong ultraviolet emission in the photoluminescence and cathodo-luminescence spectra without defect related emission (for most conditions), which proves that high-quality ZnO structures are formed by our technique with a strong potentials for optical and optoelectronic devices, with excellent control on undesirable defect emissions.

It has been seen that hydrothermal oxidation of zinc in NaCl solution (which has not been attempted before our group) is highly desirable than in pure water, as defect emission seen in case of the later tends to diminish in case of the former solution.

Furthermore, Zn-Ni alloy films have been formed by electrodeposition. Varying amount of nickel (upto about 17 at%) has been incorporated in these films by

suitable choice of electrolysis conditions. It has surprisingly seen that Wurtzite ZnO nanorods are formed retaining all the nickel, allowing to form ZnO nanorods heavily doped by nickel (17%). This doping level has never been achieved before without formation of nickel oxide impurity phases.

The wire diameter decreases with Ni content, up to about 20-50 nm for the $Zn_{0.83}Ni_{0.17}O$ nanowires formed in NaCl solution at 100°C. A strong ultra-violet emission is seen in the photoluminescence spectra obtained at 10 K and room temperature. Nickel doping itself has been observed to quench / diminish the defect emission in PL spectra. For instance, substantial visible emission exhibited by un-doped ZnO nano-structures formed in pure water at 100°C becomes negligible by nickel doping and almost completely vanishes for the samples prepared in chloride solution, due to higher crystalline quality.

In order to investigate the effects of post growth heat treatment on the crystallinity of ZnO nanostructures formed by above technique, as well as, on the emission characteristics, annealing in air (oxygen rich) and organ (oxygen deficient) environment has been performed at 500 °C for 2 hours. Although annealing has been often attempted to remove the defects, but it has never been proved effective to anneal out the defects. The same has been confirmed in this study that in the samples that don't have defects in the as-fabricated form, relatively intense emission in the visible region is seen as related with oxygen vacancies (green) and its interstitials (orange-red) after annealing in argon and air, respectively. This is also accompanied by decrease in the intensity of UV emission, particularly after annealing in air. This further confirms the viability of our techniques to form ZnO 1-D nanostructures without defect-related emissions for UV devices.

Anyway, it has also been seen that intense green emission can be achieved in these nanostructure if annealed in argon atmosphere. In addition, possibility to employ ZnO nanorods with pure UV emission and their treatment to exhibit tuned emission in the visible region, and the use of phosphors, and hetero/homo junctions, etc., also remains open, although further investigation on similar lines as have been followed for single-crystal GaN films in literatures is required to reach an appropriate conclusion in this direction.

Gold nanoparticles have been formed on the ZnO nano-structures formed hydrothermal oxidation of electrodeposited zinc in water.

Prior to attachment of gold, the surface is etched by potassium iodide. The appearance of prismatic surfaces is mildly affected by etching; while, the top ends are badly affected giving rough appearance. In addition, visible (yellow) emission is greatly enhanced; apparently due to increase in oxygen vacancies.

The gold particles have been attached to the etched-nanostructures by dipping nanostructures in $HAuCl_4$ solution. Granular deposits are formed mostly on the etch pits, although rest of the surfaces is also covered by gold as indicated by EDS analysis. An interesting observation is that the defect emission intensified by etching almost completely vanished after gold deposition. This may partly be due to oxidation / oxygenation of ZnO nanostructures in the gold solution, along with the deposition of gold. Photocatalytic activity of the ZnO has also enhanced by attaching the gold nano-particles to the ZnO nanostructures.

Next section covers the optical properties of thin films of ZnO deposited through various methods and its multilayer structure with Germanium. Initially, the effect of oxygen partial pressure during the sputter deposition on the structure and thickness of ZnO thin films has been studied in next section. The stoichiometry and thickness have been observed to be highly dependent on the oxygen partial pressure. In pure argon, zinc is about 55 at%, while the Zn to O ratio becomes unity at initially threshold level of 10% oxygen in the sputtering chamber. The thickness of the films decreases by oxygen in the chamber. Considering these two facts, 10% oxygen in the sputtering chamber is most appropriate. The films follow the columnar growth along c-axis. The omega scans suggest that c-axis of most crystals remained within an angle of 1-3^o with respect to the sample's normal. Increase in oxygen in the sputtering chamber generally lowers this dispersion. For mutual in-plane orientation / dispersion of columnar crystals, phi scans were performed for (101) or (104) planes. The six-fold symmetry, particularly for the sample grown in argon confirms the tendency to follow epitaxial growth, although with certain degree of dispersion in mutual in-plane orientation possibly responsible for columnar (polycrystalline) nature of the films. Anyway, mutual misorientation remains small possibly indicating small angle boundaries among individual crystals / columns.

Possibly highly strained layer is formed initially which menifests itself by additional peaks in the phi-scan of the films with relatively smaller thickness (formed at higher oxygen partial pressure in the sputtering chamber), these peaks form of pair of triads. This intermediate strained layer is possibly affected by trigonal substrate. As the film thickness increases by lowering the oxygen in the chamber (in the present work), contribution of this intermediate layer diminishes as seen by XRD analysis. Anyway, it has been noticed that although ZnO films with excellent growth along c-axis can be formed by sputtering with some oxygen in the sputtering chamber, growth rate is lowered and contribution of strained layer intensifies.

PLD has also been attempted in air for the growth of ZnO film. In spite of higher growth rate, crystalline quality of these films as observed by omega and phi-scans in XRD measurements was excellent. Hence, ZnO film sputter-deposited in pure argon and PLD ZnO films formed on c-plane sapphire and p-GaN substrates have been compared for other structural, optical and electrical properties. Atomic force microscopy exhibited the surface roughness of 4.33 nm and 12.99 nm for PLD and sputtered ZnO films, respectively. In photoluminescence (PL) measurements, a strong UV emission was observed at 3.30 eV for both ZnO films. However, deep level emission was observed at around 2.61 eV in PLD film, but it had a wide range from 2.61 to 2.29 eV in case of sputter-deposited film. From the transmission spectra, the optical band gap values were found to be 3.29 and 3.28 eV for PLD and sputtered ZnO films, respectively. Hall measurement revealed the resistivity values of 0.0792 and 0.4832 Ω-cm and carrier concentrations of 2.28 × 1018 and 1.73 × 1018 cm-3 for respective PLD and sputtered films. Current-voltage (I-V) curves clearly demonstrated the n-ZnO/p-GaN heterojunction with turn on voltage of 3.8 and 5.2 V for PLD and sputtered deposited samples, respectively.

ZnO-Ge multilayer thin film structures have been deposited by the electron beam evaporation of ZnO and thermal evaporation of Ge on glass substrates. X-ray diffraction showed the amorphous nature of the layered structures. The optical properties exhibited the formation of quantum wells that affected the quantum confinement effects. Various optical and optoelectronic parameters were calculated for multilayer film from the transmission and reflectance data.

11 References:

[1] M. Shinkai, M. Yanase, M. Suzuki, H. Hiroyuki, T. Wakabayashi, J. Yoshida, and T. Kobayashi, "Intracellular hyperthermia for cancer using magnetite cationic liposomes". Journal of Magnetism and Magnetic Materials, vol. 194, pp. 176-184, 1999.

[2] U. O. Häfeli and G. J. Pauer, "In vitro and in vivo toxicity of magnetic microspheres". Journal of Magnetism and Magnetic Materials, vol. 194, pp. 76-82, 1999.

[3] M. Goryll, L. Vescan, K. Schmidt, S. Mesters, H. Lüth, and K. Szot, "Size distribution of Ge islands grown on Si (001)". Applied physics letters, vol. 71, pp. 410-412, 1997.

[4] Y. Niquet, G. Allan, C. Delerue, and M. Lannoo, "Quantum confinement in germanium nanocrystals". Applied physics letters, vol. 77, pp. 1182-1184, 2000.

[5] A. Henglein, "Small-particle research: physicochemical properties of extremely small colloidal metal and semiconductor particles". Chemical Reviews, vol. 89, pp. 1861-1873, 1989/12/01 1989.

[6] H. Weller, "Quantized Semiconductor Particles: A novel state of matter for materials science". Advanced Materials, vol. 5, pp. 88-95, 1993.

[7] H. Weller, H. M. Schmidt, U. Koch, A. Fojtik, S. Baral, A. Henglein, W. Kunath, K. Weiss, and E. Dieman, "Photochemistry of colloidal semiconductors. Onset of light absorption as a function of size of extremely small CdS particles". Chemical Physics Letters, vol. 124, pp. 557-560, 1986.

[8] D. Hayes, O. I. Micic, M. T. Nenadovic, V. Swayambunathan, and D. Meisel, "Radiolytic production and properties of ultrasmall cadmium sulfide particles". The Journal of Physical Chemistry, vol. 93, pp. 4603-4608, 1989/06/01 1989.

[9] A. Hernández Battez, R. González, J. L. Viesca, J. E. Fernández, J. M. Díaz Fernández, A. Machado, R. Chou, and J. Riba, "CuO, ZrO2 and ZnO nanoparticles as antiwear additive in oil lubricants". Wear, vol. 265, pp. 422-428, 2008.

[10] H. G. Völz, J. Kischkewitz, P. Woditsch, A. Westerhaus, W.-D. Griebler, M. De Liedekerke, G. Buxbaum, H. Printzen, M. Mansmann, D. Räde, G. Trenczek, V. Wilhelm, S. Schwarz, H. Wienand, J. Adel, G. Adrian, K. Brandt, W. B. Cork, H. Winkeler, W. Mayer, K. Schneider, L. Leitner, H. Kathrein, E. Schwab, H. Jakusch, M. Ohlinger, R. Veitch, G. Etzrodt, G. Pfaff, K.-D. Franz, R. Emmert, K. Nitta, R. Besold, and H. Gaedcke, "Pigments, Inorganic," in *Ullmann's Encyclopedia of Industrial Chemistry*, ed: Wiley-VCH Verlag GmbH & Co. KGaA, 2000.

[11] C. Klingshirn, "ZnO: From basics towards applications". physica status solidi (b), vol. 244, pp. 3027-3073, 2007.

[12] Z. R. Tian, J. A. Voigt, J. Liu, B. McKenzie, M. J. McDermott, M. A. Rodriguez, H. Konishi, and H. Xu, "Complex and oriented ZnO nanostructures". Nature materials, vol. 2, pp. 821-826, 2003.

[13] Z. L. Wang, "Splendid one-dimensional nanostructures of zinc oxide: a new nanomaterial family for nanotechnology". ACS Nano, vol. 2, pp. 1987-1992, 2008.

[14] S. K. Arya, S. Saha, J. E. Ramirez-Vick, V. Gupta, S. Bhansali, and S. P. Singh, "Recent advances in ZnO nanostructures and thin films for biosensor applications: review". Analytica chimica acta, vol. 737, pp. 1-21, 2012.

[15] J. Wu and D. Xue, "Progress of science and technology of ZnO as advanced material". Science of Advanced Materials, vol. 3, pp. 127-149, 2011.

[16] Z. L. Wang, "Zinc oxide nanostructures: growth, properties and applications". Journal of Physics: Condensed Matter, vol. 16, p. R829, 2004.

[17] A. Mang and K. Reimann, "Band gaps, crystal-field splitting, spin-orbit coupling, and exciton binding energies in ZnO under hydrostatic pressure". Solid State Communications, vol. 94, pp. 251-254, 1995.

[18] J. Muth, J. Lee, I. Shmagin, R. Kolbas, H. Casey Jr, B. Keller, U. Mishra, and S. DenBaars, "Absorption coefficient, energy gap, exciton binding energy, and recombination lifetime of GaN obtained from transmission measurements". Applied physics letters, vol. 71, pp. 2572-2574, 1997.

[19] E. Ohshima, H. Ogino, I. Niikura, K. Maeda, M. Sato, M. Ito, and T. Fukuda, "Growth of the 2-in-size bulk ZnO single crystals by the hydrothermal method". Journal of Crystal Growth, vol. 260, pp. 166-170, 2004.

[20] K. Maeda, M. Sato, I. Niikura, and T. Fukuda, "Growth of 2 inch ZnO bulk single crystal by the hydrothermal method". Semiconductor Science and Technology, vol. 20, p. S49, 2005.

[21] S. W. Lee, H. D. Cho, G. Panin, and T. Won Kang, "Vertical ZnO nanorod/Si contact light-emitting diode". Applied physics letters, vol. 98, pp. 093110-093110-3, 2011.

[22] D. C. Look, "Recent advances in ZnO materials and devices". Materials Science and Engineering: B, vol. 80, pp. 383-387, 2001.

[23] J. Zhou, N. S. Xu, and Z. L. Wang, "Dissolving behavior and stability of ZnO wires in biofluids: a study on biodegradability and biocompatibility of ZnO nanostructures". Advanced Materials, vol. 18, pp. 2432-2435, 2006.

[24] D. C. Reynolds, D. C. Look, and B. Jogai, "Optically pumped ultraviolet lasing from ZnO". Solid State Communications, vol. 99, pp. 873-875, 1996.

[25] P. Yang, H. Yan, S. Mao, R. Russo, J. Johnson, R. Saykally, N. Morris, J. Pham, R. He, and H. J. Choi, "Controlled Growth of ZnO Nanowires and Their Optical Properties". Advanced Functional Materials, vol. 12, pp. 323-331, 2002.

[26] X. Jiaqiang, C. Yuping, C. Daoyong, and S. Jianian, "Hydrothermal synthesis and gas sensing characters of ZnO nanorods". Sensors and Actuators B: Chemical, vol. 113, pp. 526-531, 2006.

[27] K.-S. Weissenrieder and J. Müller, "Conductivity model for sputtered ZnO-thin film gas sensors". Thin Solid Films, vol. 300, pp. 30-41, 1997.

[28] S. Pearton, D. Norton, Y. Heo, L. Tien, M. Ivill, Y. Li, B. Kang, F. Ren, J. Kelly, and A. Hebard, "ZnO spintronics and nanowire devices". Journal of Electronic Materials, vol. 35, pp. 862-868, 2006.

[29] P. Sharma, A. Gupta, K. Rao, F. J. Owens, R. Sharma, R. Ahuja, J. O. Guillen, B. Johansson, and G. Gehring, "Ferromagnetism above room temperature in bulk and transparent thin films of Mn-doped ZnO". Nature materials, vol. 2, pp. 673-677, 2003.

[30] C. Jagadish and S. J. Pearton, *Zinc oxide bulk, thin films and nanostructures: processing, properties, and applications*: Elsevier, 2011.

[31] K. Vanheusden, W. Warren, C. Seager, D. Tallant, J. Voigt, and B. Gnade, "Mechanisms behind green photoluminescence in ZnO phosphor powders". Journal of Applied Physics, vol. 79, pp. 7983-7990, 1996.

[32] M. Ramanachalam, A. Rohatgi, W. Carter, J. Schaffer, and T. Gupta, "Photoluminescence study of ZnO varistor stability". Journal of Electronic Materials, vol. 24, pp. 413-419, 1995.

[33] Z. L. Wang and J. Song, "Piezoelectric Nanogenerators Based on Zinc Oxide Nanowire Arrays". Science, vol. 312, pp. 242-246, April 14, 2006 2006.

[34] N. K. Zayer, R. Greef, K. Rogers, A. Grellier, and C. N. Pannell, "In situ monitoring of sputtered zinc oxide films for piezoelectric transducers". Thin Solid Films, vol. 352, pp. 179-184, 1999.

[35] K. Matsubara, P. Fons, K. Iwata, A. Yamada, K. Sakurai, H. Tampo, and S. Niki, "ZnO transparent conducting films deposited by pulsed laser deposition for solar cell applications". Thin Solid Films, vol. 431, pp. 369-372, 2003.

[36] T. Minami, "New n-type transparent conducting oxides". Mrs Bulletin, vol. 25, pp. 38-44, 2000.

[37] Y. I. Alivov, E. Kalinina, A. Cherenkov, D. C. Look, B. Ataev, A. Omaev, M. Chukichev, and D. Bagnall, "Fabrication and characterization of n-ZnO/p-AlGaN heterojunction light-emitting diodes on 6H-SiC substrates". Applied physics letters, vol. 83, pp. 4719-4721, 2003.

[38] Ü. Özgür, Y. I. Alivov, C. Liu, A. Teke, M. A. Reshchikov, S. Doğan, V. Avrutin, S.-J. Cho, and H. Morkoç, "A comprehensive review of ZnO materials and devices". Journal of Applied Physics, vol. 98, pp. -, 2005.

[39] W. L. Hughes and Z. L. Wang, "Formation of piezoelectric single-crystal nanorings and nanobows". Journal of the American Chemical Society, vol. 126, pp. 6703-6709, 2004.

[40] M. H. Huang, S. Mao, H. Feick, H. Yan, Y. Wu, H. Kind, E. Weber, R. Russo, and P. Yang, "Room-temperature ultraviolet nanowire nanolasers". Science, vol. 292, pp. 1897-1899, 2001.

[41] C. Jagadish and S. Pearton, *Zinc Oxide Bulk, Thin Films and Nanostructures*: Elsevier, 2006.

[42] Ü. Özgür, Y. I. Alivov, C. Liu, A. Teke, M. Reshchikov, S. Doğan, V. Avrutin, S.-J. Cho, and H. Morkoc, "A comprehensive review of ZnO materials and devices". Journal of Applied Physics, vol. 98, p. 041301, 2005.

[43] A. B. Djurišić and Y. H. Leung, "Optical Properties of ZnO Nanostructures". Small, vol. 2, pp. 944-961, 2006.

[44] X. Meng, D. Shen, J. Zhang, D. Zhao, Y. Lu, L. Dong, Z. Zhang, Y. Liu, and X. Fan, "The structural and optical properties of ZnO nanorod arrays". Solid State Communications, vol. 135, pp. 179-182, 2005.

[45] Y. Chen, J. Jiang, Z. He, Y. Su, D. Cai, and L. Chen, "Growth mechanism and characterization of ZnO microbelts and self-assembled microcombs". Materials Letters, vol. 59, pp. 3280-3283, 2005.

[46] P. H. Kasai, "Electron spin resonance studies of donors and acceptors in ZnO". Physical Review, vol. 130, p. 989, 1963.

[47] S. Yamauchi, Y. Goto, and T. Hariu, "Photoluminescence studies of undoped and nitrogen-doped ZnO layers grown by plasma-assisted epitaxy". Journal of Crystal Growth, vol. 260, pp. 1-6, 2004.

[48] X. Liu, X. Wu, H. Cao, and R. Chang, "Growth mechanism and properties of ZnO nanorods synthesized by plasma-enhanced chemical vapor deposition". Journal of Applied Physics, vol. 95, pp. 3141-3147, 2004.

[49] D. Li, Y. H. Leung, A. B. Djurišić, Z. T. Liu, M. H. Xie, S. L. Shi, S. J. Xu, and W. K. Chan, "Different origins of visible luminescence in ZnO nanostructures fabricated by the chemical and evaporation methods". Applied Physics Letters, vol. 85, pp. 1601-1603, 2004.

[50] L. E. Greene, M. Law, J. Goldberger, F. Kim, J. C. Johnson, Y. Zhang, R. J. Saykally, and P. Yang, "Low-temperature wafer-scale production of ZnO nanowire arrays". Angewandte Chemie International Edition, vol. 42, pp. 3031-3034, 2003.

[51] F. Tuomisto, K. Saarinen, D. C. Look, and G. C. Farlow, "Introduction and recovery of point defects in electron-irradiated ZnO". Physical Review B, vol. 72, p. 085206, 2005.

[52] X. Yang, G. Du, X. Wang, J. Wang, B. Liu, Y. Zhang, D. Liu, D. Liu, H. Ong, and S. Yang, "Effect of post-thermal annealing on properties of ZnO thin film grown on c-Al 2 O 3 by metal-organic chemical vapor deposition". Journal of Crystal Growth, vol. 252, pp. 275-278, 2003.

[53] M. Liu, A. Kitai, and P. Mascher, "Point defects and luminescence centres in zinc oxide and zinc oxide doped with manganese". Journal of Luminescence, vol. 54, pp. 35-42, 1992.

[54] G. Manabu, O. Naoko, O. Kenichi, and K. Mikio, "Photoluminescent and Structural Properties of Precipitated ZnO Fine Particles". Japanese Journal of Applied Physics, vol. 42, p. 481, 2003.

[55] A. Janotti and C. G. Van de Walle, "Native point defects in ZnO". Physical Review B, vol. 76, p. 165202, 2007.

[56] T. Kogure and Y. Bando, "Formation of ZnO nanocrystals in the cubic phase was reported by electron-beam induced oxidation of ZnS surfaces during TEM observations". J Electron Microsc, vol. 47, p. 7903, 1993.

[57] A. B. M. A. Ashrafi, A. Ueta, A. Avramescu, H. Kumano, I. Suemune, Y.-W. Ok, and T.-Y. Seong, "Growth and characterization of hypothetical zinc-blende ZnO films on GaAs(001) substrates with ZnS buffer layers". Applied physics letters, vol. 76, pp. 550-552, 2000.

[58] C. H. Bates, W. B. White, and R. Roy, "New high-pressure polymorph of zinc oxide". Science, vol. 137, pp. 993-993, 1962.

[59] A. Ashrafi and C. Jagadish, "Review of zincblende ZnO: stability of metastable ZnO phases". Journal of Applied Physics, vol. 102, p. 071101, 2007.

[60] J. E. Jaffe, J. A. Snyder, Z. Lin, and A. C. Hess, "LDA and GGA calculations for high-pressure phase transitions in ZnO and MgO". Physical Review B, vol. 62, p. 1660, 2000.

[61] M. Gomi, N. Oohira, K. Ozaki, and M. Koyano, "Photoluminescent and structural properties of precipitated ZnO fine particles". Japanese Journal of Applied Physics, vol. 42, p. 481, 2003.

[62] Z. Fan, P.-c. Chang, J. G. Lu, E. C. Walter, R. M. Penner, C.-h. Lin, and H. P. Lee, "Photoluminescence and polarized photodetection of single ZnO nanowires". Applied physics letters, vol. 85, pp. 6128-6130, 2004.

[63] Q. Zhao, P. Klason, M. Willander, H. Zhong, W. Lu, and J. Yang, "Deep-level emissions influenced by O and Zn implantations in ZnO". Applied physics letters, vol. 87, pp. 211912-211912, 2005.

[64] Y. Heo, D. Norton, and S. Pearton, "Origin of green luminescence in ZnO thin film grown by molecular-beam epitaxy". Journal of Applied Physics, vol. 98, p. 073502, 2005.

[65] Y. Leung, K. Tam, A. Djurišić, M. Xie, W. Chan, D. Lu, and W. Ge, "Zno nanoshells: Synthesis, structure, and optical properties". Journal of Crystal Growth, vol. 283, pp. 134-140, 2005.

[66] D. Reynolds, D. C. Look, and B. Jogai, "Fine structure on the green band in ZnO". Journal of Applied Physics, vol. 89, pp. 6189-6191, 2001.

[67] A. Van Dijken, E. Meulenkamp, D. Vanmaekelbergh, and A. Meijerink, "Identification of the transition responsible for the visible emission in ZnO using quantum size effects". Journal of Luminescence, vol. 90, pp. 123-128, 2000.

[68] A. van Dijken, E. A. Meulenkamp, D. Vanmaekelbergh, and A. Meijerink, "The kinetics of the radiative and nonradiative processes in nanocrystalline

ZnO particles upon photoexcitation". The Journal of Physical Chemistry B, vol. 104, pp. 1715-1723, 2000.

[69] K. Vanheusden, C. Seager, W. t. Warren, D. Tallant, and J. Voigt, "Correlation between photoluminescence and oxygen vacancies in ZnO phosphors". Applied physics letters, vol. 68, pp. 403-405, 1996.

[70] D. C. Reynolds, D. C. Look, B. Jogai, and H. Morkoc, "Similarities in the bandedge and deep-centre photoluminescence mechanisms of ZnO and GaN". Solid State Communications, vol. 101, pp. 643-646, 1997.

[71] F. Kröger and H. Vink, "The origin of the fluorescence in self-activated ZnS, CdS, and ZnO". The Journal of Chemical Physics, vol. 22, pp. 250-252, 1954.

[72] S. Studenikin, N. Golego, and M. Cocivera, "Fabrication of green and orange photoluminescent, undoped ZnO films using spray pyrolysis". Journal of Applied Physics, vol. 84, pp. 2287-2294, 1998.

[73] M. Willander, O. Nur, Q. Zhao, L. Yang, M. Lorenz, B. Cao, J. Z. Pérez, C. Czekalla, G. Zimmermann, and M. Grundmann, "Zinc oxide nanorod based photonic devices: recent progress in growth, light emitting diodes and lasers". Nanotechnology, vol. 20, p. 332001, 2009.

[74] T. M. Børseth, B. Svensson, A. Y. Kuznetsov, P. Klason, Q. Zhao, and M. Willander, "Identification of oxygen and zinc vacancy optical signals in ZnO". Applied physics letters, vol. 89, p. 262112, 2006.

[75] P. Klason, T. M. Børseth, Q. X. Zhao, B. G. Svensson, A. Y. Kuznetsov, P. J. Bergman, and M. Willander, "Temperature dependence and decay times of zinc and oxygen vacancy related photoluminescence bands in zinc oxide". Solid State Communications, vol. 145, pp. 321-326, 2008.

[76] C. H. Ahn, Y. Y. Kim, D. C. Kim, S. K. Mohanta, and H. K. Cho, "A comparative analysis of deep level emission in ZnO layers deposited by various methods". Journal of Applied Physics, vol. 105, p. 13502, 2009.

[77] R. Dingle, "Luminescent transitions associated with divalent copper impurities and the green emission from semiconducting zinc oxide". Physical review letters, vol. 23, p. 579, 1969.

[78] C. G. Van de Walle, "Hydrogen as a cause of doping in zinc oxide". Physical review letters, vol. 85, p. 1012, 2000.

[79] R. Deng, X. Zhang, E. Zhang, Y. Liang, Z. Liu, H. Xu, and S. Hark, "Planar Defects in Sn-Doped Single-Crystal ZnO Nanobelts". The Journal of Physical Chemistry C, vol. 111, pp. 13013-13015, 2007/09/01 2007.

[80] S. Fujihara, Y. Ogawa, and A. Kasai, "Tunable Visible Photoluminescence from ZnO Thin Films through Mg-Doping and Annealing". Chemistry of Materials, vol. 16, pp. 2965-2968, 2004/07/01 2004.

[81] D. Chu, Y.-P. Zeng, and D. Jiang, "Synthesis of Room-Temperature Ferromagnetic Co-Doped ZnO Nanocrystals under a High Magnetic Field". The Journal of Physical Chemistry C, vol. 111, pp. 5893-5897, 2007/04/01 2007.

[82] F. Ahmed, N. Arshi, M. Anwar, S. H. Lee, E. S. Byon, N. J. Lyu, and B. H. Koo, "Effect of Ni substitution on structural, morphological and magnetic properties of Zn 1-x Ni x O nanorods". Current Applied Physics, vol. 12, pp. S174-S177, 2012.

[83] J. Zhao, L. Wang, X. Yan, Y. Yang, Y. Lei, J. Zhou, Y. Huang, Y. Gu, and Y. Zhang, "Structure and photocatalytic activity of Ni-doped ZnO nanorods". Materials Research Bulletin, vol. 46, pp. 1207-1210, 2011.

[84] F. Ahmed, N. Arshi, M. S. Anwar, S. H. Lee, E. S. Byon, N. J. Lyu, and B. H. Koo, "Effect of Ni substitution on structural, morphological and magnetic properties of Zn1-xNixO nanorods". Current Applied Physics, vol. 12, pp. S174-S177, 2012.

[85] L.-N. Tong, T. Cheng, H.-B. Han, J.-L. Hu, X.-M. He, Y. Tong, and C. M. Schneider, "Photoluminescence studies on structural defects and room temperature ferromagnetism in Ni and Ni–H doped ZnO nanoparticles". Journal of Applied Physics, vol. 108, pp. -, 2010.

[86] R. Saravanan, K. Santhi, N. Sivakumar, V. Narayanan, and A. Stephen, "Synthesis and characterization of ZnO and Ni doped ZnO nanorods by thermal decomposition method for spintronics application". Materials Characterization, vol. 67, pp. 10-16, 2012.

[87] J. Liu, M. Yu, and W. Zhou, "Fabrication of Mn-doped ZnO diluted magnetic semiconductor nanostructures by chemical vapor deposition". Journal of Applied Physics, vol. 99, p. 08M119, 2006.

[88] X. Yan, D. Hu, H. Li, L. Li, X. Chong, and Y. Wang, "Nanostructure and optical properties of M doped ZnO (M= Ni, Mn) thin films prepared by sol–gel process". Physica B: Condensed Matter, vol. 406, pp. 3956-3962, 2011.

[89] X. Ma and C. Lou, "The dilute magnetic and optical properties of Mn-doped ZnO nanowires". Journal of Nanomaterials, vol. 2011, p. 48, 2011.

[90] Z. W. Pan, S. M. Mahurin, S. Dai, and D. H. Lowndes, "Nanowire Array Gratings with ZnO Combs". Nano Letters, vol. 5, pp. 723-727, 2005/04/01 2005.

[91] R. S. Wagner and W. C. Ellis, "VAPOR-LIQUID-SOLID MECHANISM OF SINGLE CRYSTAL GROWTH". Applied Physics Letters, vol. 4, pp. 89-90, 1964.

[92] WangWang, C. J. Summers, and Z. L. Wang, "Large-Scale Hexagonal-Patterned Growth of Aligned ZnO Nanorods for Nano-optoelectronics and Nanosensor Arrays". Nano Letters, vol. 4, pp. 423-426, 2004/03/01 2004.

[93] WangWang, Song, P. Li, J. H. Ryou, R. D. Dupuis, C. J. Summers, and Z. L. Wang, "Growth of Uniformly Aligned ZnO Nanowire Heterojunction Arrays on GaN, AlN, and Al0.5Ga0.5N Substrates". Journal of the American Chemical Society, vol. 127, pp. 7920-7923, 2005/06/01 2005.

[94] X. Meng, B. Lin, B. Gu, J. Zhu, and Z. Fu, "A simple growth route towards ZnO thin films and nanorods". Solid State Communications, vol. 135, pp. 411-415, 2005.

[95] J. J. Wu and S. C. Liu, "Low-Temperature Growth of Well-Aligned ZnO Nanorods by Chemical Vapor Deposition". Advanced Materials, vol. 14, pp. 215-218, 2002.

[96] Y.-J. Kim, C.-H. Lee, Y. J. Hong, G.-C. Yi, S. S. Kim, and H. Cheong, "Controlled selective growth of ZnO nanorod and microrod arrays on Si substrates by a wet chemical method". Applied Physics Letters, vol. 89, pp. -, 2006.

[97] L. Vayssieres, "Growth of Arrayed Nanorods and Nanowires of ZnO from Aqueous Solutions". Advanced Materials, vol. 15, pp. 464-466, 2003.

[98] Y. Zhao, D. O. Wang, and K. C. Martin, "Preparation of Aplysia Sensory-motor Neuronal Cell Cultures". Journal of visualized experiments : JoVE, p. 1355, 2009.

[99] J. Bae, E. L. Shim, Y. Park, H. Kim, J. M. Kim, C. J. Kang, and Y. J. Choi, "Direct observation of enhanced cathodoluminescence emissions from ZnO nanocones compared with ZnO nanowire arrays". Nanotechnology, vol. 22, p. 285711, 2011.

[100] T. Thomas, S. Chatman, J. Wells, L. Emberley, M. A. Rasheed, and K. M. Poduska, "Lateral Heterogeneities in ZnO Electrodeposits and Their Impact on Electrical and Optical Properties". ECS Solid State Letters, vol. 1, pp. P35-P37, January 1, 2012 2012.

[101] L. Yuan, C. Wang, R. Cai, Y. Wang, and G. Zhou, "Temperature-dependent growth mechanism and microstructure of ZnO nanostructures grown from the thermal oxidation of zinc". Journal of Crystal Growth, vol. 390, pp. 101-108, 2014.

[102] N. Goswami and A. Sahai, "Structural transformation in nickel doped zinc oxide nanostructures". Materials Research Bulletin, vol. 48, pp. 346-351, 2013.

[103] Y. C. Kong, D. P. Yu, B. Zhang, W. Fang, and S. Q. Feng, "Ultraviolet-emitting ZnO nanowires synthesized by a physical vapor deposition approach". Applied Physics Letters, vol. 78, pp. 407-409, 2001.

[104] A. Hadi, H. Hajghassem, and M. Dousti, "Ultra-fine UV photoluminescence emission at room temperature from an individual ZnO nanorod". Journal of the Korean Physical Society, vol. 62, pp. 800-803, 2013/03/01 2013.

[105] Y. W. Heo, D. P. Norton, L. C. Tien, Y. Kwon, B. S. Kang, F. Ren, S. J. Pearton, and J. R. LaRoche, "ZnO nanowire growth and devices". Materials Science and Engineering: R: Reports, vol. 47, pp. 1-47, 2004.

[106] I. Isakov, M. Panfilova, M. J. L. Sourribes, and P. A. Warburton, "Growth of ZnO and ZnMgO nanowires by Au-catalysed molecular-beam epitaxy". physica status solidi (c), vol. 10, pp. 1308-1313, 2013.

[107] K. Miyamoto, M. Sano, H. Kato, and T. Yao, "High-electron-mobility ZnO epilayers grown by plasma-assisted molecular beam epitaxy". Journal of Crystal Growth, vol. 265, pp. 34-40, 2004.

[108] D. C. Look, D. C. Reynolds, C. W. Litton, R. L. Jones, D. B. Eason, and G. Cantwell, "Characterization of homoepitaxial p-type ZnO grown by molecular beam epitaxy". Applied physics letters, vol. 81, pp. 1830-1832, 2002.

[109] K. B. Sundaram and A. Khan, "Characterization and optimization of zinc oxide films by r.f. magnetron sputtering". Thin Solid Films, vol. 295, pp. 87-91, 1997.

[110] M. H. Huang, Y. Wu, H. Feick, N. Tran, E. Weber, and P. Yang, "Catalytic Growth of Zinc Oxide Nanowires by Vapor Transport". Advanced Materials, vol. 13, pp. 113-116, 2001.

[111] H. Kim, J. Moon, and H. Lee, "Growth of ZnO nanorods on various substrates by electrodeposition". Electronic Materials Letters, vol. 5, pp. 135-138, 2009/09/01 2009.

[112] L. Xu, Y. Guo, Q. Liao, J. Zhang, and D. Xu, "Morphological Control of ZnO Nanostructures by Electrodeposition". The Journal of Physical Chemistry B, vol. 109, pp. 13519-13522, 2005/07/01 2005.

[113] O. Lupan, T. Pauporté, B. Viana, I. M. Tiginyanu, V. V. Ursaki, and R. Cortès, "Epitaxial Electrodeposition of ZnO Nanowire Arrays on p-GaN for Efficient UV-Light-Emitting Diode Fabrication". ACS Applied Materials & Interfaces, vol. 2, pp. 2083-2090, 2010/07/28 2010.

[114] Q. Xu, Q. Cheng, Z. Zhang, R. Hong, X. Chen, Z. Wu, and F. Zhang, "Synthesis of ZnO nanostructures by spontaneous oxidation of Zn films on p-type silicon substrates". Journal of Alloys and Compounds, vol. 590, pp. 260-265, 2014.

[115] C. F. Guo, Y. Wang, and Q. Liu, "Ultrathin ZnO Nanostructures Synthesized by Thermal Oxidation of Hexagonal Zn Micro/Nanostructures". Journal of Nanoscience and Nanotechnology, vol. 10, pp. 7167-7170, 2010.

[116] R.-q. Chen, C.-w. Zou, X.-d. Yan, and W. Gao, "Zinc oxide nanostructures and porous films produced by oxidation of zinc precursors in wet-oxygen atmosphere". Progress in Natural Science: Materials International, vol. 21, pp. 81-96, 2011.

[117] F. J. Humphreys and M. Hatherly. (2004). *Recrystallization and Related Annealing Phenomena (Second ed.)*.

[118] B. D. Cullity and S. R. Stock. (2001). *Elements of X ray diffraction (Third ed.)*.

[119] C. Kittel. (1996). *Introduction to Solid State Physics (Seventh ed.)*.

[120] G. Binnig, C. F. Quate, and C. Gerber, "Atomic force microscope". Physical review letters, vol. 56, p. 930, 1986.

[121] C. Quate, "The AFM as a tool for surface imaging". Surface Science, vol. 299, pp. 980-995, 1994.

[122] D. Sarid, *Scanning force microscopy: with applications to electric, magnetic, and atomic forces* vol. 88: Oxford University Press New York, 1994.

[123] G. Meyer and N. M. Amer, "Novel optical approach to atomic force microscopy". Applied physics letters, vol. 53, pp. 1045-1047, 1988.

[124] V. Cosslett, "Fifty years of instrumental development of the electron microscope". Advances in Optical and Electron Microscopy, vol. 10, pp. 215-267, 1987.

[125] L. De Broglie, "Waves and quanta". Nature, vol. 112, pp. 540-540, 1923.

[126] J. I. Goldstein, D. E. Newbury, P. Echlin, D. C. Joy, C. Fiori, and E. Lifshin, *Scanning electron microscopy and X-ray microanalysis. A text for biologists, materials scientists, and geologists*: Plenum Publishing Corporation, 1981.

[127] T. Everhart and R. Thornley, "Wide-band detector for micro-microampere low-energy electron currents". Journal of scientific instruments, vol. 37, p. 246, 1960.

[128] R. Schumacker and R. Lomax, "SEM Basics". A beginner's guide to structural equation modeling, pp. 61-78, 2004.

[129] S. L. Flegler, J. W. Heckman, and K. L. Klomparens, *Scanning and transmission electron microscopy: an introduction*: WH Freeman New York, 1993.

[130] P. J. Goodhew, J. Humphreys, and R. Beanland, *Electron microscopy and analysis*: CRC Press, 2000.

[131] S. Amelinckx, D. van Dyck, J. van Landuyt, and G. van Tendeloo, *Handbook of Microscopy, Handbook of Microscopy: Applications in Materials Science, Solid-State Physics, and Chemistry. Methods II*: John Wiley & Sons, 2008.

[132] H. Leamy, "Charge collection scanning electron microscopy". Journal of Applied Physics, vol. 53, pp. R51-R80, 1982.

[133] K. Kanda, "Energy dispersive X-ray spectrometer," ed: Google Patents, 1991.

[134] D. Shindo and T. Oikawa, "Energy Dispersive X-ray Spectroscopy," in *Analytical Electron Microscopy for Materials Science*, ed: Springer, 2002, pp. 81-102.

[135] K. Heinrich, D. Newbury, and R. Myklebust, "Energy dispersive X-ray spectrometry". Gaithersburg, Md, 23-25 Apr. 1979, p. 1981, 1979.

[136] R. Van Grieken and A. Markowicz, *Handbook of X-ray Spectrometry*: CRC Press, 2001.

[137] R. Jenkins, *Quantitative X-ray spectrometry*: CRC Press, 1995.

[138] D. K. Schroder, *Semiconductor material and device characterization*: John Wiley & Sons, 2006.

[139] P. E. Flewitt and R. K. Wild, *Physical methods for materials characterisation*: CRC Press, 2003.

[140] M. Went and M. Vos, "Rutherford backscattering using electrons as projectiles: underlying principles and possible applications". Nuclear Instruments and Methods in Physics Research Section B: Beam Interactions with Materials and Atoms, vol. 266, pp. 998-1011, 2008.

[141] L. Palmetshofer, "Rutherford back-scattering spectroscopy (RBS)". Surface and Thin Film Analysis: A Compendium of Principles, Instrumentation, and Applications, 2011.

[142] A. Markwitz, W. Matz, B. Schmidt, and R. Grötzschel, "Depth profile analysis: STEM-EDX vs. RBS". Surface and interface analysis, vol. 26, pp. 359-366, 1998.

[143] H. Metzner, M. Gossla, and T. Hahn, "Rutherford backscattering spectroscopy of rough films: Theoretical considerations". Nuclear Instruments and Methods in Physics Research Section B: Beam Interactions with Materials and Atoms, vol. 124, pp. 567-574, 1997.

[144] K. Kimura, K. Ohshima, and M. h. Mannami, "Monolayer analysis in Rutherford backscattering spectroscopy". Applied physics letters, vol. 64, pp. 2232-2234, 1994.

[145] W. Vandervorst and T. Clarysse, "On the determination of dopant/carrier distributions". Journal of Vacuum Science & Technology B, vol. 10, pp. 302-315, 1992.

[146] H. B. Bebb and E. Williams, "Photoluminescence I: theory". Semiconductors and semimetals, vol. 8, pp. 181-320, 1972.

[147] P. Dean, "Photoluminescence as a diagnostic of semiconductors". Progress in Crystal Growth and Characterization, vol. 5, pp. 89-174, 1982.

[148] N. F. Mott and E. A. Davis, *Electronic processes in non-crystalline materials*: Oxford University Press, 2012.

[149] C. Hogarth and M. Ghauri, "The preparation of cadmium phosphate and cadmium zinc phosphate glasses and their electrical and optical properties". Journal of Materials Science, vol. 14, pp. 1641-1646, 1979.

[150] G. P. Smestad, *Optoelectronics of solar cells*: SPIE press, 2002.

[151] M. C. Lovell, A. J. Avery, and M. W. Vernon. (1984). *Physical Properties of Materials*.

[152] H. G. Cha, D. I. Kang, T. H. Kwon, and Y. S. Kang, "Enhanced photoluminescence of single crystalline ZnO nanotubes in ZnAl2O4 shell". CrystEngComm, vol. 14, pp. 1205-1209, 2012.

[153] Z. L. Wang, "Zinc oxide nanostructures: growth, properties and applications". JOURNAL OF PHYSICS: CONDENSED MATTER, vol. 16, pp. R829-R858, 2004.

[154] H. Zeng, W. Cai, P. Liu, X. Xu, H. Zhou, C. Klingshirn, and H. Kalt, "ZnO-Based Hollow Nanoparticles by Selective Etching: Elimination and Reconstruction of Metal−Semiconductor Interface, Improvement of Blue Emission and Photocatalysis". ACS Nano, vol. 2, pp. 1661-1670, 2008/08/01 2008.

[155] Y. Han, X. Wu, G. Shen, B. Dierre, L. Gong, F. Qu, Y. Bando, T. Sekiguchi, F. Filippo, and D. Golberg, "Solution Growth and Cathodoluminescence of Novel SnO2 Core−Shell Homogeneous Microspheres". The Journal of Physical Chemistry C, vol. 114, pp. 8235-8240, 2010/05/13 2010.

[156] H. Zeng, G. Duan, Y. Li, S. Yang, X. Xu, and W. Cai, "Blue Luminescence of ZnO Nanoparticles Based on Non-Equilibrium Processes: Defect Origins and Emission Controls". Advanced Functional Materials, vol. 20, pp. 561-572, 2010.

[157] J. H. Choy, E. S. Jang, J. H. Won, J. H. Chung, D. J. Jang, and Y. W. Kim, "Soft Solution Route to Directionally Grown ZnO Nanorod Arrays on Si Wafer; Room-Temperature Ultraviolet Laser". Advanced Materials, vol. 15, pp. 1911-1914, 2003.

[158] Z. K. Tang, G. K. L. Wong, P. Yu, M. Kawasaki, A. Ohtomo, H. Koinuma, and Y. Segawa, "Room-temperature ultraviolet laser emission from self-assembled ZnO microcrystallite thin films". Applied Physics Letters, vol. 72, pp. 3270-3272, 1998.

[159] L. Xu, Q. Liao, J. Zhang, X. Ai, and D. Xu, "Single-Crystalline ZnO Nanotube Arrays on Conductive Glass Substrates by Selective Disolution of Electrodeposited ZnO Nanorods". The Journal of Physical Chemistry C, vol. 111, pp. 4549-4552, 2007/03/01 2007.

[160] M.-J. Chen, J.-R. Yang, and M. Shiojiri, "ZnO-based ultra-violet light emitting diodes and nanostructures fabricated by atomic layer deposition". Semiconductor Science and Technology, vol. 27, p. 074005, 2012.

[161] M. Ding, D. Zhao, B. Yao, S. E, Z. Guo, L. Zhang, and D. Shen, "The ultraviolet laser from individual ZnO microwire with quadrate cross section". Opt. Express, vol. 20, pp. 13657-13662, 2012.

[162] P. Yu, Z. K. Tang, G. K. L. Wong, M. Kawasaki, A. Ohtomo, H. Koinuma, and Y. Segawa, "Room-temperature gain spectra and lasing in microcrystalline ZnO thin films". Journal of Crystal Growth, vol. 184–185, pp. 601-604, 1998.

[163] R. F. Service, "Will UV Lasers Beat the Blues?". Science, vol. 276, p. 895, May 9, 1997 1997.

[164] B. Lin, Z. Fu, and Y. Jia, "Green luminescent center in undoped zinc oxide films deposited on silicon substrates". Applied Physics Letters, vol. 79, pp. 943-945, 2001.

[165] N. Bano, I. Hussain, O. Nur, M. Willander, Q. Wahab, A. Henry, H. S. Kwack, and D. Le Si Dang, "Depth-resolved cathodoluminescence study of zinc oxide nanorods catalytically grown on p-type 4H-SiC". Journal of Luminescence, vol. 130, pp. 963-968, 2010.

[166] A. Bera and D. Basak, "Correlation between the microstructure and the origin of the green luminescence in ZnO: A case study on the thin films and nanowires". Chemical Physics Letters, vol. 476, pp. 262-266, 2009.

[167] S. Sarkar and D. Basak, "A low temperature in situ facile technique to enhance ultraviolet emission of zinc oxide nanorods and its mechanistic insights". Chemical Physics Letters, vol. 516, pp. 192-198, 2011.

[168] I. Javed, W. Baiqi, L. Xiaofang, Y. Dapeng, B. He, and Y. Ronghai, "Oxygen-vacancy-induced green emission and room-temperature ferromagnetism in Ni-doped ZnO nanorods". New Journal of Physics, vol. 11, p. 063009, 2009.

[169] C. H. Ahn, Y. Y. Kim, D. C. Kim, S. K. Mohanta, and H. K. Cho, "A comparative analysis of deep level emission in ZnO layers deposited by various methods". Journal of Applied Physics, vol. 105, pp. 013502-5, 2009.

[170] T. Costas, C. Wayne, L. Flora, A. Khairi, F. Andrew, K. Demosthenes, and R. Robert, "Intrinsic photoluminescence from low temperature deposited zinc oxide thin films as a function of laser and thermal annealing". Journal of Physics D: Applied Physics, vol. 46, p. 095305, 2013.

[171] A. Rauf, M. Mehmood, M. Ahmed, M. ul Hasan, and M. Aslam, "Effects of ordering quality of the pores on the photoluminescence of porous anodic alumina prepared in oxalic acid". Journal of Luminescence, vol. 130, pp. 792-800, 2010.

[172] Y. Khan, S. K. Durrani, M. Mehmood, J. Ahmad, M. R. Khan, and S. Firdous, "Low temperature synthesis of fluorescent ZnO nanoparticles". Applied Surface Science, vol. 257, pp. 1756-1761, 2010.

[173] T. Nobis, E. M. Kaidashev, A. Rahm, M. Lorenz, J. Lenzner, and M. Grundmann, "Spatially Inhomogeneous Impurity Distribution in ZnO Micropillars". Nano Letters, vol. 4, pp. 797-800, 2004/05/01 2004.

[174] U. K. Gautam, M. Imura, C. S. Rout, Y. Bando, X. Fang, B. Dierre, L. Sakharov, A. Govindaraj, T. Sekiguchi, and D. Golberg, "Unipolar assembly of zinc oxide rods manifesting polarity-driven collective luminescence". Proceedings of the National Academy of Sciences, vol. 107, pp. 13588-13592, 2010.

[175] T. Rakshit, S. Mandal, P. Mishra, A. Dhar, I. Manna, and S. K. Ray, "Optical and Bio-Sensing Characteristics of ZnO Nanotubes Grown by Hydrothermal Method". Journal of Nanoscience and Nanotechnology, vol. 12, pp. 308-315, 2012.

[176] R. Rizwan, M. Mehmood, M. Imran, J. Ahmad, M. Aslam, and J. I. Akhter, "Deposition of nanocrystalline zinc-nickel alloys by DC plating in additive free chloride bath". MATERIALS TRANSACTIONS, vol. 48, pp. 1558-1565, 2007.

[177] B. Liu and H. Zeng, "Direct growth of enclosed ZnO nanotubes". Nano Research, vol. 2, pp. 201-209, 2009/03/01 2009.

[178] R. Khan, M. Mehmood, R. Rizwan, J. Ahmad, M. Ul Hasan, Z. Iqbal, T. Mudassar, and M. Aslam, "Corrosion behaviour of zinc‐nickel alloy

coatings electrodeposited in additive free chloride baths". Corrosion Engineering, Science and Technology, vol. 46, pp. 755-761, 2011.

[179] M. M. a. T. O. Mikito Ueda, "Atmospheric Corrosion of Zinc and Zinc Alloy using in-situ Raman spectroscopy". Electrochemical Society Proceedings, vol. 14, p. 166, 2004.

[180] Y. Li, Y. Zou, and Y. Hou, "Synthesis and characterization of simonkolleite nanodisks and their conversion into ZnO nanostructures". Crystal Research and Technology, vol. 46, pp. 305-308, 2011.

[181] N. S. Ridhuan, K. Abdul Razak, Z. Lockman, and A. Abdul Aziz, "Structural and Morphology of ZnO Nanorods Synthesized Using ZnO Seeded Growth Hydrothermal Method and Its Properties as UV Sensing". PLoS ONE, vol. 7, p. e50405, 2012.

[182] G. Jiangfeng, D. Zhaoming, D. Qingping, X. Yuan, and Z. Weihua, "Controlled Synthesis of ZnO Nanostructures by Electrodeposition Method". Journal of Nanomaterials, 2010.

[183] J. Guo, J. Xu, X. Zhuang, Y. Wang, H. Zhou, Z. Shan, P. Ren, P. Guo, Q. Zhang, Q. Wan, X. Zhu, and A. Pan, "Large photoluminescence redshift of ZnTe nanostructures: The effect of twin structures". Chemical Physics Letters, vol. 576, pp. 26-30, 2013.

[184] A. Slimane, A. Najar, R. Elafandy, D. San-Roman-Alerigi, D. Anjum, T. Ng, and B. Ooi, "On the phenomenon of large photoluminescence red shift in GaN nanoparticles". Nanoscale Research Letters, vol. 8, p. 342, 2013.

[185] A. F. Kohan, G. Ceder, D. Morgan, and C. G. Van de Walle, "First-principles study of native point defects in ZnO". Physical Review B, vol. 61, pp. 15019-15027, 2000.

[186] Z. Yu, S. Ge, Y. Zuo, G. Wang, and F. Zhang, "Vacancy-induced room-temperature ferromagnetism in ZnO rods synthesized by Ni-doped solution and hydrothermal method". Applied Surface Science, vol. 256, pp. 5813-5817, 2010.

[187] A.-J. Cheng, Y. Tzeng, Y. Zhou, M. Park, T.-h. Wu, C. Shannon, D. Wang, and W. Lee, "Thermal chemical vapor deposition growth of zinc oxide

nanostructures for dye-sensitized solar cell fabrication". Applied Physics Letters, vol. 92, pp. -, 2008.

[188] S. L. Wang, H. W. Zhu, W. H. Tang, and P. G. Li, "Propeller-Shaped ZnO Nanostructures Obtained by Chemical Vapor Deposition: Photoluminescence and Photocatalytic Properties". Journal of Nanomaterials, vol. 2012, p. 5, 2012.

[189] D. Zhang, X. Wu, N. Han, and Y. Chen, "Chemical vapor deposition preparation of nanostructured ZnO particles and their gas-sensing properties". Journal of Nanoparticle Research, vol. 15, pp. 1-10, 2013/03/21 2013.

[190] Y. H. Tong, Y. C. Liu, L. Dong, L. X. Lu, D. X. Zhao, J. Y. Zhang, Y. M. Lu, D. Z. Shen, and X. W. Fan, "Growth and optical properties of ZnO nanostructures by vapor transport process". Materials Chemistry and Physics, vol. 103, pp. 190-194, 2007.

[191] M. C. Newton, S. Firth, T. Matsuura, and P. A. Warburton, "Synthesis and characterisation of zinc oxide tetrapod nanocrystals". Journal of Physics: Conference Series, vol. 26, p. 251, 2006.

[192] N. Rusli, M. Tanikawa, M. Mahmood, K. Yasui, and A. Hashim, "Growth of High-Density Zinc Oxide Nanorods on Porous Silicon by Thermal Evaporation". Materials, vol. 5, pp. 2817-2832, 2012.

[193] Q. X. Zhao, P. Klason, and M. Willander, "Growth of ZnO nanostructures by vapor–liquid–solid method". Applied Physics A, vol. 88, pp. 27-30, 2007/07/01 2007.

[194] L.-N. Tong, T. Cheng, H.-B. Han, J.-L. Hu, X.-M. He, Y. Tong, and C. M. Schneider, "Photoluminescence studies on structural defects and room temperature ferromagnetism in Ni and Ni–H doped ZnO nanoparticles". Journal of Applied Physics, vol. 108, p. 023906, 2010.

[195] C. Cheng, G. Xu, H. Zhang, and Y. Luo, "Hydrothermal synthesis Ni-doped ZnO nanorods with room-temperature ferromagnetism". Materials Letters, vol. 62, pp. 1617-1620, 2008.

[196] A. B. Djurišić, Y. H. Leung, K. H. Tam, L. Ding, W. K. Ge, H. Y. Chen, and S. Gwo, "Green, yellow, and orange defect emission from ZnO

nanostructures: Influence of excitation wavelength". Applied Physics Letters, vol. 88, pp. -, 2006.

[197] Z. Gu, M. P. Paranthaman, J. Xu, and Z. W. Pan, "Aligned ZnO Nanorod Arrays Grown Directly on Zinc Foils and Zinc Spheres by a Low-Temperature Oxidization Method". ACS Nano, vol. 3, pp. 273-278, 2009/02/24 2009.

[198] T. Li, T. S. Herng, H. K. Liang, N. N. Bao, T. P. Chen, J. I. Wong, J. M. Xue, and J. Ding, "Strong green emission in ZnO films after H 2 surface treatment". Journal of Physics D: Applied Physics, vol. 45, p. 185102, 2012.

[199] R. Rizwan, M. Mehmood, M. Imran, J. Ahmad, M. Aslam, and J. I. Akhter, "Deposition of Nanocrystalline Zinc-Nickel Alloys by D.C. Plating in Additive Free Chloride Bath". MATERIALS TRANSACTIONS, vol. 48, pp. 1558-1565, 2007.

[200] R. Khan, M. Mehmood, R. Rizwan, J. Ahmad, M. Ul Hasan, Z. Iqbal, T. Mudassar, and M. Aslam, "Corrosion behaviour of zinc–nickel alloy coatings electrodeposited in additive free chloride baths". Corrosion Engineering, Science and Technology, vol. 46, pp. 755-761, 2011.

[201] N.-u. Rehman, M. Mehmood, R. Rizwan, M. A. Rasheed, F. C. C. Ling, and M. Younas, "Control of optical properties of ZnO nanostructures grown by a novel two-step synthesis approach". Chemical Physics Letters, vol. 609, pp. 26-32, 2014.

[202] H. Wang, M. Li, L. Jia, L. Li, G. Wang, Y. Zhang, and G. Li, "Surfactant-Assisted in situ Chemical Etching for the General Synthesis of ZnO Nanotubes Array". Nanoscale Research Letters, vol. 5, pp. 1102-1106, 2010.

[203] A. M. Lord, T. G. Maffeis, A. S. Walton, D. M. Kepaptsoglou, Q. M. Ramasse, M. B. Ward, J. Köble, and S. P. Wilks, "Factors that determine and limit the resistivity of high-quality individual ZnO nanowires". Nanotechnology, vol. 24, p. 435706, 2013.

[204] L. H. Wang, X. D. Han, Y. F. Zhang, K. Zheng, P. Liu, and Z. Zhang, "Asymmetrical quantum dot growth on tensile and compressive-strained ZnO nanowire surfaces". Acta Materialia, vol. 59, pp. 651-657, 2011.

[205] T. Al-Harbi, "Hydrothermal synthesis and optical properties of Ni doped ZnO hexagonal nanodiscs". Journal of Alloys and Compounds, vol. 509, pp. 387-390, 2011.

[206] G. Murugadoss, "Synthesis and Characterization of Transition Metals Doped ZnO Nanorods". Journal of Materials Science & Technology, vol. 28, pp. 587-593, 2012.

[207] E. Burstein, " nomalous Optical Absorption Limit in InSb". Physics Review, vol. 93, pp. 632--633, Feb 1954.

[208] T. S. Moss, "The Interpretation of the Properties of Indium Antimonide". Proceedings of the Physical Society. Section B, vol. 67, p. 775, 1954.

[209] S. A. M. Lima, F. A. Sigoli, M. Jafelicci Jr, and M. R. Davolos, "Luminescent properties and lattice defects correlation on zinc oxide". International Journal of Inorganic Materials, vol. 3, pp. 749-754, 2001.

[210] A. K. Srivastava and J. Kumar, "Effect of zinc addition and vacuum annealing time on the properties of spin-coated low-cost transparent conducting 1 at% Ga–ZnO thin films". Science and Technology of Advanced Materials, vol. 14, p. 065002, 2013.

[211] M. Willander, O. Nur, J. R. Sadaf, M. I. Qadir, S. Zaman, A. Zainelabdin, N. Bano, and I. Hussain, "Luminescence from Zinc Oxide Nanostructures and Polymers and their Hybrid Devices". Materials, vol. 3, pp. 2643-2667, 2010.

[212] V. Nikitenko, "Optics and Spectroscopy of Point Defects in ZnO," in *Zinc Oxide — A Material for Micro- and Optoelectronic Applications*. vol. 194, N. Nickel and E. Terukov, Eds., ed: Springer Netherlands, 2005, pp. 69-81.

[213] S. H. Kim, A. Umar, Y.-B. Hahn, A. Al-Hajry, and M. Abaker, "Low-Temperature Growth of Aligned ZnO Nanorods: Effect of Annealing Gases on the Structural and Optical Properties". Journal of Nanoscience and Nanotechnology, vol. 14, pp. 4564-4569, 2014.

[214] D. Wang, Z. Wang, G. Ping, D. Chen, M. Fan, L. Bai, L. Qin, C. Lv, and K. Shu, "Facile Synthesis of Waxberry-Like ZnO Nanospheres for High Performance Photocatalysis". Science of Advanced Materials, vol. 5, pp. 1642-1648, 2013.

[215] J. Wang, F. Qu, and X. Wu, "Photocatalytic Degradation of Organic Dyes with Hierarchical Ag₂ O/ZnO Heterostructures". Science of Advanced Materials, vol. 5, pp. 1364-1371, 2013.

[216] A. R. Ghasemi, M. M. Doroodmand, M. H. Sheikhi, and S. Nasresfahani, "Fabrication of Methane Sensor Using Inter-Digitated Electrode, Modified with Ag₂O, SiO₂, ZnO and MgO Nanoparticles-Mixed Multi-Walled Carbon Nanotubes as Specific Nanomaterials". Journal of Nanoengineering and Nanomanufacturing, vol. 3, pp. 202-210, 2013.

[217] V. N. Singh, G. Partheepan, and A. Kumar, "Growth of ZnO Nanostructures and Its Morphology/Structure Dependent Luminescent Properties". Journal of Nanoengineering and Nanomanufacturing, vol. 3, pp. 276-280, 2013.

[218] L. Kumar and M. Mall, "Ambient Atmosphere Dependent Photovoltaic Parameters of P3HT:ZnO Based Hybrid Solar Cells". Science of Advanced Materials, vol. 5, pp. 1231-1235, 2013.

[219] H. Usui, T. Kono, and H. Sakaguchi, "Electrochemical Properties of Metal/ZnO Composites Synthesized by Co-Precipitation Method for Li-Ion Battery Anode". Journal of Nanoengineering and Nanomanufacturing, vol. 3, pp. 326-330, 2013.

[220] J. Wang, F. Qu, and X. Wu, "Synthesis of Ultra-Thin ZnO Nanosheets: Photocatalytic and Superhydrophilic Properties". Science of Advanced Materials, vol. 5, pp. 1052-1059, 2013.

[221] C. Periasamy and P. Chakrabarti, "Effect of Temperature on the Electrical Characteristics of Nanostructured n-ZnO/p-Si Heterojunction Diode". Science of Advanced Materials, vol. 5, pp. 1384-1391, 2013.

[222] R. H. Bari, S. B. Patil, and A. R. Bari, "Chemically Sprayed Nanocomposite SnO₂–ZnO Thin Film for Ethanol Gas Sensor". Journal of Nanoengineering and Nanomanufacturing, vol. 3, pp. 10-14, 2013.

[223] A. Kumar, S. Rahman, S. N. Kazim, Z. A. Ansari, and S. G. Ansari, "Application of Glutathione Coated ZnO Nanoparticles to Study the Oxidative Stress in Bacterial Cells". Materials Focus, vol. 2, pp. 148-154, 2013.

[224] C. Zhang, S. Zhou, K. Li, S. Song, and D. Xue, "Color-Tunable ZnO Quantum Dots Emitter: Size Effect Study and a Kinetic Control of Crystallization". Materials Focus, vol. 2, pp. 11-19, 2013.

[225] D. Wang, Z. Li, T. Kawaharamura, M. Furuta, T. Narusawa, and C. Li, "Well-arrayed ZnO nanostructures formed by multi-annealing processes at low temperature". physica status solidi (c), vol. 9, pp. 194-197, 2012.

[226] Y. H. Leung, X. Y. Chen, A. M. C. Ng, M. Y. Guo, F. Z. Liu, A. B. Djurišić, W. K. Chan, X. Q. Shi, and M. A. Van Hove, "Green emission in ZnO nanostructures—Examination of the roles of oxygen and zinc vacancies". Applied Surface Science, vol. 271, pp. 202-209, 2013.

[227] Q. Li, Y. Chen, X. Zhang, Y. Su, and C. Jia, "Annealing effect on the morphologies and photoluminescence properties of ZnO nanocombs". Journal of Physics and Chemistry of Solids, vol. 70, pp. 1482-1486, 2009.

[228] K. A. Eswar, J. Rouhi, H. F. Husairi, M. Rusop, and S. Abdullah, "Annealing Heat Treatment of ZnO Nanoparticles Grown on Porous Si Substrate Using Spin-Coating Method". Advances in Materials Science and Engineering, vol. 2014, p. 6, 2014.

[229] G. H. Mhlongo, D. E. Motaung, S. S. Nkosi, H. C. Swart, G. F. Malgas, K. T. Hillie, and B. W. Mwakikunga, "Temperature-dependence on the structural, optical, and paramagnetic properties of ZnO nanostructures". Applied Surface Science, vol. 293, pp. 62-70, 2014.

[230] N. M. A. Hadia, S. García-Granda, and J. R. García, "Effect of the Temperature on Structural and Optical Properties of Zinc Oxide Nanoparticles". Journal of Nanoscience and Nanotechnology, vol. 14, pp. 5443-5448, 2014.

[231] B. Allabergenov, S.-H. Chung, S. M. Jeong, S. Kim, and B. Choi, "Enhanced blue photoluminescence realized by copper diffusion doping of ZnO thin films". Optical Materials Express, vol. 3, pp. 1733-1741, 2013.

[232] C. Tsakonas, W. Cranton, F. Li, K. Abusabee, A. Flewitt, D. Koutsogeorgis, and R. Ranson, "Intrinsic photoluminescence from low temperature deposited

zinc oxide thin films as a function of laser and thermal annealing". Journal of Physics D: Applied Physics, vol. 46, p. 095305, 2013.

[233] A. B. Djurišić, W. C. H. Choy, V. A. L. Roy, Y. H. Leung, C. Y. Kwong, K. W. Cheah, T. K. Gundu Rao, W. K. Chan, H. Fei Lui, and C. Surya, "Photoluminescence and Electron Paramagnetic Resonance of ZnO Tetrapod Structures". Advanced Functional Materials, vol. 14, pp. 856-864, 2004.

[234] M. Wang, Y. Zhou, Y. Zhang, E. Jung Kim, S. Hong Hahn, and S. Gie Seong, "Near-infrared photoluminescence from ZnO". Applied Physics Letters, vol. 100, pp. -, 2012.

[235] R. B. M. Cross, M. M. D. Souza, and E. M. S. Narayanan, "A low temperature combination method for the production of ZnO nanowires". Nanotechnology, vol. 16, p. 2188, 2005.

[236] J. Liu, S. Lee, Y. H. Ahn, J.-Y. Park, and K. H. Koh, "Tailoring the visible photoluminescence of mass-produced ZnO nanowires". Journal of Physics D: Applied Physics, vol. 42, p. 095401, 2009.

[237] L. E. Halliburton, N. C. Giles, N. Y. Garces, M. Luo, C. Xu, L. Bai, and L. A. Boatner, "Production of native donors in ZnO by annealing at high temperature in Zn vapor". Applied Physics Letters, vol. 87, pp. -, 2005.

[238] A. Janotti and C. G. Van de Walle, "Oxygen vacancies in ZnO". Applied Physics Letters, vol. 87, pp. -, 2005.

[239] Q. Zhu, C. Xie, H. Li, and Q. Yang, "Comparative study of ZnO nanorod array and nanoparticle film in photoelectric response and charge storage". Journal of Alloys and Compounds, vol. 585, pp. 267-276, 2014.

[240] Z. Wang, C. Lin, X. Liu, G. Li, Y. Luo, Z. Quan, H. Xiang, and J. Lin, "Tunable Photoluminescent and Cathodoluminescent Properties of ZnO and ZnO:Zn Phosphors". The Journal of Physical Chemistry B, vol. 110, pp. 9469-9476, 2006/05/01 2006.

[241] A. van Dijken, E. A. Meulenkamp, D. Vanmaekelbergh, and A. Meijerink, "The luminescence of nanocrystalline ZnO particles: the mechanism of the ultraviolet and visible emission". Journal of Luminescence, vol. 87–89, pp. 454-456, 2000.

[242] Z.-M. Liao, H.-Z. Zhang, Y.-B. Zhou, J. Xu, J.-M. Zhang, and D.-P. Yu, "Surface effects on photoluminescence of single ZnO nanowires". Physics Letters A, vol. 372, pp. 4505-4509, 2008.

[243] C. W. Zou, Y. F. Rao, A. Alyamani, W. Chu, M. J. Chen, D. A. Patterson, E. A. C. Emanuelsson, and W. Gao, "Heterogeneous Lollipop-like V2O5/ZnO Array: A Promising Composite Nanostructure for Visible Light Photocatalysis". Langmuir, vol. 26, pp. 11615-11620, 2010/07/20 2010.

[244] L.-J. Tzeng, C.-L. Cheng, and Y.-F. Chen, "Enhancement of band-edge emission induced by defect transition in the composite of ZnO nanorods and CdSe/ZnS quantum dots". Optics Letters, vol. 33, pp. 569-571, 2008/03/15 2008.

[245] H. Y. Yang, S. F. Yu, S. P. Lau, X. Zhang, D. D. Sun, and G. Jun, "Direct Growth of ZnO Nanocrystals onto the Surface of Porous TiO2 Nanotube Arrays for Highly Efficient and Recyclable Photocatalysts". Small, vol. 5, pp. 2260-2264, 2009.

[246] S.-M. Lam, J.-C. Sin, A. Z. Abdullah, and A. R. Mohamed, "ZnO nanorods surface-decorated by WO3 nanoparticles for photocatalytic degradation of endocrine disruptors under a compact fluorescent lamp". Ceramics International, vol. 39, pp. 2343-2352, 2013.

[247] Y. Sun, Q. Zhao, J. Gao, Y. Ye, W. Wang, R. Zhu, J. Xu, L. Chen, J. Yang, L. Dai, Z.-m. Liao, and D. Yu, "In situ growth, structure characterization, and enhanced photocatalysis of high-quality, single-crystalline ZnTe/ZnO branched nanoheterostructures". Nanoscale, vol. 3, pp. 4418-4426, 2011.

[248] Y. Yang and T. Liu, "Fabrication and characterization of graphene oxide/zinc oxide nanorods hybrid". Applied Surface Science, vol. 257, pp. 8950-8954, 2011.

[249] C. Xu, L. Cao, G. Su, W. Liu, H. Liu, Y. Yu, and X. Qu, "Preparation of ZnO/Cu2O compound photocatalyst and application in treating organic dyes". Journal of Hazardous Materials, vol. 176, pp. 807-813, 2010.

[250] G. Merga, L. C. Cass, D. M. Chipman, and D. Meisel, "Probing Silver Nanoparticles During Catalytic H2 Evolution". Journal of the American Chemical Society, vol. 130, pp. 7067-7076, 2008/06/01 2008.

[251] V. Subramanian, E. E. Wolf, and P. V. Kamat, "Catalysis with TiO2/Gold Nanocomposites. Effect of Metal Particle Size on the Fermi Level Equilibration". Journal of the American Chemical Society, vol. 126, pp. 4943-4950, 2004/04/01 2004.

[252] Y. Wei, Y. Li, X. Liu, Y. Xian, G. Shi, and L. Jin, "ZnO nanorods/Au hybrid nanocomposites for glucose biosensor". Biosensors and Bioelectronics, vol. 26, pp. 275-278, 2010.

[253] T. Bora, H. H. Kyaw, S. Sarkar, S. K. Pal, and J. Dutta, "Highly efficient ZnO/Au Schottky barrier dye-sensitized solar cells: Role of gold nanoparticles on the charge-transfer process". Beilstein Journal of Nanotechnology, vol. 2, pp. 681-690, 2011.

[254] N. Udawatte, M. Lee, J. Kim, and D. Lee, "Well-Defined Au/ZnO Nanoparticle Composites Exhibiting Enhanced Photocatalytic Activities". ACS Applied Materials & Interfaces, vol. 3, pp. 4531-4538, 2011/11/23 2011.

[255] S. Ikeda, N. Sugiyama, B. Pal, G. Marci, L. Palmisano, H. Noguchi, K. Uosaki, and B. Ohtani, "Photocatalytic activity of transition-metal-loaded titanium(IV) oxide powders suspended in aqueous solutions: Correlation with electron-hole recombination kinetics". Physical Chemistry Chemical Physics, vol. 3, pp. 267-273, 2001.

[256] A. Dawson and P. V. Kamat, "Semiconductor−Metal Nanocomposites. Photoinduced Fusion and Photocatalysis of Gold-Capped TiO2 (TiO2/Gold) Nanoparticles". The Journal of Physical Chemistry B, vol. 105, pp. 960-966, 2001/02/01 2001.

[257] E. Szabó-Bárdos, H. Czili, and A. Horváth, "Photocatalytic oxidation of oxalic acid enhanced by silver deposition on a TiO2 surface". Journal of Photochemistry and Photobiology A: Chemistry, vol. 154, pp. 195-201, 2003.

[258] B. Nikoobakht, C. Burda, M. Braun, M. Hun, and M. A. El-Sayed, "The Quenching of CdSe Quantum Dots Photoluminescence by Gold Nanoparticles in Solution¶". Photochemistry and Photobiology, vol. 75, pp. 591-597, 2002.

[259] T.-H. Lin, T.-T. Chen, C.-L. Cheng, H.-Y. Lin, and Y.-F. Chen, "Selectively enhanced band gap emission inZnO/Ag2O nanocomposites". Optics Express, vol. 17, pp. 4342-4347, 2009/03/16 2009.

[260] E. S. P. Leong, S. F. Yu, M. K. Chong, O. K. Tan, and K. Pita, "Metal-oxide-SiO₂ composite ZnO lasers". Photonics Technology Letters, IEEE, vol. 17, pp. 1815-1817, 2005.

[261] X. Zhang, I. Suemune, H. Kumano, Z. Yao, and S. Huang, "Room temperature ultraviolet lasing action in high-quality ZnO thin films". Journal of Luminescence, vol. 122, pp. 828-830, 2007.

[262] S. Chu, M. Olmedo, Z. Yang, J. Kong, and J. Liu, "Electrically pumped ultraviolet ZnO diode lasers on Si". Applied Physics Letters, vol. 93, pp. 181106-181106-3, 2008.

[263] S. Krishnamoorthy and A. A. Iliadis, "Properties of high sensitivity ZnO surface acoustic wave sensors on SiO 2/(100) Si substrates". Solid-State Electronics, vol. 52, pp. 1710-1716, 2008.

[264] S. Kumar, G.-H. Kim, K. Sreenivas, and R. Tandon, "ZnO based surface acoustic wave ultraviolet photo sensor". Journal of electroceramics, vol. 22, pp. 198-202, 2009.

[265] V. Chivukula, D. Ciplys, M. Shur, and P. Dutta, "ZnO nanoparticle surface acoustic wave UV sensor". Applied Physics Letters, vol. 96, pp. 233512-233512-3, 2010.

[266] M. Reshchikov, J. Xie, B. Hertog, and A. Osinsky, "Yellow luminescence in ZnO layers grown on sapphire". Journal of Applied Physics, vol. 103, pp. 103514-103514-8, 2008.

[267] J. Zhao, L. Hu, Z. Wang, J. Sun, and Z. Wang, "ZnO thin films on Si (111) grown by pulsed laser deposition from metallic Zn target". Applied Surface Science, vol. 253, pp. 841-845, 2006.

[268] M. Purica, E. Budianu, E. Rusu, M. Danila, and R. Gavrila, "Optical and structural investigation of ZnO thin films prepared by chemical vapor deposition (CVD)". Thin Solid Films, vol. 403, pp. 485-488, 2002.

[269] Y. Zhang, G. Du, X. Wang, W. Li, X. Yang, Y. Ma, B. Zhao, H. Yang, D. Liu, and S. Yang, "X-ray photoelectron spectroscopy study of ZnO films grown by metal-organic chemical vapor deposition". Journal of crystal growth, vol. 252, pp. 180-183, 2003.

[270] Y. Nakanishi, A. Miyake, H. Kominami, T. Aoki, Y. Hatanaka, and G. Shimaoka, "Preparation of ZnO thin films for high-resolution field emission display by electron beam evaporation". Applied Surface Science, vol. 142, pp. 233-236, 1999.

[271] S.-R. Jian, H.-G. Chen, G.-J. Chen, J. S. Jang, and J.-Y. Juang, "Structural and nanomechanical properties of a-plane ZnO thin films deposited under different oxygen partial pressures". Current Applied Physics, vol. 12, pp. 849-853, 2012.

[272] S.-Y. Pung, K.-L. Choy, X. Hou, and C. Shan, "Preferential growth of ZnO thin films by the atomic layer deposition technique". Nanotechnology, vol. 19, p. 435609, 2008.

[273] V. Assuncao, E. Fortunato, A. Marques, H. Aguas, I. Ferreira, M. Costa, and R. Martins, "Influence of the deposition pressure on the properties of transparent and conductive ZnO: Ga thin-film produced by rf sputtering at room temperature". Thin Solid Films, vol. 427, pp. 401-405, 2003.

[274] R. Behrisch and W. Eckstein, *Sputtering by Particle Bombardment*. Heidelberg, Germany: Springer-Verlag Berlin Heidelberg, 2007.

[275] M. A. Hernández-Fenollosa, L. C. Damonte, and B. Marí, "Defects in electron irradiated ZnO single crystals". Superlattices and Microstructures, vol. 38, pp. 336-343, 2005.

[276] J. J. Ding, S. Y. Ma, H. X. Chen, X. F. Shi, T. T. Zhou, and L. M. Mao, "Influence of Al-doping on the structure and optical properties of ZnO films". Physica B: Condensed Matter, vol. 404, pp. 2439-2443, 2009.

[277] A. Teke, Ü. Özgür, S. Doğan, X. Gu, H. Morkoç, B. Nemeth, J. Nause, and H. Everitt, "Excitonic fine structure and recombination dynamics in single-crystalline ZnO". Physical Review B, vol. 70, p. 195207, 2004.

[278] X. W. Sun and H. S. Kwok, "Optical properties of epitaxially grown zinc oxide films on sapphire by pulsed laser deposition". Journal of Applied Physics, vol. 86, pp. 408-411, 1999.

[279] P. Zu, Z. K. Tang, G. K. L. Wong, M. Kawasaki, A. Ohtomo, H. Koinuma, and Y. Segawa, "Ultraviolet spontaneous and stimulated emissions from ZnO microcrystallite thin films at room temperature". Solid State Communications, vol. 103, pp. 459-463, 1997.

[280] R. Hong, H. Qi, J. Huang, H. He, Z. Fan, and J. Shao, "Influence of oxygen partial pressure on the structure and photoluminescence of direct current reactive magnetron sputtering ZnO thin films". Thin Solid Films, vol. 473, pp. 58-62, 2005.

[281] E. Sonmez, S. Aydin, M. Yilmaz, M. T. Yurtcan, T. Karacali, and M. Ertugrul, "Study of Structural and Optical Properties of Zinc Oxide Rods Grown on Glasses by Chemical Spray Pyrolysis". Journal of Nanomaterials, vol. 2012, p. 950793, 2012.

[282] K. Uma, S. Ananthakumar, R. Mangalaraja, T. Soga, and T. Jimbo, "Growth and Improvement of ZnO Nanostructure Using Aged Solution by Flow Coating Process". Advances in Materials Physics and Chemistry, vol. 3, pp. 194-200, 2013.

[283] K. Minegishi, Y. Koiwai, Y. Kikuchi, K. Yano, M. Kasuga, and A. Shimizu, "Growth of p-type zinc oxide films by chemical vapor deposition". Japanese Journal of Applied Physics, vol. 36, p. L1453, 1997.

[284] Y. Ryu, S. Zhu, D. C. Look, J. Wrobel, H. Jeong, and H. White, "Synthesis of p-type ZnO films". Journal of Crystal Growth, vol. 216, pp. 330-334, 2000.

[285] D. C. Look, D. Reynolds, C. Litton, R. Jones, D. Eason, and G. Cantwell, "Characterization of homoepitaxial p-type ZnO grown by molecular beam epitaxy". Applied physics letters, vol. 81, pp. 1830-1832, 2002.

[286] D. C. Look and B. Claflin, "P-type doping and devices based on ZnO". physica status solidi (b), vol. 241, pp. 624-630, 2004.

[287] G. T. Du, W. F. Liu, J. M. Bian, L. Z. Hu, H. W. Liang, X. S. Wang, A. M. Liu, and T. P. Yang, "Room temperature defect related electroluminescence from ZnO homojunctions grown by ultrasonic spray pyrolysis". Applied Physics Letters, vol. 89, pp. 052113-3, 2006.

[288] A. Tsukazaki, A. Ohtomo, T. Onuma, M. Ohtani, T. Makino, M. Sumiya, K. Ohtani, S. F. Chichibu, S. Fuke, Y. Segawa, H. Ohno, H. Koinuma, and M. Kawasaki, "Repeated temperature modulation epitaxy for p-type doping and light-emitting diode based on ZnO". Nat Mater, vol. 4, pp. 42-46, 2005.

[289] H. S. Kim, F. Lugo, S. J. Pearton, D. P. Norton, Y.-L. Wang, and F. Ren, "Phosphorus doped ZnO light emitting diodes fabricated via pulsed laser deposition". Applied Physics Letters, vol. 92, pp. 112108-3, 2008.

[290] L. G. Wang and A. Zunger, "Cluster-Doping Approach for Wide-Gap Semiconductors: The Case of p-Type ZnO". Physical Review Letters, vol. 90, p. 256401, 2003.

[291] H.-M. Huang, C.-C. Kuo, C.-Y. Chang, Y.-T. Lin, T.-C. Lu, L.-W. Tu, and W.-F. Hsieh, "Growth and Characteristics of a-Plane GaN on ZnO Heterostructure". Journal of The Electrochemical Society, vol. 159, pp. H290-H292, January 1, 2012 2012.

[292] S. C. Hung, P. J. Huang, C. E. Chan, W. Y. Uen, F. Ren, S. J. Pearton, T. N. Yang, C. C. Chiang, S. M. Lan, and G. C. Chi, "Nanostructured surface morphology of ZnO grown on p-type GaN and Si by metal organic chemical vapor deposition". Applied Surface Science, vol. 255, pp. 3016-3018, 2008.

[293] H. Huang, G. Fang, Y. Li, S. Li, X. Mo, H. Long, H. Wang, D. L. Carroll, and X. Zhao, "Improved and color tunable electroluminescence from n-ZnO/HfO[sub 2]/p-GaN heterojunction light emitting diodes". Applied Physics Letters, vol. 100, pp. 233502-4, 2012.

[294] W. S. Han, Y. Y. Kim, B. H. Kong, and H. K. Cho, "Ultraviolet light emitting diode with n-ZnO:Ga/i-ZnO/p-GaN:Mg heterojunction". Thin Solid Films, vol. 517, pp. 5106-5109, 2009.

[295] X. D. Chen, C. C. Ling, S. Fung, C. D. Beling, Y. F. Mei, R. K. Y. Fu, G. G. Siu, and P. K. Chu, "Current transport studies of ZnO/p-Si heterostructures grown by plasma immersion ion implantation and deposition". Applied Physics Letters, vol. 88, pp. 132104-3, 2006.

[296] S. T. Tan, X. W. Sun, J. L. Zhao, S. Iwan, Z. H. Cen, T. P. Chen, J. D. Ye, G. Q. Lo, D. L. Kwong, and K. L. Teo, "Ultraviolet and visible electroluminescence from n-ZnO/SiO[sub x]/(n,p)-Si heterostructured light-emitting diodes". Applied Physics Letters, vol. 93, pp. 013506-3, 2008.

[297] J. B. You, X. W. Zhang, S. G. Zhang, H. R. Tan, J. Ying, Z. G. Yin, Q. S. Zhu, and P. K. Chu, "Electroluminescence behavior of ZnO/Si heterojunctions: Energy band alignment and interfacial microstructure". Journal of Applied Physics, vol. 107, pp. 083701-5, 2010.

[298] H. Long, G. Fang, H. Huang, X. Mo, W. Xia, B. Dong, X. Meng, and X. Zhao, "Ultraviolet electroluminescence from ZnO/NiO-based heterojunction light-emitting diodes". Applied Physics Letters, vol. 95, pp. 013509-3, 2009.

[299] Y. Y. Xi, Y. F. Hsu, A. B. Djurisic, A. M. C. Ng, W. K. Chan, H. L. Tam, and K. W. Cheah, "NiO/ZnO light emitting diodes by solution-based growth". Applied Physics Letters, vol. 92, pp. 113505-3, 2008.

[300] T. Shu-Yi, H. Min-Hsiung, and L. Yang-Ming, "Heterojunction photodiodes based on p-NiO/ n-ZnO for ultraviolet detection," in *Nano/Micro Engineered and Molecular Systems (NEMS), 2011 IEEE International Conference on*, 2011, pp. 1184-1187.

[301] R. D. Vispute, V. Talyansky, S. Choopun, R. P. Sharma, T. Venkatesan, M. He, X. Tang, J. B. Halpern, M. G. Spencer, Y. X. Li, L. G. Salamanca-Riba, A. A. Iliadis, and K. A. Jones, "Heteroepitaxy of ZnO on GaN and its implications for fabrication of hybrid optoelectronic devices". Applied Physics Letters, vol. 73, pp. 348-350, 1998.

[302] Y. Nakanishi, A. Miyake, H. Kominami, T. Aoki, Y. Hatanaka, and G. Shimaoka, "Preparation of ZnO thin films for high-resolution field emission display by electron beam evaporation". Applied Surface Science, vol. 142, pp. 233-236, 1999.

[303] E. Dalchiele, P. Giorgi, R. Marotti, F. Martın, J. Ramos-Barrado, R. Ayouci, and D. Leinen, "Electrodeposition of ZnO thin films on n-Si (100)". Solar energy materials and solar cells, vol. 70, pp. 245-254, 2001.

[304] Z. Hai, F. Guojia, Z. Yongdan, L. Nishuang, W. Haoning, H. Huihui, L. Songzhan, and Z. Xingzhong, "A device with two kinds of functions — Ultraviolet photodetector and electroluminescence: Fabrication and carrier transport mechanism". EPL (Europhysics Letters), vol. 97, p. 68001, 2012.

[305] G.-H. Lee, D.-h. Bae, and W.-J. Lee, "Effect of bottom layer thickness on crystalline quality and surface roughness of ZnO film prepared by multi-step deposition process". Journal of Ceramic Processing Research, vol. 13, pp. 229-232, 2012.

[306] A. Kumar, S. Jeedigunta, I. Tarasov, and S. Ostapenko, "Photoluminescence Studies of Epitaxial ZnO Thin Films on Si (100) Substrates by Pulsed Laser Deposition". The AZO Journal of Materials Online, vol. 6, 2010.

[307] W. Zhao-yang, H. Li-zhong, Z. Jie, S. Jie, and W. Zhi-jun, "Effect of the variation of temperature on the structural and optical properties of ZnO thin films prepared on Si (1 1 1) substrates using PLD". Vacuum, vol. 78, pp. 53-57, 2005.

[308] A. Aravind, M. K. Jayaraj, M. Kumar, and R. Chandra, "The dependence of structural and optical properties of PLD grown ZnO films on ablation parameters". Applied Surface Science, vol. 286, pp. 54-60, 2013.

[309] H. S. Kim, S. J. Pearton, D. P. Norton, and F. Ren, "Pulsed laser deposition of high-quality ZnO films using a high temperature deposited ZnO buffer layer". Applied Physics A, vol. 91, pp. 255-259, 2008/05/01 2008.

[310] J. B. You, X. W. Zhang, S. G. Zhang, J. X. Wang, Z. G. Yin, H. R. Tan, W. J. Zhang, P. K. Chu, B. Cui, A. M. Wowchak, A. M. Dabiran, and P. P. Chow, "Improved electroluminescence from n-ZnO/AlN/p-GaN heterojunction light-emitting diodes". Applied Physics Letters, vol. 96, pp. 201102-3, 2010.

[311] M. J. C. H. C. Chen, Y. H. Huang, W. C. Sun, W. C. Li, J. R. Yang, H. Kuan, and M. Shiojiri, "White-Light Electroluminescence From n-ZnO/p-GaN

Heterojunction Light-Emitting Diodes at Reverse Breakdown Bias". IEEE TRANSACTIONS ON ELECTRON DEVICES, vol. 58, 2011.

[312] C.-S. Son, S.-M. Kim, Y.-H. Kim, S.-I. Kim, Y. T. Kim, K. H. Yoon, I.-H. Choi, and H. C. Lopez, "Deposition-Temperature Dependence of ZnO/Si Grown by Pulsed Laser Deposition". Journal of the Korean Physical Society, vol. 45, pp. S685-S688, 2004.

[313] S. A. M. Lima, F. A. Sigoli, M. Jafelicci, and M. R. Davolos, "Luminescent properties and lattice defects correlation on zinc oxide". International Journal of Inorganic Materials, vol. 3, pp. 749-754, Nov 2001.

[314] T. P. Rao and M. C. Santhoshkumar, "Effect of thickness on structural, optical and electrical properties of nanostructured ZnO thin films by spray pyrolysis". Applied Surface Science, vol. 255, pp. 4579-4584, 2009.

[315] S. Mahmoud, A. H. Eid, and H. Omar, "Optical characteristics of bismuth sulfide (Bi2S3) thin films". Fizika A, vol. 6, pp. 111-120, 1997.

[316] J.-L. Zhao, X.-M. Li, J.-M. Bian, W.-D. Yu, and X.-D. Gao, "Structural, optical and electrical properties of ZnO films grown by pulsed laser deposition (PLD)". Journal of Crystal Growth, vol. 276, pp. 507-512, 2005.

[317] I. Hamberg and C. G. Granqvist, "Evaporated Sn-doped In[sub 2]O[sub 3] films: Basic optical properties and applications to energy-efficient windows". Journal of Applied Physics, vol. 60, pp. R123-R160, 1986.

[318] F. K. Shan and Y. S. Yu, "Optical properties of pure and Al doped ZnO thin films fabricated with plasma produced by excimer laser". Thin Solid Films, vol. 435, pp. 174-178, 2003.

[319] B. J. Lokhande and M. D. Uplane, "Structural, optical and electrical studies on spray deposited highly oriented ZnO films". Applied Surface Science, vol. 167, pp. 243-246, 2000.

[320] M. A. Martínez, J. Herrero, and M. T. Gutiérrez, "Properties of RF sputtered zinc oxide based thin films made from different targets". Solar energy materials and solar cells, vol. 31, pp. 489-498, 1994.

[321] T. K. Subramanyam, B. Srinivasulu Naidu, and S. Uthanna, "Structure and Optical Properties of dc Reactive Magnetron Sputtered Zinc Oxide Films". Crystal Research and Technology, vol. 34, pp. 981-988, 1999.

[322] Y. Qu, T. A. Gessert, T. J. Coutts, and R. Noufi, "Study of ion-beam-sputtered ZnO films as a function of deposition temperature". Journal of Vacuum Science & Technology A, vol. 12, pp. 1507-1512, 1994.

[323] S. Salim, M. Kamal, A. Salem, and T. Bahr, "Characteristic behaviour of thermaly evaporated CdIn 2 Se 4 thin films". Journal of Applied Sciences Research, vol. 8, 2012.

[324] P. Beckmann and A. Spizzichino, *The Scattering of Electromagnetic Waves from Rough Surfaces*: Pergamon Press, Oxford, 1963.

[325] A. Ashour, M. A. Kaid, N. Z. El-Sayed, and A. A. Ibrahim, "Physical properties of ZnO thin films deposited by spray pyrolysis technique". Applied Surface Science, vol. 252, pp. 7844-7848, 2006.

[326] M. Ramzan, M. Wasiq, A. Rana, S. Ali, and M. Nadeem, "Characterization of e-beam evaporated hafnium oxide thin films on post thermal annealing". Applied Surface Science, vol. 283, pp. 617-622, 2013.

[327] T. K. Hamad, "Refractive index dispersion and analysis of the optical parameters of (PMMA/PVA) thin film". Journal of Al-Nahrain University, vol. 16, pp. 164-170, 2013.

[328] M. El-Nahhas, H. Abdel-Khalek, and E. Salem, "Optical Properties of 3, 4, 9, 10-Perylenetetracarboxylic Diimide (PTCDI) Organic Thin Films as a Function of Post-Annealing Temperatures". American Journal of Materials Science, vol. 2, pp. 131-137, 2012.

[329] N. A. Lange, M. Gordon, and B. S. Forker, *Handbook of Chemistry*: McGraw Hill, New York, 1961.

[330] E. M. Bachari, G. Baud, S. Ben Amor, and M. Jacquet, "Structural and optical properties of sputtered ZnO films". Thin Solid Films, vol. 348, pp. 165-172, 1999.

[331] N. Shakti and P. S. Gupta, "Structural and optical properties of Sol-gel prepared ZnO thin film". Applied Physics Research, vol. 2, pp. 19-28, 2010.

[332] M. H. Mamat, M. Z. Sahdan, S. Amizam, H. A. Rafaie, Z. Khusaimi, A. Z. Ahmed, S. Abdullah, and M. Rusop, "The effect of annealing temperatures on zinc oxide thin films properties for electronic devices application," in *Semiconductor Electronics, 2008. ICSE 2008. IEEE International Conference on*, 2008, pp. 566-570.

[333] E. Fortunato, V. Assunção, A. Gonçalves, A. Marques, H. Águas, L. Pereira, I. Ferreira, P. Vilarinho, and R. Martins, "High quality conductive gallium-doped zinc oxide films deposited at room temperature". Thin Solid Films, vol. 451–452, pp. 443-447, 2004.

[334] S. I. Bhat, P. M. Rao, A. P. G. Bhat, and D. K. Avasthi, "Irradiation effects on the optical properties of a new NLO mixed borate crystal". Surface and Coatings Technology, vol. 158–159, pp. 725-728, 2002.

[335] N. Ponpandian, P. Balaya, and A. Narayanasamy, "Electrical conductivity and dielectric behaviour of nanocrystalline NiFe 2 O 4 spinel". Journal of Physics: Condensed Matter, vol. 14, p. 3221, 2002.

[336] W. H. Steier, A. Chen, S.-S. Lee, S. Garner, H. Zhang, V. Chuyanov, L. R. Dalton, F. Wang, A. S. Ren, C. Zhang, G. Todorova, A. Harper, H. R. Fetterman, D. Chen, A. Udupa, D. Bhattacharya, and B. Tsap, "Polymer electro-optic devices for integrated optics". Chemical Physics, vol. 245, pp. 487-506, 1999.

[337] P. Sharma and S. C. Katyal, "Calculation of optical constants in a-Ge10Se90-xTex (x = 0, 30, 40) thin films". Journal of Optoelectronics and Advanced Materials, vol. 9, pp. 2000-2004, 2007.

[338] A. F. Kohan, G. Ceder, D. Morgan, and C. G. Van de Walle, "First-principles study of native point defects in ZnO". Phys. Rev. B, vol. 61, pp. 15019-15027, 2000.

[339] C. G. Van de Walle, "Hydrogen as a Cause of Doping in Zinc Oxide". Phys. Rev. Lett., vol. 85, pp. 1012-1015, 2000.

[340] C.-H. Chen, S.-J. Chang, S.-P. Chang, M.-J. Li, I.-C. Chen, T.-J. Hsueh, and C.-L. Hsu, "Electroluminescence from n-ZnO nanowires/p-GaN

heterostructure light-emitting diodes". Applied Physics Letters, vol. 95, p. 223101, 2009.

[341] P. Nunes, B. Fernandes, E. Fortunato, P. Vilarinho, and R. Martins, "Performances presented by zinc oxide thin films deposited by spray pyrolysis". Thin Solid Films, vol. 337, pp. 176-179, 1999.

[342] D. J. Goyal, C. Agashe, M. G. Takwale, B. R. Marathe, and V. G. Bhide, "Development of transparent and conductive ZnO films by spray pyrolysis". Journal of Materials Science, vol. 27, pp. 4705-4708, 1992.

[343] A. Sanchez-Juarez, A. Tiburcio-Silver, and A. Ortiz, "Properties of fluorine-doped ZnO deposited onto glass by spray pyrolysis". Solar Energy Materials and Solar Cells, vol. 52, pp. 301-311, 1998.

[344] S. Faÿ, U. Kroll, C. Bucher, E. Vallat-Sauvain, and A. Shah, "Low pressure chemical vapour deposition of ZnO layers for thin-film solar cells: temperature-induced morphological changes". Solar Energy Materials and Solar Cells, vol. 86, pp. 385-397, 2005.

[345] N. Ohashi, K. Kataoka, T. Ohgaki, T. Miyagi, H. Haneda, and K. Morinaga, "Synthesis of zinc oxide varistors with a breakdown voltage of three volts using an intergranular glass phase in the bismuth--boron--oxide system". Applied Physics Letters, vol. 83, pp. 4857-4859, 2003.

[346] D. H. Fan, Z. Y. Ning, and M. F. Jiang, "Characteristics and luminescence of Ge doped ZnO films prepared by alternate radio frequency magnetron sputtering". Applied Surface Science, vol. 245, pp. 414-419, 2005.

[347] T. Makino, Y. Segawa, S. Yoshida, A. Tsukazaki, A. Ohtomo, and M. Kawasaki, "Gallium concentration dependence of room-temperature near-band-edge luminescence in n-type ZnO:Ga". Applied Physics Letters, vol. 85, pp. 759-761, 2004.

[348] H.-Y. Lee, H.-J. Ko, and T. Yao, "Effect of Ag photodoping on deep-level emission spectra of ZnO epitaxial films". Applied Physics Letters, vol. 82, pp. 523-525, 2003.

[349] L. Gong, J. Lu, and Z. Ye, "Transparent and conductive Ga-doped ZnO films grown by RF magnetron sputtering on polycarbonate substrates". Solar Energy Materials and Solar Cells, vol. 94, pp. 937-941, 2010.

[350] J. G. Lu, Z. Z. Ye, Y. J. Zeng, L. P. Zhu, L. Wang, J. Yuan, B. H. Zhao, Q. L. Liang, and J. A. Phys, vol. 100, p. 073714, 2006.

[351] B. Singh, Z. A. Khan, I. Khan, and S. Ghosh, "Highly conducting zinc oxide thin films achieved without postgrowth annealing". Applied Physics Letters, vol. 97, pp. 241903-3, 2010.

[352] A. F. Khan, M. Mehmood, M. Aslam, and S. I. Shah, "Nanostructured multilayer TiO2–Ge films with quantum confinement effects for photovoltaic applications". Journal of Colloid and Interface Science, vol. 343, pp. 271-280, 2010.

[353] S. A. Shah, A. F. Khan, A. Khan, N. A. Rahim, and M. Mehmood, "Multilayer Si/Ge thin films with quantum confinement effects for photovoltaic applications". Applied Surface Science, vol. 296, pp. 185-188, 2014.

[354] U. Pal, G. Casarrubias Segura, and O. Zarate Corona, "Preparation of Ge/ZnO nanocomposites by radio frequency alternate sputtering". Solar Energy Materials and Solar Cells, vol. 76, pp. 305-312, 2003.

[355] G. Raghavan and R. Rajaraman, "Role of defects in metal mediated crystallization in Al/a-Ge multilayers". Physical Review B, vol. 68, p. 012104, 2003.

[356] T. Zheng, Z. Li, J. Chen, K. Shen, and K. Sun, "Transitions of microstructure and photoluminescence properties of the Ge/ZnO multilayer films in certain annealing temperature region". Applied Surface Science, vol. 252, pp. 8482-8486, 2006.

[357] M. I. Alonso, M. Garriga, A. Bernardi, A. R. Goñi, A. F. Lopeandia, G. Garcia, J. Rodríguez-Viejo, and J. L. Lábár, "Ellipsometric study of crystallization of amorphous Ge thin films embedded in SiO2". Thin Solid Films, vol. 516, pp. 4277-4281, 2008.

[358] J. Jouhannaud, J. Rossignol, and D. Stuerga, "Rapid synthesis of tin (IV) oxide nanoparticles by microwave induced thermohydrolysis". Journal of Solid State Chemistry, vol. 181, pp. 1439-1444, 2008.

[359] M. Y. Nadeem and W. Ahmed, "Optical Properties of ZnS Thin Films". Turkish Journal of Physics, vol. 24, pp. 651-659, 2000.

[360] I. C. Ndukwe, "Solution growth, characterization and applications of zinc sulphide thin films". Solar Energy Materials and Solar Cells, vol. 40, pp. 123-131, 1996.

[361] J. Lee, "Effects of oxygen concentration on the properties of sputtered SnO2:Sb films deposited at low temperature". Thin Solid Films, vol. 516, pp. 1386-1390, 2008.

[362] G. Frank, E. Kauer, and H. Köstlin, "Transparent heat-reflecting coatings based on highly doped semiconductors". Thin Solid Films, vol. 77, pp. 107-118, 1981.